Wireless Capsule Endoscope for Targeted Drug Delivery

by

Stephen Woods

April 2016

A thesis submitted for the degree of
Doctor of Philosophy of Imperial College London
and the Diploma of Imperial College

Department of Electrical and Electronic Engineering
Imperial College London
South Kensington, London SW7 2AZ

Declaration of Originality

I declare that the contents of my thesis is original and of my own work and that it has not been submitted to any other institution for any other degree award. All information sourced from published work has been acknowledged and a bibliography list has been given for each chapter.

Copyright Declaration

The copyright of this thesis rests with the author and is made available under a Creative Commons Attribution Non-Commercial No Derivatives licence. Researchers are free to copy, distribute or transmit the thesis on the condition that they attribute it, that they do not use it for commercial purposes and that they do not alter, transform or build upon it. For any reuse or redistribution, researchers must make clear to others the licence terms of this work.

Abstract

The diagnosis and treatment of pathologies of the gastrointestinal (GI) tract are performed routinely by gastroenterologists using endoscopes and colonoscopes, however the small intestinal tract is beyond the reach of these conventional systems. Attempts have been made to access the small intestines with wireless capsule endoscopes (WCE). These pill-sized cameras take pictures of the intestinal wall and then relay them back for evaluation. This practice enables the detection and diagnosis of pathologies of the GI tract such as Crohn's disease, small intestinal tumours such as lymphoma and small intestinal cancer. The problems with these systems are that they have limited diagnostic capabilities and they do not offer the ability to perform therapy to the affected areas leaving only the options of administering large quantities of drugs or surgical intervention.

To address the issue of administering therapy in the small intestinal tract this thesis presents an active swallowable microrobotic platform which has novel functionality enabling the microrobot to treat pathologies through a targeted drug delivery system. This thesis first reviews the state-of-the-art in WCE through the evaluation of current and past literature. A review of current practises such as flexible sigmoidoscopy, virtual colonoscopy and wireless capsule endoscopy are presented. The following sections review the state-of-the-art in methods of resisting peristalsis, drug targeting systems and drug delivery. A review of actuators is presented, in the context of WCE, with a view to evaluate their acceptability in adding functionality to current WCEs.

The thesis presents a novel biologically-inspired holding mechanism which overcomes the issue of resisting natural peristalsis in the GI tract. An analysis of the two components of peristaltic force, circumferential and longitudinal peristaltic contractions, are presented to ensure correct functionality of the holding mechanism. A detailed analysis of the motorised method employed to deploy the expanding mechanism is described and a 5:1 scale prototype is presented which characterises the gearbox and validates the holding mechanism.

The functionality of WCE is further extended by the inclusion of a novel targeting mechanism capable of delivering a metered dose of medication to a target site of interest in the GI tract. A solution to the problem of positioning a needle within a 360 degree envelope, operating the needle and safely retracting the needle in the GI tract is discussed. A comprehensive analysis of the mechanism to manoeuvre the needle is presented and validation of the mechanism is demonstrated through the evaluation of scale prototypes.

Finally a drug delivery system is presented which can expel a 1 ml dose of medication, stored onboard the capsule, into the subcutaneous tissue of the GI tract wall. An analysis of the force required to expel the medication in a set period of time is presented and the design and analysis of a variable pitch conical compression spring which will be used to deliver the medication is discussed. A thermo mechanical trigger mechanism is presented which will be employed to release the compressed conical spring. Experimental results using 1:1 scale prototype parts validate the performance of the mechanisms.

To my wife Jennifer

Acknowledgements

I have been very fortunate in finding my supervisor Dr Timothy Constandinou who believed in my work and was willing to support me through the long process of developing the next generation of wireless capsule endoscopes. I would like to thank Tim for all his guidance and insightful comments which enabled me to take confidence in the decisions I was making. I would also like to thank members of the Centre for Bio-Inspired Technology who have given me ideas and encouragement over the years.

I am very grateful to Terry Waldock, Chairman of Duckworth & Kent Ltd. for financial support throughout my research. Also at Duckworth & Kent Ltd. I would like to thank David Levy, Head of Engineering, for his help and advice in preparing and assembling the prototypes and also Stuart Cracknell for his help in preparing the prototypes for testing. I would also like to thank Stuart for taking the time to listen to my ideas and for offering me useful suggestions.

Finally I would like to thank my wife Jennifer for her support and encouragement over the long and difficult journey to completing my PhD.

Contents

1 Introduction **5**

1.1 Motivation 5

1.2 Background 6

1.3 Unmet Clinical Needs of Endoscopy 7

1.4 Research Objectives 7

1.5 Overview 8

1.5.1 Wireless Capsule Endoscopy: Background and the State-of-the-Art . 8

1.5.2 Towards a WCE for Targeted Drug Delivery 9

1.5.3 Attaining Equilibrium: Design, Analysis and Evaluation 9

1.5.4 Targeted Drug Delivery: Design, Analysis and Evaluation 10

1.5.5 Drug Delivery System: Design, Analysis and Evaluation 10

1.5.6 Conclusion 10

1.6 Publication Output 11

2 Wireless Capsule Endoscopy: Background and the State-of-the-Art **15**

2.1 Overview 15

2.2 Background 15

2.2.1 Current Practices 16

2.2.2 Clinical Benefits 17
2.2.3 Target Market Segment 18
2.2.4 Commercial WCE Systems 19
2.2.5 Biology of the GI Tract 21
2.3 WCE Components 23
2.3.1 WCE Essential System Features 24
2.3.2 Methods of Resisting Peristalsis 26
2.3.3 Drug Targeting Systems 34
2.3.4 Drug Delivery Systems 41
2.3.5 WCE Localisation 43
2.3.6 Methods of Obtaining Biopsy Samples 45
2.3.7 Evaluation of Micro Actuators 54
2.3.8 Fabrication Methods for Prototype Realisation 62
2.4 WCE Systems 68
2.4.1 Volume Limitations 68
2.4.2 Development Status 69
2.5 Summary 69

3 Towards a WCE for Targeted Drug Delivery 82

3.1 Overview 82
3.1.1 Key Research Aims and Objectives 83
3.1.2 Design Methodology 84
3.1.3 Analysis of Optimal Microrobot Volume 84
3.1.4 Actuators 85

3.1.5 Investigation into the Microrobotic Platform Attaining Equilibrium 86
3.2 Performance Considerations . . . 88
3.2.1 Stages of Operation . . . 88
3.2.2 Electronics . . . 89
3.2.3 Power Distribution . . . 89
3.2.4 Energy Requirement . . . 93
3.2.5 Usability . . . 95
3.2.6 Ingress Protection . . . 96
3.3 Summary . . . 96
3.3.1 Microrobotic Platform Technical Specification . . . 96

4 Attaining Equilibrium: Design, Analysis and Evaluation 101
4.1 Introduction . . . 101
4.2 Overview . . . 101
4.3 Resisting Peristalsis . . . 102
4.3.1 Holding Mechanism . . . 103
4.3.2 Gear Train . . . 104
4.3.3 Gear Tooth Loading Analysis . . . 108
4.4 Analysis of Holding Mechanism . . . 113
4.4.1 Circumferential Peristaltic Force Analysis . . . 113
4.4.2 Longitudinal Peristaltic Force Analysis . . . 127
4.5 Prototype Manufacture . . . 130
4.5.1 Gear Train Prototyping . . . 131
4.5.2 Holding Mechanism Prototyping . . . 135

4.6 Measurement and Characterisation of the Holding Mechanism 139
4.6.1 Motor Torque Protocol 139
4.6.2 Gearbox Torque Protocol 142
4.6.3 Holding Mechanism Protocol 145
4.7 Summary 148

5 Targeted Drug Delivery: Design, Analysis and Evaluation 151

5.1 Introduction 151
5.2 Overview 151
5.3 Targeted drug delivery 153
5.3.1 Needle Positioning 153
5.3.2 Needle Deployment 155
5.3.3 Needle Cam Spring Design Analysis 157
5.3.4 Requirements for Needle Penetration 160
5.4 Analysis of Needle Positioning Mechanism 161
5.4.1 Anticlockwise Motion: Needle Positioning 161
5.4.2 Clockwise Motion: Needle Deployment 169
5.5 Prototype Manufacture 171
5.5.1 SLA Alpha Prototyping 171
5.5.2 Needle Positioning Mechanism Prototyping 174
5.5.3 Needle Deployment 175
5.5.4 Needle Positioning Mechanism Performance 176
5.6 Measurement and Characterisation of the Needle Positioning Mechanism . . 177
5.6.1 Needle Funnel Arm Deflection Protocol 178

5.6.2 Durability and Performance of Needle Funnel Arms 181
5.6.3 Needle Funnel Ratchet Arm Deflection Protocol 183
5.6.4 Durability and Performance of Needle Funnel Ratchet Arms 186
5.7 Summary 188

6 Drug Delivery System: Design, Analysis and Evaluation 191
6.1 Introduction 191
6.2 Overview 191
6.3 Drug Delivery System 193
6.3.1 Drug Delivery 194
6.3.2 Spring Design Analysis 196
6.3.3 Trigger Mechanism 197
6.4 Measurement and Characterisation of the Drug Delivery System 199
6.4.1 Drug Delivery Performance Protocol 200
6.4.2 Spring Deflection Protocol 204
6.5 Summary 208

7 Conclusion 212
7.1 Contributions 212
7.2 Recommendations for Future Work 214
7.2.1 Gastrointestinal Biopsy 215
7.2.2 Pancreas 216
7.2.3 Electrosurgery 216
7.2.4 Surgical Tools 216

A Holding Mechanism Concept Designs **218**

A.1 Holding Mechanism Concepts 219

B Targeting Mechanism Concept Designs **222**

B.1 Targeting Mechanism Concepts 223

C Medication Delivery Concept Designs **225**

C.1 Medication Delivery Concepts 226

D Volume Comparison of the Proposed Concepts **228**

D.1 Volume Comparison 229

E Bending Trials **230**

E.1 PEEK Beam Bending Trial 231

F Detailed Engineering Drawings **233**

List of Figures

2.1 PillCam™ SB(R) developed for visualising the small bowel and PillCam™ ESO developed for visualising the oesophagus 19

2.2 Component parts of the WCE and a system overview including sensor array and location guide 20

2.3 Example of images taken by WCE 21

2.4 Sections of the alimentary canal 22

2.5 Immobilisable in-vivo sensing device 28

2.6 CAD conceptual three-legged anchoring capsule 29

2.7 Prototype of frontal clamping capsule 30

2.8 Prototype of the 12-legged endoscopic capsular robot 32

2.9 Concept of the proposed electrical stimulus capsule 33

2.10 Enterion capsule 35

2.11 InteliSite drug delivery system 37

2.12 Philips Intellicap 38

2.13 Electronically controlled pill 39

2.14 Inflatable reservoir for releasing medication into the GI tract 41

2.15 OdoCapsule conceptual design 42

2.16 Gamma scintigraphy of a delivery to the small intestines 44

2.17 Capsule with two orthogonally orientated permanent magnets for real time 6D localisation and orientation in the GI tract 44

2.18 System and device for in-vivo biopsy 46

2.19 Magnetically driven body-tissue sample device 48

2.20 Hollow needle tissue sampling configuratio 49

2.21 Tissue sampling mechanism with a microactuator for microbiopsy in capsular endoscopes 50

2.22 Prototype micro-biopsy module 52

2.23 Self-propelling endoscope 53

2.24 Piezoelectric squiggle motor manufactured by New Scale Technologies . . . 54

2.25 Namiki four stage geared micromotor 55

2.26 Prototype of the SMA leg actuator for a legged endoscopic capsule 58

2.27 Locomotive mechanism driven by SMA springs for capsule-type endoscopes 59

2.28 SMA flat springs to halt the progress of an oesophageal WCE 60

3.1 Schematic representation of existing capsule geometry based on the PillCam^{TM} by Given Imaging Ltd. 84

3.2 Peristaltic forces (P_e) acting on the microrobot with the lumen shown fully dilated to highlight the extent of the interaction required to achieve equilibrium 87

3.3 Flow chart showing the stages of operation 88

3.4 Circuit schematic of the power supply requirement for the microrobot . . . 90

3.5 Cut-through view of the microrobot with the five main sections labelled . . 91

3.6 Rotary encoder: concentric tracks and registration contact a) and contact pins embedded in the needle funnel b) 92

3.7 Power supply assembly 95

4.1 Microrobot concept design capable of resisting peristaltic pressure through an integrated holding mechanism. Holding mechanism shown fully open . . 102

4.2 Vertically orientated micromotor driving a bevel gear set 104

4.3 Two-legged design showing the central spur gear being driven by the bevel gear. The legs are fully expanded to accommodate a circumference of 60.4 mm 105

4.4 Gear tooth loading modelled as a cantilever beam 109

4.5 Von Mises FEA 2D isoareas analysis of a stainless steel 304, 0.1 module gear tooth profile with a radial component load of 1.473 N 111

4.6 Microrobot holding mechanism shown fully open and the external circumferential peristaltic force P_c acting on the microrobot at six positions 114

4.7 Holding mechanism shown fully closed 115

4.8 Circumferential forces P_{c1} and P_{c5} acting towards the centre of the microrobot 116

4.9 Circumferential force P_{c1} results in a perpendicular component force (P_{p1}) and a reaction force F_{p1} acting on the microrobot's leg 117

4.10 Graph plotting the reaction force F_{p1} of a full zero to 90 degrees opening cycle of the microrobot's leg 118

4.11 Circumferential forces P_{c2} and P_{c4} acting towards the centre of the microrobot 119

4.12 Circumferential force acting on the microrobot's tie bar P_{c2} 120

4.13 Graph plotting the reaction force F_{p2} of a full zero to 90 degrees opening cycle of the microrobot's tie bar 121

4.14 Circumferential peristaltic force acting on the microrobot's centre support P_{c3} 122

4.15 Circumferential force acting on the microrobot's centre support P_{c3} 123

4.16 Graph plotting the reaction force F_{p3} of a full zero to 90 degrees opening cycle of the microrobot's centre support 124

4.17 Graph plotting the combined individual estimated reaction forces F_{p1}, F_{p2}, F_{p3}, F_{p4}, F_{p5} and F_{p6} for a full zero to 90 degree leg operating cycle 125

4.18 Von Mises FEA 2D isoareas analysis of the holding mechanism's leg modelled in stainless steel 304 126

4.19 External longitudinal peristaltic force P_L acting on the microrobot at six positions 127

4.20 Four main leg supports A, B, C and D which will be subjected to the combined longitudinal peristaltic force acting on the holding mechanism 128

4.21 Plot of the holding mechanism bending profile for the longitudinal peristaltic force acting on leg support B modelled in stainless steel 304 129

4.22 5:1 scale prototype of the holding mechanism's gear train manufactured from Nylon 6 and gearbox modelled in PMMA 131

4.23 CNC milled 8 tooth spur gear manufactured from Nylon 6. The profile of the teeth are obscured by significant burring 132

4.24 Bevel gear set manufactured by SLA in Accura 60 and bevel gear cover manufactured by CNC milling from PMMA 134

4.25 Individual parts of the holding mechanism: assembled gearbox, retaining plate, M3 screws, legs, centre support, tie bars and pins 135

4.26 Holding mechanism fully collapsed. The shape of the distal end of the legs has been designed to accommodate cables 137

4.27 Holding mechanism fully expanded. The peg in the centre support slot prevents over expansion of the mechanism 137

4.28 Holding mechanism fully extended with retaining plate secured in position and titanium pins fitted to secure the tie bars 138

4.29 Layout of the test fixture to determine the output torque of the 9 V DC motor and 16:1 gearbox at 52m A 140

4.30 Deliverable motor torque test set-up comprising: a motor controller driving a 9 V DC motor and 16:1 planetary gearhead attached to a 20 mm long arm 141

4.31 Layout of the test fixture to determine the efficiency of the 5:1 scale prototype gearbox with an input motor torque of 4.96 mNm 142

4.32 Gearbox efficiency test set-up comprising: a rocker switch connected to a motor controller which is controlling the gearbox input motor 144

4.33 Load profile of a typical 40 mm long arm deflection with a motor input torque of 4.96 mNm 145

4.34 Test set-up used to measure the load being delivered to the holding mechanism's legs, tie bars and centre support 146

4.35 Experimental set-up of the holding mechanism's opening cycle with a 2.5 N cylindrical dynamometer interfaced with the leg tip (P_{c1}) 149

5.1 Microrobot concept design capable of delivering 1 ml of targeted medication. Needle shown fully extended 152

5.2 Needle positioning mechanism: needle funnel a), ratchet driving the needle funnel and needle b), and enlarged view of the protrusions c) 154

5.3 Needle positioning mechanism extended cantilever 155

5.4 Needle cam operating cycle: stored position a), needle ready to exit b), full stroke c), and retracted position d) 155

5.5 Needle cam linear displacement profile 156

5.6 360 degree needle cam operating cycle: stored position a), full stroke b), needle returning to the stored position c), and retracted position d) 157

5.7 360 degree needle cam linear displacement profile 158

5.8 Needle cam spring in the stored position and at full extension 158

5.9 Needle cam spring stages of operation 159

5.10 Von Mises FEA 2D isoareas and displacement analysis of a PEEK needle funnel arm with a point load of 12.55 mN 165

5.11 Free-body diagram of the extended cantilever needle funnel design 168

5.12 Free-body diagram of the forces acting on the needle funnel arm end 170

5.13 1:1 scale SLA prototypes 172

5.14 Assembled needle positioning mechanism 173

5.15 5:1 scale prototypes of the body and ratchets, needle cam, needle and spring, retaining plate and needle funnel 175

5.16 Assembled needle positioning components. Retaining plate has been removed for clarity 176

5.17 Needle positioning mechanism at maximum extension. Retaining plate has been removed for clarity 176

5.18 Left: Layout of needle funnel arm deflection fixture; Right: Experimental set-up 178

5.19 Needle funnel arm load deflection profile of a 0.85 mm deflection 179

5.20 Top left: Needle funnel arms; Bottom left: Needle funnel assembly; Right: TESA Vision 200 measuring system 181

5.21 Plot of the measured arm dimension across the tips of two prototype needle funnels during repeated manual cycling 182

5.22 Prototype needle funnels CNC machined from Nylon 6. The ratchet arms can be seen in the centre of the parts 183

5.23 Left: Layout of needle funnel ratchet arm deflection fixture; Right: Experimental set-up 184

5.24 Needle funnel ratchet arms engaged with the ratchet 186

5.25 Plot of the measured arm dimension between the tips of two prototype needle funnels during repeated manual cycling 187

6.1 Microrobot concept design capable of delivering 1 ml of targeted medication. Needle shown fully extended and the medication partially deployed 192

6.2 Conical compression spring configurations, 7.5 coils fully expanded with a variable pitch a) collapsed section view b) and fully coiled position c) 193

6.3 Cut-through view of the thermo mechanical trigger mechanism. Heat shield shown suspended above the igniter and Nylon wire 197

6.4 Layout of the medication performance delivery test fixture a), vertical needle configuration b) and horizontal needle configuration c) 201

6.5 Left: Vertical needle configuration; Right: Horizontal needle configuration . 202

6.6 Left: Medication delivery force experimental set-up; Right: Needle delivering liquid into a chicken breast test piece 203

6.7 Overlay of three plots of the measured delivery force required to deliver a 1 ml volume of water into chicken breast flesh 204

6.8 Variable pitch conical compression spring deflection load test fixture 206

6.9 1:1 scale prototype stainless steel variable pitch conical compression spring . 207

6.10 Left: Conical spring held vertically between two supports and further supported via a mandrel; Right: Spring in the fully compressed configuration . 208

6.11 Load profile of a typical spring compression 209

7.1 Microrobot concept design capable of resisting peristaltic pressure through an integrated holding mechanism and delivering 1 ml targeted medication . 213

A.1 Design concept 1 - two axially aligned legs operated by a centrally aligned leadscrew and micromotor 219

A.2 Design concept 2 - two-legged mechanism 220

A.3 Design concept 3 - section view through the small intestines (a) three-legged mechanism (b) 221

A.4 Three-legged design - legs in the stored position (a) legs in the fully extended position (b) 221

B.1 Design concept 4 - a centrally aligned micromotor and leadscrew for the operation of the needle and deployment of medication 223

B.2 Design concept 5 - micromotor combination for needle advancement and retraction 224

B.3 Design concept 6 - rotating medication platform driven independently from the needle operating micromotor 224

C.1 Design concept 7 - spring activated medication delivery mechanism and autonomous needle operation 226

C.2 Design concept 8 - novel single micromotor configuration performing two separate operations 227

E.1 Von Mises FEA 2D isoareas analysis (a) and plan view of PEEK test piece at 42.4X magnification (b) 231

F.1 Final assembly drawing 234

F.2 CAD layout drawing of the needle CAM 235

F.3 CAD layout drawing of the leg cover 236

F.4 CAD layout drawing of the gearbox - legs 237

F.5 CAD layout drawing of the needle carrier 238

F.6 CAD layout drawing of the main body 239

F.7 CAD layout drawing of the 16 teeth needle funnel ratchet 240

F.8 CAD layout drawing of the 0.1 mod spur gears 241

F.9 CAD layout drawing of the 0.2 mod bevel gear set 242

F.10 CAD layout drawing of the bevel gear cover 243

F.11 CAD layout drawing of the expanding leg (right) 244

F.12 CAD layout drawing of the expanding leg (left) 245

F.13 CAD layout drawing of the centre support 246

F.14 CAD layout drawing of the leg tie 247

F.15 CAD layout drawing of the needle funnel 248

F.16 CAD layout drawing of the 16 teeth cam ratchet 249

F.17 CAD layout drawing of the flexible contact PCB 250

F.18 CAD layout drawing of the leg pivot pin 251

F.19 CAD layout drawing of the domed top 252

F.20 CAD layout drawing of the case pin 253

F.21 CAD layout drawing of the contact pin 254

F.22 CAD layout drawing of the flexible needle funnel PCB 255

F.23 CAD layout drawing of the case pin (large) 256

F.24 CAD layout drawing of the needle grinding details 257

F.25 CAD layout drawing of the variable pitch conical compression spring 258

List of Tables

2.1 Review of simple mechanisms which can interact with actuators 27

2.2 Comparison of pH levels in the GI tract [59] 39

2.3 Power to volume merit index 56

2.4 Actuator characteristics evaluation matrix 62

2.5 Comparison of manufacturing methods suitable for prototyping low volume high precision components 67

2.6 Comparison of WCE systems as discussed in the literature review 71

3.1 Microrobotic platform technical specification 98

4.1 Calculated gear train output from an input of 1,543 RPM 106

4.2 Bevel gear and spur gear design parameters 108

4.3 Statistical measured data for the 0.5 module, 8 tooth spur gears 133

4.4 Measured force from each of the circumferential peristaltic positions (P_c) and calculated perpendicular component forces which have been further evaluated 147

5.1 Material selection matrix 162

5.2 Resulting load (P) for the selected material properties 163

5.3 Induced stress (σ_{max}) in the needle positioning arm 164

5.4 Average recorded loads developed through a deflection range of 0.75 mm to 1.05 mm for each of the needle funnel arms 180

5.5 Average measured loads developed through a deflection range of 0.55 mm to 0.75 mm for each of the needle funnel ratchet arms 185

D.1 Concept design volume merit index 229

Table of Acronyms

ASIC	Application specific integrated circuit
CAD	Computer aided design
CCD	Charge-coupled device
CMOS	Complementary metal oxide semiconductor
CNC	Computer numerical control
CT	Computerised tomography
DOF	Degrees of freedom
EDM	Electrical discharge machining
EPIC	Electro-pyrotechnic initiator thin film chip
FCC	Federal Communications Commission
FDA	Food and drug administration
FEA	Finite element analysis
GERD	Gastroesophageal reflux disease
GI	Gastrointestinal
LED	Light emitting diode
LiGA	Lithographie galvanoformung abformung
LiPo	Lithium-ion polymer
MEMS	Microelectromechanical systems
MIM	Metal injection moulding
MIS	Minimally invasive surgery
MRI	Magnetic resonance imaging
MSFF	Maximum static frictional force
OGIB	Obscure gastrointestinal bleeding
PCB	Printed circuit board
PDMS	Polydimethylsiloxane
PEEK	Polyetheretherketone
PMMA	Polymethylmethacrylate
PVC	Polyvinyl chloride
Ra	Arithmetic average
RF	Radio frequency
RP	Rapid prototyping
RPM	Revolutions per minute
SBA	Small bowel angiodysplasias
SMA	Shape memory alloy
SMD	Surface mount device
SOI	Site of interest
WCE	Wireless capsule endoscope
WEDM	Wire electrical discharge machining
WMTS	Wireless medical telemetry service

Table of Latin Symbols

A	Area [m^2]
A_x	Reaction force [N]
A'	Cross-sectional area [mm^2]
b	Beam width [mm]
b_t	Face width [mm]
c	Perpendicular distance from the neutral axis [mm]
C_p	Specific heat [$\mathrm{J\,g^{-1}\,{}^\circ C^{-1}}$]
d	Wire diameter [mm]
d_1	Diameter of pinion [mm]
D	Mean spring diameter [mm]
E	Young's modulus [$\mathrm{N\,m^{-2}}$]
E_i	Electrical energy for ignition [J]
F	Force [N]
F_c	Circumferential force [N]
F_L	Longitudinal force [N]
F_p	Reaction force [N]
F_{pen}	Penetration force [N]
F_t	Force at tooth pitch circle [N]
G	Modulus of rigidity [$\mathrm{N\,m^{-2}}$]
h	Beam height [mm]
h_t	Tooth depth [mm]
I_x	Moment of inertia through section $x-x$ for a solid rectangular beam [mm^4]
I_y	Moment of inertia through section $y-y$ for a solid rectangular beam [mm^4]
I_o	Moment of inertia [$\mathrm{kg\,m}^2$]
k	Radius of gyration [mm]
K_c	Curvature correction factor
K_e	Effective length factor
K_v	Velocity factor
L	Length [m]
L_e	Effective length [m]
L_t	Spring travel [mm]
m	Mass [kg]
M	Moment [N m]
M_n	Normal module
n	Active coils
N_d	Number of teeth on driver
N_f	Number of teeth on follower
N	RPM [rev/min]

Table of Latin Symbols Continued

P	Beam load [N]
P_c	Circumferential peristaltic force [N]
P_{cr}	Critical load [N]
P_e	Peristaltic forces [N]
P_L	Longitudinal peristaltic force [N]
P_p	Perpendicular component force [N]
P_{pen}	Penetration pressure [Pa]
P_1	Subcutaneous pressure [Pa]
P_2	Medication delivery pressure [Pa]
Q	Centroid of area $A^{'}$ [mm^3]
Q_f	Flow rate [$m^3\,s^{-1}$]
r	Radius [mm]
r_{tn}	Resistivity [$\mu\Omega$ x cm]
R	Breaking force [N]
R_e	Reynolds number
R_{tn}	Heating element resistance [Ω]
S	Spring constant [$N\,m^{-1}$]
t	Tooth thickness [mm]
t_w	Beam segment width [mm]
t_r	Rise time [s]
T	Torque [N m]
v	Velocity [$m\,s^{-1}$]
V	Internal resultant shear force [N]
V_p	Pitch line velocity [$m\,s^{-1}$]
y	Lewis form factor
$\bar{y}^{'}$	Distance from the neutral axis to the centroid of $A^{'}$ [mm]
z	Number of teeth

Table of Greek Symbols

ΔP	Pressure difference [Pa]
ΔT	Adiabatic temperature [°C]
α	Angular acceleration [rads s^{-2}]
ω	Angular velocity [rads s^{-1}]
ρ	Density [g cm^{-3}]
δ	Deflection [mm]
η	Efficiency
η_v	Viscosity [Pa s]
σ_{max}	Maximum normal stress [N mm^{-2}]
Φ	Pressure angle [Deg]
Θ	Protrusion angle [Deg]
τ	Shear stress [N mm^{-2}]

Chapter 1

Introduction

1.1 Motivation

There is a growing requirement for surgical procedures to be less traumatic to patients and require shorter procedure times [1]. These issues are currently being tackled by employing minimally invasive surgery (MIS). MIS encompasses many surgical procedures in which a surgeon uses long-handled instruments through a body cavity or a small entry incision to perform a surgical procedure such as abdominal surgery (laparoscopy).

It is proposed that the application of microrobots to assist remotely in performing surgical procedures in the gastrointestinal (GI) tract, such as treating colorectal cancer which is the fourth most common cancer in the UK [2], will greatly increase patient recovery times and improve surgical outcomes. However the clinical need to treat pathologies of the GI tract is not being met by today's technology. It is reasoned that reconfiguring, adapting and exploiting the latest microscale actuation technology, coupled with creative and innovative design, will allow increased functionality to be built into conventional WCEs for the purpose of delivering therapy to a site of interest in the GI tract. The increased functionality will lead to the exploration and treatment of pathologies of the GI tract which were previously inaccessible using conventional flexible colonoscopes, resulting in improved procedure times and comfort for patients. Ultimately the increased functionality will facilitate the treatment of a larger patient group.

1.2 Background

Conventional surgical procedures rely on an incision long enough for a surgeon to be able to observe and manipulate the target operating site with their instruments and fingers. A great deal of damage and trauma can be caused to the bone and surrounding tissue in the process of reaching the surgical site of interest before the curative procedure can commence. Therefore it is of great benefit to the surgeon and the patient to minimise this trauma as it will reduce surgical complications and promote faster recovery times.

One approach towards trauma reduction is MIS. This involves a surgeon inserting long rigid instruments through a small incision to reach a target operating site. The incision is generally no longer than 10 mm because restricting the incision avoids excessive damage to the surrounding tissue and organs.

Although MIS can be seen to bring benefits to the surgeon and to the patient, it also brings with it certain disadvantages and limitations [3]. As the surgeon is now removed from direct contact with the operating site they will have lost any sense of touch and feel with which to aid recognition of the tissue and organs. Instead they must rely on the feedback generated from operating the surgical instruments. Moreover the reduced access impacts the surgeon's ability to manipulate the tools as the 10 mm incision limits the number of degrees of freedom (DOF) the tools can perform through. These problems together can result in reduced dexterity which will not only increase the surgeon's strain but also increase the possibility of error and lead to potentially longer operating times.

The problem of accessibility in MIS can potentially be overcome by the application of microrobots [4]. Introducing a microrobot into the body via an incision or through a natural orifice can offer greater DOF to the surgeon who can now perform the surgical procedure remotely using the microrobot.

An early example of a basic system can be found in colonoscopy. The M2A is a wireless swallowable capsule endoscope developed by Given Imaging Ltd. [5] in 2000 to overcome the problem of examining the small intestine. The capsule which is 11.0 mm in diameter and 25.0 mm long comprises a complementary metal oxide semiconductor (CMOS) camera, four illuminating light emitting diodes (LEDs), a radio frequency (RF) module and a power supply. The problem with this system is that it does not offer the ability to perform therapy to the affected areas leaving only the options of either administering large quantities of drugs or surgical intervention.

The microrobot solutions to MIS use a variety of systems to control and operate their various functions, but there are limitations such as power consumption when operating drive motors and space constraints for actuators. However developments in micro actuators [6], micromotors and the use of shape memory alloys (SMA) [7] may provide solutions for future *in-vivo* surgical microrobots.

1.3 Unmet Clinical Needs of Endoscopy

There are a number of wireless capsule endoscopes (WCE) on the market which meet the medical need for evaluating the appearance of the inside of the GI tract and there are also capsules which can deliver medication to a region of the GI tract. However these systems are unable to meet some clinical needs, principally the ability to perform targeted therapy to an affected area of the small intestines.

There is a clinical need to target and treat pathologies of the GI tract such as ulcerative colitis, polyps and Crohn's disease [8]. These pathologies are currently being treated by using conventional endoscopes in the upper and lower regions of the GI tract but the middle section, the jejunum and ileum, are only reachable through viewing a series of pictures from a WCE. The WCE does not meet the clinical need to directly treat these pathologies of the small intestines. For example if a polyp which required treatment, such as its removal, was detected by a WCE in the GI tract the operator would be required to revert back to conventional endoscopy to perform the procedure.

1.4 Research Objectives

The aim of this research is to develop a platform to achieve targeted drug delivery in the next-generation WCE. A WCE with increased functionality such as the ability to propel medication through a needle rather than allowing it to disperse throughout the GI tract would meet the clinical need for targeting a specific location in the GI tract. The WCE would also be more effective due to the advantages of the shorter discharge time and the more accurate positioning of the medication. The shorter time will allow for the correct dosage to be delivered to the required location without it being diluted over the delivery time from the natural passing of the GI tract or from being dispersed by the constant movement from natural peristalsis.

A microrobot with an onboard camera and a targeting system which has the capability of delivering 1 ml of medication directly into a target site would fulfil the unmet need of visibly targeting a site with therapy. The drug delivery system when operated would allow a lower dose of medication to be delivered to the target site, this in turn could improve the patient's recovery time. There is also a medical need to diagnose small intestinal Crohn's disease [9]. This can be achieved by taking a sample of the intestinal tissue, however conventional WCE cannot perform this function. A microrobot with a targeting biopsy function combined with an onboard camera would be a significant advancement in the diagnosis and treatment of small intestinal Crohn's disease.

Current literature suggests that there is a clinical advantage in monitoring pH levels during the capsule's passage through the GI tract as this can give an approximation of the location of the capsule. Also restricting the capsule's progress through the GI tract for a sufficient length of time would enable the pH data to be used for other analytical purposes such as identifying pathological states associated with abnormal pH levels [10] and diagnosing gastroesophageal reflux disease (GERD) [11].

1.5 Overview

This section presents an overview of the subject matter covered in each of the following six chapters.

1.5.1 Wireless Capsule Endoscopy: Background and the State-of-the-Art

This chapter reviews the state-of-the-art in WCE through the evaluation of current and past literature. A review of current practises such as flexible sigmoidoscopy, virtual colonoscopy and wireless capsule endoscopy are presented along with the clinical benefits of performing endoluminal capsule monitoring. An appraisal of the target market for the diagnosis and treatment of colorectal cancer is presented and a review of the available commercial systems and how the systems operate is discussed. The biology of the GI tract and the movement patterns required to process foodstuff such as segmentation and peristalsis is reviewed. The following sections focus on methods of resisting peristalsis, drug targeting systems, drug delivery systems and methods of performing biopsies in the GI tract. A review of actuators is presented, in the context of WCE, with a view to evaluate their acceptability in adding functionality to current WCEs. The chapter concludes with a comparison of the WCE

systems discussed in the literature review.

1.5.2 Towards a WCE for Targeted Drug Delivery

This chapter sets out the aims and objectives for this research project. A methodology to identify key constraints and requirements of the microrobot is presented. The design methodology presents three research questions, which have been chosen for their impact on the design of the microrobot at the early design concept stage. The first question addresses the physical geometry of the microrobot asking what would be the optimal device volume for a disposable platform. The second question looks at what actuator technology is best suited for the application and the third question relates to the stopping requirement of the microrobot, in particular the stopping and holding forces required to resist peristaltic contractions in the GI tract without damaging tissue. A review of the stages of operation is presented to evaluate what will be required to achieve a successful WCE procedure. The chapter concludes with a comprehensive technical specification of the microrobotic platform.

1.5.3 Attaining Equilibrium: Design, Analysis and Evaluation

This chapter presents a novel biologically-inspired holding mechanism based on the order of insects known as the Coleoptera. Using the biologically-inspired concept of a pair of folded wings protected by an outer case as a basic premise, a compact holding mechanism is presented which can be incorporated into the next generation of WCE for the purpose of resisting natural peristalsis in the GI tract. This chapter describes the requirements of WCE and discusses the detailed analysis of the holding mechanism. The gear train, which is an important part of the mechanism, is described and an analysis of the micro-metre gear teeth, in the context of torque delivery, is presented. An analysis of the two components of peristaltic force, circumferential and longitudinal peristaltic contractions, are presented to ensure correct functionality of the holding mechanism. A fully functioning prototype of the holding mechanism is evaluated and the prototyping methods selected to produce the component parts of the holding mechanism are discussed. A series of experiments, using 5:1 scale prototype parts, is presented which characterises the gearbox and validates the holding mechanism.

1.5.4 Targeted Drug Delivery: Design, Analysis and Evaluation

This chapter presents a novel targeting mechanism capable of delivering a metered dose of medication to a target site of interest in the GI tract. Building on the medical motivation given in Chapter 1 and the design specification presented in Chapter 3 this chapter focuses on finding a solution to the problem of positioning a needle in the GI tract, operating the needle and safely retracting the needle. The requirements for needle penetration are discussed and a comprehensive analysis of the mechanism chosen to manoeuvre a dispensing needle is presented. The analysis focuses on the critical features of the proposed mechanism. To ensure that the needle positioning mechanism performs mechanically an analysis of the geometry, and also of the materials the mechanism could potentially be manufactured from, is reviewed. Prototypes of the mechanism are presented and an evaluation of their performance is discussed. The final section presents the measurement and characterisation of the needle positioning mechanism through two 5:1 scale prototypes.

1.5.5 Drug Delivery System: Design, Analysis and Evaluation

This chapter presents a drug delivery system. A novel actuator is considered for its suitability to expel a 1 ml dose of medication, stored onboard the capsule, into the subcutaneous tissue of the GI tract wall. An analysis of the force required to expel the medication in a set period of time is presented and the design and analysis of a variable pitch conical stainless steel spring which will be used to deliver the medication is discussed. A thermo mechanical trigger mechanism is presented which will be employed to release the compressed conical spring. This method of triggering the spring relies on the Joule's effect to heat an igniter which in turn ignites a pyrogen that melts a Nylon wire. The Nylon wire is employed to retain the coiled spring. A method of overcoming the issue of power distribution through the microrobot is discussed. The solution takes into consideration the requirement for the holding mechanism to rotate 360 degrees and also allows for the medication chamber to be manually filled. A series of experiments using 1:1 scale prototype parts are presented which validate the drug delivery system.

1.5.6 Conclusion

This chapter discusses the contributions which have been presented in each of the preceding chapters. The research presents a WCE with increased functionality resulting in the de-

velopment of the world's first microrobot with the capability of delivering targeted therapy in the GI tract. A discussion of the adaptability of the novel mechanisms and how they can be reconfigured to perform a number of procedures, such as gastrointestinal biopsy, is presented in the future work.

1.6 Publication Output

Parts of this research have been published in journals and conference proceedings. The journal article 'Wireless Capsule Endoscope for Targeted Drug Delivery: Mechanics and Design Considerations' has been listed on the 'most downloaded articles in the past month (published in the past 3 years)' list published by IEEE Transactions on Biomedical Engineering. Its position was 15th in May 2015 and it finished 19th in September 2015.

Journal Publications

- S. P. Woods and T. G. Constandinou, "A Compact Targeted Drug Delivery Mechanism for a Next Generation Wireless Capsule Endoscope," *Journal of Micro-Bio Robotics*, vol. 11, no. 1, pp. 19-34, 2016. doi:10.1007/s12213-016-0088-9.
  This article contains content which contributed to Chapters 2, 3 and 6.

- S. P. Woods and T. G. Constandinou, "Engineering Micro Mechanical Systems for the Next Generation Wireless Capsule Endoscopy," *Biomedical Research International*, vol. 2015, Article ID 741867, 14 pages, 2015. doi:10.1155/2015/741867.
  This paper contains content which contributed to Chapter 2 and Chapter 4.

- S. P. Woods and T. G. Constandinou, "Wireless Capsule Endoscope for Targeted Drug Delivery: Mechanics and Design Considerations," *Transactions on Biomedical Engineering*, vol. 60, no. 4, pp. 945-953, 2013.
  This article contains content which contributed to Chapter 4 and Chapter 5.

Conference Publications

- S. P. Woods and T. G. Constandinou, "A Novel Holding Mechanism for Next Generation Active Wireless Capsule Endoscopy," *Proc. IEEE International Conference of the Engineering in Medicine and Biology Society*, pp. 1181-1185, 2015.
  This paper contains content which contributed to Chapter 2 and Chapter 4.

- S. P. Woods and T. G. Constandinou, "Towards a Micropositioning System for Targeted Drug Delivery in Wireless Capsule Endoscopy," *Proc. IEEE International Conference of the Engineering in Medicine and Biology Society*, pp. 7372-7375, 2011. This article contains content which contributed to Chapter 5.

Press Articles

- M. Piesing "Medical robotics: Would you trust a robot with a scalpel?", *The Observer (London)*, October 10th, 2014.
- "IDC Models revolutionary Robotic Pill receives 'thumbs up' from US technology website", *IDC Design Lines*, February 13th, 2013.
- B. Plackett "The Future Of Medicine: Your Surgeon in a Pill", *Tech Page One*, February 12th, 2013.
- "The 'robotic pill' - SLA prototyping in miniature", *Design Products & Applications*, October 18th, 2012.
- "IDC Models produces Robotic Pill, a revolutionary new treatment for cancer", *IDC Design Lines*, October 18th, 2012.

References

[1] F. Tendick, S. S. Sastry, R. S. Fearing, and M. Cohn, "Applications of micromechatronics in minimally invasive surgery," *Mechatronics, IEEE/ASME Transactions on*, vol. 3, pp. 34–42, 1998.

[2] Office for National Statistics, "Cancer registration statistics, England, 2011," 2013.

[3] D. Qinjun, "Study on medical robot system of minimally invasive surgery," *Complex Medical Engineering, IEEE/ICME International Conference on Complex Medical Engineering*, pp. 76–81, 2007.

[4] M. C. Carrozza, P. Dario, and L. P. S. Jay, "Micromechatronics in surgery," *Transactions of the Institute of Measurement and Control*, vol. 25, pp. 309–337, 2003.

[5] G. D. Meron, "The development of the swallowable video capsule (M2A)," *Gastrointestinal Endoscopy*, vol. 52, pp. 817–819, 2000.

[6] J. Peirs, D. Reynaerts, and H. Van Brussel, "A miniature manipulator for integration in a self-propelling endoscope," *Sensors and Actuators A: Physical*, vol. 92, pp. 343–349, 2001.

[7] A. Menciassi, A. Moglia, S. Gorini, G. Pernorio, C. Stefanini, and P. Dario, "Shape memory alloy clamping devices of a capsule for monitoring tasks in the gastrointestinal tract," *Journal of Micromechanics and Microengineering*, vol. 15, pp. 2045–2055, 2005.

[8] N. I. Goldfarb, L. T. Pizzi, J. P. Fuhr, C. Salvador, V. Sikirica, A. Kornbluth, and B. Lewis, "Diagnosing crohn's disease: An economic analysis comparing wireless capsule endoscopy with traditional diagnostic procedures," *Disease Management*, vol. 7, pp. 292–304, 2004.

[9] P. Swain, "Wireless capsule endoscopy and crohn's disease," *Gut*, vol. 54, pp. 323–326, 2005.

[10] E. A. Johannessen, W. Lei, C. Wyse, D. R. S. Cumming, and J. M. Cooper, "Biocompatibility of a lab-on-a-pill sensor in artificial gastrointestinal environments," *Biomedical Engineering, IEEE Transactions on*, vol. 53, pp. 2333–2340, 2006.

[11] J. L. Gonzalez-Guillaumin, D. C. Sadowski, K. V. I. S. Kaler, and M. P. Mintchev, "Ingestible capsule for impedance and pH monitoring in the esophagus," *Biomedical Engineering, IEEE Transactions on*, vol. 54, pp. 2231–2236, 2007.

Chapter 2

Wireless Capsule Endoscopy: Background and the State-of-the-Art

2.1 Overview

MIS offers reduced trauma to patients through the manipulation of tools through small incisions [1]. However introducing a microrobot into the body through a natural orifice can offer greater DOF to the surgeon. This chapter investigates the current solutions available for the exploration of the GI tract. It focuses on methods for diagnosing pathologies of the small intestine (ileum) and of the large intestine (colon). The emphasis is placed on WCE methods rather than methods such as push enthrascopy as WCE offers the surgeon greater DOF due to the ability to operate the microrobot remotely.

2.2 Background

The introduction of the first flexible colonoscope in 1963 was followed by the first commercial colonoscope manufactured by Olympus Corp. in 1969 [2]. The flexible colonoscope has enabled colonoscopy to become the standard procedure for examining the appearance of the internal surface of the full length of the colon. The colonoscopy procedure involves an examiner, usually a doctor, introducing a 2 m long flexible tube that is approximately 13.2 mm in diameter into the large intestine. The progress can be monitored through an

eye piece on the instrument or via a monitor.

The procedure is performed to investigate abdominal pain, diarrhoea and abnormalities found on colon X-rays or CT scans. The procedure normally takes between 15 and 60 minutes for the instrument to be fully retracted through the whole length of the large intestine. Medication is often given to make the patient sleepy and relaxed as colonoscopy often gives a feeling of pressure, cramping, and bloating but does not cause any significant pain.

Endoscopists complain of the technical difficulties involved in managing the long, flexible instruments and of the difficulty in navigating the tight angles of the colon. These issues are particularly important to newly trained surgeons as inexperience can lead to increased procedure times and the potential to cause damage to the intestinal wall such as small tears or even perforation [3]. The main limitation of the colonoscopy procedure is that the colonoscopes are unable to reach the full length of the GI tract leaving the small intestine unexamined.

2.2.1 Current Practices

There are alternative procedures to colonoscopy currently being used to investigate the GI tract however they also have limitations, they are:

- X-ray performed with a barium enema. This procedure can miss lesions, also if lesions are found colonoscopy may still be required to biopsy or remove the abnormality.
- Flexible sigmoidoscopy. This procedure examines the descending colon (left side of the colon) and the sigmoid colon (lower part of the large bowel) for signs of disease. It is a limited procedure which is used at an early stage to diagnose symptoms such as unexplained anaemia, visible rectal bleeding and positive haemoccult stools.
- Virtual colonoscopy uses a CT scan to construct a virtual image of the colon. It can find hidden polyps, obstructions, fistulas and abscesses however it has several limitations [4]:
    - Polyps less than 5.0 mm in size cannot be found.
    - It is not as accurate as colonoscopy at finding flat cancers or lesions that are not protruding.

  - It cannot remove polyps. If they are found then a colonoscopy must be performed to remove them.
  - The main disadvantage is high doses of radiation exposure.

- Wireless capsule endoscopy uses a swallowed video capsule to take photographs of the inside of the GI tract [5]. One major advantage of the procedure is that the patient is not confined to a hospital environment. The limitations with the procedure are:
  - Rapid transit of the capsule can miss abnormalities due to blurred photographs.
  - Relies on peristalsis to progress through the GI tract.
  - Batteries can fail before examining the entire tract due to slow transit.
  - If abnormalities are found it can be difficult to determine where they are located.
  - Capsules can be retained causing an obstruction that will require surgical removal.
  - Reviewing the photographs is very time consuming.

2.2.2 Clinical Benefits

Endoluminal capsule monitoring devices such as the M2A, Given Images [6], Olympus EndoCapsule [7] or the MiRo, IntroMedic Corporation [8] are particularly clinically beneficial for diagnoses in the small intestine [9], which is extremely challenging to access without them. They are able to detect a number of diseases such as:

- Obscure gastrointestinal bleeding (OGIB). OGIB is persistent or reccurring bleeding which cannot be explained. The origin of the persistent bleeding is unknown even after initial endoscopic evaluations [10]. The OGIB procedure accounts for 60%-70% of all WCE examinations worldwide [11].
- Coeliac disease. Coeliac disease occurs in genetically predisposed individuals. It is an adverse reaction to the gluten protein found in wheat, rye and barley. It can cause diarrhoea, abdominal pain, bloating, weight loss and a failure to thrive due to the reduced ability of the small intestines to absorb nutrients [12].
- Angiodysplasias. Small bowel angiodysplasias (SBA) accounts for 15% of GI bleeding cases. SBA is a collection of friable blood vessels just under the inner intestinal lining.

The vessels are susceptible to recurrent haemorrhaging as the ageing process reduces the surrounding muscle layer [13].

- Small intestinal tumours such as lymphoma, carcinoid tumours and adenocarcinoma (small intestinal cancer).
- Crohn's disease. Crohn's disease can affect any part of the GI tract. It is a chronic inflammatory bowel disease found in genetically susceptible individuals. The disease can be triggered by immunological, bacterial or environmental factors. The symptoms include diarrhoea, weight loss, abdominal pain and vomiting however it may also cause skin rashes, arthritis and chronic anaemia [4].

Being able to detect pathologies of the GI tract using endoluminal capsule monitoring devices offers the potential to diagnosing a wide selection of patients.

2.2.3 Target Market Segment

The statistics for cancer in the UK show that the three most common cancers found in men are prostate (25.6%), lung (13.8%) and colorectal (13.6%) and the three most common cancers for women are breast (30.7%), lung (11.6%) and colorectal (11.2%) [14]. As is evident from the statistics colorectal cancer is the fourth most common cancer in the UK and it represents a significant percentage of patients. Published figures for 2010 show that approximately 40,700 people (22,834 men and 17,861 women) were diagnosed with colorectal cancer in the UK and that there were 15,708 deaths attributed to colorectal cancer [15]. The global picture shows that an estimated 1.24 million cases of colorectal cancer were diagnosed in 2008.

The statistics reveal that there is potentially a large market for the diagnosis and treatment of colorectal cancer which is why the market has responded with new generation products like the Pillcam SB3 developed by Given Images and the EndoCapsule manufactured by Olympus Medical Systems Corporation. GlobalData estimates that the market for WCE systems, valued at $163.5 million (£100 m) in 2008, is forecast to grow by an average 7% annually during the next seven years to reach $261.3 million (£161.3 m) by 2015 [16]. The estimated sales figures appear to be in line with reported sales of WCE, for example since 2001 it is reported that Given Images' PillCam capsules have been used in more than 2 million patients worldwide [17]. As WCE are becoming the gold standard for inspecting

the GI tract it is not unrealistic to expect the market to grow as predicted or even exceed expectations.

2.2.4 Commercial WCE Systems

There are a number of commercial WCE systems available on the market for visualisation of the GI tract such as the M2A, Given Images [6], the Olympus EndoCapsule [7] or the MiRo, IntroMedic Corporation [8]. However the market leader is the M2A developed by Dr Gabi Iddan. Dr Iddan and Dr Gavriel Meron founded the Israeli Company Given Imaging in 1998 and produced the first WCE in 2000. The technology was founded on the idea of miniaturising missile imaging technology so that it could be utilised in a medical device that could explore the GI tract.

The M2A capsule was renamed PillCam^{TM} SB(R) in September 2004 (Figure 2.1), having received its CE approval in May 2001, it then gained FDA approval in August 2011. In 2006 the PillCam^{TM} SB(R) retailed at \$450 (£270) each and was supplied in packs of ten. The accompanying RAPID® Application Software and Workstation retailed at \$17,000 (£10,520) and the Data Recorder (DR2), which is reusable and includes a belt pack, aerial harness and batteries, retailed at \$4,995 (£3,000) [18]. The PillCam^{TM} SB(R) has proven a useful medical tool as by May 2009 Given Images had sold 1 million devices. The PillCam^{TM} contains light emitting diodes, a camera, a lens, batteries, an antenna and a radiofrequency transmitter. The complete system is outlined in Figure 2.2.



Figure 2.1: PillCam^{TM} SB(R) developed for visualising the small bowel and PillCam^{TM} ESO developed for visualising the oesophagus [17]

The holding unit contains a magnet which renders the WCE inoperative. Removing the WCE from the holding unit activates the device. This method of activation ensures

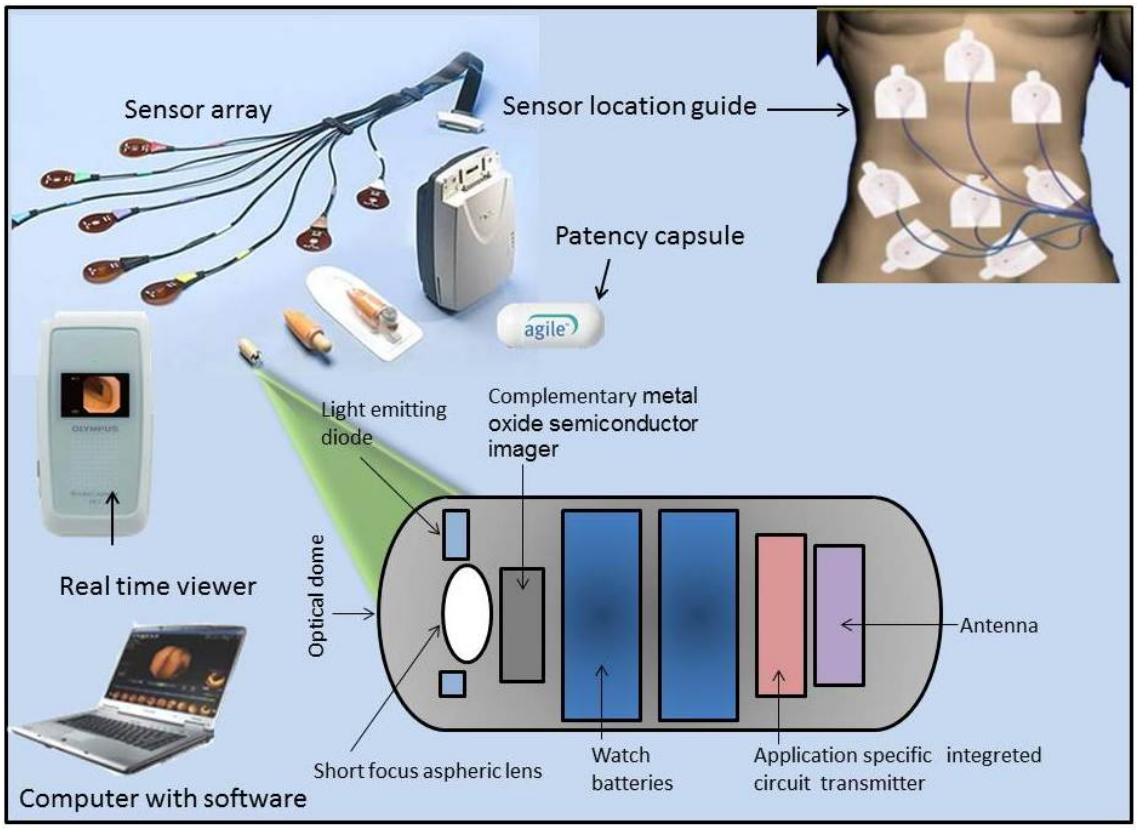


Figure 2.2: Component parts of the WCE and a system overview including sensor array and location guide [19]

the batteries have not deteriorated during storage and that they have enough capacity to complete the 7 to 8 hour transit through the intestinal tract. The capsule records images of the intestinal tract, approximately 2 every second, and transmits them to a receiver worn on a belt-pack by the patient. A series of sensors is placed in specific locations across the abdomen. These sensors are connected by wires to a receiver unit where the transmitted images are recorded. The sensor array and recorder unit can be worn under normal clothing. The position of the capsule is triangulated using the sensor array as the capsule passes through the GI tract, this technique achieves a positional accuracy of $\pm 3\,\text{cm}$. Once the examination procedure has been completed the image recording unit is connected to a computer workstation where dedicated software (RAPID®) is used to evaluate the data. The software allows the user to watch the captured images at varying speeds both forwards or backwards and also label individual frames for future reference.

Many clinical studies have been carried out using WCE for the purpose of detecting

diseases of the small bowel. The type of images which are captured by the procedure and viewed through the dedicated software are displayed in Figure 2.3.

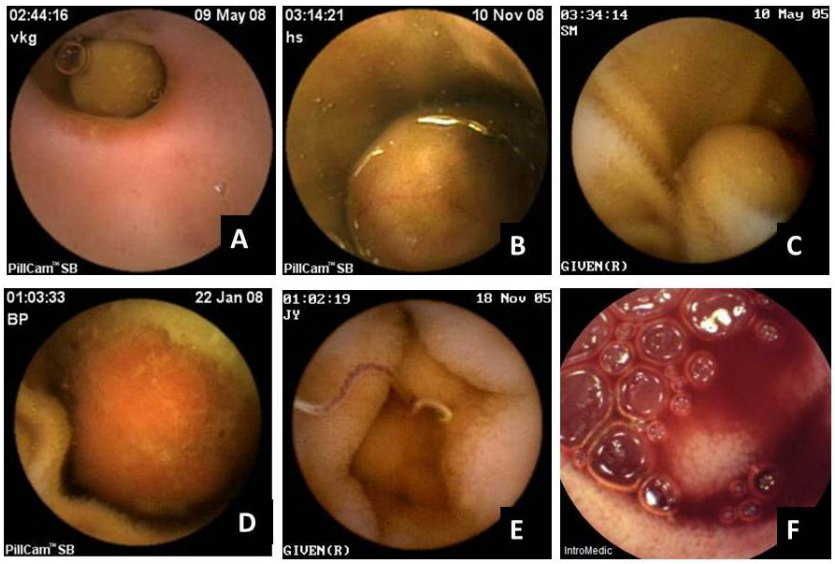


Figure 2.3: Example of images taken by WCE. Pictures of patients with intestinal stricture due to tuberculosis with enterolith (A), small bowel tumors (B, C, D), hookworm (E) and active bleeding without an identifiable causative lesion (F) [19]

As can be seen from Figure 2.3 WCE offers the ability to diagnose a diverse range of pathologies which can be observed in the small intestines. For example Figure 2.3 A) shows an image of a patient who has an intestinal stricture due to tuberculosis with enterolith, a mineral concretion, while Figure 2.3 E) shows a hookworm infestation which is commonly detected by the WCE procedure.

2.2.5 Biology of the GI Tract

The biology of the GI tract presents many challenges to a successful examination by WCE. From the negotiation of the pylorus into the duodenum, to obtaining a clear visualisation of the lumen wall, there are a series of obstacles to be overcome. The GI tract can vary greatly from patient to patient however the average diameter in adults of the large colon is approximately 60.0 mm and the average diameter of the small intestines is approximately 20.0 mm [20]. In addition, the GI tract is a slippery environment as the viscoelastic walls are covered by a 1.0 mm to 2.0 mm [21] thick layer of lubricating mucosa which can have a coefficient of friction as low as 10^{-3} [22]. To put the slippery environment into perspective

the coefficient of friction for the lubricating mucosa can be compared to Teflon® which has a coefficient of friction four times higher [23].

2.2.5.1 Movement Analysis of the GI Tract

Once swallowed the WCE will pass through the alimentary canal, Figure 2.4. The particular section of interest for diagnosis and treatment is the small intestines as this section is very difficult to access. The small intestines comprise of the duodenum, the jejunum and the ileum. These three sections make up the longest part of the alimentary canal at 6.25 m [24]. The duodenum is C shaped and its mouth, the pylorus, extends from the stomach giving this section a degree of stability. The jejunum and the ileum are free to move, however their natural state is collapsed.

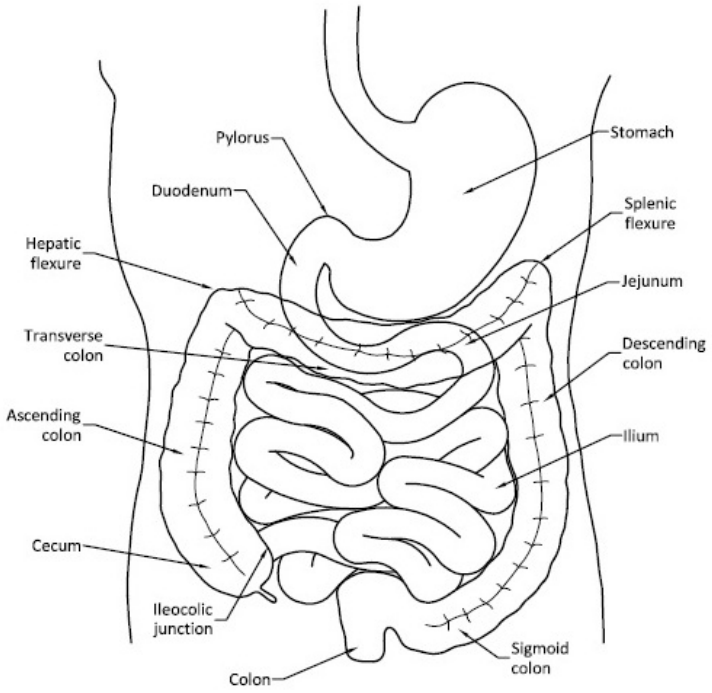


Figure 2.4: Sections of the alimentary canal

In order to process foodstuff, a liquid mixture called chyme, the small intestines uses a series of movement patterns. These patterns, segmentation and peristalsis [20], cause the chyme to progress through the tract. Segmentation is a contraction of the duodenum for the purpose of mixing food. There are two processes involved, they are eccentric contractions

and concentric contraction. The first generates very little intraluminal pressure and the second can generate pressures as high as 20 mmHg [20]. The frequency of the contractions is dependent on eating patterns, becoming stronger as chyme is being processed. Peristalsis is the process of moving chyme through the intestinal tract from the stomach to the colon by means of a series of muscle contractions acting in a wave pattern. The muscle contraction acts in two planes, circumferential and longitudinal. Miftahof (2005) [25] has developed a mathematical model to describe the dynamics of the electromechanical wave phenomenon of a segment of the gut. They report that the active force of contraction in the longitudinal direction to have an amplitude of 17.2 g/cm and an amplitude of 26.9 g/cm in the circumferential direction.

The process of peristalsis allows food to pass through the GI tract. The time it takes for this process to be completed can vary between patients with normal transit times ranging from 20 hours to 56 hours [26]. Transit times of the small bowel range from 15 minutes to 5 hours with the mean average time taking 84 minutes [27].

Prior to administering a WCE it is common practice to determine if the patient is suitable for the capsule endoscopy procedure. This is achieved through the administering of a patency capsule. Patency capsules check the patient is not suffering from known or suspected strictures and that the GI tract is open and unobstructed. If the patency capsule becomes stuck in the GI tract it will dissolve over a period of time however if the capsule is passed within normal time parameters the patient can be assessed for the WCE procedure.

2.3 WCE Components

The development of GI endoscopes with more DOF offers greater advantages to the endoscopists and to the patient [28]. An early pioneer of active endoscopes was Koji Ikuta (1988) [29] and co-workers who developed a SMA actuated multi-DOF endoscope with electric resistance feedback. The snake-like robot could be guided around obstacles using SMAs. Other systems include the in-pipe inspection robot developed by Toshio Fukuda (1989) [30] and the inchworm-like locomotion system, that exploited inflatable balloons and rubber bellows as actuators, developed by Joel Burdick (1994) [31, 32]. The problem with these prior devices is that they all use wires connected to an outside source to power the cameras and actuators and as a result make the procedure uncomfortable for the patient. However to help overcome this issue local sedation is often administered.

Significant advances in the field of medical devices have been made with the introduction of WCE [5]. Replacing the standard endoscopy procedure with a swallowable capsule will benefit the patient in terms of increased comfort and safety and a larger number of patients can be screened more effectively. As comfort is improved and the indignity of the procedure reduced the target screening group will also be increased. However commercial WCE have some limitations one being the lack of an active locomotion system which restricts the ability to navigate through the GI tract and another the inability to perform therapy to an area of interest for example delivering medication to a specific pathogen such as an ulcer.

Researchers are developing technologies which will overcome these issues such as in the area of active locomotion. The addition of active locomotion to a WCE will expand the diagnostic capabilities of the device and enable the surgeon to perform endoscopy in a totally controlled manner.

2.3.1 WCE Essential System Features

In order to achieve a successful examination of the GI tract or perform a procedure such as obtaining a biopsy sample from a specific location, a WCE must possess a number of essential system features. These system features can be categorised into five main areas:

- Vision system
- Telemetry system
- Central processing unit
- Locomotion/holding
- Power unit

The vision system, which can either be a CMOS or CCD image sensor, is illuminated by a minimum of 4 white SMT LEDs. CMOS image sensors consume less power than CCD image sensors however they have lower picture quality. The image sensor must possess sufficient resolution and field of view to determine macroscopic abnormalities of the intestinal mucosa. Typically these features are 0.1 mm and 140 degrees [33] respectively with a depth of view of between 1.0 mm to 30.0 mm and a 1:8 magnification.

The telemetry system will transmit approximately 55,000 compressed video frames over the 7 to 8 hour examination period [34] and also any readings which have been taken, such as pH levels, to an external receiver worn on the body. The external receiver comprises a series of leads placed over the abdomen and connected to a recording unit. The radio frequency transmitter must be compact and consume minimal power, it must also be optimised for transmission through the human body. The allowable limits for the intensity of the radiated field about the abdomen has been determined by the Federal Communications Commission (FCC) for Wireless Medical Telemetry Service (WMTS) to be in a band of 608 MHz to 614 MHz however higher frequencies can also be used such as 1,395 MHz to 1,400 MHz [35].

The onboard central processing unit is responsible for controlling all of the functions of the WCE, such as the telemetry system, power management (i.e. DC/DC conversion), timing and the control of actuators. The controller is implemented in a custom ASIC.

In order for a WCE to perform therapeutic activities it must be capable of resisting peristalsis or actively moving to a desired location in the GI tract. To accomplish this task micro actuators integrated into the WCE are utilised or an external approach can be used where magnetic fields are used to control the position of the capsule.

The power unit, which generally consists of one or two silver oxide button cell batteries, is the most important feature of the WCE as it facilitates all the required operations. The limiting factor for power management is the available space onboard the capsule to accommodate the batteries. Alternative wireless power transfer methods are available however they also require onboard space and large external equipment to operate them.

Different system features can be combined to perform a multitude of medical procedures such as combining two cameras, one at the front and one at the back of the capsule, to allow for a greater area of inspection of the GI tract. However system features are restricted by the geometry of the capsule as the addition of a second camera would prohibit the inclusion of other system features such as a holding mechanism.

2.3.1.1 Simple Mechanisms

Mechanisms, which consist of a system of parts operating together to achieve a particular function, have historically been used for a range of purposes from timekeeping [36] to the production of clothing [37]. However in order for mechanisms to operate they are required to interact with actuators, such as micromotors. Simple mechanisms facilitate the desired

movement and offer a potential mechanical advantage to the system. There are a number of methods for translating the actuator motion into useful motion, some of the general methods are gears, pulleys, cams, screws, levers and ratchets. A description of the advantages and disadvantages of these general methods used in the next generation of WCE is outlined in Table 2.1.

These mechanisms are universal therefore only mechanisms used in WCE will be reviewed as they share key characteristics. The following sections review a number of WCE system features such as methods of obtaining a biopsy sample in the small intestines and methods for resisting peristalsis. The final section presents a review of fabrication methods suitable for realising prototypes.

2.3.2 Methods of Resisting Peristalsis

For a WCE to deliver therapeutic treatment to the GI tract it must firstly overcome peristalsis. To this end researchers have proposed many methods to halt the progress of a capsule such as balloon insulfflation and harnessing magnetic fields. Having the ability to temporarily resist peristalsis by means of an anchoring mechanism overcomes the problem of relying on the operator's judgement in determining the optimum time to deploy a therapeutic treatment.

2.3.2.1 Holding

There are three methods employed for halting the progress of a WCE by enabling it to resist the natural movement from peristalsis. One utilises micro-actuator mechanisms embedded within the capsule, such as the paddling based microrobot developed by Park et al. (2007) [38]. The second approach exploits external magnetic fields to control the position of the capsule [39] and the third approach applies a stimulus to the GI tract to inhibit peristalsis [40].

There has been much development in the field of magnetic control of WCE such as the magnetic shell employed by Carpi et al. [39]. This system looks to modify existing WCE with the addition of a magnetic shell. The shell can be used to guide the WCE by means of an external magnetic field, however this system requires large equipment to perform the procedure and there is also an increase in the diameter of the WCE making it more difficult to swallow.

Table 2.1: Review of simple mechanisms which can interact with actuators

Actuation method	**Advantages**	**Disadvantages**
Gears	Can transmit high torque without slipping Gear trains can deliver a mechanical advantage through a gear ratio Gear trains output a definite velocity ratio Standard gear modules of 0.5 to 14 can be selected to determine the size of the gear Drive direction can be reversed	Low module (<0.5) gears are difficult to manufacture Expensive to manufacture compared to pulleys Lubrication may be required Misalignment of gears will produce vibration, noise and quickly damage the gear train Replacing damaged gears can be difficult and costly
Pulleys	A set of pulleys offers a mechanical advantage Compared to gears it is a simple system which requires no lubrication Crowned pulleys can self-centre a belt through the use of convex curve or V-forms Face widths can be the same as the belt width There is a degree of overload protection due to potential slipping of the belt Large shaft centre distances can be accommodated Slight misalignment of pulleys can be tolerated Belts are easily replaced compared to gears	Flanges at the sides of the pulley are undesirable due to the belt's tendency to crawl against them Large crowns can cause the belt to break where belt curvature changes rapidly between pulley centres Relies on friction to deliver power with a potential for varying velocity ratios as the belt can slip Belts may be strained if tight pulley radii are used Unsuitable for high speeds and high torque transmission More space is required compared to a gear train Open belt pulley can be unsafe
Cams	An open track or a closed track can be used to drive the follower A closed track has positive drive throughout the cycle Rotational motion can be translated into variable linear motion The shape of the cam determines the motion of the follower	Initial start up can generate shock at the beginning and end of the stroke An open track requires a sprung follower to guarantee contact through the cycle The interaction between the cam and follower can generate noise and vibration
Screws	Can translate rotational motion into linear motion Threads on a leadscrew can engage with threads on a nut resulting in either rotational movement of the leadscrew with a static nut or the nut advancing with a static screw The pitch of a thread can vary the linear movement relative to the rotational speed of the screw Rotation of fine pitched screw threads can exert large axial loads Thread forms are easy to generate using conventional CNC machines	V-form threads generate high frictional force making them unsuitable for power transmission Trapezoidal threads generate radial pressure on the nut causing uneven motion of the nut Threads can wear quickly due to the high degree of friction Square threads are more difficult to manufacture compared to trapezoidal threads A large volume of space is required to accommodate a driven leadscrew assembly
Levers	A rigid beam pivoting at a fixed point may offer a mechanical advantage by amplifying the input load An oscillating lever can be used to translate into a linear movement	Pinned joints are required which can be complicated to produce An incorrectly positioned pivot can negate any mechanical advantage Space constraints may limit the achievable mechanical advantage
Ratchets	Can transmit intermittent motion Pawls prevents reverse motion of the ratchet Coarse pitched teeth can produce fine feeds with multiple pawls	Can only be used for slowing a drive system down The pawl produces a jerking action which may result in noise and vibration A second pawl may be required to prevent the drive pawl from pulling the ratchet wheel backwards Pawls may require springing to guarantee correct engagement

2.3.2.2 Immobilisable In-Vivo Sensing Device

The patent proposed by Gilad and Iddan (2004) [41] attempts to temporarily halt the progress of a capsule by deploying two anchors into the intestinal wall, Figure 2.5.

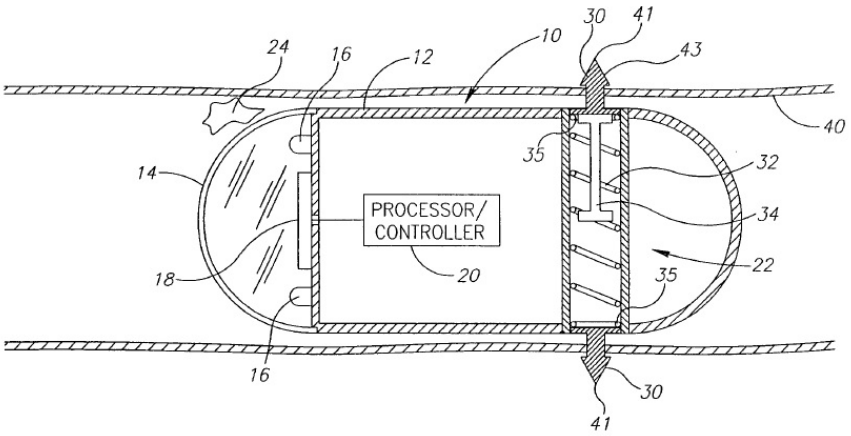


Figure 2.5: Immobilisable in-vivo sensing device [41]

The capsule contains an immobilisation unit to immobilise, hold or otherwise arrest the motion of the capsule. The immobilisation unit is contained in a separate chamber in the body completely sealed from any of the other components. The exit holes for the anchors are also sealed with film to prevent ingress from the liquid environment.

The immobilisation unit contains two anchors separated by a spring and a fuse joined to the anchors. The ends of the spring are soldered to the fuse to ensure a good connection and to prime the mechanism. The anchors have a 0.5 mm - 2.0 mm point capable of piercing the endoluminal walls. The anchors are activated by breaking the ferrite fuse which is triggered through the presence of transmitted radio waves or through the application of an electrical charge. When the fuse breaks, the pointed anchors are pushed by the spring through an aperture in the capsule case and through the wall of the GI tract.

The anchors are made from a biodegradable material such as caramel, biodegradable plastic resins or starches, such as gelatine or wax. The anchors are released from the GI tract by the process of degradation or becoming soluble due to exposure to the moist conditions in the GI tract. An anti-biotic coating may be applied to the anchors to counter any possible injuries encountered through their application.

The distance the anchors extend from the capsule case would appear insufficient to penetrate through the 2.0 mm to 3.0 mm thick GI tract wall. Also the compliant nature of the intestinal wall would suggest that it would move out of the way of the anchors rather than resisting their force and allowing them to penetrate. Further, a perforated intestinal wall is an unwanted outcome of small intestinal endoscopy [3].

2.3.2.3 Micropatterned Adhesive Anchoring Mechanism

An alternative method for anchoring to the intestinal wall which reduces the risk of injury to the intestinal tissue is proposed by Glass et al. (2008) [42]. They propose a three-legged anchoring mechanism which utilises micropatterned adhesives for resisting peristalsis, Figure 2.6.

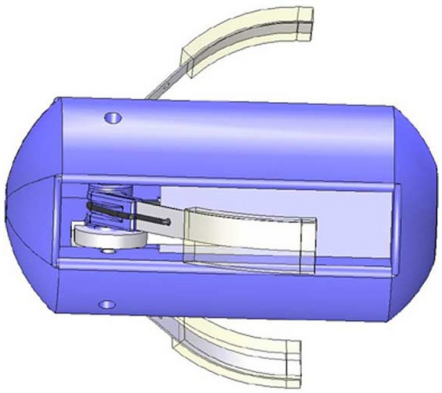


Figure 2.6: CAD conceptual three-legged anchoring capsule [42]

Once an area of interest has been identified in the GI tract by the passing of a standard microcapsule, the proposed three-legged capsule would be used to follow up the procedure and further investigate any areas of interest or perform localised therapy.

The anchoring mechanism consists of three axially aligned legs equally spaced around the capsule. Each leg is connected to a cylindrical pulley which is free to rotate. One end of a cable is secured to the capsule while the other end is secured to the upper end of the leg. The normal state of the cables is relaxed with the legs in the closed position. The leg pulleys are connected to the base of the capsule via rubber springs. When the anchoring mechanism is activated micromotors or SMA wires pull the cables, this results in a torque being applied to the pulleys which can now rotate the legs opening them outwards. At

the same time the rotation applies a torque to the rubber spring resulting in an opposing torque, this counter torque is the means of returning the legs to the closed position when the cable torque has been removed.

To secure the capsule to the wall the ends of the legs have a pad which is coated with a micropattern of adhesive. The adhesive is a biocompatible polymer, polydimethylsiloxane (PDMS). The advantage of using an adhesive to secure the capsule to the wall is that no additional energy is required to maintain the bond after adhesion has occurred and that it requires very little power to remove it due to the peeling action of the arm mechanism.

Although the adhesive pads are embedded in the side of the capsule they are potentially vulnerable to contamination from the environment as the adhesive layer has no protective covering. As the capsule passes through the stomach and negotiates its way around the intestines it is very likely that the adhesive pads will become contaminated with particulates. This contamination will significantly reduce the effectiveness of the pads adhering to the intestinal wall. The patient would be required to overcome the obstacle of swallowing a sticky capsule.

2.3.2.4 Integrated Frontal Clamping System

Menciassi et al. (2005) [43] propose a system for clamping to the wall of the GI tract for the purpose of long-term monitoring. The system is to be integrated into a WCE to achieve accurate visualisation of a target location and long-term pH monitoring, Figure 2.7.

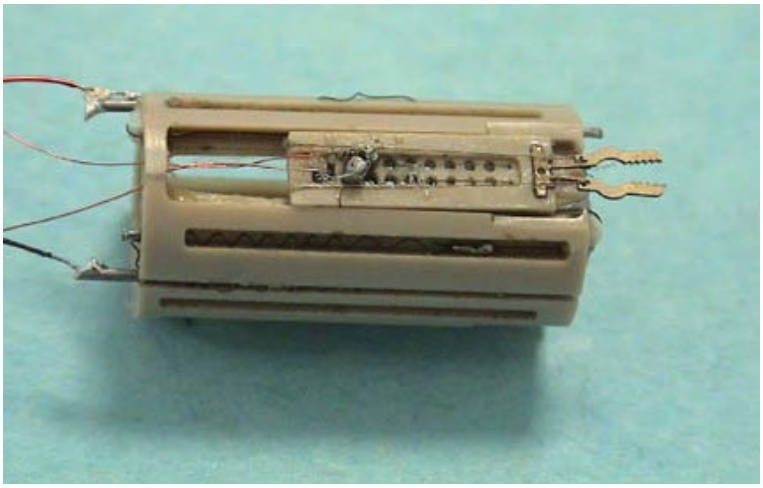


Figure 2.7: Prototype of frontal clamping capsule [43]

The clamping system utilises three grasping units which extend forwards from the capsule and can be activated to clamp to the intestinal wall. The orientation of the three grasping units has been chosen specifically for the advantage of obtaining visual feedback of the whole clamping procedure. The disadvantage with this orientation as opposed to a laterally orientated clamp is the reduced effectiveness of the grasping units as the intestinal wall is normally collapsed onto the capsule case and not in front of it.

The clamping mechanism is a combination of two subsystems, one system to operate the protrusion and return of the grasping unit and another system to operate the opening of the grasping unit. The clamper unit slides in a groove which runs parallel to the capsule's body and is the vehicle which moves the grasping unit. The clamper unit is driven by thermally activating a 100 μm diameter SMA wire which is housed in a trench that runs alongside the groove. The wire has been coiled to generate the large forces required to slide the clamper unit forwards to bring it into contact with the intestinal wall.

The grasping unit comprises two arms made from SMA, this material has been selected for its superelastic properties. The arms are normally in a closed position which is achieved by virtue of a flexure joint which biases the arms. The arms are activated by heating a 20.0 mm long by 50 μm diameter SMA wire which has been fixed into holes in the arms. The heating causes the wire to contract which opens the arms. The method of operation minimises the power consumption of the system.

2.3.2.5 Legged Anchoring Mechanism

Current devices lack the ability to control their speed and direction relying on natural peristalsis to move them through the GI tract. A solution that overcomes this problem is the robotic legged locomotion device developed by Valdastri et al. (2009) [44], Figure 2.8.

The 12-legged endoscopic capsular microrobot features two sets of six legs integrated into the capsule (Figure 2.8). These propel the device through the GI tract and help to uniformly distend collapsed colon tissue making visualisation easier. The dimensions of the device, not including the power supply but including the snap-on vision system, is 11.1 mm in diameter and 33.0 mm long.

The legs are operated via their connection to a nut which moves axially up and down a leadscrew. The set of legs simultaneously open and close as the nut translates the leadscrew, with each set of legs being independently controlled by a motor and gearbox. The number of

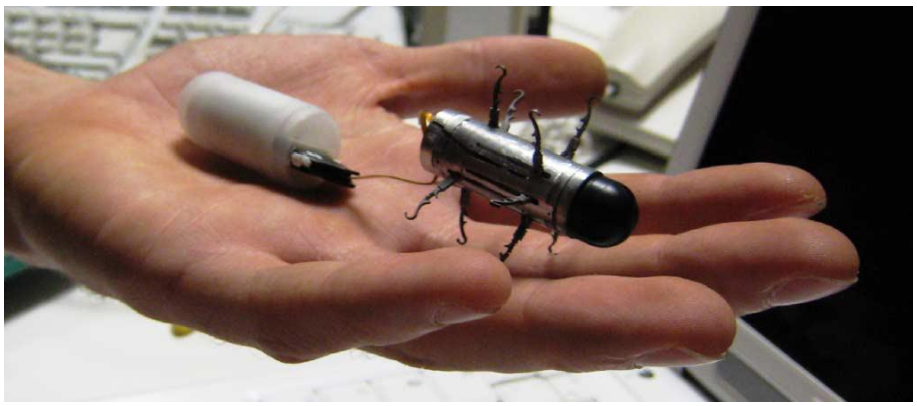


Figure 2.8: Prototype of the 12-legged endoscopic capsular robot [44]

legs distributes the contact force over the colon wall reducing slippage, however a different configuration of the leg ends such as a shaped paddle may distribute the contact force more evenly minimising the number of legs while still supporting the tissue.

The design of the legs would appear to allow only for forward movement, this is also evident in the design of the knee joints as they are designed to allow the leg to flex when moving forward. Although the design permits navigation of sharp corners like the colon's splenic flexure it does not look possible to return to an earlier position for re-evaluation.

The device requires 184 mA under full load, this is supplied by a 100 mA·h battery which is sufficient to provide enough energy to complete an entire 30 minute colon transit. However, as the batteries selected are 10.0 mm diameter by 30.0 mm long there is insufficient room in the device to carry the power supply. The solution that has been adopted is to trail the batteries behind within a capsule, however this bimodular power solution may not be acceptable to the medical profession or to the patient.

An issue with this method of active locomotion is how effective the device will be at performing targeted therapy. The capsule is suspended evenly in the centre of the GI tract to make movement easier as there is equal space around the capsule for the legs to operate in. However performing therapeutic activities to the side of the wall will be difficult due to the further reach needed for tools to contact the intestinal surface. The problem may be further compounded by the viscoelastic property of the intestines preventing good grip or manipulation of the tissue.

The fundamental limitation of this system in performing therapeutic activities is the

overall volume of the capsule which prevents it from being swallowed. The overall volume would be a result of the tools for performing therapeutic activities being combined with the existing volume for the leg mechanism and the volume of the trailing power supply.

2.3.2.6 Electrical Stimulation

An alternative approach to controlling the progress and direction of a WCE is through electrical stimulation. Woo et al. (2010) [45] propose a capsule which can contract the small intestine using electrical stimuli, Figure 2.9.

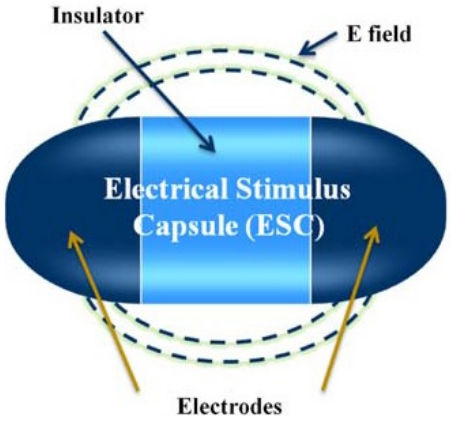


Figure 2.9: Concept of the proposed electrical stimulus capsule [45]

Stimulating the tissue of the GI tract with an electrical charge can cause a contraction of the muscle and prevent the capsule from moving. The method employed by Woo et al. is to contract the tissue in contact with the centre of the capsule by applying a high frequency electrical stimuli (>5Hz) to the stainless steel (SUS316L) electrodes at each end of the capsule. The length of the insulating material between the electrodes determines the contraction force and affects the overall length of the approximate 11.0 mm diameter capsule which has been optimised at 35.0 mm long. A maximum static frictional force (MSFF) of 56.5 $\pm$9.77 gf can be generated using the parameters of 5 ms pulses of 20V at a frequency of 10 Hz. The MSFF is sufficient to hold the capsule against peristalsis for a period of 60 minutes.

Research carried out by Mosse et al. (2001) [46] showed that small diameter electrical stimulated devices (15 mm) moved very slowly (approximately 1 mm/sec) compared to larger diameters. Mosse et al. proposed an ovoid shaped capsule with an inclusive taper of

40 degrees at the front, a length of 38.0 mm and a diameter of 23.0 mm. The acrylic device uses two stainless steel electrodes positioned 180 degrees apart and mounted on the front of the taper. With the optimised settings of 30 ms pulses of 20 mA at a frequency of 15 Hz the capsule resulted in a speed of 4 mm/sec.

A limitation with the design proposed by Woo et al. (2010) [45] is that the capsule can only stop, it does not have the ability to travel in either direction. This issue has been overcome by Mosse et al. (2001) [46] by applying contacts at the front and back of the capsule. However the large diameter and increased length of Mosse's capsule will make it very difficult to swallow and navigate the tight turns of the GI tract. Previous research carried out by Woo et al. (2009) [47] presents a capsule which also has contacts on the front and back. Its dimensions are 22.0 mm long with a diameter of 11.0 mm making the capsules volume comparable with conventional WCE. However once the onboard components such as the electrical stimulation unit, RF receiver, antenna and batteries have been included it only leaves a volume of approximately 0.76 cm^3 of useful space.

There are a number of issues with electrical stimulation which may prevent it from becoming a viable option for navigating the GI tract. One such issue is the electrical sensitivity of the liver which makes it potentially susceptible to damage from the electrical discharge. In addition the natural movement patterns from peristalsis could be interrupted [45].

2.3.3 Drug Targeting Systems

At present there are two main types of drug targeting systems available that can be swallowed for targeting the GI tract, they are non-disintegrating drug delivery devices and coated capsules which can target the small intestines (enteric).

Enteric coated capsules are orally administered capsules that use a barrier to protect them from gastric juices, this enables the release of the medication in the small intestine. This type of system is known as a delayed release dosage form [48] and commercially available products come in the form of tablets or pellets filled into hard gelatine capsules. They are generally used to protect the medication from attack by enzymes or low pH levels in the stomach. They can also be used where drugs irritate the gastric mucosa causing nausea.

The enteric coated capsule relies on the thickness of the coating applied to it to control the release of the drug into the GI tract. If too much or too little coating is applied it

may not properly disperse in the required position within the GI tract. This puts greater emphasis on the control of the manufacturing process requiring the employment of skilled staff to ensure consistency.

Non-disintegrating drug targeting systems are pill sized capsules capable of being swallowed. They are made from FDA approved materials which can pass through the GI tract without being affected by the changing environment. They offer the ability to perform regional drug absorption treatment within the GI tract. There are a number of patents relating to drug delivery [49, 50] however there are only three commercial companies selling regional drug absorption services, they are Phaeton Research with the Enterion capsule [51], Innovative Devices LLC with InteliSite [52] and Philips Electronics with IntelliCap [53].

2.3.3.1 Site-Specific Drug Delivery

The Enterion capsule [51] manufactured by Phaeton Research is a site-specific drug delivery capsule commercially available for delivering drugs to a specific location in the alimentary canal. It is administered with a standard volume of water (240 ml) [54] and relies on natural peristalsis to move it through the body, Figure 2.10.

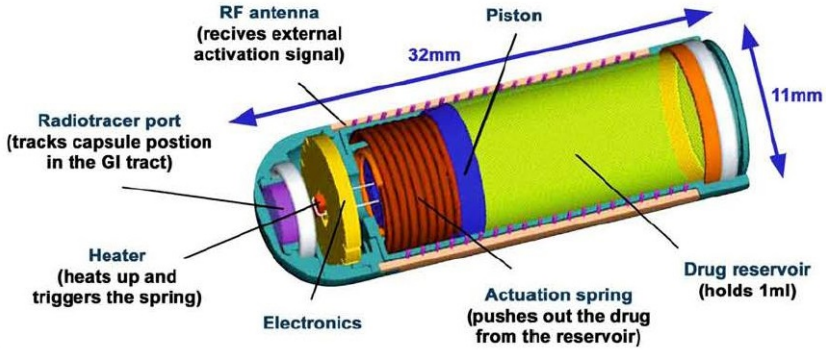


Figure 2.10: Enterion capsule [51]

The device is manufactured from FDA approved plastics and has a capacity of storing 1 ml of medication in a drug reservoir. The method of delivering the medication offers an advantage over other capsules as the medication may be in a liquid, powder or solid form. The drug reservoir and the requirement that the device be swallowed have influenced the

size of the capsule which is 11.0 mm in diameter and 32.0 mm in length. These dimensions are contradictory to the general geometric boundaries for swallowing stated in the literature which are a maximum diameter of 12.0 mm and a maximum length of 25.0 mm [55] however studies carried out by Conner et al. (2009) [56] have shown that capsules of larger dimensions (Ø11.0 x 32.0 mm long) are capable of being swallowed by subjects aged 18 to 65 years.

The loading of the medication is performed simply by removing a bung at the rear of the capsule and filling up the drug reservoir. The bung relies on an elastomeric o-ring to seal the rear port. The o-ring is a cheap and efficient way of sealing the aperture against leaks and the design utilises the non-linear force profile of a rolling compressed o-ring to stop it from accidentally being opened.

The medication is administered through the use of a stored energy source, i.e. a compressed spring which when triggered operates a cylindrical piston. The piston expels the medication through the rear aperture at the same time as ejecting the bung. The speed of expulsion will be rapid propelling the detached bung outwards. The bung is then free to continue on until it is excreted naturally. Although the size of the bung is relatively small compared with the capsule the shape of the bung does not appear to facilitate easy expulsion from the body.

2.3.3.2 Releasing the medication

The activation spring propels the medication from the drug reservoir. The spring is held in position by an anchoring mechanism which consists of a thin thread connected to the piston and to a heating element which is mounted on a circular printed circuit board. The anchoring mechanism works by heating the thin thread until it becomes weak and breaks releasing the spring and hence operating the piston. The heating element which is a resistor is triggered by an externally applied radiation. When the device passes through an electromagnetic field at the frequency an onboard receiver is tuned to, the induced current powers the resistor which heats the thin thread.

The configuration of the anchoring mechanism assembly does not appear to be a simple task to prepare for loading into the capsule as the thin thread is required to be fixed in position while it is under the compressive force from the spring. Also these components are positioned deep within the housing of the capsule compounding the assembly problem.

The 1 ml of medication can be expelled at a target region in the GI tract such as the

jejunum, ileum, ascending colon or descending colon. It cannot target specific pathogens such as tumours or ulcers because it releases its payload as a bolus form. This has the effect of spreading the medication over a section of lumen as the capsule is under constant movement from peristalsis and has no means of stopping and holding its position.

Tracking the capsule's position through the GI tract is by means of a gamma-emitting radionuclide and a gamma camera. There is no visual identification of a target site as it relies on the position from the gamma-emitting radionuclide tracer. The radioactive dose of 0.49 mill-Sieverts (mSv) is less than one-fifth of the annual radiation dose that each person would receive in one year (2.6 mSv) [54] however this may become problematic if the procedure were required to be performed for multiple treatments over a short period of time.

2.3.3.3 Liquid or Powder Drug Delivery

The InteliSite is a drug delivery system manufactured by Innovative Devices LLC [52] which overcomes the problem of losing the cap in the GI tract by employing a system which opens ports on the side of the device releasing the drugs into the GI tract, Figure 2.11.

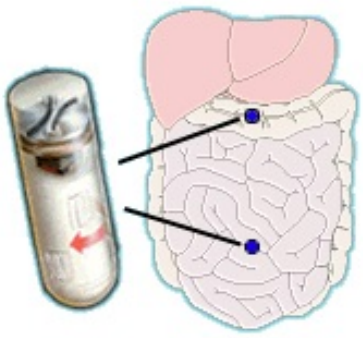


Figure 2.11: InteliSite drug delivery system [52]

The InteliSite has a 1 ml reservoir capable of being loaded with either a liquid or a powder drug formulation. The dimensions of the capsule are comparable with the Enterion capsule at 10.0 mm in diameter and 35.0 mm long.

The drugs are administered when the capsule is exposed to a radio frequency magnetic field. The magnetic field causes two SMA wires to heat up and straighten out. This action causes an inner sleeve which has a series of slots in it to rotate aligning it with a series of

slots in the outer surface. This action allows the drugs to be released into the GI tract. The device has no means to propel the drug from the capsule into the GI tract instead it relies on the natural turbulence generated from the capsule passing through the GI tract to disperse the medication. This method would appear to be an inefficient means of targeting a specific site as it will be slow and unreliable.

2.3.3.4 Electronically Controlled Drug Delivery

Philips Research has developed IntelliCap [53] an intelligent pill for electronically controlled drug delivery in the GI tract. This device uses a micro pump to propel the medication into the GI tract, Figure 2.12.



Figure 2.12: Philips Intellicap [53]

The dimensions of the capsule are similar to the M2A by Given Imaging Ltd. [6] at Ø11.0 mm by 26.0 mm long. The IntelliCap incorporates a microprocessor, battery, pH sensor, temperature sensor, RF wireless transceiver, fluid pump and drug reservoir. The literature does not specify the capacity of the drug reservoir or the type of medication it can dispense however from the dimensions and the onboard equipment stated it would appear that there will be very little room for the medication and that it can only deliver liquids.

The microprocessor controls the delivery of the drug through the internal fluid pump which can disperse the medication in different delivery profiles such as burst, progressive release or a multi-location dosing. Before the IntelliCap is swallowed it can be programmed to deliver the drug at a pre-planned target location. As the pill passes naturally through the GI tract it monitors the pH levels. The pill uses this information to determine its position as the pH value varies depending on its location in the GI tract.

The IntelliCap can communicate pH levels and temperature readings to an external control unit which has the ability to record the data and also to transmit additional commands

back to the pill. The use of external medical imaging equipment such as magnetic resonance imaging (MRI) or computerised tomography (CT) scans are proposed if greater accuracy is required in locating the position of the IntelliCap before it delivers its medication.

2.3.3.5 Electronically Controlled Pill

Philips Electronics N.V. owns a number of patents relating to ingestible electronic capsules [57, 58]. One such patent is the electronically controlled pill designed by Gerardus Langereis and George Likourezos (2006) [59]. The electronically controlled pill (Figure 2.13) provides a delivery system using at least one sensor to sense a change in pH levels. This change in pH level triggers a valve, pump or hatch to release the medication. The pill can be custom programmed to a patient's medical profile.

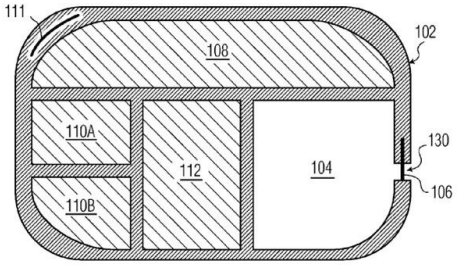


Figure 2.13: Electronically controlled pill [59]

The pill stores data relating to pH levels in a look-up table. The look-up table correlates the sensed pH levels with the pill's position within the GI tract. This method of tracking is similar to the method used in the IntelliCap by Philips Research [53]. An example of the pH levels in the various areas of the GI tract can be seen in Table 2.2.

Table 2.2: Comparison of pH levels in the GI tract [59]

Position in GI Tract	**Mouth**	**Oesophagus**	**Stomach**	**Small Intestine**	**Colon**
pH Level	7.4-7.7	6.3-6.9	4.0-4.8	7.0-9.0	4.0-6.5

The pill is activated by pushing a button before swallowing or an alternative method is to use a dissolvable outer layer which when swallowed will dissolve away revealing electrodes of a switch which will close a circuit.

2.3.3.6 Interpreting pH Data

The data from the look-up table could potentially be interpreted incorrectly. As can be seen from Table 2.2, the pill could appear to be in the stomach with a pH level of between 4.0 and 4.8 but actually be in the colon with a pH reading between 4.0 and 6.5. It would appear that Philips have tried to overcome this problem by introducing a timing element which is activated when the pill is swallowed. They also propose an alternative method of physically locating the pill by using magnets to interact with a metallic liner imbedded in the outer shell. The location is achieved by placing a magnetic detector on the abdomen of the patient. This method will only give a position relative to x and y in the body, it does not specify where exactly it is along the GI tract. Therefore targeting a precise point becomes difficult as, owing to the mobility of the ileum structure, there is no guarantee that the target coordinates will lead to the same site as a previous passing.

The pill uses the pH readings and the timing circuitry to determine its relative position within the GI tract however the tract can vary in length depending on the patient's age, gender, size and many other factors. The average length of the small intestines is 6.25 m [60] however this length can differ enormously between patients, therefore the position of the capsule within the GI tract cannot be specifically known using this system.

To release the medication a signal is sent from a logic circuit to the release controller which controls the amount the valve opens. The medication is released from the medicament reservoir by slowly opening the valve or by pumping slowly using a pump valve to dispense the medication in a controlled manner. The suggested valve system used by the pill would be a microfluidic system similar to those used by inkjet printers. These microfluidic systems can precisely control the quantity of medicament being released. Using such a valve system is questionable in this application as the release rate would appear to be restricted by the maximum aperture size of the valve and the physical size of the pump. This system would also be restricted to liquids as the valve can be easily clogged.

The release controller is a micro-electromechanical mechanism capable of generating a variable voltage level and supplying it to the electronically controlled valve for opening and closing it. The release controller is a transistor or D/A circuit that provides voltages to the valve causing it to open and close.

2.3.4 Drug Delivery Systems

There are a number of methods employed by pharmacologists to administer drugs to the GI tract, the most common being enteric coated capsules. This method employs a coating on the capsule which when swallowed starts to be dissolved by the enzymes in the intestines. Over a period of time the capsule will pass through the intestinal tract and release the medication however this method is not reliable for targeting specific locations of the tract therefore researchers have looked for alternatives methods.

2.3.4.1 Determining the GI Tract Length

The telemetric capsule developed by Lambert et al. (1991) [61] overcomes the problem of location by using a plastic cogwheel to measure the length of the tract. As the 10.0 mm diameter plastic cogwheel rotates, due to the pressure applied to it from the intestinal wall, it contacts a flexible thin plate which has a strain gauge bonded to it. Each rotation of the wheel bends the thin plate three times causing variations in resistance in the strain gauge. The resistance variations are transmitted to a receiver.

The capsule has an interchangeable tip used for either aspirating or releasing a liquid into the GI tract. The tip is controlled by a magnetic switch which is activated by a permanent magnet being brought into close proximity to the capsule (closer than 15 cm). The switch triggers a micro furnace to heat up a strip of plastic which breaks after two seconds causing a clip to open, this releases a compressed spring which starts the delivery (Figure 2.14). The plastic strip is destroyed each time the capsule is deployed and needs replacing.

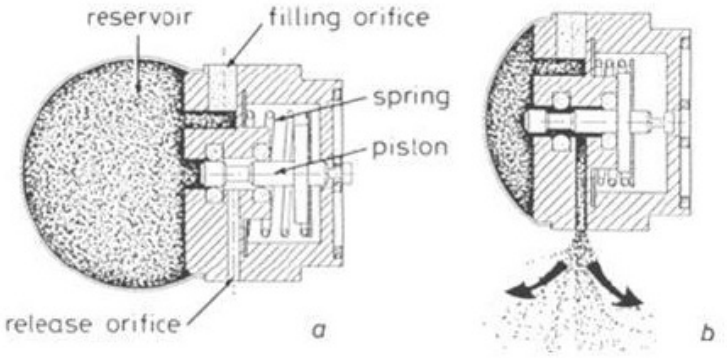


Figure 2.14: Inflatable reservoir for releasing medication into the GI tract [61]

The drug delivery tip utilises an inflatable elastic reservoir to store 1 ml of medication. A

port on the side of the capsule allows for easy filling of the reservoir using a syringe, a tight Silastic joint prevents the medication from escaping. When the mechanism is activated the piston moves forward opening the way for the medication to flow through, propelled from the contraction of the expanded reservoir and delivering the medication into the GI tract.

The use of an expandable elastic material for storing and delivering the medication makes for a simple and user friendly system, however the expanded bubble may be difficult to swallow because of its shape and the high friction properties of the material. The medication will be expelled quickly into the GI tract however there will be no directional control over the discharge as the release orifice is fixed in a side position. This coupled with the lack of a camera suggests limited effectiveness. Using a wheel to measure distance is common practice however the single wheel configuration may not allow for continuous contact with the GI tract wall as the digestive tract will twist and turn potentially disengaging the wheel. This will result in unreliable positional data.

2.3.4.2 Odometer Measuring Method

Karargyris et al. (2015) [62] propose the OdoCapsule which provides video stability and positional information while navigating the GI tract, Figure 2.15.

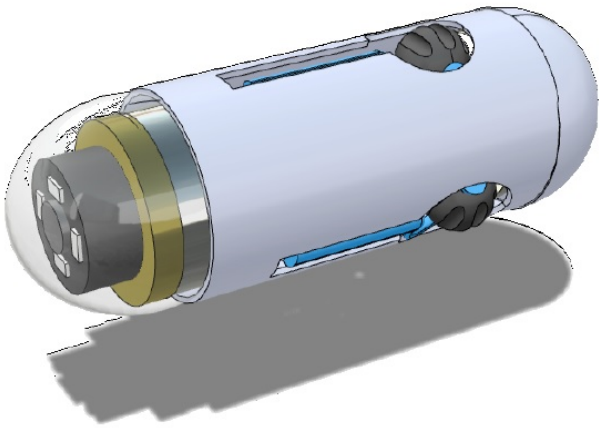


Figure 2.15: OdoCapsule conceptual design [62]

The system, which is based on previous work carried out by Bourbakis et al. (2010) [63, 64], utilises three positional sensor wheels as opposed to the one wheel approach proposed by Lambert et al. (1991) [61]. The capsule's three sensor wheels are mounted on 15 mm long legs which protrude out of the 13 mm diameter by 30 mm long capsule by 35° due

to torsion springs. The springs extend the wheels from the capsule's body so that they make contact with the GI tract wall. Frictional forces between the intestinal wall and the wheels cause the wheels to rotate. The rotating wheels emit electromagnetic peaks which are received by precision sensors on the control board of the capsule allowing the progress of the capsule to be monitored. The legs are retracted and extended by a micromotor which pulls or releases a cable connected to each of the three legs.

There is a risk that the capsule may enter the pyloric opening in reverse which could result in one of the legs becoming stuck in the intestinal wall tissue due to the angle of the open legs. However this scenario has been considered and the solution reported is to monitor the feedback from the rotating wheels. If a steady state has been recorded for one of the wheels the micromotor retracts the legs for a short period of time then releases them to continue. This method of recovering the legs from a stuck position would rely on sufficient torque from the micromotor to overcome the force imposed by the collapsed tissue.

2.3.5 WCE Localisation

Returning to a site of interest to perform further diagnosis or to administer therapy in the small intestines presents many challenges. The mechanical method of employing wheels proposed by Lambert et al. [61] and Karargyris et al. [62] may offer a potential solution however relocating the site of a previously captured image, in relation to the position and orientation of the capsule, is still a challenge to achieve. Further the unrestrained, slippery, compliant environment of the small intestine adds greater complexity to the problem. Therefore alternative methods of tracking a capsule's position which do not use a mechanical means of interaction with the GI tract wall have been proposed by researchers, for example using magnets or using radioactive isotopes.

2.3.5.1 Gamma Scintigraphy

The InteliSite capsule [52] can be tracked through the GI tract using gamma scintigraphy (Figure 2.16) which will detect Indium (^{111}In) or Technetium ($^{99\,m}$Tc) gamma isotopes which have been incorporated into the capsule. As with the Enterion capsule there is no visual identification of a target site as it relies on the position from the gamma-emitting radionuclide tracer.

As can be seen from Figure 2.16 gamma scintigraphy provides very little information

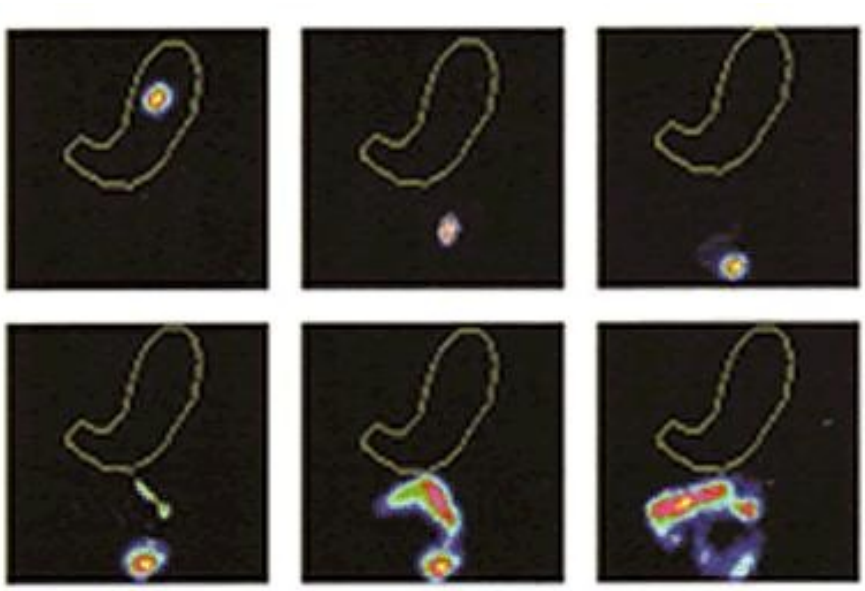


Figure 2.16: Gamma scintigraphy of a delivery to the small intestines [65]

regarding the location of the capsule. The capsule can clearly be seen leaving the stomach however once it enters the small intestines its position relative to the stomach is lost. This method is also incapable of providing detailed macroscopic recognition of the intraluminal surface of the GI tract making diagnosis of pathologies impossible.

2.3.5.2 Magnet Based Localisation

The capsule proposed by Song et al. (2009) [66] utilises a system based on two magnets for real time 6 degrees localisation and orientation in the GI tract, Figure 2.17.

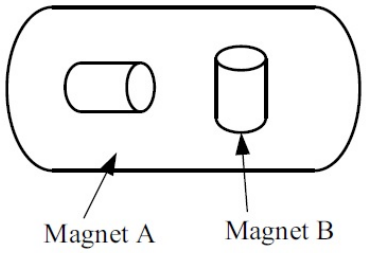


Figure 2.17: Capsule with two orthogonally orientated permanent magnets for real time 6D localisation and orientation in the GI tract [66]

A tracking system, which is worn outside the body, is proposed for the detection of magnetic fields generated by two permanent magnets onboard the capsule. The tracking system uses a sensor array utilising 64 3-axis magnetic sensors positioned equally between 4 planes of a 0.5 m^3 frame to track the movements and position of a capsule in real time.

Two orthogonally orientated permanent magnets with diameters of 6.0 mm and lengths of 4.0 mm are incorporated into a capsule (Fig. 2.17). The magnetic field intensity of the magnets is relative to their distance, using an algorithm based on the mathematic model of the magnetic field the capsules 3D location and 3D orientation can be calculated.

The system accuracy is reported to have an average error of 2.1 mm for the capsule's localisation and an average orientation error of 2.1 degrees. However these results are based on two magnets with diameters of 6.0 mm and lengths of 8.0 mm positioned 100.0 mm apart.

The benefit of using a permanent magnet to realise the localisation of a capsule is that it generates a magnetic signal wirelessly without the need for an onboard power supply. However there may be issues scaling down the technology to achieve the full 6D orientation information as reducing the distance between the two magnets increase the average localisation and orientation errors. Using a conventional capsule geometry as a standard for comparison the furthest distance the two magnets could be positioned apart would be 13.7 mm. This distance is significantly lower than the 100.0 mm test distance, and it also excludes the area required for a camera system, therefore the positional errors may exceed the limits required for reliable localisation.

2.3.6 Methods of Obtaining Biopsy Samples

It is not only difficult to determine the location of a capsule in the small intestines but it is also challenging to diagnose pathologies of the small intestinal mucosa. To identify abnormalities of the small intestine, barium studies or enteroscopy can be performed, however these procedures are limited in their ability to diagnose pathologies of the small intestines [67]. An important diagnostic procedure is biopsy. Small intestinal biopsies involve the removal of cells or a sample of tissue from the tract wall [68]. A conventional biopsy procedure uses an endoscope which is inserted into the mouth and fed into the small intestines through the stomach. If larger sections of tissue are required to be removed a thin flexible tube with a small cutting instrument attached to the end is used, this method also gives a greater reach than conventional endoscopes.

2.3.6.1 Small Intestinal Biopsy

The biopsy procedure is a necessary means of diagnosing pathologies early such as in the diagnosis of small intestinal Crohn's disease [69]. There are few risks involved in small bowel biopsy with patients who are cooperative, however there can be some complications such as perforations, haemorrhages or pain due to infection from bacteria. Also the procedure is uncomfortable for the patient and requires the throat to be anaesthetised. The fundamental problem with the biopsy procedure is that it is virtually impossible to reach the total length of the small intestines with conventional enteroscopy.

There are a number of researchers involved in realising methods of improving these procedures such as the intracorporeal videoprobe developed by Arena et al. (2005) [70]. This device seeks to reduce the optical lens system of the rigid endoscope by employing a camera directly at the tip, this reduction in size will allow for greater capacity for incorporating diagnosis equipment.

2.3.6.2 Tissue Interaction and Intervention

There are a number of patents relating to tissue interaction and intervention [49, 71]. Some of the more significant patents are discussed by Moglia et al. (2008) [72] and Toennies et al. (2010) [73] however these papers fail to cover the more important features of some of the patents such as the patent filed by Christopher Swain (2005) for his 'Method, system and device for in-vivo biopsy' [74].

Swain proposes a system which uses one or more devices for obtaining images and a sample from endo-luminal areas of the body, Figure 2.18.

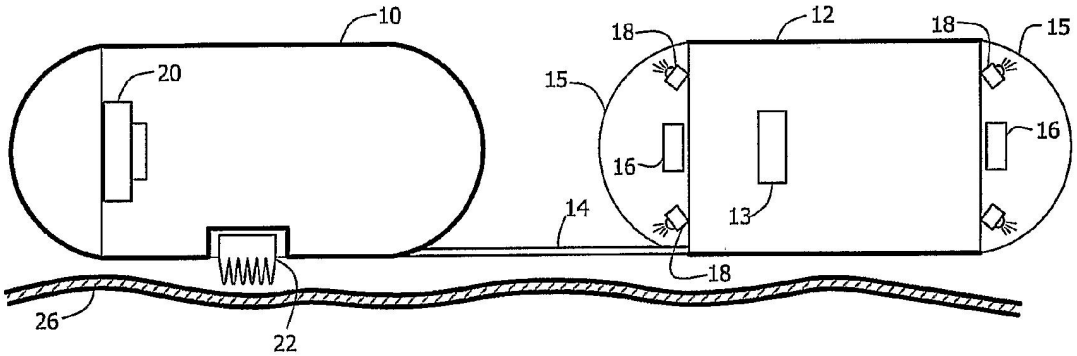


Figure 2.18: System and device for in-vivo biopsy [74]

The devices may be connected via a thread, tube, cable, wire or flexible narrow shaft. The connection may be from a few millimetres to a few centimetres in length and could be an electrical or purely a physical connection. It is proposed that the flexible connection between the two devices could make swallowing the system easier when compared to a single rigid device of the same mass. Although this would appear true it may prove more difficult to swallow the tethered devices as the gap between the devices would prevent the patient from swallowing the system in one go, this may trigger the patients gag reflex prohibiting them from swallowing any further devices.

The devices are configured such that one link or lobe would contain a camera and an illumination unit positioned behind a transparent dome. The other link would contain a power source and a biopsy or sampling mechanism with provision for storing the sample. The advantage of this arrangement is that an operator may visualise the procedure. The biopsy mechanism depicted in Figure 2.18 is not explained in the patent, however there are a number of other mechanisms described such as the articulated arm which may extend from the device to grasp and collect a tissue sample. Further tissue samples are collected by the release of a curved flat spring which is used to move the articulated arm when it grasps a sample. Another embodiment proposes an electrical motor which could drive a cog and screw to extend or retract the articulated arm. The forward movement of the arm could be used to close the jaws of the grasping mechanism. A further embodiment is proposed which overcomes the problem of positioning the biopsy mechanism by linking it to the second module with a rigid drive shaft. The second module has a motor which can rotate the first module via the rigid drive shaft. Balloons and fins are proposed to stabilise or hold the second module in position while samples are being taken.

Swain's proposed system relies on two opposing modules to provide the means of obtaining a sample of the GI tract, although it states that the proposed solutions could be combined to perform this function it does not suggest any alternative means of achieving a targeted sample collection.

Platt et al. (2009) [75] suggest that a large amount of force is required to grasp and tear a tissue sample away from an organ. The described methods of operating the articulated arm do not appear to be able to generate a mechanical advantage high enough to generate sufficient forces to remove a tissue sample.

2.3.6.3 Magnetically Driven Body-Tissue Sample Device

The capsule medical device for obtaining a body-tissue sample proposed by Tanaka Shinsuke (2009) [76] seeks to overcome the limitations of two modules by combining the required features into one device, Figure 2.19.

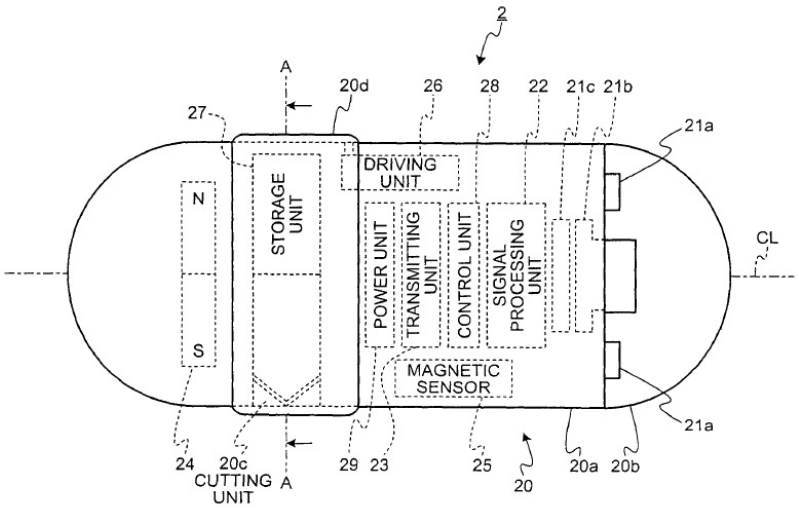


Figure 2.19: Magnetically driven body-tissue sample device [76]

A cutting unit with a 'V' shaped blade is protected by a movable cover. In order to take a tissue sample the capsule is manipulated into the intestinal wall by virtue of a generated external rotating magnetic field. The magnetic field acts on an internal magnet causing the capsule to move in the desired direction. Once the capsule is pressed firmly against the intestinal wall the magnetic sensor senses the external magnetic field and causes the driving unit to slide the outer cover back revealing the blade. It is proposed that the tissue will fall into a cavity between the blade and the capsule wall where it can be removed and stored in a storage unit. The tissue is removed by means of the external rotating magnetic field acting on the internal magnet and causing the capsule to rotate. The rotation will generate a circumferential torque which will act on the tissue resulting in a sample being taken.

The device has the capability of taking images of the intestinal wall and relaying them back to the operator for inspection and position recognition. It is proposed that the image system could be used to determine when and what samples are to be taken, however the method proposed for orientating the blade will make selecting the precise spot very difficult.

The cutting unit cover significantly extends outside of the capsule's body interrupting the smooth outer surface of the capsule, this could potentially make it very difficult to swallow.

2.3.6.4 Hollow Needle Tissue Sampling

Shinsuke (2009) [76] also proposes a modification to the first embodiment (previously described), which relates to a method for extracting and retaining the in-vivo tissue sample. Figure 2.20 shows two phases of the extraction, phase C1 shows the needle in the forward position and phase C2 shows the needle collecting a tissue sample.

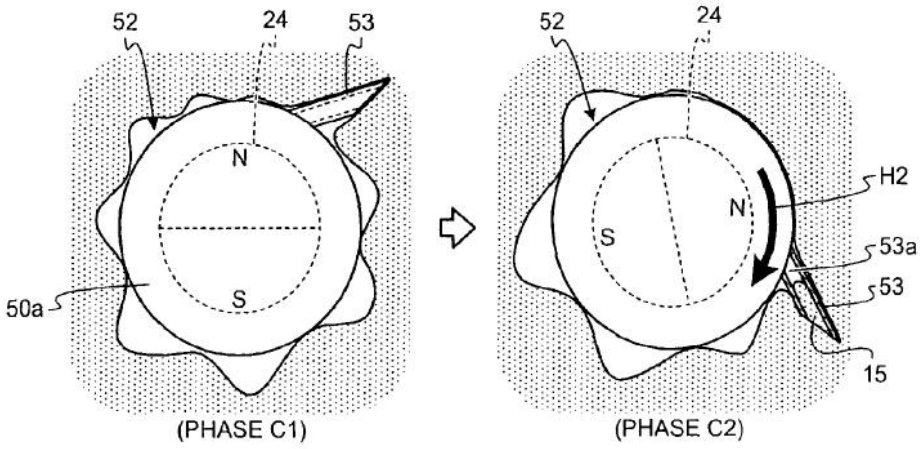


Figure 2.20: Hollow needle tissue sampling configuration [76]

A hollow needle with a pointed tip is extended through a hole in the capsule casing for the purpose of obtaining a tissue sample. The needle is controlled through an extending and withdrawing system that is activated by applying a current to an SMA coil. When heated through the application of a current the SMA coil shrinks exerting a driving force to the needle and extending it forwards. The extended needle is rotated due to the torque generated by the magnetic field, this rotation forces tissue into the hollow needle. A suction pump which is connected to the hollow needle through a flexible tube sucks up the tissue sample from the hollow needle and stores it in a storage unit. Removing the current from the SMA coil causes it to return to its original shape as it does this it retracts the hollow needle back inside the capsule.

The proposed method for extracting a tissue sample could potentially result in a perfo-

rated intestine. When the capsule is rotated to force the tissue into the hollow needle the tip of the extended needle could act like a knife, making a circumferential incision in the intestinal wall.

2.3.6.5 Micro-Biopsy Actuator

Park et al. (2008) [77] have developed an actuator for small intestinal biopsy which can be integrated into a conventional capsule endoscope, Figure 2.21.

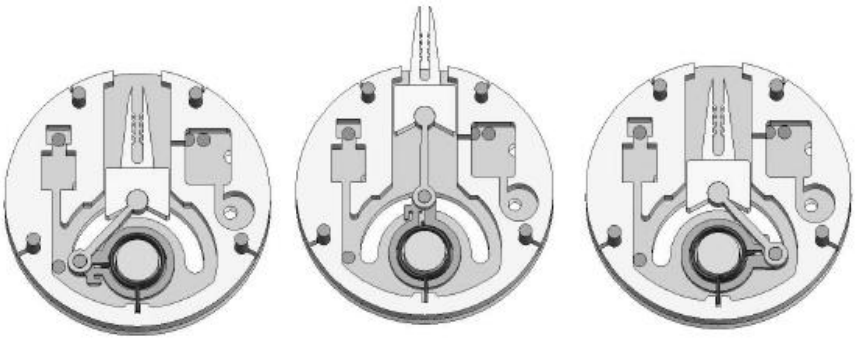


Figure 2.21: Tissue sampling mechanism with a microactuator for microbiopsy in capsular endoscopes [77]

The microactuator has been manufactured through a LiGA (Lithographie, Galvanoformung, Abformung) process. The process comprises three steps: applying an X-ray mask (1.0 mm thick PMMA), X-ray irradiation and electroplating. A full description of the fabrication steps are presented in [78]. The dimensions are 10.0 mm in diameter by 1.8 mm thick. The actuator comprises three main component parts: a microspike for taking the biopsy, a torsion spring actuator and an SMA heating wire triggering mechanism. The microspike is propelled forwards and backwards through the operation of a slider-crank mechanism. The slider crank comprises a connecting rod which is attached to a torsion spring at one end and the microspike at the other. A polymer string holds the torsion spring in position by anchoring it to a series of small fixing posts. This fixing method allows the polymer string to be routed across the PCB mounting board and across an SMA heating wire. When a current is applied to the SMA wire it heats up and melts the polymer string and hence releases the torsion spring which in turn propels the microspike forwards and then backwards to the stored position.

The intention is to incorporate the compact actuator into an existing capsule endoscope

such as the MiRo [8]. However Park states that for a complete operation to be performed further functionality such as the ability to hold position in the GI tract while taking a sample would be required from the WCE. To achieve this functionality it has been suggested that the autonomous moving functionality of the legged locomotion device developed by Stefanini et al. [79] and a frontal clamping system developed by Menciassi et al. [80] could be adapted. However combining these systems presents limitations due to the available space and also the effectiveness of the frontal clamping approach, as the frontal clamping approach may not necessarily clamp tissue in an orientation which guarantees contact with the GI tract wall and the microspike.

The biopsy spike, which is based on previous work carried out by Byun et al. (2005) [81], successfully removed a sample of tissue. However the microactuator can only be operated once with no control of the sampling direction and the tissue sample has limited protection while travelling through the remainder of the GI tract. Also the complexity of the polymer string configuration and the delicate positioning of the SMA wire would prove very difficult to reset by an unskilled operator.

The geometry specified for the slider crank allows a maximum stroke length of 4.3 mm. This stroke length may be required to guarantee a sufficient sample volume has been collected however there is a possibility of perforating the GI tract wall as the average wall thickness is between 2.0 mm and 3.0 mm thick [82].

2.3.6.6 Rotational Micro-Biopsy Device

Kong et al. (2005) [83] have developed a rotational micro-biopsy module which has been integrated into a WCE specifically to perform a biopsy of the small intestines. It is a compact design with a diameter of 10.0 mm and a thickness of 2.0 mm. The thickness is approximately 10% thicker than the design proposed by Park et al. (2008) [77], Figure 2.22.

The module utilises an eccentrically mounted razorblade configuration to remove a section of the GI wall. The release of a torsion spring causes the tissue-cutting razorblade to protrude from the side wall of the capsule. The blade rotates 120 degrees at a force of 10 N removing a sample of the wall as it rotates. The continued rotation of the blade causes the sample to be sealed into the WCE. The seal is achieved by the alignment of the blade edge with the capsule body.

The razorblade trigger mechanism is a paraffin block which restrains the blade against

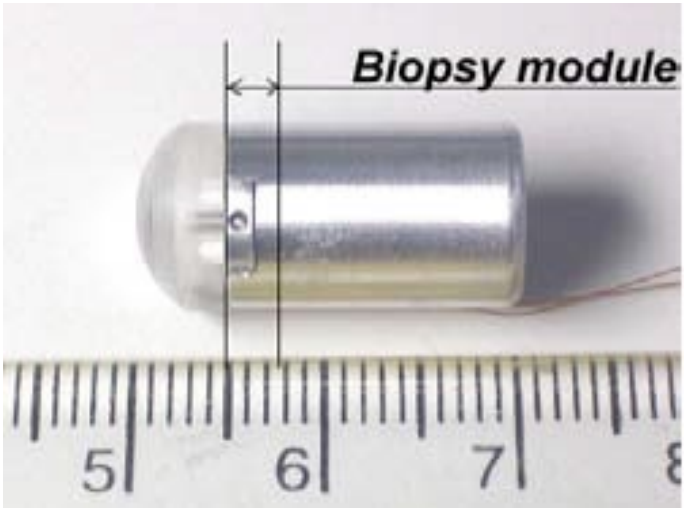


Figure 2.22: Prototype micro-biopsy module [83]

the torque from the torsion spring. The blade is released when the WCE receives a trigger signal causing the paraffin block to melt at 42 °C. The low melting temperature ensures the intestines remain undamaged. The power requirement to operate the trigger was measured at 300 mA for 1.7 seconds and it is intended that it will be supplied by an onboard battery.

There are a number of foreseeable problems with the biopsy module. The first and most important is that the blade needs to remove a sample of between 1.0 mm to 2.0 mm in depth [83] to guarantee a useful tissue sample has been retrieved. Unfortunately this cannot be guaranteed as the system relies on the WCE adhering to the intestinal wall and there are no means of achieving this with the WCE. A second problem is in obtaining a sample from a specific location. As the capsule is free to rotate as it passes through the GI tract the unpredictable orientation means relying on chance to target the required point.

2.3.6.7 Miniature Manipulator

A miniature manipulator mounted at the front of an endoscopic system is proposed by Peirs et al. (2000) [84], Figure 2.23.

This self-propelling system could be adapted to overcome the problem of retrieving a biopsy sample from the intestinal wall. The device uses two clamping modules which utilise a series of perforations to hold the intestinal wall through an applied vacuum. The modules are connected by an expansion/contraction bellow which allows the clamping modules to

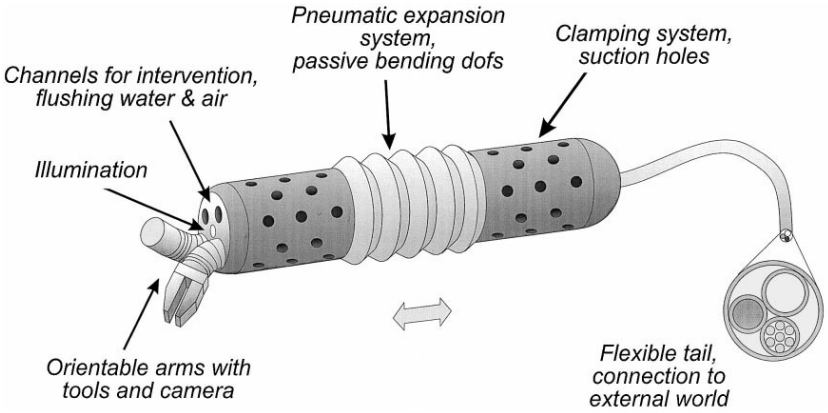


Figure 2.23: Self-propelling endoscope [84]

move independently.

A hydraulically controlled actuator was chosen over SMA and electric actuators to control a Stewart platform due to the high force which can be generated. The Stewart platform has 3 DOF which would be utilised to position the micro tools. The disadvantage with the hydraulic system is that it requires a hydraulic circuit to drive it as it cannot be driven electronically. It is proposed that the hydraulic power required to drive the actuators be supplied by an umbilical cord. The proposed configuration of the Stewart platform takes advantage of high stiffness and the possibility of having a tool channel running through the centre. The miniature hydraulic manipulator has an outer diameter of 12.0 mm and a length of 30.0 mm. The platform is driven by three hydraulic pistons connected to the platform by ball joints which give the platform the ability to move. It is proposed that two Stewart platforms could be combined to give 6 DOF however at the proposed dimensions it would result in an extremely large device.

The proposed device has two main issues which prevent it from retrieving a tissue sample from the small intestines. The first and most important issue is that the large volume of the device prevents it from being swallowed or if accessing the small intestines through the large intestines it would not be capable of navigating through the ileocolic valve. Secondly the power to drive the modules is supplied by a trailing wire this prevents the device from being totally autonomous and is also potentially disconcerting for the patient.

2.3.7 Evaluation of Micro Actuators

WCE are passive medical devices, however for these devices to be useful surgical tools they are required to perform tasks such as a biopsy or electro surgery. To achieve the given task a degree of mechanical movement is required of the tools. For example a needle must move forwards to pierce tissue or the jaw of a clamp must close to obtain a sample. The kinematics of the tools performing the curative treatment can be achieved through the application of actuators. There are a number of actuators available such as SMA actuators, piezoelectric actuators and micromotors. Choosing the correct actuator for a given task requires the consideration of a number of factors such as the available space, the type of movement and the peak power consumption. Many researchers have adopted SMA actuators as they have a high degree of allowable strain which takes advantage of the limited space for the deliverable force.

2.3.7.1 Piezoelectric Squiggle Motor

An actuator solution for controlling an injection system or biopsy system could be the use of a piezoelectric linear motor to drive a mechanism directly. These motors use the piezoelectric effect to drive the actuation. The piezoelectric effect is the change in a material's geometry due to an applied electric charge or a mechanical stress changing a solid's shape which will result in a proportional electrical charge [85]. There are problems with piezoelectric actuators such as they require displacement amplification mechanisms to obtain a useful stroke length and they also require large voltages (100 V) to activate them [84].

Non-conductive materials such as quartz (SiO_2) exhibit the piezoelectric effect and can be utilised in such applications as displacement transducers. The Squiggle piezoelectric linear motor manufactured by New Scale Technologies [86] utilises the piezoelectric effect to vibrate a leadscrew causing it to travel forwards and backwards, Figure 2.24.

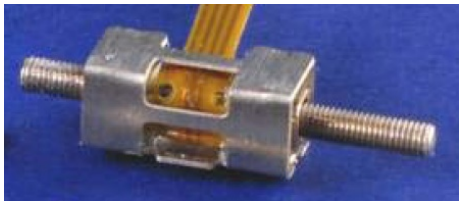


Figure 2.24: Piezoelectric squiggle motor manufactured by New Scale Technologies [86]

The Squiggle motor (SQL-RV-1.8-6-12) is one of the smallest piezoelectric motors in the world with a package size of 6.0 mm long by 2.8 mm square and a leadscrew of 12.0 mm long. The motor has a high positioning resolution of 0.5 μm and a stall force (4.5 V input) of 0.5 N which makes it a good candidate for operating mechanical mechanisms.

An alternative to the piezoelectric Squiggle motor is a micromotor. Micromotors could potentially be used to drive the mechanisms directly. An examination of the latest available technology in micromotors shows that there are a limited number of micromotors on the market which could fit within the package size of a conventional WCE and have a useful torque capability at a low RPM.

2.3.7.2 Micromotor power comparison

One micromotor which appears to have the required specifications is the Ø1.5 mm x 10.5 mm long geared micromotor manufactured by Namiki (no. 10-010) [87], Figure 2.25.

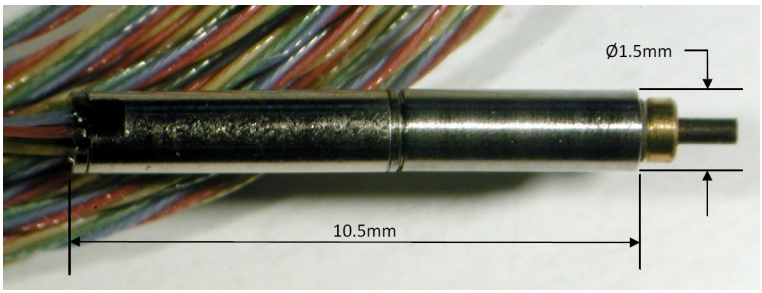


Figure 2.25: Namiki four stage geared micromotor

The four stage geared micromotor operates at 60 mW and runs at 76 RPM, this produces a stall torque of 1.6 mNm. The Namiki motor can be compared with the specifications of three alternative motors: a Ø6.0 mm x 3.75 mm long motor manufactured by Maxon Motor (EC 6) [88], a Ø1.9 mm x 10.82 mm long micromotor manufactured by Faulhaber (02/1)[89] and the Squiggle motor. An important criterion is the micromotor's maximum power output. A comparison of the four motors using a merit index to compare the power output against the motor's volume (Table 2.3) shows that the Squiggle motor is far superior to the other motors as the higher the merit index the more powerful the motor is for its size. However the Squiggle motor operates in a linear orientation compared to the rotational output of the micromotors.

The Namiki micromotor can be evaluated for its ability to perform the task of moving

Table 2.3: Power to volume merit index

	Maxon	**Namiki**	**Faulhaber**	**Squiggle**
Power mW	30	60	130	340
Volume cm^3	0.071	0.019	0.029	0.053
Merit Index*	0.422	3.157	4.482	6.415

*A higher merit index represents a more powerful motor for its volume

a 0.13 g mass of stainless steel. The stainless steel would replicate the mass of an injection system or biopsy system.

The torque required to move the mass of stainless steel can be calculated using the following equation:

$$T = I_o \alpha \tag{2.1}$$

Where α is the angular acceleration and can be calculated at 265.3 rads/s^2 from the motor's performance data [90, 91] and I_o is the moment of inertia which can be expressed as mk^2 where m is the mass concentrated at a radius, the Radius of Gyration (k), which would be 5.0 mm. This concentrated mass (0.13 g) would be a worst case scenario as it assumes the total volume to be moved is positioned at the extreme limit of the microrobot.

The results of the initial torque analysis show that a torque of 0.86 μNm would be required to operate the mechanism. Although the Namiki micromotor is capable of delivering a significantly higher torque than what is theoretically required provision would need to be made for the inherent friction in the mechanism and for any load which would be generated by the mechanism itself.

2.3.7.3 Shape memory alloy actuators

An alternative to micromotors as an actuator mechanism are SMA such as superelastic nitinol which is an alloy of approximately 50% nickel and 50% titanium. The superelastic properties of nitinol allow large amounts of deformation to take place without permanently damaging the lattice structure of the material. This allowable strain makes it possible to

create super springs which would be triggered by heating. The disadvantages of using SMAs are that they require high power consumption [92] and they can affect their environment as a result of heating. Also they are unable to fully recover their original configuration after cooling due to twinning of the atomic crystal [80]. This can be overcome by detwinning the lattice by using a secondary process which would apply a bias to the spring.

SMA wires can be employed to drive mechanisms. The wire could be orientated in a pulley configuration minimizing volume and attaining a mechanical advantage from the pulley. The approximate relationship between the pulley's radius (r) and the length (L) of wire required to rotate the pulley through an angle (θ) have been determined by Gorini, et al. (2006) [92] and is given by:

$$L = \frac{\pi r \theta}{0.04 \cdot 180} \tag{2.2}$$

The 0.04 represents a 4% contraction of the wire due to the Joules effect. By considering a pulley with a radius (r) of 0.9 mm and a required rotation (θ) of 90 degrees the theoretical length (L) of the wire would be 35.3 mm. The actuator mechanism would require a longer wire to operate efficiently as the theoretical model does not take into account the friction in the system and the drop in performance of the wire due to multiple operations. Also the wire would need to overcome the resistance imposed by a second wire which would be required to return the pulley to its original configuration. A consideration of the difficulty in manufacturing and assembling such small and complex components would need to be taken into account when designing such a mechanism.

2.3.7.4 SMA Wire Based Actuator for a Legged Endoscopic Capsule

Gorini et al. (2006) [92] propose the use of SMA wires to operate an actuator for a six legged endoscopic capsule, Figure 2.26.

The proposed miniaturised leg mechanism is to be integrated into a WCE for the purpose of locomotion in the GI tact. The mechanism comprises three main components: a PEEK prismatic support with dimensions of 3.4 mm x 25.0 mm x 3.2 mm, the leg and the SMA wire system. The operation of the leg is through the activation of two 100 μm diameter SMA wires connected to a brass micro pulley. The right hand wire is wrapped clockwise around the pulley and the left hand wire is wrapped anticlockwise around the pulley, with the ends of the wires fixed to the prismatic support.

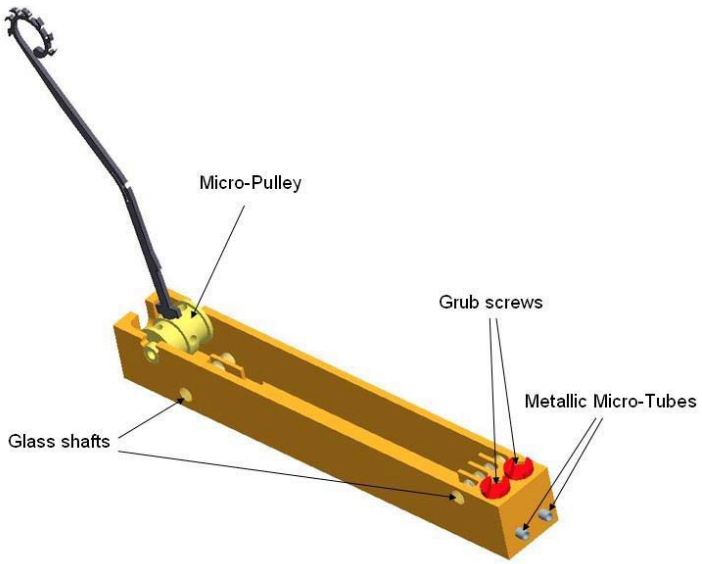


Figure 2.26: Prototype of the SMA leg actuator for a legged endoscopic capsule [92]

Applying a current of 360 mA and 10 V for a period of 4 s to the left hand wire causes the wire to contract by 6% and rotate the pulley approximately 135 degrees. After an unreported period of cooling time the right hand wire is activated bringing the leg back inside the prismatic support. The degree of leg rotation is dictated by the length of contraction of the 100.0 mm long SMA wire however the geometry of the prismatic support limits the length of wire which can be used. This issue has been overcome by the addition of glass shafts mounted in the prismatic support which allow the wire to be wrapped around them without shortcutting the circuit. The SMA wire is 40.0 mm longer than required to fully open the leg as compensation for the resistance from the antagonist SMA wire during the rotation of the pulley is required.

The wire pulley offers a mechanical advantage which would help to combat the large lever force being generated by the distance between the leg pivot and tip and also to help overcome the resistance from the antagonist wire. However the combined volume of six leg modules equates to 1.6 cm^3, comparing this volume to a conventional WCE shows that there would only be 0.4 cm^3 of usable space left for components such as a surgical tool, camera, battery or RF module.

A disadvantage of SMAs is that they have a high power consumption [93] which results in a localised elevated temperature at the site of the actuator. This may result in damage

to the surrounding area. Also the performance of the SMA will reduce over a number of cycles compounding the problem of the wires' ability to return to their original state.

2.3.7.5 SMA Spring Driven Locomotive Mechanism

A two-way linear actuator mechanism driven by SMA springs is proposed by Kim et al. (2005) [94] for the purpose of locomotion in capsule-type endoscopes, Figure 2.27.

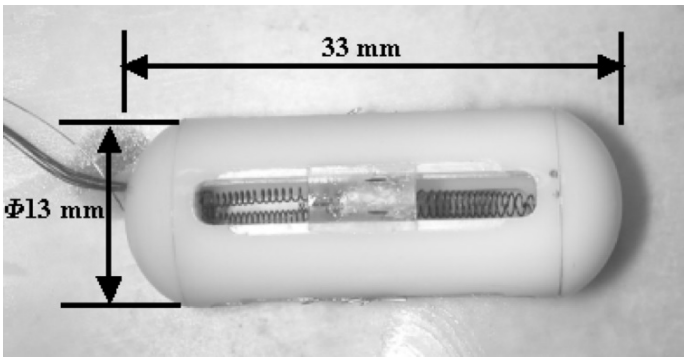


Figure 2.27: Locomotive mechanism driven by SMA springs for capsule-type endoscopes [94]

The 33.0 mm long by 13.0 mm diameter capsule is intended to navigate the GI tract by means of four sliding clamps which have been arranged around the outside surface of the capsule body. The core of the capsule has a 7.6 mm diameter hollow which is reserved for components such as an RF module, camera and batteries.

The four sliding clamps carry micro hooks which protrude from the capsule by 400-600 μm. The purpose of the clamps and hooks are to replicate the motion of insects such as the earth worm by mimicking its setae. The 180 μm diameter angled hooks are similar to those reported previously by Lee et al. (2004) [95]. The capsule moves forwards through a sequence of independent clamp movements which are driven by four two-way linear actuators. The two-way linear actuators comprise of two SMA springs which are connected to either side of the clamp and are activated independently through the Joules effect. When the forward spring is contracted for a period of 2 s it pulls the clamp forwards at which point the clamp grips the surface of the GI tract. The forward spring is allowed to cool for a period of 5 s before the rear spring is contracted. The contraction of the rear spring pulls the capsule forwards with a maximum stroke length of 7.5 mm. This sequence is repeated with each sliding clamp being activated in turn to propel the capsule through the GI tract

at a rate of 110 mm/min. The SMA springs reach a maximum operating temperature of 70 °C with an applied current of 400 mA and a voltage of less than 2 V.

The SMA springs are fabricated through a shape setting heat treatment process where the 150 μm diameter wire is wrapped around an M1 bolt which acts as a mandrel and heat treated for approximately 30 minutes at 400-500 °C. The result is a shape set spring with 18 turns, a diameter of 1.0 mm and a length of 4.5 mm. The total length of the spring is set to 19.5 mm which generates a maximum force of 135.9 g when contracted.

The contraction force generated by the SMA spring is sufficient to propel a commercial WCE which has a weight of approximately 10 g. However the reliability of the spikes to make adequate contact with the intestinal wall may result in clamping failures that will cause a decrease in locomotion speed or even a total failure to move. The large diameter of the capsule and overall length will make it difficult to swallow. This, combined with the fact that the spikes are always protruding from the side of the capsule, adds even greater difficulty to the swallowing process. The direction of the spikes may also cause complications if the capsule orientation is in reverse when it is travelling through the intestines and also when it is excreted.

2.3.7.6 SMA Sheet Oesophageal Stopping Mechanism

The procedure of inspecting the lining of the oesophagus using a flexible endoscope is routine however it is also a very uncomfortable procedure for the patient. Tognarelli et al. (2009) [96] propose SMA flat springs to halt the progress of an oesophageal WCE for the purpose of inspecting the oesophagus lining, Figure 2.28.

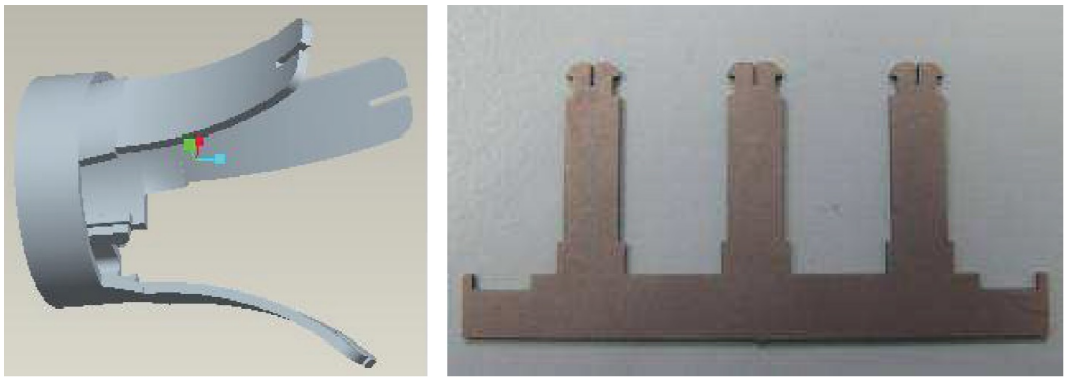


Figure 2.28: SMA flat springs to halt the progress of an oesophageal WCE [96]

The transit time through the oesophagus is rapid therefore a stopping mechanism must have a quick response time. The 11.0 mm in diameter by 31.0 mm long capsule developed by Tognarelli et al. [96] can deploy a stopping mechanism suddenly to halt its progress through the oesophagus. The stopping mechanism consists of three equally spaced SMA flaps, a DC brushless motor, a pulley, a gear set and three 0.15 mm diameter Kevlar wires. Rather than being triggered by the Joules effect the SMA legs have been set in an open position to take advantage of the superelastic properties of the material. The DC motor is connected to the gear set and pulley and is used to wind the legs into a cavity in the capsule body by virtue of the Kevlar wire which connects the tip of the legs to the pulley. When the wire is released the flaps return to their original open position and halt the progress of the capsule.

The thin Kevlar wires may prove difficult to assemble to the pulley mechanism and also prove potentially unreliable in operation due to the tendency of the wires to get tangled up. In addition the sudden release of the SMA flaps could cause trauma to the oesophageal wall lining as the shape of the legs focuses the spring load to the leg tip. The authors attempt to overcome this problem by suggesting a silicone coating could be applied to the legs however a more substantial dampening effect may be required.

2.3.7.7 Actuator characteristics comparison

The various actuator mechanisms described offer a diverse range of potential solutions to control mechanical movement. With each actuator system having a number of advantages and disadvantages. To gain a better overview and to help understand the various options an evaluation matrix has been created using a set of criteria relating to the actuators' characteristics (Table 2.4). The matrix will give a quantitative assessment of the performance of each method.

The evaluation matrix highlights the problems associated with completing a task such as controlling the position of a biopsy mechanism within the GI tract. For example the linear movement of the piezoelectric actuators and SMA actuators will make positioning a clamping jaw angularly very difficult whereas micromotors would have little difficulty with this task, however the position of the jaw would need to be determined therefore space for an encoder system would also be required.

Table 2.4: Actuator characteristics evaluation matrix

Characteristics	**Micromotor**	**Piezoelectric**	**SMA**
Voltage	<5 V	>100 V	>2 V
Displacement	unlimited	0.2%	>30%
Force	high	high	medium
Speed	<1 kHz	∼10 kHz	∼0.1 Hz
Compactness	poor	good	good
Motion type	rotation	linear	linear

2.3.8 Fabrication Methods for Prototype Realisation

In order to realise a WCE which has additional functionality, such as active locomotion or a mechanism for performing a biopsy, consideration must be given to the manufacture of the component parts which make up the mechanism, specifically the mechanical components as these require a number of process routes before they can be realised. The difficulty in producing parts for conceptual evaluation and for prototype testing is not just the financial limitations due to the cost of producing low numbers of components but also in selecting the right process which is capable of producing the small component features which are inevitably required when dealing with mechanisms which must fit in package sizes $<3.0\,\mathrm{cm}^3$.

There are a number of manufacturing processes available for the production of small components parts. However producing features as small as $50\,\mu$m can prove very challenging using conventional machining techniques such as computer numerical controlled (CNC) milling or CNC turning. There are alternative manufacturing processes, for example semiconductor device fabrication techniques have been adapted to fabricate microelectromechanical systems (MEMS). Scaling up this type of technology may offer advantages in producing complex mechanical systems however it is restricted to 2D structures and it is also limited to a small selection of materials such as silicon which have limited mechanical properties [97]. Therefore conventional manufacturing processes must be adapted to achieve the required outcome. The following section will discuss seven manufacturing routes suitable for fabricating small complex parts and which are also readily accessible.

2.3.8.1 Conventional Machining

Conventional machining practices refer to CNC turning and CNC milling, these manufacturing processes are the most common method for material removal. They use a single or multiple point cutting tool to remove material from a securely held workpiece to generate the desired shape.

Horizontal fixed head CNC lathes are used for producing cylindrical shapes, tapers, threads and flat faces on any type of round, square or hexagonal stock. They have between 2 to 6 axes which allows for greater flexibility when features such as milled pockets or holes off the centre line are required [98]. CNC milling machines are used for generating flat surfaces, profiles, holes and tapped holes however contours with external radii can be produced with suitable cutting tools.

The tools used for material removal must have a hardness greater than the material which is being cut. The efficiency of the cutting process relies on a number of factors such as: the hardness of the material being cut, the hardness and toughness of the cutting tool, the design of the cutting tool, the type of cutting fluid used, the metal removal rate, the surface finish required, the required tolerances and the speeds and feeds used.

The accuracy of the turning process will depend on the type of machine tool being used with typical achievable tolerances being $\pm 0.5\,\mathrm{mm}$ for rough turning and $\pm 0.1\,\mathrm{mm}$ for fine turning. However, given the correct conditions even finer tolerances of $\pm 0.01\,\mathrm{mm}$ can be achieved. The surface finish (arithmetic average = R_a) achievable for turning is between $\mathrm{R}_a = 0.05\,\mu\mathrm{m}$ to $25\,\mu\mathrm{m}$ with typical values between $\mathrm{R}_a = 0.05\,\mu\mathrm{m}$ to $5\,\mu\mathrm{m}$ being achieved.

Conventional CNC milling offers a great deal of flexibility for the production of complex features. Part geometry can typically be held to $\pm 0.1\,\mathrm{mm}$ with surface finishes of between $\mathrm{R}_a = 0.2\,\mu\mathrm{m}$ to $10\,\mu\mathrm{m}$ however machine tool technology is available that can give even greater control of the surface finish and geometry of a workpiece for example the KERN Pyramid Nano is a five-axis CNC machining centre it is capable of a positional accuracy of $\pm 0.3\,\mu\mathrm{m}$ and it can generate surface finishes as low as $\mathrm{R}_a = 0.05\,\mu\mathrm{m}$.

Although high degrees of accuracy and good surface finish can be achieved through either turning or milling both processes rely on the skill of the machine setter to produce and maintain them.

2.3.8.2 Injection Moulding

Injection moulding offers the ability to produce small complex polymer components. The process is most commonly used with thermoplastics however thermosets and elastomers may also be processed.

The injection moulding process involves polymer granules being fed from a hopper into a cylinder containing a motor-driven screw plasticizer. The granules are heated then forced along by a rotating screw until it reaches a plasticized state. The rotating screw acts as a ram to inject the material under high pressure, up to 200 MPa, through sprues into a mould tool. Once the part has solidified, through the cooling of the mould tool, it is then ejected from the tool [99].

The process can produce complex shapes with fine detail and surface finishes in the range of $R_a = 0.2\,\mu$m to $1.6\,\mu$m [100] however allowance for material shrinkage must be taken and large changes in section should be avoided. Features such as small re-entrant angles, screw threads and inserts can be produced however these increase the complexity of the tool increasing tooling costs. Tooling costs can be high however prototype mouldings can be made using single cavity moulds of cheaper materials such as aluminium.

2.3.8.3 Metal Injection Moulding

Metal injection moulding (MIM) offers the flexibility of plastic injection moulding to produce small highly complex shaped components from metal or ceramic powder which cannot be manufactured through conventional methods. The process involves mixing fine grained powders in the range of $0.5\,\mu$m to $20\,\mu$m with an organic binder agent such as a wax or a thermoplastic to create a feedstock. Conventional injection moulding machines can be used to inject the feedstock, under high pressure, into an oversized die to create a 'green' moulded part, which will shrink in the following process stages. The 'green' part undergoes a de-binderising process where it is heated in a low temperature oven to vaporize the binder agent leaving a porous 'brown' component. The final stage involves sintering the 'brown' component in a computer controlled vacuum or controlled atmosphere furnace. The powder particles are fused together at high temperatures shrinking and densifying the component.

Densities as high as 98% of the theoretical material density can be achieved with the MIM process and further post-sintering processes can be performed such as heat treatment, plating or machining if additional features are required. The process can be used to produce

parts as small as 1 mm with tolerance as low as ±0.025 mm and with surface finishes in the range of R_a = 0.4 μm to 1.6 μm however wall thicknesses are limited to between 0.2 mm to 10 mm and overall component size does not generally exceed 100 mm also component thickness/width ratio is limited to 3:1 [99].

2.3.8.4 Rapid Prototyping

Rapid Prototyping (RP) provides the opportunity to realise ideas in a quick and cost effective manner. There are three material addition RP based systems available commercially they are: liquid based, powder based and solid based [101]. The most common RP system is stereolithography addition (SLA) which is a liquid based system. The system uses a vat of photosensitive liquid resin which cures under the exposure to ultra violate light to produce solid three dimensional models.

The process starts with a closed 3D STL model generated in a CAD package. The SLA system then divides the model into thin cross-sectional layers from 0.025 mm to 0.5 mm thick [102]. The part is then built up as the focused laser beam prints the thin layer pattern onto the surface of the photosensitive liquid resin by virtue of mirrors. The laser beam diameter is in the range of 0.25±0.025 mm for the standard process and 0.075±0.015 mm for high resolution. Once the pattern hardens the platform can move down below the level of the liquid by one layer thickness which is typically between 0.05 mm to 0.1 mm thick. A sweeper then moves across the vat to cover any exposed surface with resin and then the process of printing the next layer begins. This method is repeated until the model is complete, the final operation is to cure the part to complete the polymerization.

RP systems can produce complex 3D models in a variety of materials. The finished models have the inherent properties of the materials from which they have been manufactured. This gives the advantage that the parts can be used directly in the finished product. For example Accura 60 is a resin which simulates the properties of polycarbonate it has a tensile strength of between 58 MPa to 68 MPa. Models can also be used to generate moulds which can then make further copies of the model in the desired material.

Part sizes are restricted to the maximum build envelope of the system for example the Viper si2 SLA system has a maximum build envelope in standard mode of 250 x 250 x 250 mm XYZ however this is reduced to 125 x 125 x 250 mm XYZ if high resolution parts are required. Dimensional accuracy of parts over the build envelope range between 0.125 mm to

0.25 mm XY however over smaller component sizes the accuracy can be as low as <0.05 mm XY [103]. The surface finish of a component is significantly influenced by the nature of the layered process and leads to a common problem of stair-stepping. Surface finishes of between $R_a = 5\,\mu$m to $40\,\mu$m [101] can be achieved however it is greatly dependent on the component's surface angle. Attention to the orientation of the part during modelling can minimise the stepping effect and reduce any post-finishing processes.

2.3.8.5 Electrical Discharge Machining

Electrical discharge machining (EDM) utilises the intense heat of an electric spark to remove any electrically conductive material. There are two basic methods of EDM, wire eroding and die sinking. The first method uses a wire in a similar action to a bandsaw to produce profiles in a workpiece, the second method uses a form tool which is sunk into the workpiece leaving an impression of the tool.

The form tool method offers a high degree of flexibility for prototyping complex parts as the tool is a mirror image of the required profile. A number of different shaped tools can be used successively to produce the required shape reducing the cost of producing a complex form tool. The form tool (cathode) is slowly fed into the workpiece leaving a slight gap between them, the gap is flooded with a dielectric fluid which assists the erosion process and the removal of metal particles. The metal or graphite form tool will also erode at a wear ratio of 3:1 for metallic electrodes and between 3:1 to 100:1 for graphite electrodes [99].

Controlling the spark gap between the work piece and the tool, which can vary between $20\,\mu$m to $120\,\mu$m, and also controlling the frequency and energy of the pulsed DC power supply enables the volume of material which can be removed and the surface finish of the work piece to be precisely managed. A typical tolerance of ± 0.025 mm can be achieved however ± 0.005 mm can be achieved under ideal conditions. Surface finishes are typically in the range of $R_a = 1.6\,\mu$m to $4.8\,\mu$m however the actual finish depends on production parameters as higher current densities will result in a rougher finish. Very high surface finishes can be achieved such as a mirror finish ($R_a = 0.05\,\mu$m) however these are time consuming to produce compared to roughing finishes which are fast to produce but can have a surface finish as high as $R_a = 15\,\mu$m [104].

Wire electrical discharge machining (WEDM) may offer greater degrees of flexibility for

prototyping as complex profiles can be produced directly through CNC control of the work-table eliminating the requirement to produce a form tool. The cutting speed is dependent on the material thickness the wire is passing through rather than the complexity of the form being produced. Wire electrodes can be manufactured from a number of materials, for example: tungsten, molybdenum or brass-covered steel. The choice of material will affect the degree of cutting accuracy achieved due to the tension obtained from the wire. Typical wire diameters range between 50 μm to 300 μm thick allowing fine features to be produced with surface finishes ranging between $R_a = 0.75\,\mu$m to 1.25 μm however there is an overcut of 20 μm to 50 μm and the spark produces a recast layer and a heat effected zone of between 2 μm to 120 μm deep which may require secondary finishing [99].

2.3.8.6 Comparison of Fabrication Methods for Component Realisation

The various manufacturing methods described for making low volume high precision component parts have been compared and their process parameters tabulated, Table 2.5.

Table 2.5: Comparison of manufacturing methods suitable for prototyping low volume high precision components

Manufacturing process	**Number of machine axes**	**General tolerance (mm)**	**Typical surface finish $R_a = \mu$m**	**Material**
CNC turning	3	±0.1	0.05 - 5	Various
CNC milling	3	±0.1	0.2 - 10	Various
Injection moulding	1	±0.2	0.2 - 1.6	Polymers
MIM	1	±0.025[1]	0.4 - 1.6	Metals & ceramics
RP - SLA	3	<0.05[2]	5 - 40	Polymers
EDM - Form tool	1	±0.025	1.6 - 4.8	Metals
EDM - Wire	2	±0.013	0.75 - 1.25	Sheet metals

[1] Based on dimensions ⩽5 mm
[2] Based on dimensions ⩽6.3 mm in the XY direction

Table 2.5 shows a comparison of manufacturing methods suitable for prototyping small scale component parts which require a high degree of accuracy and surface finish. The manufacturing processes described are readily available and offer the potential to make prototypes with small scale features however these processes are limited. For example generating parts through RP offers a quick and cheap solution to prototype realisation however the surface finish generated by the process may require further hand work to fully

achieve the required outcome, this can prove very difficult if the parts are too small to handle.

Producing prototypes which meet intended requirements will generally involve a compromise either between part accuracy, surface finish, size or cost. The selected manufacturing method will satisfy the majority of requirements however the designer will ultimately decide which parameters are the most important and therefore which can be compromised.

2.4 WCE Systems

Table 2.6 is a comparison of the non-disintegrating capsules discussed in the literature review. The positions marked with a '-' signify that the feature is unavailable or that details relating to the module's function have not been published in the literature. As can be seen from Table 2.6 the WCEs have many different modules however all possible modules are not contained in any one capsule. A good example of this is the Intellicap [53] which appears to have the greatest selection of modules although it doesn't possess the ability to maintain a static position or have active locomotion capabilities. It is a commercial capsule that uses time and pH sensing to track its movements through the GI tract and it is capable of bidirectional communication whereas the majority of the other capsules either have not got this function or they are only capable of unidirectional communication. The device is powered by a battery as opposed to magnetism or being tethered and is capable of delivering a liquid medication.

2.4.1 Volume Limitations

The standard volume for WCE is $2.0\,\mathrm{cm}^3$ this has been established by the M2A capsule developed by Given Imaging Ltd. [6] in 2000. This volume has been proven to be easily swallowed by the majority of patients who undergo the WCE procedure. The predominant feature of the M2A capsule is its ability to take images of the GI tract. Other capsules, such as the Intellicap, have looked to improve the functionality of this capsule by developing means of performing therapeutic and diagnostic activities.

The additional features incorporated into the Intellicap allow for a therapy to be delivered to a location in the GI tract with only a small increase in the volume of the capsule to $2.1\,\mathrm{cm}^3$ however this additional functionality is at the expense of the vision capability.

Table 2.6 presents the varying capsule volumes. It can be seen that the majority of the capsules have a volume greater than the standard volume and that a number of capsules such as the electrical stimulus capsule developed by Mosses [46], which has a volume of $5.7\,cm^3$, also exceed the limitations for swallowing, set at approximately $3.0\,cm^3$ [56]. The six legged endoscopic capsule developed by Gorini et al. (2006) [92] presents a volume that is lower than the standard volume however the volume only represent the geometry for the actuators as they do not report the total capsule volume.

2.4.2 Development Status

The development status of the capsules can be grouped into four main categories, commercial, concept, patent and prototype. The type of category a capsule is in has great significance as it highlights the development status of the technology. For example the Enterion, InteliSite and IntelliCap capsules are all commercial capsules capable of delivering medication to the GI tract. The technology involved in these capsules has been proven to work through clinical trials. These capsules can be compared to the capsule proposed by Langereis et al. [59] which also delivers medication to the GI tract, however the capsule is currently only in patent form and as such has not been realised.

The level of technology and the viability of a capsule is further exemplified by the capsule proposed by Shinsuke [76]. This capsule possesses a large number of modules, it is capable of obtaining a biopsy sample and taking images of the GI tract. However the capsule has not been realised as it is also in patent form therefore the viability of the technology and the practical issue of compressing the technology into a standard volume is in question as they do not report any clinical results or specify the total volume of the capsule.

2.5 Summary

There are clear benefits to the patient and the clinical practice from using WCE for the purpose of exploration and diagnosis of the GI tract. The capabilities of this technology, which include diagnosing pathologies of the small intestines like Crohn's disease and ulcerative colitis, enable a painless procedure for the patient and result in reduced costs for the clinical practice administering the procedure as a trained surgeon or a clinical setting is not required for the procedure to be performed. However there are significant limitations with WCE as the systems are unable to meet all the clinical needs, such as performing targeted

therapy to an affected area of the small intestines, taking multiple biopsy samples from specific locations or actively navigating to a site of interest. These limitations are principally due to the restrictions of the available space onboard the WCE which prevents all the features being incorporated into one device. However with advancements in technology and design the potential of WCE can be further expanded.

The challenge is to develop microscale actuator systems which can be incorporated into conventional WCE geometry and also be produced using convention manufacturing techniques. The following chapter will discuss the requirements for a WCE system to perform targeted therapy in the GI tract and outline the research objectives.

Table 2.6: Comparison of WCE systems as discussed in the literature review

WCE	Ref.	Status	Volume	Tracking	Telemetry	Sensing	Power	Motion	Vision	Therapy	Actuator
M2A	[6]	Commercial	2.0 cm^3	RF	U	-	B	N	CMOS	-	-
Endocapsule	[7]	Commercial	2.1 cm^3	RF	U	-	B	N	CCD	-	-
MiRo	[8]	Commercial	1.9 cm^3	EF	U	-	B	N	CMOS	-	-
Park (2007)	[38]	Prototype	3.7 cm^3	-	-	-	Te	A	-	-	Motor
Carpi	[39]	Prototype	3.2 cm^3	Fluoroscopy	U	-	B	N, M	Camera	-	-
Gilad	[41]	Patent	-	RF, Time	Bi	pH, T	B	N, Sp	Camera	-	Spring
Glass	[42]	Prototype	2.2 cm^3	-	Bi	-	B	N, Sp	Camera	-	SMA wire/Motor
Menciassi	[43]	Prototype	2.9 cm^3	-	-	pH	Te	N, Sp	Camera	-	SMA wire
Valdastri	[44]	Prototype	3.0 cm^3	-	Bi	-	Te/B	A	Camera	-	Motor
Woo (2010)	[45]	Prototype	3.0 cm^{3*}	-	-	-	Te	E	-	-	-
Mosse	[46]	Prototype	5.7 cm^3	-	-	-	Te	E	-	-	-
Woo (2009)	[47]	Prototype	1.7 cm^3	RF	U	-	B	E	-	-	-
Enterion	[51]	Commercial	2.9 cm^3	Radionuclide	-	-	M	N	-	L,P,S	Spring
InteliSite	[52]	Commercial	2.6 cm^3	Radionuclide	-	-	M	N	-	L	SMA wire
IntelliCap	[53]	Commercial	2.1 cm^3	Time, pH	Bi	pH, T	B	N	-	L	Microfluidic
Langereis	[59]	Patent	-	Time, pH	U	pH	B	N	-	L	Microfluidic
Lambert	[61]	Prototype	3.5 cm^3	Wheel	U	-	B	N	-	L	Spring
Karargyris	[62]	Prototype	3.7 cm^3	Wheel	Bi	pH	B	N	CMOS	-	Spring/Motor
Bourbakis	[63]	Concept	3.0 cm^3	Wheel	-	-	B	N	Camera	-	Spring
Song	[66]	Concept	-	M	-	-	-	N	-	-	-
Swain	[74]	Patent	-	-	Bi	-	Te/B	N	Camera	Biopsy	Motor
Shinsuke	[76]	Patent	-	RF	Bi	-	M	N	Camera	Biopsy	SMA wire
Park (2008)	[77]	Prototype	-	-	Bi	-	B	N	Camera	Biopsy	Spring
Kong	[83]	Prototype	1.6 cm^{3*}	-	U	-	B	N	-	Biopsy	Spring
Peirs	[84]	Prototype	3.2 cm^3	-	-	-	Te	N	-	Biopsy	Hydraulic
Gorini	[92]	Prototype	1.6 $cm^{3\circ}$	-	-	-	B	A	-	-	SMA wire
Kim	[94]	Prototype	3.8 cm^3	RF	-	-	B	A	Camera	-	SMA spring
Tognarelli	[96]	Prototype	2.9 cm^3	-	U	-	B	N, Sp	CMOS	-	SMA flat/Motor

- = data unavailable, A = active locomotion, B = battery, Bi = bidirectional communication, E = electrical stimulus, EF = electrical field propagation, L = liquid medication, M = magnetism, N = natural peristalsis, P = powder medication, S = solids medication, Sp = static position, T = temperature, Te = tethered, U = unidirectional communication

* Estimated from published data

° Volume represents actuators only

References

[1] M. C. Carrozza, P. Dario, and L. P. S. Jay, "Micromechatronics in surgery," *Transactions of the Institute of Measurement and Control*, vol. 25, pp. 309–337, 2003.

[2] J. M. Church, *Endoscopy of the colon, rectum, and anus.* Igaku-Shoin, 1995.

[3] S. Phee, W. Ng, I. Chen, F. Seow-Choen, and B. Davies, "Locomotion and steering aspects in automation of colonoscopy. I. A literature review," *Engineering in Medicine and Biology Magazine, IEEE*, vol. 16, pp. 85–96, 1997.

[4] D. C. Baumgart and W. J. Sandborn, "Crohn's disease," *The Lancet*, vol. 380, no. 9853, pp. 1590–1605, 2012.

[5] G. Iddan, G. Meron, A. Glukhovsky, and P. Swain, "Wireless capsule endoscopy," *Nature*, vol. 405, p. 417, 2000.

[6] G. D. Meron, "The development of the swallowable video capsule (M2A)," *Gastrointestinal Endoscopy*, vol. 52, pp. 817–819, 2000.

[7] D. R. Cave, D. E. Fleischer, J. A. Leighton, D. O. Faigel, R. I. Heigh, V. K. Sharma, C. J. Gostout, E. Rajan, K. Mergener, A. Foley, M. Lee, and K. Bhattacharya, "A multicenter randomized comparison of the endocapsule and the pillcam SB," *Gastrointestinal Endoscopy*, vol. 68, no. 3, pp. 487–494, 2008.

[8] S. Bang, J. Y. Park, S. Jeong, Y. H. Kim, H. B. Shim, T. S. Kim, D. H. Lee, and S. Y. Song, "First clinical trial of the MiRo capsule endoscope by using a novel transmission technology: electric-field propagation," *Gastrointestinal Endoscopy*, vol. 69, no. 2, pp. 253–259, 2009.

[9] B. MacFadyen and A. Cuschieri, "Endoluminal surgery," *Surgical Endoscopy And Other Interventional Techniques*, vol. 19, no. 1, pp. 1–3, 2005.

[10] J. A. Leighton, J. Goldstein, W. Hirota, B. C. Jacobson, J. F. Johanson, J. Mallery, K. Peterson, J. Waring, R. D. Fanelli, J. Wheeler-Harbaugh, T. H. Baron, and D. O. Faigel, "Obscure gastrointestinal bleeding," *Gastrointestinal Endoscopy*, vol. 58, no. 5, pp. 650–655, 2003.

[11] A. Koulaouzidis, E. Rondonotti, and A. Karargyris, "Small-bowel capsule endoscopy: A ten-point contemporary review," *World Journal of Gastroenterol*, vol. 19, pp. 3726–3746, 2013.

[12] J. F. Ludvigsson, D. A. Leffler, J. C. Bai, F. Biagi, A. Fasano, P. H. R. Green, M. Hadjivassiliou, K. Kaukinen, C. P. Kelly, J. N. Leonard, K. E. A. Lundin, J. A. Murray, D. S. Sanders, M. M. Walker, F. Zingone, and C. Ciacci, "The Oslo definitions for coeliac disease and related terms," *Gut*, vol. 62, no. 1, pp. 43–52, 2013.

[13] G. Holleran, B. Hall, M. Hussey, and D. McNamara, "Small bowel angiodysplasia and novel disease associations: a cohort study," *Scandinavian Journal of Gastroenterology*, vol. 48, no. 4, pp. 433–438, 2013.

[14] Office for National Statistics, "Cancer registration statistics, England, 2011," 2013.

[15] Cancer Research UK, "Bowel cancer, 2013."

[16] J. R. Padhi, "10 of the best - Part two," *Medical Device Developments*, vol. 4, pp. 16–18, 2010.

[17] www.givenimaging.com [Accessed 10 October 2013].

[18] D. S. Mishkin, R. Chuttani, J. Croffie, J. DiSario, J. Liu, R. Shah, L. Somogyi, W. Tierney, L. M. Wong Kee Song, and B. T. Petersen, "Asge technology status evaluation report: wireless capsule endoscopy," *Gastrointestinal endoscopy*, vol. 63, no. 4, pp. 539–545, 2006.

[19] U. C. Ghoshal, "Capsule endoscopy: A new era of gastrointestinal endoscopy," *Endoscopy of GI Tract*, pp. 75–88, 2013.

[20] W. Xiaona, M. Q. H. Meng, and C. Yawen, "Physiological factors of the small intestine in design of active capsule endoscopy," *Engineering in Medicine and Biology Society, 2005. IEEE-EMBS 2005. 27th Annual International Conference of the*, pp. 2942–2945, 2005.

[21] A. Allen, D. A. Hutton, A. J. Leonard, J. P. Pearson, and L. A. Sellers, "The role of mucus in the protection of the gastroduodenal mucosa," *Scandinavian Journal of Gastroenterology*, vol. 21, pp. 71–78, 1986.

[22] X. Wang and M. Q. H. Meng, "Study of frictional properties of the small intestine for design of active capsule endoscope," in *Biomedical Robotics and Biomechatronics, 2006. BioRob 2006. The First IEEE/RAS-EMBS International Conference on*, pp. 124–129, 2006.

[23] E. Oberg, F. D. Jones, H. L. Horton, and H. H. Ryffel, *Machinerys hand book*. New York: Industrial Press Inc., 23rd ed., 1990, pp. 2201-2203.

[24] H. Gray, *Grays anatomy*. London: Greenwich Editions, 2005, pp. 606-607.

[25] R. Miftahof, "The wave phenomena in smooth muscle syncytia," *Silico Biology*, vol. 5, pp. 479–498, 2005.

[26] B. R. Southwell, M. C. C. Clarke, J. Sutcliffe, and J. M. Hutson, "Colonic transit studies: normal values for adults and children with comparison of radiological and scintigraphic methods," *Pediatric surgery international*, vol. 25, pp. 559–572, 2009.

[27] S. K. Kim, "Small intestine transit time in the normal small bowel study," *American Journal of Roentgenology*, vol. 104, pp. 522–524, 1968.

[28] A. Menciassi, M. Quirini, and P. Dario, "Microrobotics for future gastrointestinal endoscop," *Minimally Invasive Therapy and Allied Technologies*, vol. 16, pp. 91–100, 2007.

[29] K. Ikuta, M. Tsukamoto, and S. Hirose, "Shape memory alloy servo actuator system with electric resistance feedback and application for active endoscope," *Robotics and Automation, 1988. Proceedings., 1988 IEEE International Conference on*, vol. 1, pp. 427–430, 1988.

[30] T. Fukuda, H. Hosokai, and M. Uemura, "Rubber gas actuator driven by hydrogen storage alloy for in-pipe inspection mobile robot with flexible structure," *Robotics and Automation, 1989. Proceedings., 1989 IEEE International Conference on*, vol. 3, pp. 1847–1852, 1989.

[31] W. S. Grundfest, J. W. Burdick IV, and A. B. Slatkin, "Robotic endoscopy," 1994.

[32] A. B. Slatkin, J. Burdick, and W. Grundfest, "The development of a robotic endoscope," *Intelligent Robots and Systems 95. 'Human Robot Interaction and Cooperative Robots', Proceedings. 1995 IEEE/RSJ International Conference on*, vol. 2, pp. 162–171, 1995.

[33] A. Moglia, A. Menciassi, M. Schurr, and P. Dario, "Wireless capsule endoscopy: from diagnostic devices to multipurpose robotic systems," *Biomedical Microdevices*, vol. 9, no. 2, pp. 235–243, 2007.

[34] S. Tsevas, D. K. Iakovidis, D. Maroulis, and E. Pavlakis, "Automatic frame reduction of wireless capsule endoscopy video," in *BioInformatics and BioEngineering, 2008. BIBE 2008. 8th IEEE International Conference on*, pp. 1–6, 2008.

[35] Z. Wang, E. Lim, T. Tillo, and F. Yu, "Review of the wireless capsule transmitting and receiving antennas," *Wireless Communications and Networks - Recent Advances*, pp. 27–46, 2012.

[36] M. Thomi and R. Studer, "Watch mechanism incorporating two barrels," 1982. US Patent 4,363,553.

[37] J. A. Transue, "Retractable needle basting mechanism," 1978. US Patent 4,123,983.

[38] H. Park, S. Park, E. Yoon, B. Kim, J. Park, and S. Park, "Paddling based microrobot for capsule endoscopes," in *Robotics and Automation, 2007 IEEE International Conference on*, pp. 3377–3382, 2007.

[39] F. Carpi, S. Galbiati, and A. Carpi, "Controlled navigation of endoscopic capsules: concept and preliminary experimental investigations," *IEEE Transactions on Biomedical Engineering*, vol. 54, pp. 2028–2036, 2007.

[40] S. H. Woo, T. W. Kim, Z. Mohy-Ud-Din, I. Y. Park, and J. Cho, "Small intestinal model for electrically propelled capsule endoscopy," *BioMedical Engineering OnLine*, vol. 10, no. 1, p. 108, 2011.

[41] Z. Gilad and G. J. Iddan, "Immobilizable in vivo sensing device," Given Imaging Ltd, 2004.

[42] P. Glass, E. Cheung, and M. Sitti, "A legged anchoring mechanism for capsule endoscopes using micropatterned adhesives," *IEEE Transactions on Biomedical Engineering*, vol. 55, pp. 2759–2767, 2008.

[43] A. Menciassi, S. Gorini, A. Moglia, G. Pernorio, C. Stefanini, and P. Dario, "Clamping tools of a capsule for monitoring the gastrointestinal tract - problem analysis and preliminary technological activity," *IEEE International Conference on Robotics and Automation (ICRA)*, vol. 1-4, pp. 1309–1314, 2005.

[44] P. Valdastri, R. J. Webster, C. Quaglia, M. Quirini, A. Menciassi, and P. Dario, "A new mechanism for mesoscale legged locomotion in compliant tubular environments," *IEEE Transactions on Robotics*, vol. 25, pp. 1047–1057, 2009.

[45] S. Woo, T. Kim, and J. Cho, "Stopping mechanism for capsule endoscope using electrical stimulus," *Medical & Biological Engineering & Computing*, vol. 48, no. 1, pp. 97–102, 2010.

[46] A. Mosse, T. Mills, M. Appleyard, S. Kadirkamanathan and P. Swain, "Electrical stimulation for propelling endoscopes," *Gastrointestinal Endoscopy*, vol. 54, pp. 79–83, 2001.

[47] S. H. Woo, T. W. Kim, J. H. Lee, P. U. Kim, C. H. Won, and J. H. Cho, "Implemented edge shape of an electrical stimulus capsule," *The International Journal of Medical Robotics and Computer Assisted Surgery*, vol. 5, no. 1, pp. 59–65, 2009.

[48] R. A. Scott and E. T. Cole, "Enteric and colonic delivery using HPMC capsules," Warner-Lambert Company, 2001.

[49] S. Jin, "Magnetic navigation system for diagnosis, biopsy and delivery vehicles," Glen E. Books, 2004.

[50] K. Mohseni, "Guided capsule for wireless endoscopy, biopsy and drug deliver," Regents of the university of Colorado, 2004.

[51] P. J. Houzego, P. N. Morgan, P. H. Hirst, D. J. Westland, and I. R. Wilding, "Ingestible device for the release of substances at distinct locations in the alimentary canal," USA: Phaeton Research Limited, 2005.

[52] M. E. McGirr, S. M. McAllister, E. E. Peters, A. W. Vickers, A. F. Parr, and A. W. Basit, "The use of the intelisite companion device to deliver mucoadhesive polymers to the dog colon," *European Journal of Pharmaceutical Sciences*, vol. 36, no. 4-5, pp. 386–391, 2009.

[53] www.research.philips.com [Accessed 5 May 2010].

[54] Q. Clinical, "Innovations in early development," 2003.

[55] E. Rondonotti, J. M. Herrerias, M. Pennazio, A. Caunedo, M. Mascarenhas-Saraiva, and R. de Franchis, "Complications, limitations, and failures of capsule endoscopy: a review of 733 cases," *Gastrointestinal Endoscopy*, vol. 62, pp. 712–716, 2005.

[56] A. Connor, P. Evans, J. Doto, C. Ellis, and D. E. Martin, "An oral human drug absorption study to assess the impact of site of delivery on the bioavailability of bevirimat," *The Journal of Clinical Pharmacology*, vol. 49, pp. 606–612, 2009.

[57] J. F. Dijksman, F. T. D. Jongh, M. G. Pardoel, C. J. Malaurie, Y. O. J. G. Droinet, A. Pierik, J. M. Rensen, J. Shimizu, H. Zou, and R. Albu, "Ingestible electronic capsule and in vivo drug delivery or diagnostic system," Koninklijke Philips Electronics N.V., 2010.

[58] K. Trovato and G. Spekowlus, "Electronically and remotely controlled pill and system for delivering at least one medicament," Koninklijke Philips Electronics N.V., 2006.

[59] G. R. Langereis and G. Likourezos, "Electronically controlled pill," Koninklijke Philips Electronics N.V., 2006.

[60] S. R. Snell, *Clinical anatomy for medical students.* Boston: Little, Brown and Company, 2nd ed., 1981, pp. 187-191.

[61] A. Lambert, F. Vaxman, F. Crenner, T. Wittmann, and J. F. Grenier, "Autonomous telemetric capsule to explore the small bowel," *Medical and Biological Engineering and Computing*, vol. 29, pp. 191–196, 1991.

[62] A. Karargyris and A. Koulaouzidis, "Odocapsule: next-generation wireless capsule endoscopy with accurate lesion localization and video stabilization capabilities," *Biomedical Engineering, IEEE Transactions on*, vol. 62, no. 1, pp. 352–360, 2015.

[63] N. Bourbakis, G. Giakos, and A. Karargyris, "Design of new-generation robotic capsules for therapeutic and diagnostic endoscopy," in *Imaging Systems and Techniques (IST), 2010 IEEE International Conference on*, pp. 1–6, 2010.

[64] A. Karargyris and A. Koulaouzidis, "Capsule-odometer: A concept to improve accurate lesion localisation," *World Journal of Gastroenterology*, vol. 19, no. 35, pp. 5943–5946, 2013.

[65] www.quotientbioresearch.com [Accessed 10 January 2014].

[66] S. Song, C. Hu, M. Li, W. Yang, and M.-H. Meng, "Two-magnet-based 6D-localization and orientation for wireless capsule endoscope," in *Robotics and Biomimetics (ROBIO), 2009 IEEE International Conference on*, pp. 2338–2343, 2009.

[67] T. Ang, K. Fock, T. Ng, E. Teo, and Y. Tan, "Clinical utility, safety and tolerability of capsule endoscopy in urban southeast asian population," *World Journal of Gastroenterology*, vol. 9, pp. 2313–2316, 2003.

[68] M. S. Dunnill and R. Whitehead, "A method for the quantitation of small intestinal biopsy specimens," *Journal of Clinical Pathology*, vol. 25, pp. 243–246, 1972.

[69] Z. Z. Ge, Y. B. Hu, and S. D. Xiao, "Capsule endoscopy in diagnosis of small bowel crohn's disease," *World Journal of Gastroenterology*, vol. 10, pp. 1349–1352, 2004.

[70] A. Arena, M. Boulougoura, H. S. Chowdrey, P. Dario, C. Harendt, K. M. Irion, V. Kodogiannis, B. Lenaerts, A. Menciassi, R. Puers, C. Scherjon, and D. Turgis, "Intracorporeal videoprobe (IVP)," *Studies in Health Technology and Informatics*, vol. 114, pp. 167–174, 2005.

[71] K. Mohseni, "Guided capsule for wireless endoscopy, biopsy and drug deliver," Regents of the university of Colorado, 2004.

[72] A. Moglia, A. Menciassi, and P. Dario, "Recent patents on wireless capsule endoscopy," *Recent Patents on Biomedical Engineering*, vol. 1, pp. 24–33, 2008.

[73] J. L. Toennies, G. Tortora, M. Simi, P. Valdastri, and R. J. Webster III, "Swallowable medical devices for diagnosis and surgery: the state of the art," *Journal of Mechanical Engineering Science*, vol. 224, pp. 1397–1414, 2010.

[74] C. Swain, "Method, system and device for in-vivo biopsy," Given Imaging Ltd, 2005.

[75] S. R. Platt, J. A. Hawks, and M. E. Rentschler, "Vision and task assistance using modular wireless in vivo surgical robots," *Biomedical Engineering, IEEE Transactions on*, vol. 56, pp. 1700–1710, 2009.

[76] T. Shinsuke, "Capsule medical device for obtaining a body-tissue sample," Olympus Medical Systems Corporation, 2009.

[77] S. Park, K. Koo, S. Min Bang, J. Y. Park, S. Song, and D. Dan Cho, "A novel microactuator for microbiopsy in capsular endoscopes," *Journal of Micromechanics and Microengineering*, vol. 18, pp. 209–218, 2008.

[78] S. Park, K. Koo, G. Kim, S. M. Bang, S. Y. Song, J. Byun, C. Chu, and D. Cho, "A novel micro-biopsy actuator for capsular endoscope using LiGA process," in *Solid-State Sensors, Actuators and Microsystems Conference, 2007. Transducers 2007. International*, pp. 209–212, 2007.

[79] C. Stefanini, A. Menciassi, and P. Dario, "Modeling and experiments on a legged microrobot locomoting in a tubular, compliant and slippery environment," *The International Journal of Robotics Research*, vol. 25, no. 5-6, pp. 551–560, 2006.

[80] A. Menciassi, A. Moglia, S. Gorini, G. Pernorio, C. Stefanini, and P. Dario, "Shape memory alloy clamping devices of a capsule for monitoring tasks in the gastrointestinal tract," *Journal of Micromechanics and Microengineering*, vol. 15, pp. 2045–2055, 2005.

[81] S. Byun, J. Lim, S. Paik, A. Lee, K. Koo, S. Park, J. Park, B. Choi, J. Seo, K. Kim, H. Chung, S. Song, D. Jeon, and D. Cho, "Barbed micro-spikes for micro-scale biopsy," *Journal of Micromechanics and Microengineering*, vol. 15, pp. 1279–1284, 2005.

[82] L. Phee, D. Accoto, A. Menciassi, C. Stefanini, M. Chiara, Carrozza, and P. Dario, "Analysis and development of locomotion devices for the gastrointestinal tract," *IEEE Transactions on Biomedical Engineering*, vol. 49, pp. 613–616, 2002.

[83] K. Kong, J. Cha, D. Jeon, and D. Dan Cho, "A rotational micro biopsy device for the capsule endoscope," *Intelligent Robots and Systems, 2005. (IROS 2005). 2005 IEEE/RSJ International Conference on*, pp. 1839–1843, 2005.

[84] J. Peirs, D. Reynaerts, and H. Van Brussel, "Design of miniature parallel manipulators for integration in a self-propelling endoscope," *Sensors and Actuators A: Physical*, vol. 85, pp. 409–417, 2000.

[85] E. Doebelin, *Measurement systems: Application and design.* London: McGraw Hill, 4th ed., 1990, pp. 261-262.

[86] www.newscaletech.com [Accessed 27 May 2010].

[87] www.namiki.net [Accessed 19 May 2010].

[88] www.maxonmotor.co.uk [Accessed 21 March 2010].

[89] www.faulhaber.com [Accessed 21 March 2010].

[90] Namiki, "Micro geared motor technical specification data sheet," Namiki Precision of Europe SA, 2011.

[91] T. Aoyagi, "Namiki SBL015PG1609 rise time measurement," Namiki Precision of Europe SA, 2011.

[92] S. Gorini, M. Quirini, A. Menciassi, G. Pernorio, C. Stefanini, and P. Dario, "A novel SMA-based actuator for a legged endoscopic capsule," *Biomedical Robotics and Biomechatronics, 2006. BioRob 2006. The First IEEE/RAS-EMBS International Conference on*, pp. 443–449, 2006.

[93] J. M. Hollerbach, I. W. Hunter, and J. Ballantyne, "A comparative analysis of actuator technologies for robotics," *Robotics Review 2, MIT Press*, pp. 299–342, 1991.

[94] B. Kim, S. Lee, J. H. Park, and J. Park, "Design and fabrication of a locomotive mechanism for capsule-type endoscopes using shape memory alloys (SMAs)," *Mechatronics, IEEE/ASME Transactions on*, vol. 10, pp. 77–86, feb. 2005.

[95] Y. P. Lee, B. Kim, M. G. Lee, and J. Park, "Locomotive mechanism design and fabrication of biomimetic micro robot using shape memory alloy," in *Robotics and Automation, 2004. Proceedings. ICRA '04. 2004 IEEE International Conference on*, vol. 5, pp. 5007–5012, 2004.

[96] S. Tognarelli, C. Quaglia, P. Valdastri, E. Susilo, A. Menciassi, and P. Dario, "Innovative stopping mechanism for esophageal wireless capsular endoscopy," *in Procedings of the Eurosensors XXIII Conferance*, pp. 485–488, 2009.

[97] C. Quaglia, E. Buselli, R. J. Webster III, P. Valdastri, A. Menciassi, and P. Dario, "An endoscopic capsule robot: a meso-scale engineering case study," *Journal of Micromechanics and Microengineering*, vol. 19, pp. 1–11, 2009.

[98] P. Smid, *A comprehensive Guide to Practical CNC Programming. CNC Programming Handbook*. Editorial Industrial Press, Inc. Segunda edición. Nueva York, EUA, 2003.

[99] F. Walters, *Fundamentals of Manufacturing for Engineers*. UCL Press Limited, London, 1996.

[100] "CES selector 4.1: Various technical data sheets," Granta Design Ltd, 2006.

[101] R. I. Campbell, M. Martorelli, and H. S. Lee, "Surface roughness visualisation for rapid prototyping models," *Computer-Aided Design*, vol. 34, no. 10, pp. 717–725, 2002.

[102] C. K. Chua, K. F. Leong, and C. S. Lim, *Rapid Prototyping: Principles and Applications*. World Scientific Publishing Co., 2003.

[103] B. Wang, *Integrated Product, Process and Enterprise Design (Manufacturing Systems Engineering Series)*, vol. 2. Springer, US, 1997.

[104] J. A. Schey, *Introduction to manufacturing processes*. McGraw-Hill Book Co, Singapore, 2nd ed., 1987.

Chapter 3

Towards a WCE for Targeted Drug Delivery

3.1 Overview

This chapter will evaluate the medical and technical challenges in performing both diagnosis and therapeutic procedures simultaneously with a remotely operated microrobot within the GI tract.

The aim will be to develop a swallowable microrobotic platform which has novel functionality such as a targeted drug delivery system combined with constant pH monitoring. The particular challenge with designing a microrobotic system which can perform a surgical procedure such as targeted drug delivery is in the allowable working envelope for the microrobot. As the microrobot is to be swallowed it requires a small package size of approximately 12.0 mm diameter by 25.0 mm long. The small package size of the microrobot places great constraints on the component parts such as the electronics and actuator mechanisms. A particular problem is in generating sufficient strength and operating forces from the miniaturised components.

The research project will investigate novel methods of stopping and holding the microrobot against natural peristalsis in the small intestines. The development of a novel system which can deliver a metered dose of medication to a specifically targeted site will also be investigated. These systems will involve the design and analysis of innovative micromechanical mechanisms. The mechanisms will be responsible for deploying the stopping arms and controlling the position and deployment of the medication in a $\sim$20.0 mm diameter

section of lumen. Potential technologies to investigate which could drive these mechanisms are piezoelectric actuators, DC electric micromotors and SMA.

3.1.1 Key Research Aims and Objectives

This research project aims to develop a next generation microrobotic platform for targeted drug delivery in the GI tract. Given the constraints of capsule endoscopy and the design objectives identified above it is clear that it will be a very challenging task to achieve this aim. There are a number of specific research objectives that will need to be addressed, they are:

- To investigate and analyse a new method of attaining equilibrium in the GI tract. This will involve developing a novel microscale mechanism capable of resisting peristalsis and gravity to hold the microrobot in a static state for a specified period. There are a number of factors which will influence the mechanism such as the limited available space and the availability of microactuators with sufficient torque to perform the given task. Also there are safety issues to overcome such as the possibility of the mechanism damaging tissue or even perforating the GI tract wall.
- To research and develop a new method for targeting a specific location in the GI tract. This will involve developing a number of solutions which combined will allow the microrobot the ability to return to a site of interest (SOI) and position a needle within a specified arc to target a pathogen. The specific challenge will be to develop a mechanism which is capable of positioning a needle within a 360 degree envelope and hit a SOI with controlled accuracy.
- To explore and evaluate a new method of delivering a metered dose of medication to a specific location in the GI tract. Once the microrobot has reached the SOI the challenge will be to dispense the onboard medication through a needle into the GI tract wall. To achieve this objective a compact remotely operated triggering solution will be required to release a stored energy device. The specific challenge will be to develop a mechanism which will operate with minimal power consumption yet occupy minimal space.

The outcome of the three objectives will be combined and integrated into a WCE to give additional functionality that will allow a metered dose of medication to be delivered to

a specific location in the GI tract. The following section presents a methodology to identify key constraints and requirements of the microrobot.

3.1.2 Design Methodology

Three research questions have been posed for the starting point of the critical evaluation and analysis of a microrobotic platform which is capable of performing microscale diagnosis and targeted therapy. Each question focuses on a particular issue which has been chosen for its impact on the design of the microrobot at the early design concept stage. The questions will be summarised, followed by a discussion of the research and analysis carried out.

3.1.3 Analysis of Optimal Microrobot Volume

The first question addresses the physical geometry of the microrobot asking what would be the optimal device volume for a disposable platform taking into account the limitations of current energy storage devices and actuator torque requirements. To address this question an investigation into the available technology was undertaken and an analysis of the physiological constraints of the GI tract.

Using the PillCam^{TM} by Given Imaging Ltd. [1] as a reference point the geometry of the capsule can be investigated. Figure 3.1 is a schematic representation of the available space when loaded with 1 ml of medication and a camera unit. The 1 ml volume of medication has been chosen as the optimum dose as it is representative of the dose published in the prior art [2] and also the quantity being used in current trials stated in the literature [3].

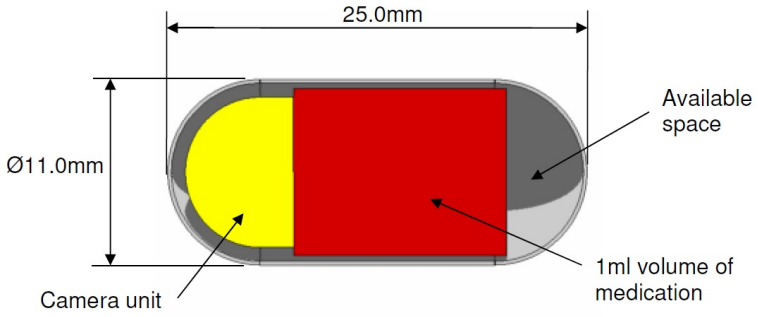


Figure 3.1: Schematic representation of existing capsule geometry based on the PillCam^{TM} by Given Imaging Ltd.

The available space that remains after the medication and camera space have been

allocated is limited, however this space will be required to house a targeting mechanism, a delivery mechanism, a holding/stopping mechanism, a pH sensor, a temperature sensor, a power supply and an RF transmitter.

Figure 3.1 highlights the potential challenges of miniaturising mechanical actuators and electronic components to fit into the $2.0\,cm^3$ package and fulfil the intended objectives. It is clearly impractical to use the dimension based on the PillCam^{TM}, therefore a more realistic approach will be to use the dimensions outlined by the Enterion capsule (Chapter 2, Figure 2.10) [4] which is 7.0 mm longer and has a square form at one end rather than a full radius. These changes in geometry result in a volume of $2.8\,cm^3$, however the new geometry remains within the boundaries for swallowing which is set at approximately $3.0\,cm^3$ [5].

The dimensions are an important consideration in the design of the microrobot as not only will it need to be swallowed but it will also be required to navigate the junctions of the GI tract. These junctions are: the pylorus, where the stomach meets the small intestines; the duodenojejunal junction, a peritoneal fold called the ligament of Treitz which holds the junction in position, and the ileocolic valve which is where the small intestines meet the large intestines and which is also the most difficult junction to navigate [6]. The consequences of the microrobot failing to navigate through the GI tract, i.e. becoming an obstruction, will result in surgical intervention.

3.1.4 Actuators

The second question relates to actuators, traditionally actuators have been adopted for use on a variety of platforms such as in robotics for the control of movement or in machines to perform operations [7]. However with the increasing demand for small scale technology there are greater demands being placed on actuators. For example faster and more powerful actuators with higher torque/mass ratios are required if mechanisms are to be driven directly. Driving mechanisms directly eliminates the need for bulky mechanical parts such as linkages and gearboxes and results in a more efficient system. However actuator performance is severely restricted by volume constraints.

There are a number of actuators readily available for controlling mechanisms such as micromotors, piezoelectric actuators and SMA actuators, these have already been discussed and summarised in Chapter 2, Section 2.3.7.7, however an application where actuators are combined to produce a mechanism capable of controlling the position of a needle would be

the Stewart platform.

The Stewart platform offers a degree of rigidity and could be used to control an injection system as it has the ability to control the position of a needle tip within the GI tract. It is reasoned that a Stewart platform with 3 DOF, i.e. movement up and down, tilt forward and backward and pivot side to side could be used to offer limited control of a needle tip. However the total volume of the mechanism when each of the actuators are combined would leave insufficient remaining capacity to incorporate all the other required features. Therefore the focus will be to use micromotors to drive novel mechanisms as they will give the greatest degrees of flexibility due to the unlimited displacement and low voltage consumption compared to other actuators (Chapter 2, Table 2.4).

Micromotors manufactured by Namiki and Faulhaber will be explored for their ability to operate micromechanical mechanisms as they appear to offer a greater selection of motors for this application.

3.1.5 Investigation into the Microrobotic Platform Attaining Equilibrium

The third question relates to the stopping requirement of the microrobot, in particular the stopping and holding forces required to resist peristaltic contractions in the GI tract without damaging tissue.

The question of force being applied to the GI tract wall highlighted the possibility of the GI tract suffering from post-operative ileus. As a result of the GI tract being handled the wall can cease to function. This point required further investigation and clarification as it could have an impact on the design of the stopping mechanism.

After consulting a medical doctor [8] it was confirmed that post-operative ileus is usually associated with metabolic abnormalities or with the GI tract being handled such as in laparotomies or abdominal surgery and is not associated with endoscopy or with the use of WCE. This means that the design and configuration of the legs will not be restricted to simple shapes and low applied forces. It has been determined by Egorov et al. (2002) [9] that the values of maximal stress and destructive strain for the transverse small bowel are 0.9 MPa and 140% respectively. These tensile figures can be used to guide the design of the legs and feet.

There has been much work carried out in leg design in the literature [10, 11] though

these designs relate to robots which are trying to walk in the GI tract rather than just stopping and holding position. Consequently there will be different requirements imposed on the design of the legs such as the configuration of the legs and the shape of the feet. The shape of the feet will play an important part in the analysis of the interaction with the GI tract wall as they will be required to overcome the 1-2 mm thick layer of lubricant mucosa [12] that coats the wall and which can have a coefficient of friction as low as 10^{-3} [13].

The microrobot's legs and feet will be required to overcome the peristaltic force imposed by the GI tract and the gravitational force acting on the mass of the microrobot to maintain a state of static equilibrium. Figure 3.2 shows the peristaltic forces (P_e) acting on the microrobot with the lumen shown fully dilated to highlight the extent of the interaction required from the microrobot to achieve equilibrium.

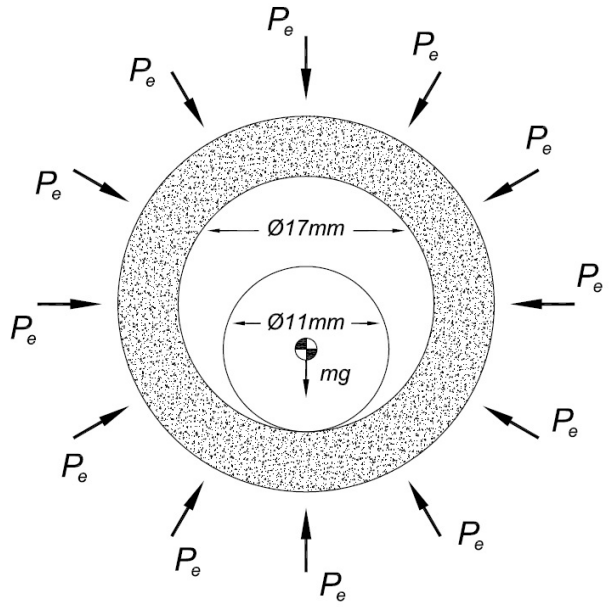


Figure 3.2: Peristaltic forces (P_e) acting on the microrobot with the lumen shown fully dilated to highlight the extent of the interaction required to achieve equilibrium

The legs and feet of the microrobot will be required to accommodate the movement patterns of the GI tract which are segmentation and contraction [14]. These patterns will affect the loading acting on the legs. The feet will be required to accommodate the smooth surface of the lower part of the ileum and the thicker more closely set plicae circulares wall of the jejunum [15]. Inspiration for the design of the legs and feet will be drawn from nature such as from the cockroach which shows a great aptitude for negotiating difficult terrains

[16] or from the gecko whose foot hairs (setae) enable it to adhere to surfaces due to the accumulative action of the setae intermolecular bonding with the surface [17].

3.2 Performance Considerations

There are a number of considerations which will need to be addressed in order for the microrobot to achieve a successful WCE procedure, some of the more important considerations are as follows:

3.2.1 Stages of Operation

The microrobot will be required to perform targeted drug delivery and therapeutic activities. To analyse the sequence of actions the microrobot will be performing, a flow chart of the process has been devised, Figure 3.3.

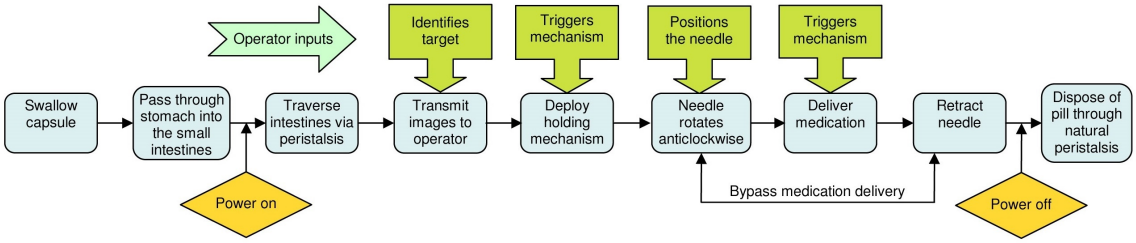


Figure 3.3: Flow chart showing the stages of operation

Showing the step-by-step stages of operation of the WCE will be an aid to the designing process as it will help focus on the significant aspects of a particular step. For example the flow chart shows that the microrobot will only require power once it arrives in the GI tract. With this information we can design the system so that it automatically turns the power on when the microrobot reaches the GI tract. There are many ways in which we can achieve this such as timing or by using the sharp increase in pH value when the capsule enters the small intestines as the trigger to operate the power.

3.2.2 Electronics

The complex electronics required for the control of the microrobot will not be developed as part of this research however provision for electronic components will be made. The microrobot will require onboard space for a number of components such as a transceiver, batteries, LEDs, connectors and the imager which needs to be mounted at the front of the capsule.

An onboard embedded controller will be required to control the system functions. The flow chart (Figure 3.3) outlines a sequence of basic events which the controller will need to implement. The first task before swallowing the capsule will be to activate the microrobot. It is envisioned that the microrobot will be stored in an inactive state to save the battery life. The microrobot will be activated by bringing it into close proximity to a magnet triggering a reed switch. Once the microrobot has reached the small intestines it will be required to turn the transmission from the image sensor on. This will be achieved through timing and pH sensing. When the operator has identified the target location a signal will be transmitted to the microrobot to deploy the holding mechanism. On receiving a signal that the holding mechanism has been fully deployed the operator will transmit a further signal to the microrobot to set the position of the needle. A final signal will deploy the needle and deliver the medication. Once the medication has been delivered the controller will automatically retract the needle and holding mechanism. The operator is able to decide when to switch off transmission from the image sensor.

3.2.3 Power Distribution

The holding mechanism, positioning mechanism and medication delivery mechanism will bring increased functionality to the microrobot however this increased functionality presents the challenge of supplying power to the actuators which will be driving the mechanisms. A circuit schematic of the power distribution for the microrobot is presented in Figure 3.4. The schematic diagram is based on the anticipated layout of the microrobot.

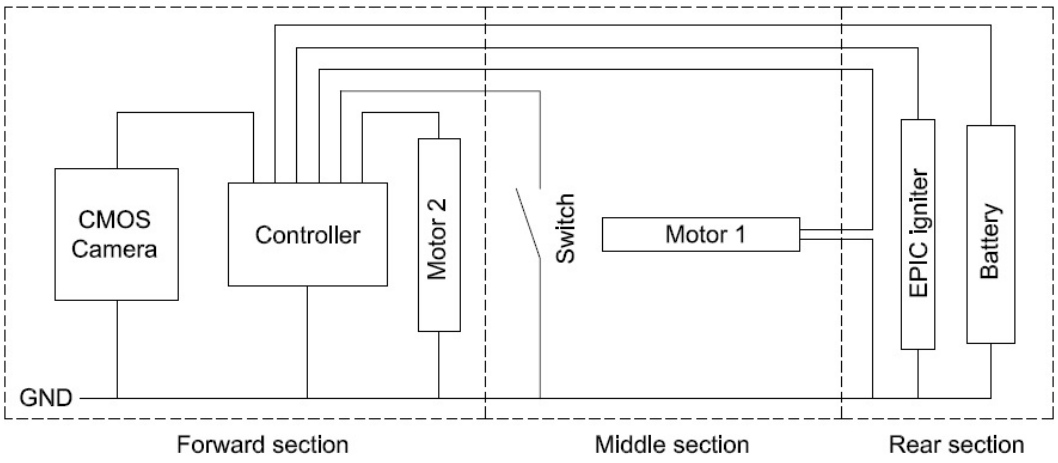


Figure 3.4: Circuit schematic of the power supply requirement for the microrobot

Figure 3.4 highlights the requirement for multiple connections to pass through the forward, middle and rear sections of the microrobot. A more precise evaluation shows that the microrobot can be split into five distinct sections which all have a demand for power:

- The visualisation and processing section
- The holding mechanism
- The needle positioning mechanism
- The medication delivery system
- The power supply section

The configuration of the five sections of the microrobot presents problems of power delivery through the device, specifically delivering power to the holding mechanism and the visualisation and processing sections. This is due to the requirement that the holding mechanism can be deployed diametrically opposite the needle. This feature requires the front section of the microrobot to rotate 360° relative to the rear section. It is assumed that the rear section will remain static due to the mass of the medication and power supply and also from the pressure generated by the GI tract wall. The needle positioning mechanism and the medication delivery system have direct access to the power supply, however the medication chamber and the micromotor driving the needle positioning mechanism inhibit

the direct passage of power to the front of the microrobot. Figure 3.5 highlights the five sections with a cut-through view of the microrobot.

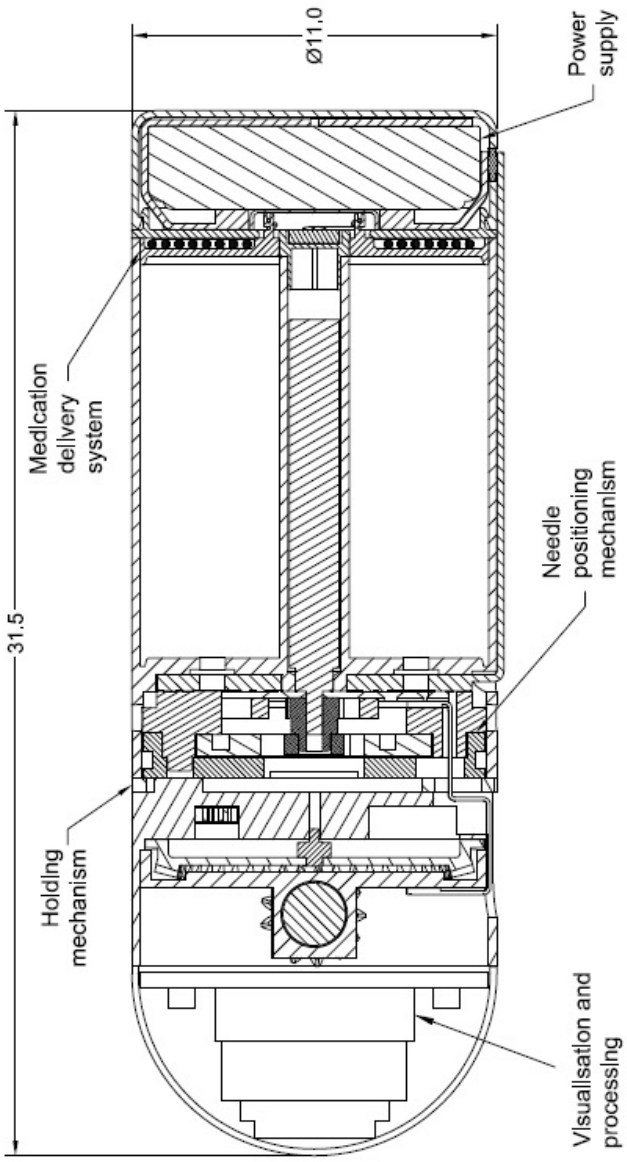


Figure 3.5: Cut-through view of the microrobot with the five main sections labelled

To overcome the issue of power distribution through the microrobot and to control the angular orientation of the needle positioning mechanism a specifically designed rotary encoder is proposed.

3.2.3.1 Rotary Encoder

A specifically designed rotary encoder mounted between the medication chamber and the needle positioning mechanism is the proposed solution for providing power through the forward section of the microrobot, Figure 3.6. The rotary encoder uses flexible PCB cabling, which adheres to the outside of the microrobot's body, to connect the power supply at the rear of the microrobot to the rotary encoder board. Utilising the outside of the microrobot bypasses the need to disrupt the medication compartment making sealing the medication chamber more straightforward.

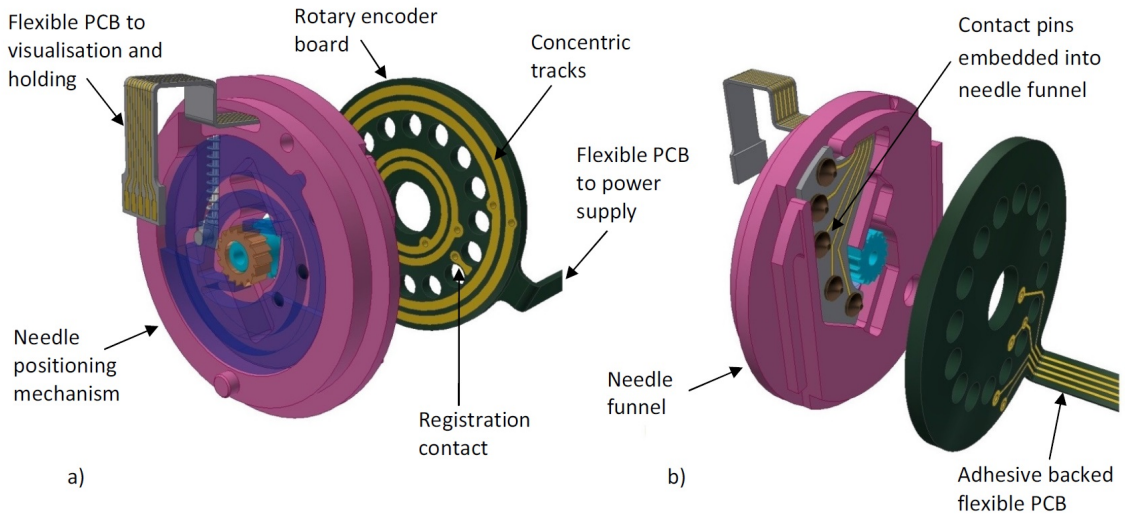


Figure 3.6: Rotary encoder: concentric tracks and registration contact a) and contact pins embedded in the needle funnel b)

The rotary encoder board, which is 0.5 mm thick, allows power to be supplied to the visualisation and processing section and to the holding mechanism while the front of the microrobot is rotating. The rotary encoder achieves this through four 0.3 mm wide concentric tracks which have been positioned to take into consideration the limitations of flexible PCB manufacture and also to accommodate the holes which allow the medication to pass through the board and into the needle funnel, Figure 3.6, a). Contact pins held in the needle positioning mechanism make contact with the tracks however they remain free to rotate with the needle funnel. A fifth contact pin is mounted in the needle funnel and used in conjunction with a registration contact on the rotary encoder board to determine the angular position of the needle and holding mechanism, Figure 3.6, b).

The contact pins align with pads on a flexible PCB board which is incorporated into the needle funnel. The pins stand proud of the needle funnel by 0.05 mm to ensure they make contact with the tracks on the rotary encoder board. The flexible PCB passes through the needle funnel and through the retaining plate. The shape of the distal end of the holding mechanism's legs have been designed to accommodate the flexible cable (Chapter 4, Figure 4.26), however the cable cannot pass through the bevel gear set which is positioned behind the holding mechanism's legs as it will be rotating. Therefore the power supply is again routed out through the side of the microrobot and then back into the space behind the bevel gear set where it can supply power to the visualisation and processing section and to the holding mechanism.

The power supply for the forward section is supplied through the onboard battery which is stored at the rear section of the microrobot. As specified the rotary encoder's flexible PCB board adheres to the outside of the microrobot's body and connects to the power supply, however the power supply is required to be removable to allow access to the medication chamber for loading.

3.2.4 Energy Requirement

The requirement for the microrobot to perform tasks such as delivering a metered dose of medication will necessitate the use of a stored energy device. This device could be in the form of a coiled spring however the camera and lighting system will require electrical energy to power them. For this purpose high performance batteries have been selected as they exhibit high energy density ratios. Energy density (Wh/L) is a measure of how much energy a battery can hold, where W is watts, h is hours and L is litres, the higher the energy density the longer the runtime will be. A second consideration will be the power density (W/L) of the battery this is a measure of how much power a battery can deliver on demand. This is significant as the actuators will only be required to work for short periods of time however they may require high power, for example, to activate a motor controller.

There are a number of battery options available such as silver oxide button cell batteries however these are not as powerful as lithium-ion polymer batteries (LiPo) which have the highest energy density ratio available at 300 Wh/L [18]. They are also rechargeable and have a slow loss of charge when not in use. Provision for button cell batteries will be incorporated into the microrobot however the limitations of space at the early design stage will not prohibit the development of the mechanisms as it is envisaged that shaped batteries

could be developed at a later stage which would take full advantage of the available space.

3.2.4.1 Power Consumption

As the space available for the power supply onboard the WCE is limited, it is essential that the needle positioning mechanism and the holding mechanism can both operate with low power consumption. The energy requirements for both mechanisms have been estimated from the peak current consumption of the Namiki motor controller (SSD04) and the Faulhaber motor controller (BLD05002S) which are stated as 800 mA at 6 V and 400 mA at 7.5 V respectively. Three revolutions of the Namiki micromotor are required for positioning and deployment of the needle; this is achieved in 3.8 s while the holding mechanism can complete a full opening and closing cycle in 1.78 s. Using a Lithium coin battery with a volume of 188 mm^3 and an energy density of 435 Wh/L (CR1025 Energizer), the mechanisms will consume at most 28.94 J of energy for each complete cycle which is only 9.8% of the available energy, offering the potential for multiple operations.

3.2.4.2 Power Supply

A compact method of connecting the power supply to the microrobot is required which will allow access to the medication chamber for filling and also connect with the flexible PCB board which links to the rotary encoder. Figure 3.7 shows the chosen design in three stages of assembly.

Figure 3.7 shows the proposed assembly of the power supply unit. The solution is a modular system which allows the medication chamber to be manually loaded and also provides a method of connecting to the rotary encoder PCB board running on the outside of the body. The solution incorporates a flexible PCB board which wraps around a silver oxide button cell battery (CR1025 Energizer), Figure 3.7, a). The battery and flexible PCB board are secured into a cap with resin to ensure the unit cannot be damaged. A contact board is also secured into the side of the cap which facilitates the connection to the rotary encoder PCB board, Figure 3.7, b). The cap and battery are fitted to the trigger mechanism via a snap fit on the trigger board, Figure 3.7, c). The assembly can be loaded onto the microrobot's body via a central lug protruding from the trigger board. The lug secures the power supply unit and also connects the power supply to the micromotor and to the EPIC device. The flexible PCB board running on the outside of the body is connected to the

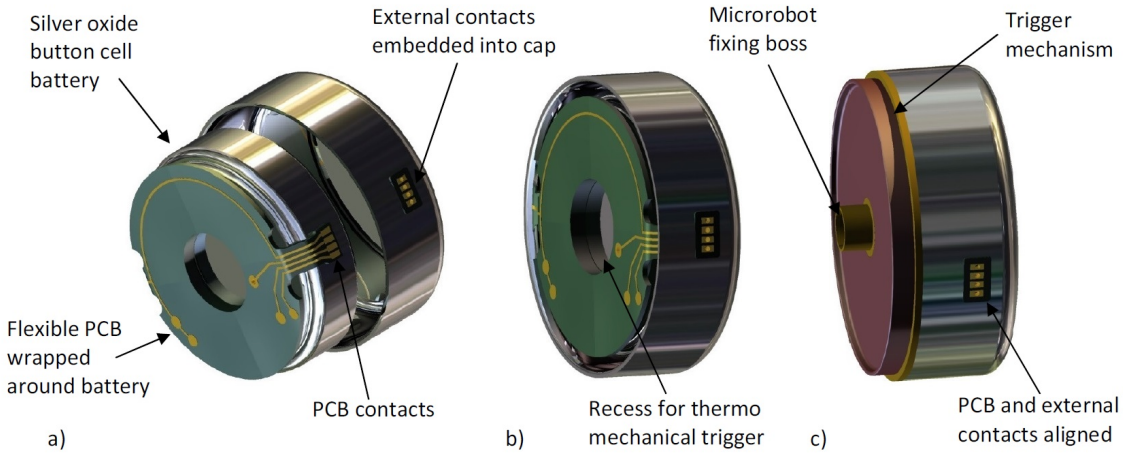


Figure 3.7: Power supply assembly: flexible PCB board wrapped around the battery a) battery and flexible PCB board secured into the cap with contacts aligned b) and trigger mechanism and power supply assembly ready to be loaded into the microrobot's body c)

contact board to complete the connection with the front of microrobot.

The proposed solution allows the medication chamber to be manually filled at the point just prior to administration. This feature gives flexibility in the choice of medication which can be prescribed to the patient therefore potentially broadening the scope of its use.

3.2.5 Usability

The microrobot will have the facility to carry onboard medication such as antibiotics or adrenaline. The medication may have a short shelf life or degrade quickly if it is not stored correctly therefore the microrobot must have the capability for the medication to be loaded at the beginning of the procedure. An influencing factor for the manual loading operation will be the decision to make the microrobot a single use device or a reusable device as there will be a degree of added complexity if the medication loading system is required to accommodate multiple loadings. For example, the medication chamber may be contaminated by the drug or the method for sealing may not withstand the sterilizing procedure. A further requirement, if the device is to be reusable, will be a replaceable power supply and the ability to reset or replace the drug delivery mechanisms.

3.2.6 Ingress Protection

The microrobot will be in a liquid environment when passing through the GI tract. This will have implications on the performance of the micromotor as any liquid ingress will prohibit the smooth functioning of the micromotor possibly resulting in total failure. The solution to the problem will be to seal the driveshaft however this may be problematic due to the small dimensions of driveshafts (Ø0.5 x 1.3 mm). Also the increased friction due to the seal will increase the torque required to drive the driveshaft reducing the available torque to drive the mechanism. Another consideration relating to ingress is the sterilization of the microrobot as general autoclaving uses steam at temperatures of 134 °C to 137 °C for three minutes. The steam which will also be pressurised will penetrate the micromotor potentially damaging component parts. The alternative is to use gas plasma (hydrogen peroxide) sterilization which uses temperatures <50 °C.

3.3 Summary

A design specification for the microrobotic platform has been derived from the gathered research data and from the prior art presented in the literature review.

3.3.1 Microrobotic Platform Technical Specification

The microrobot will need to be easily swallowed by the patient and expelled through natural means. During its journey it will be required to transmit images to an operator and perform therapeutic activities such as constant pH, temperature and pressure monitoring. It would also be required to hold itself in position while delivering a metered dose of medication to a targeted site. Some of the more important performance specifications are that the microrobot will be comparable in size with its competitors, it will be capable of navigating the ileocolic valve and it will be capable of delivering 1 ml of medication.

For the microrobot to perform targeted therapy and microscale diagnosis a list of requirements can be drawn from the design specification and broken down into specific system features for the microrobot such as the camera, power supply, systems controller, pH sensor, drug delivery system and a stopping mechanism. The detailed specifications for the microrobot's performance is outlined in Table 3.1.

The following chapters will discuss the design, analysis and validation of a microrobotic system capable of performing a therapeutic activity in the GI tract, more specifically the microrobot will have additional functionality which will allow it to target and treat pathologies in the small intestines which is the most difficult and challenging section to access. The structure of the chapters are as follows: chapter four presents the design, analysis and evaluation of a holding mechanism capable of maintaining a state of equilibrium; chapter five presents the design, analysis and evaluation of a targeting system; chapter six presents the design, analysis and evaluation of a drug delivery system capable of delivering 1 ml of medication and chapter seven presents the conclusions and further work.

Table 3.1: Microrobotic platform technical specification

System features	Requirement	Specification
Geometry	Microrobot volume	Maximum 3.0 cm^3
	Maximum diameter	11.10 mm
	Maximum length	36.0 mm
	Maximum weight	5.0 g
Vision	Image sensor	CMOS
	Viewing angle	140 deg
	Depth of view	1.0 mm to 3.0 mm
	Resolution	0.1 mm
	Magnification	Optical dome 1:8
	Illumination	4 white LEDs
	Duration	6 to 8 hours
Holding	Attaining equilibrium	Expansion
	Expand to a circumference	>53.0 mm
	Resist peristaltic contractions of:	>26.9 g/cm circumferential
		>17.2 g/cm linear
	Actuator	Micromotor
	Deployment time	Maximum 2.5 s
	Holding time	Minimum 10 s
Targeting	Tracking:	RF
		Timed transit
	Telemetry	Bidirectional
	Actuator	Micromotor
	Return to site of interest	±5.0 mm
Delivery	Delivering therapy	Liquid medication
	Delivery method	Needle
	Drug reservoir	1 ml
	Wall penetration	1.0 mm to 2.0 mm
	Needle penetration force	8.9 MPa
	Target location	±30 deg
	Actuator	Spring
	Response time	Maximum 5 s
Sensing	Monitoring:	pH level
		Temperature
		Pressure
Power	Onboard power supply	Silver oxide button cell battery
	Supply voltage	3.0 V
	Battery life	6 to 8 hours
	Duration of mechanisms	Minimum of 2 cycles
Sterilization	Sterilization method	Gas plasma (hydrogen peroxide)
	Withstand temperatures of	50 °C

References

[1] G. D. Meron, "The development of the swallowable video capsule (M2A)," *Gastrointestinal Endoscopy*, vol. 52, pp. 817–819, 2000.

[2] A. Lambert, F. Vaxman, F. Crenner, T. Wittmann, and J. F. Grenier, "Autonomous telemetric capsule to explore the small bowel," *Medical and Biological Engineering and Computing*, vol. 29, pp. 191–196, 1991.

[3] A. Parr, E. Sandefer, P. Wissel, M. McCartney, C. McClain, U. Y. Ryo, and G. Digenis, "Evaluation of the feasibility and use of a prototype remote drug delivery capsule (RDDC) for non-invasive regional drug absorption in the GI tract of man and beagle dog," *Pharmaceutical Research*, vol. 16, pp. 266–271, 1999.

[4] P. J. Houzego, P. N. Morgan, P. H. Hirst, D. J. Westland, and I. R. Wilding, "Ingestible device for the release of substances at distinct locations in the alimentary canal," USA: Phaeton Research Limited, 2005.

[5] A. Connor, P. Evans, J. Doto, C. Ellis, and D. E. Martin, "An oral human drug absorption study to assess the impact of site of delivery on the bioavailability of bevirimat," *The Journal of Clinical Pharmacology*, vol. 49, pp. 606–612, 2009.

[6] S. R. Snell, *Clinical anatomy for medical students*. Boston: Little, Brown and Company, 2nd ed., 1981, pp. 187-191.

[7] J. M. Hollerbach, I. W. Hunter, and J. Ballantyne, "A comparative analysis of actuator technologies for robotics," *Robotics Review 2, MIT Press*, pp. 299–342, 1991.

[8] N. Oliver, Clinical Research Fellow, Imperial College London, (Personal communication 18 February 2010).

[9] V. I. Egorov, I. V. Schastlivtsev, E. V. Prut, A. O. Baranov, and R. A. Turusov, "Mechanical properties of the human gastrointestinal tract," *Journal of Biomechanics*, vol. 35, pp. 1417–1425, 2002.

[10] E. Buselli, P. Valdastri, M. Quirini, A. Menciassi, and P. Dario, "Superelastic leg design optimization for an endoscopic capsule with active locomotion," *Smart Materials and Structures*, vol. 18, p. 8, 2008.

[11] C. Quaglia, E. Buselli, R. J. Webster III, P. Valdastri, A. Menciassi, and P. Dario, "An endoscopic capsule robot: a meso-scale engineering case study," *Journal of Micromechanics and Microengineering*, vol. 19, pp. 1–11, 2009.

[12] A. Allen, D. A. Hutton, A. J. Leonard, J. P. Pearson, and L. A. Sellers, "The role of mucus in the protection of the gastroduodenal mucosa," *Scandinavian Journal of Gastroenterology*, vol. 21, pp. 71–78, 1986.

[13] X. Wang and M. Q. H. Meng, "Study of frictional properties of the small intestine for design of active capsule endoscope," in *Biomedical Robotics and Biomechatronics, 2006. BioRob 2006. The First IEEE/RAS-EMBS International Conference on*, pp. 124–129, 2006.

[14] W. Xiaona, M. Q. H. Meng, and C. Yawen, "Physiological factors of the small intestine in design of active capsule endoscopy," *Engineering in Medicine and Biology Society, 2005. IEEE-EMBS 2005. 27th Annual International Conference of the*, pp. 2942–2945, 2005.

[15] H. Gray, *Grays anatomy.* London: Greenwich Editions, 2005, pp. 606-607.

[16] S. Gorini, M. Quirini, A. Menciassi, G. Pernorio, C. Stefanini, and P. Dario, "A novel SMA-based actuator for a legged endoscopic capsule," *Biomedical Robotics and Biomechatronics, 2006. BioRob 2006. The First IEEE/RAS-EMBS International Conference on*, pp. 443–449, 2006.

[17] K. Autumn, M. Sitti, Y. A. Liang, A. M. Peattie, W. R. Hansen, S. Sponberg, T. W. Kenny, R. Fearing, J. N. Israelachvili, and R. J. Full, "Evidence for van der Waals adhesion in gecko setae," *Proceedings of the National Academy of Sciences of the United States of America*, vol. 99, pp. 12252–12256, 2002.

[18] Z. Salameh and B. Kim, "Advanced lithium polymer batteries," in *Power & Energy Society General Meeting, 2009. PES '09. IEEE*, pp. 1–5, 2009.

Chapter 4

Attaining Equilibrium: Design, Analysis and Evaluation

4.1 Introduction

This chapter presents a novel biologically-inspired holding mechanism based on the order of insects known as the Coleoptera. Coleopteran's, which are more generally referred to as beetles, have two pairs of wings and include insects such as the coccinellidae (ladybird). The ladybird, which can grow to 10 mm in size, has the ability to fold away its wings behind a second hardened pair of wings which are used as a casing to protect them. Using the biologically-inspired concept of a pair of folded wings protected by an outer case as a basic premise, a compact holding mechanism can be designed which can be incorporated into the next generation of WCE for the purpose of resisting natural peristalsis in the GI tract. This chapter describes the requirements of WCE, discusses a proposed design and analysis of a holding mechanism based on the design specification presented in Chapter 3 and presents a 5:1 scale prototype holding mechanism which is validated through experimentation.

4.2 Overview

Conventional WCE have sufficiently small geometry to allow them to pass through the small intestines and navigate the ileocolic valve without becoming an obstruction. However the clinical need to target a specific location or feature within the GI tract for medication delivery or examination of the intestinal wall would require the WCE to stop. Figure 4.1

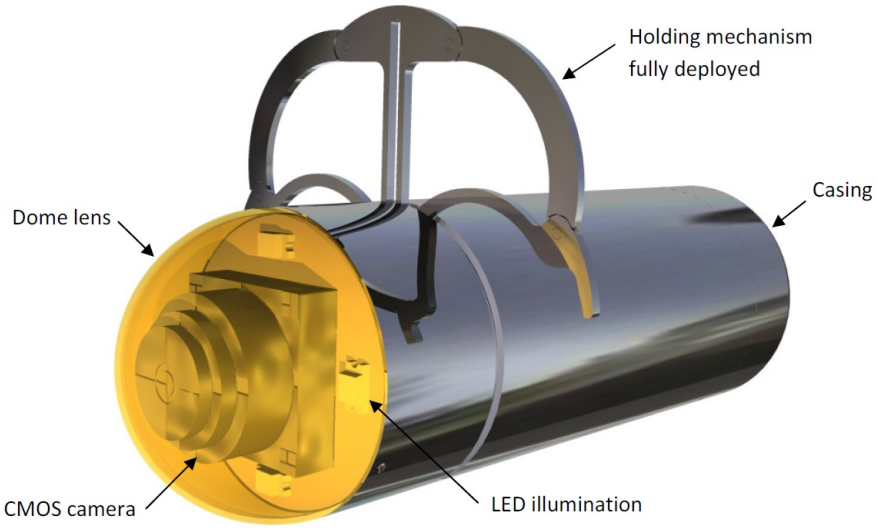


Figure 4.1: Microrobot concept design capable of resisting peristaltic pressure through an integrated holding mechanism. Holding mechanism shown fully open

shows a microrobot concept design capable of resisting peristaltic pressure through the deployment of an integrated holding mechanism.

4.3 Resisting Peristalsis

The overall geometry of the microrobot system must be capable of housing all the components necessary for the WCE to resist natural peristalsis. Therefore a simple mechanism which can expand in some way to prevent the WCE from moving when a section of the intestinal wall is being examined, or for the purpose of administering medication, is proposed. The holding mechanism must fit within the maximum volume of 3.0 cm^3, leave sufficient space for other features and expand to a minimum circumference of 53.40 mm to guarantee it occupies the 17.0 mm diameter of the small intestinal tract.

Through a process of divergent and convergent thinking [1] a method of expansion was selected to hold the microrobot against natural peristalsis. The chosen method of expansion offers greater advantages compared to alternative methods of resisting peristalsis such as balloon insufflation or electrical stimulation as it guarantees the intestinal tract is in contact with the body of the microrobot. This is an important requirement as it allows access to the GI tract wall for the purpose of administering treatment. A number of expansion

solutions have been considered, for example two, three and four leg designs were explored which utilised direct drive from a micromotor through a leadscrew or from a geared system. However operating legs via a leadscrew presents challenges of space and insufficient torque to combat the leverage action from the pivoting legs. A two leg system driven by a gear train offered the advantage of using the minimum occupied space and also a reduction in the number of pinned joints which would be required compared to a four leg approach. A further advantage of the expansion mechanism is its ability to slow down the transit of the microrobot by partially opening the legs. This feature offers the potential advantage of greater control of the delivery of the medication as more precise targeting is possible. This section concentrates on the design and analysis of the selected method of expansion which utilises a geared system to gain maximum mechanical advantage and also incorporates a number of levers and pinned joints which will allow the mechanism to unfold from the WCE's protective casing in a similar way to the unfolding of a ladybird's wings. A selection of holding concepts is presented in Appendix A.

4.3.1 Holding Mechanism

The concept holding mechanism (Figure 4.1) uses a single micromotor to open and close two legs. The two legs are connected to a central support via two pinned leg ties. The two-legged design utilises a micromotor which is orientated in a vertical position, Figure 4.2. The micromotor is connected to a bevel gear set, this allows the micromotor's rotation to be translated through 90 degrees. The bevel gear drives a gear train of spur gears, which is nested in the large bevel gear, and drives the legs in and out, Figure 4.3. This novel configuration significantly reduces the micromotor's RPM. The reduction in RPM will result in a multiplication of the micromotor's torque, this will give the legs the strength required to distend the GI tract wall and hold the microrobot in place.

To secure the microrobot in place the holding mechanism will be required to expand to a size which is sufficiently large that it resists the natural movement from peristalsis. This is achieved through an increase in circumference of the microrobot. The holding mechanism begins with a circumference of 34.5 mm however when activated the mechanism increases in size to produce a circumference of 60.4 mm which is an increase of 75%. This can be further increased to 71.25 mm by simply modifying the profile of the legs to increase the surface area in contact with the GI tract wall.

The vertical configuration of the micromotor offers the advantage of being a very com-

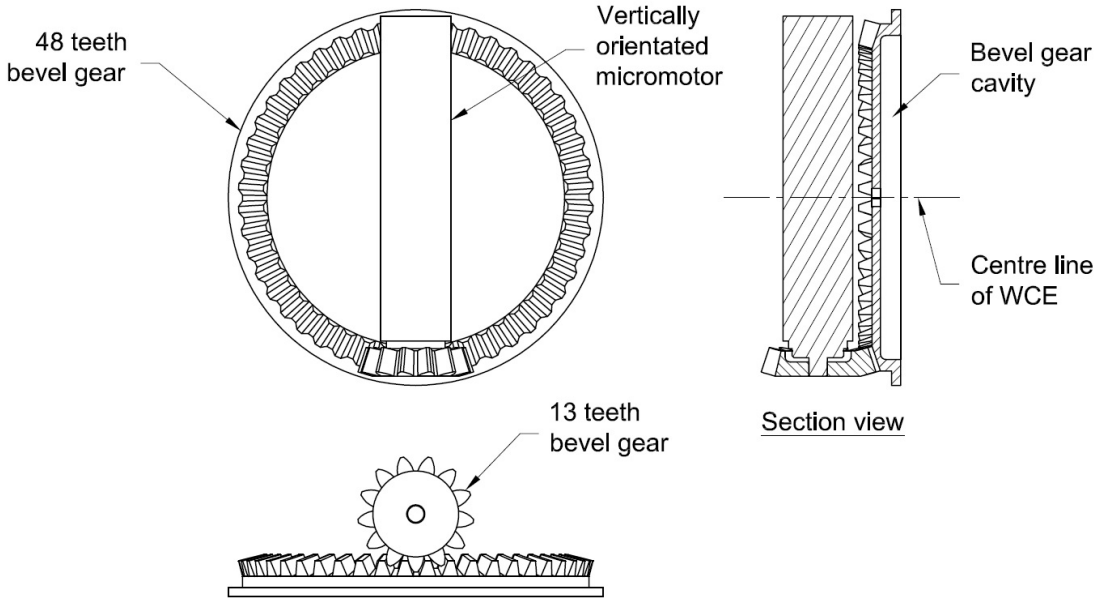


Figure 4.2: Vertically orientated micromotor driving a bevel gear set

pact design (347 mm^3) resulting in the most efficient use of space. The two legs, central support, leg ties and the microrobot case will absorb the load from the GI tract wall evenly. The compact gearing allows the rate at which the legs are deployed to be controlled by the ratio of the gear train.

4.3.2 Gear Train

For the holding mechanism to operate at a safe speed the micromotor will require the gear train to slow it down. The chosen micromotor is manufactured by Faulhaber and already has an integral gearbox, which reduces the 20,000 RPM by a factor of 13:1 (reduction absolute 324/25). This results in a starting RPM of 1,543 RPM, which is significantly high; therefore, further reductions will need to be achieved from the gear train. The output speed of a gear train can be estimated from the following equation:

$$RPM_{out} = \frac{N_{d1} \times N_{d2} \times N_{d3} \times N_{d4} \times RPM_{in}}{N_{f1} \times N_{f2} \times N_{f3} \times N_{f4}} \tag{4.1}$$

Where RPM_{in} is the input speed, N_{d1} is the number of teeth on the driving gear and

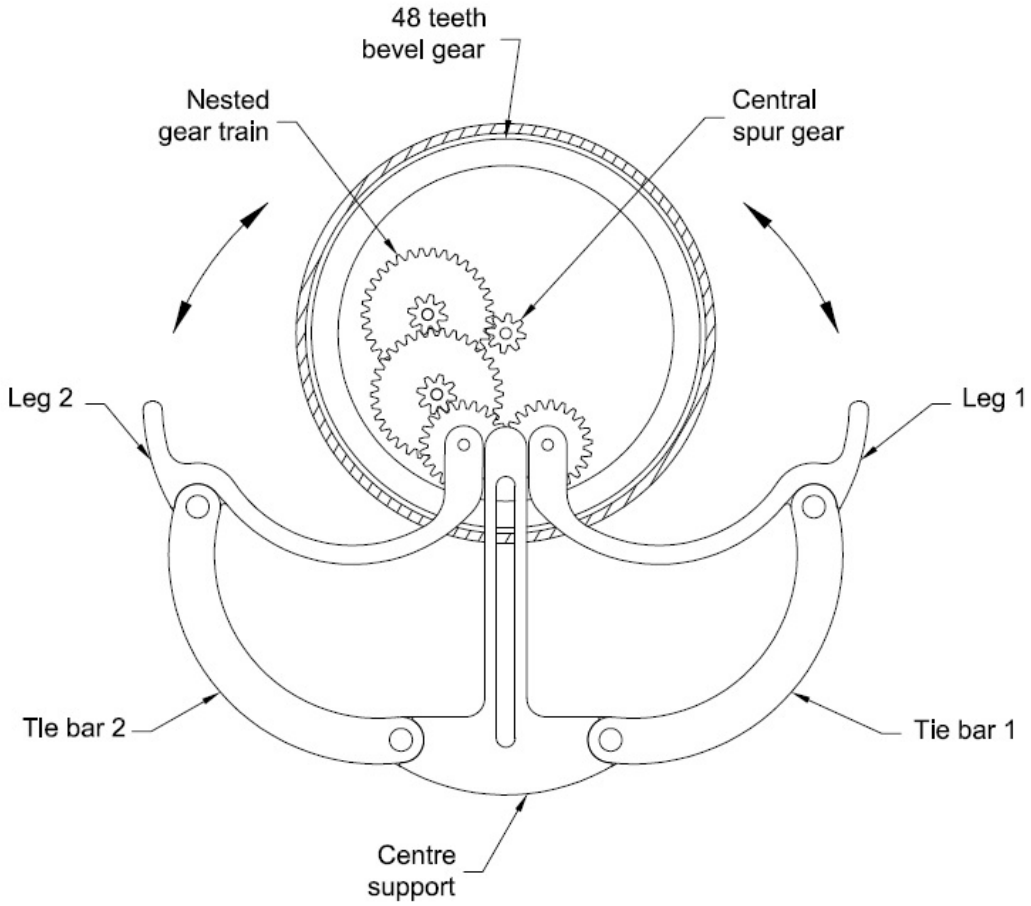


Figure 4.3: Two-legged design showing the central spur gear being driven by the bevel gear. The legs are fully expanded to accommodate a circumference of 60.4 mm

N_{f1} is the number of teeth on the follower gear. This formula can be applied to the gear train with a selection of gear teeth to determine the output RPM, Table 4.1.

Table 4.1: Calculated gear train output from an input of 1,543 RPM

Gear stages	**Micromotor and bevel gear**	**Bevel gear and spur gear**	**Second stage spur gear**	**Output spur gear**
No. of teeth on driver (d)	13	8	8	8
No. of teeth on follower (f)	48	34	34	22
Output RPM	417.93	98.34	23.14	8.41

As can be seen from Table 4.1 the number of teeth on the follower gears (f) is higher than the number of teeth on the driving gears (d), this is to ensure a rapid reduction in RPM. The target is to deploy the holding mechanism as slowly as possible as this will reduce the potential for trauma to the GI tract wall from the legs and supports. However there are limitations to the number of teeth which can be used as the chosen gear module, which is the ratio of the pitch diameter to the number of teeth on the gear, determines the overall geometry of the gear. The chosen bevel gear module is 0.2 this results in a maximum number of teeth of 48 and an overall gear diameter of 10.0 mm (Figure 4.2) as the gear has the overall limiting factor of the diameter of the microrobot. The spur gears use a module of 0.1 this results in a maximum number of teeth of 34 as the gears are required to be linked together in a train and nested in the bevel gear (Figure 4.3). They are therefore limited again to the overall diameter of the microrobot.

The gear train reduces the 1,543 RPM output from the micromotor to 8.4 RPM this allows the holding mechanism to be fully deployed in approximately 1.8 s. Based on an average transit time through the small intestines of 23 mm/min [2] the capsule would have travelled approximately 0.7 mm before the holding mechanism is fully deployed. Altering the number of teeth on the driver or follower gears will increase or decrease this figure however as stated this is severely restricted by the geometry of the microrobot. A complex multiple layered design has been chosen to achieve the speed reduction. This type of gear configuration will add to the overall length of the microrobot however the layout does leave an unused volume of 37.7 mm^3 which could be utilised to house a power supply.

An important function of the gear train is to transmit power from the micromotor to the legs, this will enable the legs to distend the luminal wall and hold the microrobot in position.

The power transmitting capacity of a gear train can be determined by the following formula:

$$T_{out} = \frac{N_{f1} \times N_{f2} \times N_{f3} \times N_{f4} \times T_{in}}{N_{d1} \times N_{d2} \times N_{d3} \times N_{d4}} \tag{4.2}$$

Where T_{in} is the input torque, N_{f1} is the number of teeth on the follower gear and N_{d1} is the number of teeth on the driving gear. Applying this formula to the gear train and using 0.15 mNm torque generated by the Faulhaber micromotor as the input torque (T_{in}) results in an estimated output torque (T_{out}) of 27.5 mNm. However the calculated output torque does not take into consideration how efficient the gear train is in transmitting power. There are a number of factors which will influence the efficiency of the gear train for example the ratio of output power to input power is significantly influenced by friction generated by the system. The friction generates heat energy which causes loss of transmitted power. Friction is dependent on the load torque and the contact between the teeth therefore the number of teeth engaged and the number of stages in the gear train will influence the efficiency of the gear train. Also bearing material and configuration coupled with the type of lubrication used will have an impact on the efficiency of the gear train. Using the number of gear stages and an estimation of a 10% loss at each stage the gear train efficiency (η) can be estimated by the following formula:

$$\eta = Stage1(90\%) \times Stage2(90\%) \times Stage3(90\%) \times Stage4(90\%) \times Stage5(90\%) \tag{4.3}$$

Table 4.1 shows four gear stages however for the purpose of the efficiency analysis (equation 4.3) a fifth stage is taken into consideration. The fifth stage does not contribute to the torque or RPM output as it has the same number of teeth on each gear. The purpose of the gear stage is to drive both the legs simultaneously. Using 90% for each stage results in an overall system efficiency of approximately 60.0% this equates to an output torque of 16.2 mNm. The design parameters for the complete gear train are specified in Table 4.2.

Table 4.2: Bevel gear and spur gear design parameters

	Number of teeth (z)	**Normal module** (m_n)	**Outside diameter** (OD)	**Pitch circle** (PC)	**Tooth depth** (h_t)	**Tooth thickness** (t)	**Pressure angle** (Φ)	**Face width** (b_t)
Bevel gear 1	13	0.2	3.0 mm	2.6 mm	0.48 mm	0.314 mm	20°	0.7 mm
Bevel gear 2	48	0.2	10.0 mm	9.6 mm	0.48 mm	0.314 mm	20°	0.7 mm
Drive gear	8	0.1	1.0 mm	0.8 mm	0.24 mm	0.157 mm	20°	0.45 mm
Follower	34	0.1	3.6 mm	3.4 mm	0.24 mm	0.157 mm	20°	0.45 mm
Drive gear 2	22	0.1	2.4 mm	2.2 mm	0.24 mm	0.157 mm	20°	0.45 mm

The gears must perform under the maximum torque delivered by the micromotor however the chosen gear modules result in very small gears therefore it is essential that the gears can withstand the stress and strain developed during an operating cycle. The next section evaluates the gears with a view to determining whether they are capable of withstanding these loads.

4.3.3 Gear Tooth Loading Analysis

The 0.1 module chosen for the gear train results in a micro-metre gear tooth profile, Figure 4.4. It is therefore important to determine if the teeth can withstand the bending loads which they will be subjected to when the micromotor is operated at its maximum RPM. The Faulhaber (02/1) (Table 2.3) micromotor will be used for the purpose of gear train analysis. It has a two stage 13:1 reduction gearbox which results in an output of 1,543 RPM and a torque of 0.15 mNm.

An involute gear tooth profile has been selected for the gears. Figure 4.4 shows the forces acting at the pitch circle of the involute tooth profile and some additional relationships between features. For the purposes of analysis the tooth can be modelled as a cantilever beam.

The contact angle between mating teeth is also known as the pressure angle (Φ) and in this application it is set at an industry standard of 20 degrees for a spur gear.

The stress figures determined by analysis are an important resource as they can be used to determine the material the gears are to be manufactured from and the manufacturing process.

The bending stress for a spur gear tooth or a straight toothed bevel gear can be obtained

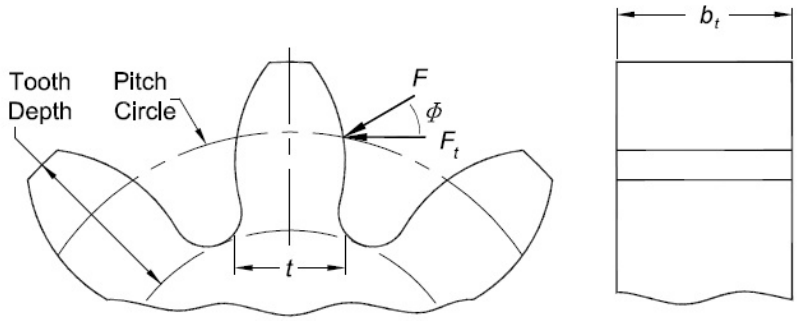


Figure 4.4: Gear tooth loading modelled as a cantilever beam

by using the Lewis formula which has been modified to take into consideration the contact impact of the gears through the addition of a velocity factor:

$$\sigma = \frac{F_t}{K_v b_t m_n y} \tag{4.4}$$

Where F_t is the load applied to the tooth, K_v is the velocity factor, b_t is the face width, m_n is the normal module and y is the Lewis form factor.

The assumptions made with the modified Lewis formula are that the full load is applied to a single tooth and the radial component force (F) is ignored, also that the force is distributed evenly over the full face width of the tooth and that the stress concentration effect of the tooth fillet is also ignored.

To calculate the load (F_t) acting at the circular pitch [3]:

$$F_t = \frac{2000 T_{f1}}{d_1} \tag{4.5}$$

Where T_{f1} is the torque on the drive gear and d_1 is the reference diameter of pinion and can be calculated by the number of teeth on the pinion (z) multiplied by the normal module (m_n).

The velocity factor K_v compensates for the dynamic effect of the gears pitch line velocity and the manufacturing method used to produce the teeth profile. For a hobbed or shaped gear the Barth's formula can be used to calculate the velocity factor [4]:

$$K_v = \frac{3.54}{3.54 + \sqrt{V_p}} \tag{4.6}$$

Where V_p is the pitch line velocity and is calculated by:

$$V_p = \frac{\pi d n}{60} \tag{4.7}$$

Where d is the pitch diameter and n is the rotating speed of the gear in revolutions per minute.

The Lewis form factor (y) is a function of tooth shape and is independent of tooth size, it also does not take into consideration the stress raiser effect of the tooth fillet. It can be calculated as follows [4]:

$$y = 0.484 - \frac{4.24}{z + 6} \tag{4.8}$$

Where z is the number of teeth on the gear.

The normal module (m_n) of a gear is the ratio of the pitch diameter to the number of teeth on the gear. The module has a direct relation to the geometry of the teeth and the overall diameter (OD), it can be calculated as follows:

$$OD = (z + 2) \times m_n \tag{4.9}$$

An example of the module's impact on the outside diameter can be shown using a module of 0.5 and 22 teeth as this would result in an outside gear diameter of 12.0 mm. If the same number of teeth were to be used with a 0.1 module the outside diameter would become 2.4 mm. Therefore the smaller the module the smaller the gear geometry which can be generated.

Applying the modified Lewis formula (equation 4.4) to the bevel gear set, which has a module of 0.2, results in a tooth bending stress of $3.57\,\mathrm{Nmm}^{-2}$ for the 13 toothed gear and $2.30\,\mathrm{Nmm}^{-2}$ for the 48 toothed gear. The calculated low figures for stress can be used to guide the design of the gears as the results suggest the gear set could be manufactured from a polymer such as PEEK. The benefit of making the 48 toothed gear from a polymer would be a simplified assembly as friction bushes can be eliminated by designing the gear

to have bearing surfaces. However applying the formula to the next gear in the train results in significantly higher levels of bending stress.

Applying the Lewis formula to the 8 toothed drive gear, which has a module of 0.1 and is connected to the 48 toothed bevel gear, yields a stress of 176.21 Nmm^{-2}. At this level of stress it would result in a polymer tooth yielding therefore a metallic gear would be required. The Lewis formula does not take into account the stress raising effect of the fillets or the stress distribution when the radial component load (F) is applied, therefore an FEA analysis has been performed to determine a more accurate level of stress distribution through the tooth, Figure 4.5.

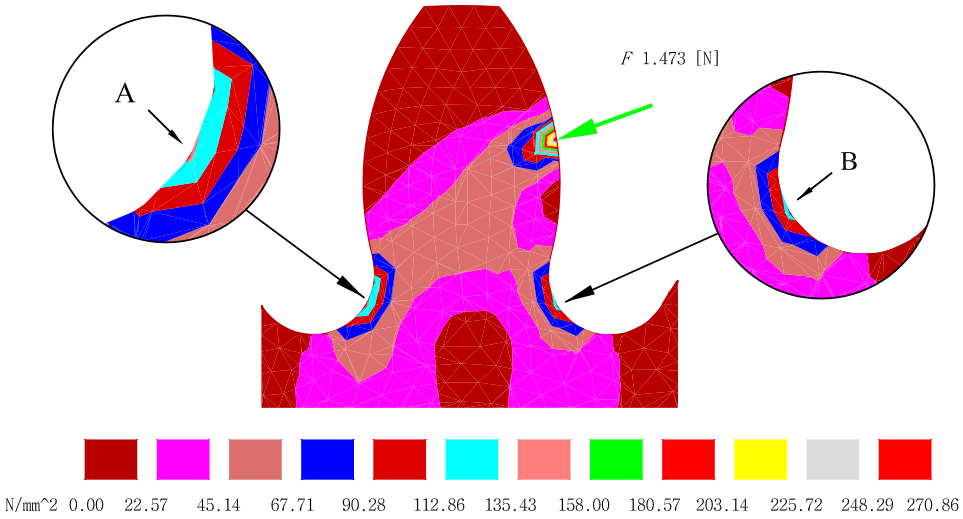


Figure 4.5: Von Mises FEA 2D isoareas analysis of a stainless steel 304, 0.1 module gear tooth profile with a radial component load of 1.473 N

Figure 4.5 shows a Von Mises FEA 2D isoareas analysis of a stainless steel 304, 0.1 module gear tooth profile with an applied radial component load of 1.473 N. The radial load F has been calculated from the applied load F_t and the pressure angle Φ. There is a distinct difference in the result for loading: Figure 4.5 A) shows the compressive stress to be 139.42 Nmm^{-2} while Figure 4.5 B) shows the tensile stress to be 121.69 Nmm^{-2}. However repeating the Von Mises FEA analysis with the load (F_t) acting on the circular pitch resulted

in similar bending stress figures to the radial component load analysis. Although the FEA figures are lower than the calculated figure ($176.21\,\mathrm{Nmm}^{-2}$) the FEA figures confirm that the 8 toothed gear must be manufactured from a metal rather than a polymer to ensure the teeth do not yield under load.

The Von Mises FEA analysis assumes a worst case scenario, that is, at any one time only one pair of teeth are in contact with each other and that they take the total load. Generally two pairs of teeth are in contact however this may drop to 1.5 depending on the degree of tooth truncation and inaccuracies in tooth profile due to the manufacturing process. Increasing the value of the face width or increasing the module would reduce the stress in the tooth, however increasing the module would result in an increase in the overall diameter of each gear in the set and hence the overall size of the gear train would increase. Also increasing the tooth thickness will influence the overall length of the microrobot due to the stack-up of dimensions. However increasing the size of the components would make manufacturing generally easier.

4.4 Analysis of Holding Mechanism

The microrobot's holding mechanism will be required to overcome the peristaltic force imposed on it by the GI tract and the gravitational force acting on it due to its mass in order for the microrobot to achieve a state of static equilibrium. There are two components of peristalsis which will potentially influence the operation of the holding mechanism, they are circumferential and longitudinal peristaltic contractions. To ensure correct functionality of the holding mechanism an analysis of the potential impact of the two components will be performed.

4.4.1 Circumferential Peristaltic Force Analysis

To attain a state of equilibrium, the external forces acting on the microrobot must be balanced for any given orientation; however angles less than 90 degrees from the horizontal can be neglected from the equilibrium analysis, as in the worst case the load would be acting vertical to the horizontal resulting in a multiplication factor of $\sin 90$ which equals 1, hence producing no net increase in load. Figure 4.6 shows the external forces acting on the legs of the microrobot. For the purpose of the force analysis the contact area has been divided into six contact points as these points will be in continuous contact with the GI tract wall throughout the deployment of the holding mechanism.

As can be seen from Figure 4.6 the external forces acting on the microrobot's legs are the circumferential peristaltic force P_c, the longitudinal peristaltic forces are neglected at this stage of the analysis as they do not contribute to the holding function. Using the figures determined by Miftahof (2005) [5] the maximum circumferential amplitude of muscle contraction is 26.9 g/cm this results in an estimated load of 687.0 mN for the total circumferential contact area of the extended legs and microrobot's body with the GI tract wall.

The micromotor employed to drive the legs must be capable of delivering an equivalent force to the legs to maintain a state of equilibrium. The force acting at each point of contact P_c can be estimated by the following formula:

$$P_c = \frac{F_c + mg}{6} \tag{4.10}$$

Where F_c is the circumferential force from the GI tract wall, m is the mass of the

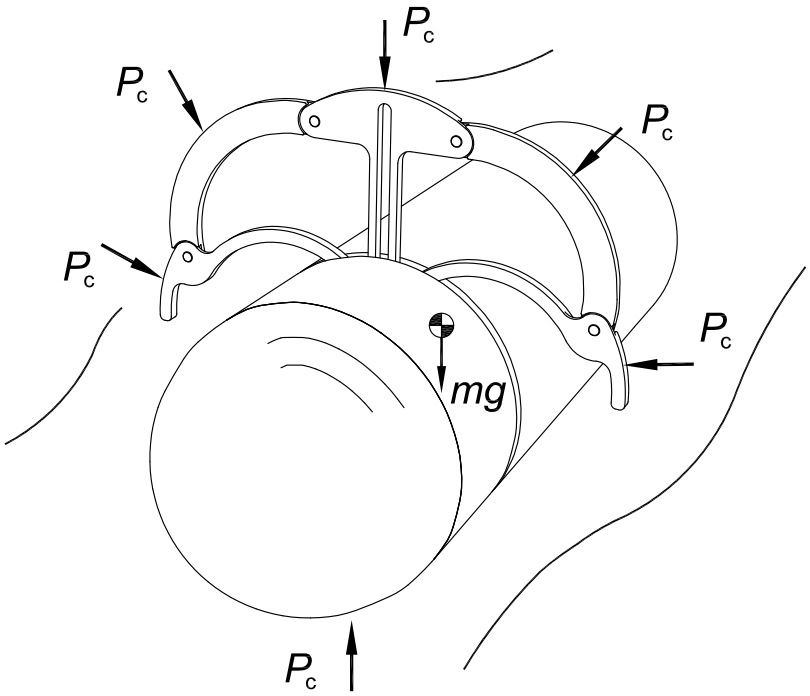


Figure 4.6: Microrobot holding mechanism shown fully open and the external circumferential peristaltic force P_c acting on the microrobot at six positions

microrobot and is estimated to be 3.45 g and g is gravity.

Using formula (4.10) the load acting at each point equates to 120.1 mN. However due to the unfolding nature of the mechanism the circumferential peristaltic force will work towards preventing the legs from opening, Figure 4.7.

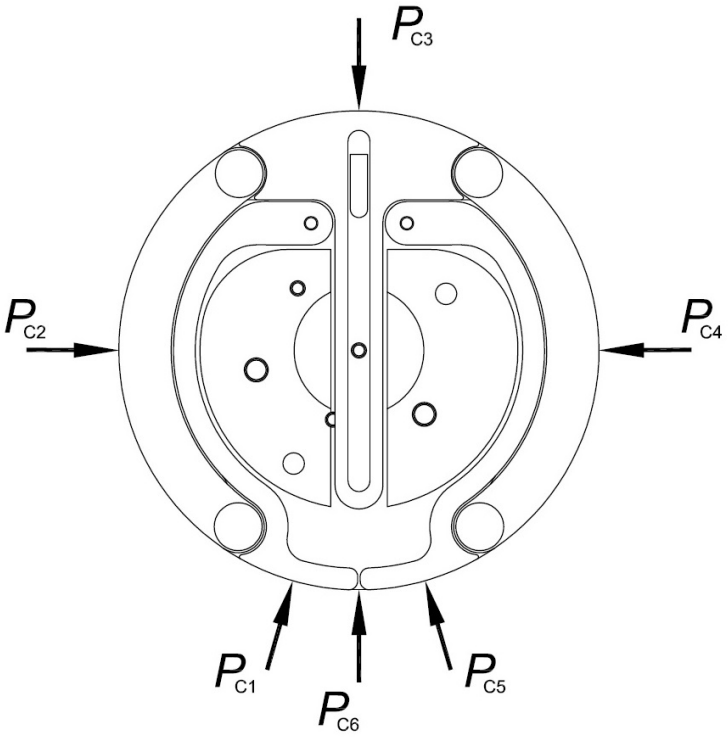


Figure 4.7: Holding mechanism shown fully closed. Circumferential peristaltic forces acting towards the centre of the microrobot prevent the holding mechanism from opening

For the purpose of simplifying the force analysis the circumferential peristaltic forces have been assigned individual identification numbers P_{c1}, P_{c2}..., Figure 4.7.

4.4.1.1 Load Points P_c Contributing to Torque

The process of operating the legs from the stored position to the fully extended position results in the circumferential peristaltic force from the GI tract wall (P_c) acting towards the centre of the microrobot, this is illustrated for P_{c1} and P_{c5} in Figure 4.8. However due to the position of the legs' pivot points the circumferential forces will be required to be broken down into their component forces as only the perpendicular component force acting on the leg pivot will work towards preventing the legs from opening P_{p1} and P_{p5}.

The circumferential forces P_{c1} and P_{c5} act on both legs with equal magnitude and

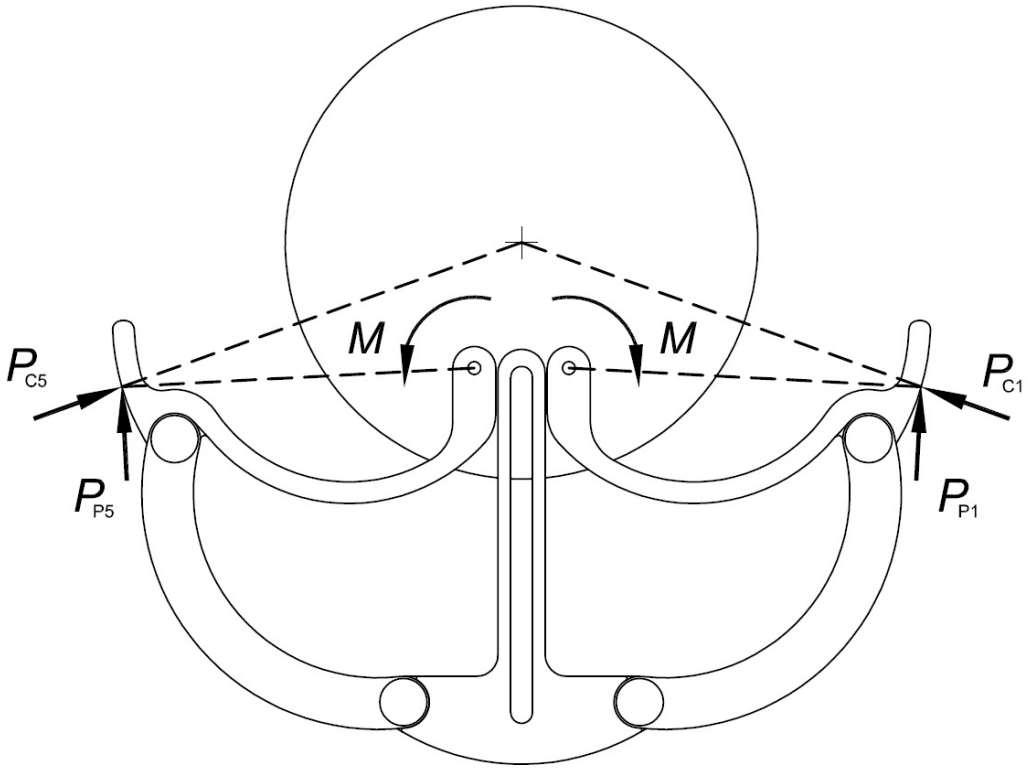


Figure 4.8: Circumferential forces P_{c1} and P_{c5} acting towards the centre of the microrobot resulting in perpendicular component forces P_{p1} and P_{p5} working to prevent the legs from opening

direction therefore, due to the legs being identical in geometrical design, only one side will require analysing. However the result of the analysis will be applicable to both legs.

To ensure the microrobot's legs can distend the GI tract wall and achieve a state of equilibrium the micromotor must deliver an equivalent or greater sum of reaction forces F_{pn} than the sum of the perpendicular component forces P_{pn}. This can be expressed as follows:

$$\sum_{n=1}^{6} F_{pn} \geq \sum_{n=1}^{6} P_{pn} \tag{4.11}$$

The magnitude of the reaction force F_{p1} (Figure 4.9) can be estimated for a leg movement through zero degrees to 90 degrees using the following formula:

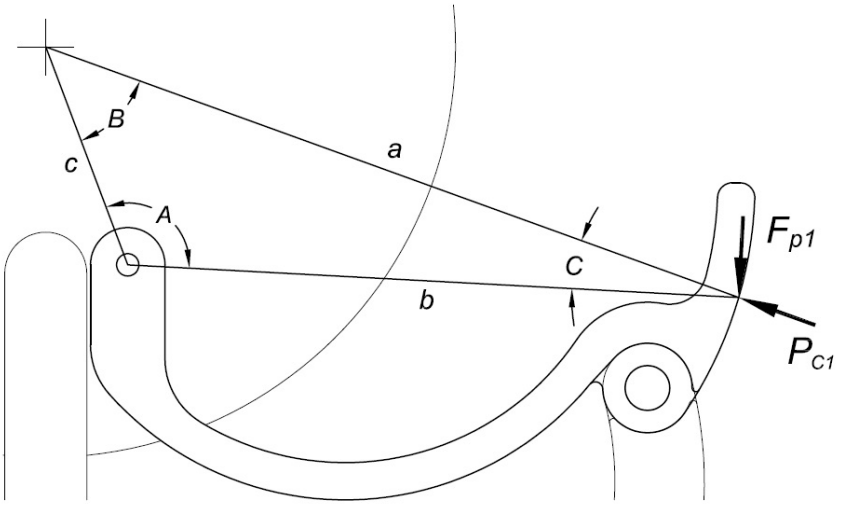


Figure 4.9: Circumferential force P_{c1} results in a perpendicular component force (P_{p1}) and a reaction force F_{p1} acting on the microrobot's leg

$$F_{p1} = P_{c1}\left(\frac{c(\sin A)}{\sqrt{b^2 + c^2 - 2bc(\cos A)}}\right) \tag{4.12}$$

Using formula (4.12) the calculated maximum reaction force acting on the leg is 45.6 mN, this occurs at an opening angle of 45 degrees. A plot of the full leg opening cycle can be seen in Figure 4.10.

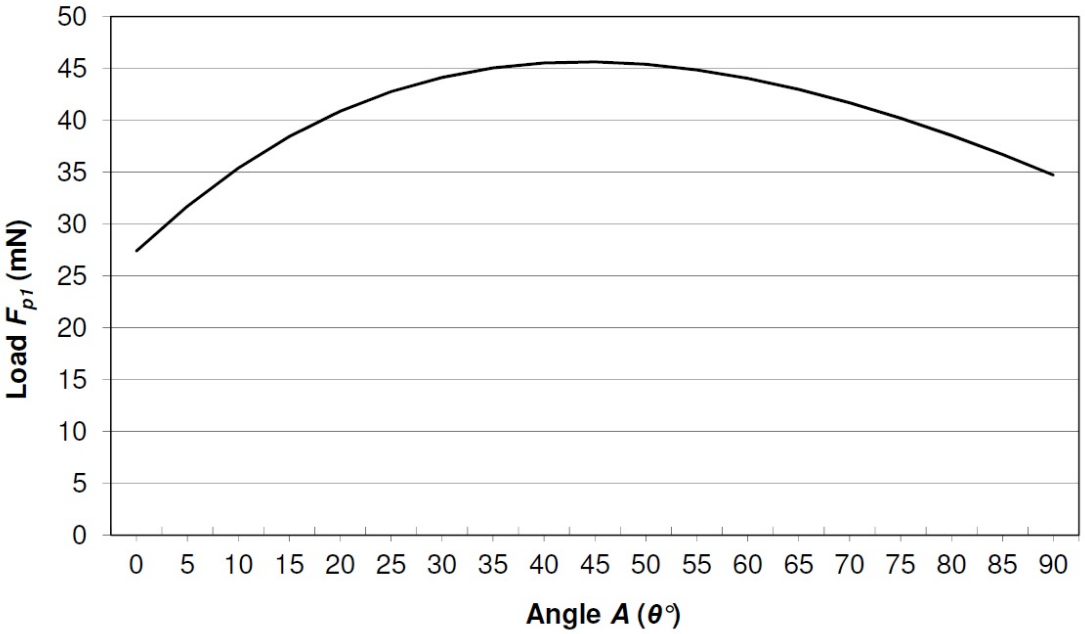


Figure 4.10: Graph plotting the reaction force F_{p1} of a full zero to 90 degrees opening cycle of the microrobot's leg

The circumferential force from the GI tract wall P_{c2} and P_{c4} will be acting on both tie bars, Figure 4.11. The tie bars link the legs to the centre support via pinned joints therefore they will contribute to the perpendicular component forces preventing the legs from opening. Similarly to the analysis of the legs only one of the perpendicular component forces F_{p2} or F_{p4} will require analysing due to the identical geometry, Figure 4.12. However both resulting forces will contribute to the total load.

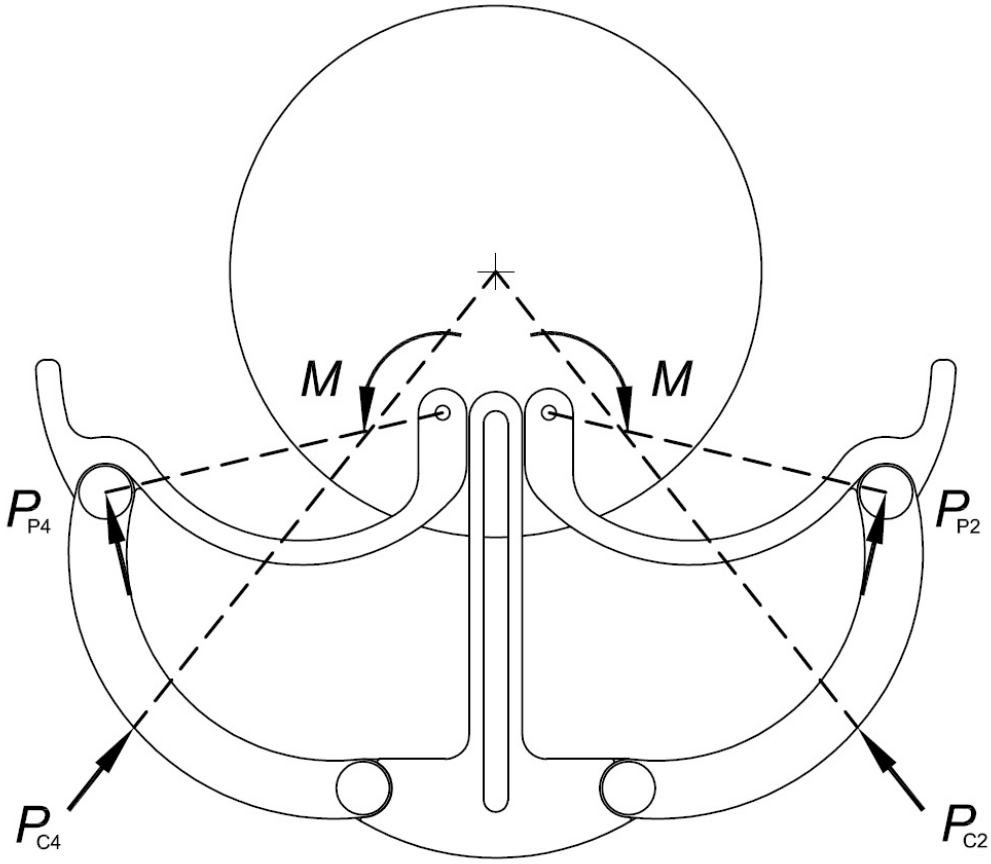


Figure 4.11: Circumferential forces P_{c2} and P_{c4} acting towards the centre of the microrobot result in perpendicular component forces P_{p2} and P_{p4} working to prevent the legs from opening

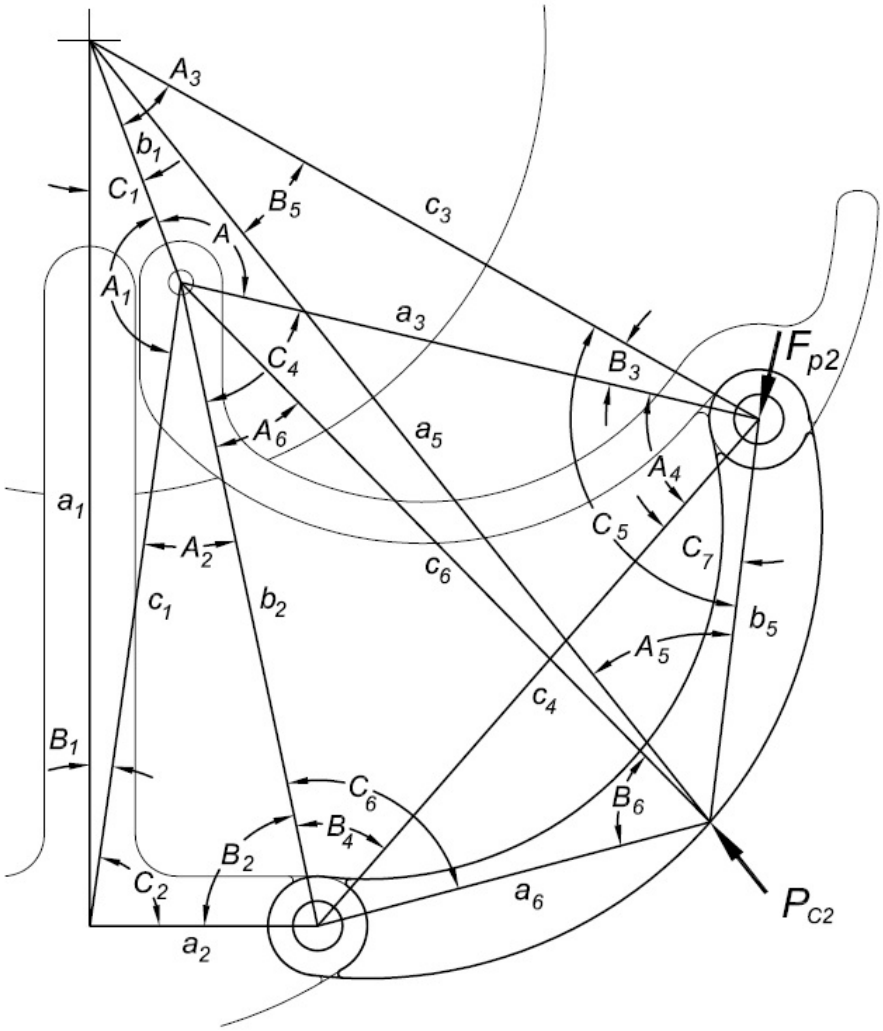


Figure 4.12: Circumferential force acting on the microrobot's tie bar P_{c2} results in a perpendicular component force (P_{p2}) and a reaction force F_{p2} acting on the microrobot's leg

The reaction force F_{p2} acting on the microrobot's leg, as a result of the circumferential force acting on the tie bar P_{c2}, can be seen in Figure 4.12 and can be estimated using the following formula:

$$F_{p2} = P_{c2} \cos\left[\tan^{-1}\left(c_3\left(\frac{\sin C_5}{b_5 - (c_3 \cos C_5)}\right)\right)\right] \sin\left[\cos^{-1}\left(\left({a_3}^2 + {b_2}^2 + {c_4}^2\right) - \left(\frac{{b_2}^2}{2a_3c_4}\right)\right) + C_7\right] \tag{4.13}$$

The 120.1 mN circumferential force acting on the tie bar (P_{c2}) equates to a reaction force F_{p2} of 83.9 mN and occurs at full extension. This can be seen in a plot of a full zero to 90 degrees opening cycle of the microrobot's tie bar in Figure 4.13.

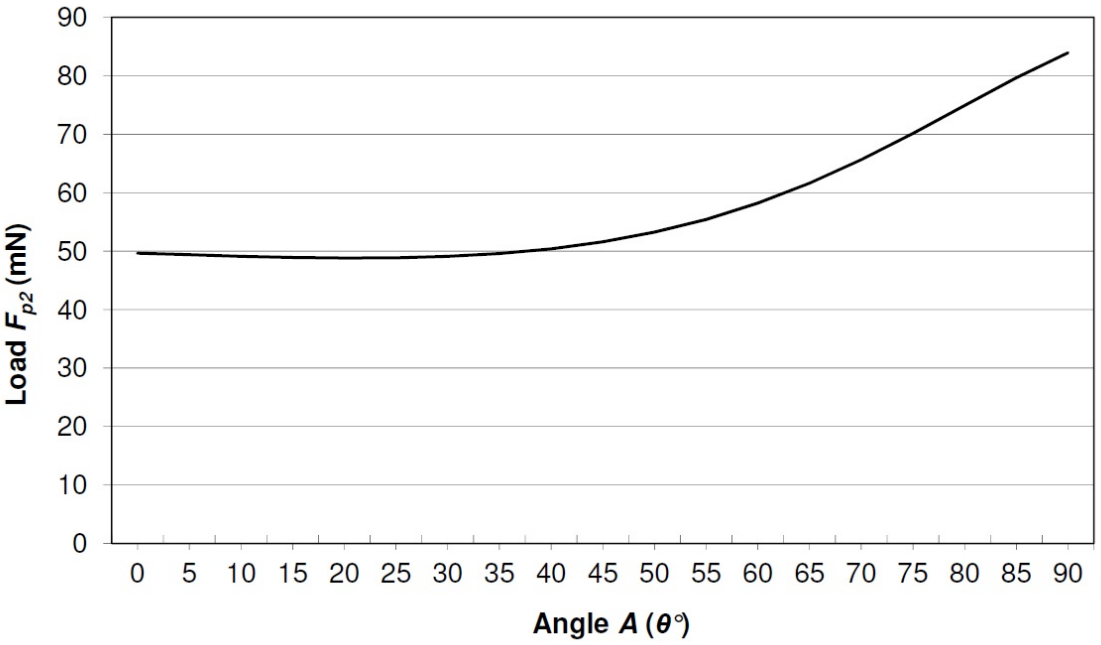


Figure 4.13: Graph plotting the reaction force F_{p2} of a full zero to 90 degrees opening cycle of the microrobot's tie bar

The circumferential peristaltic force P_{c3} acting on the centre support (Figure 4.14) would be split between the two pivot points linking the two tie bars, these two forces will result in the perpendicular component forces P_{p3} and P_{p6} which will work towards preventing the legs from opening. As the geometry and loading are symmetrical only one side of the centre support requires analysis, Figure 4.15.

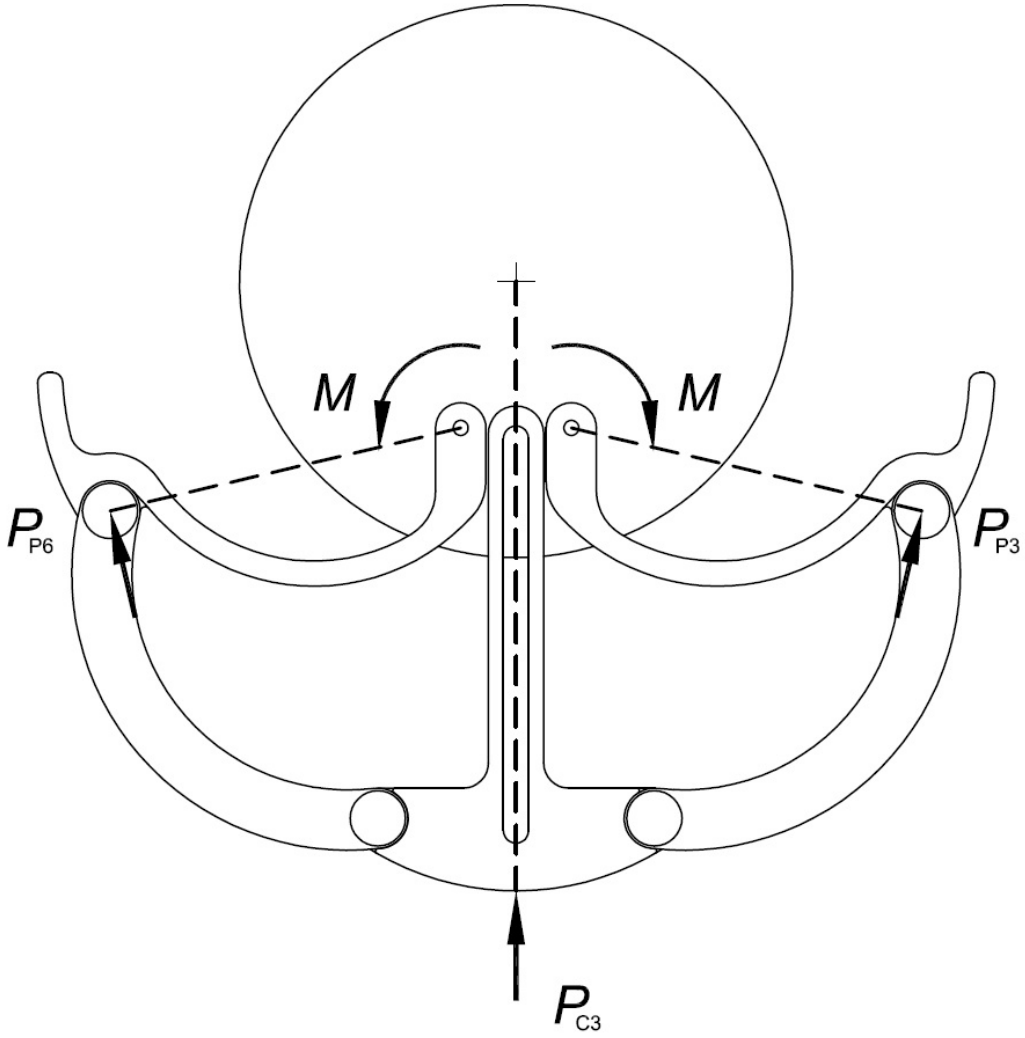


Figure 4.14: Circumferential peristaltic force acting on the microrobot's centre support P_{c3} results in perpendicular component forces P_{p3} and P_{p6} which will be working to prevent the legs from opening

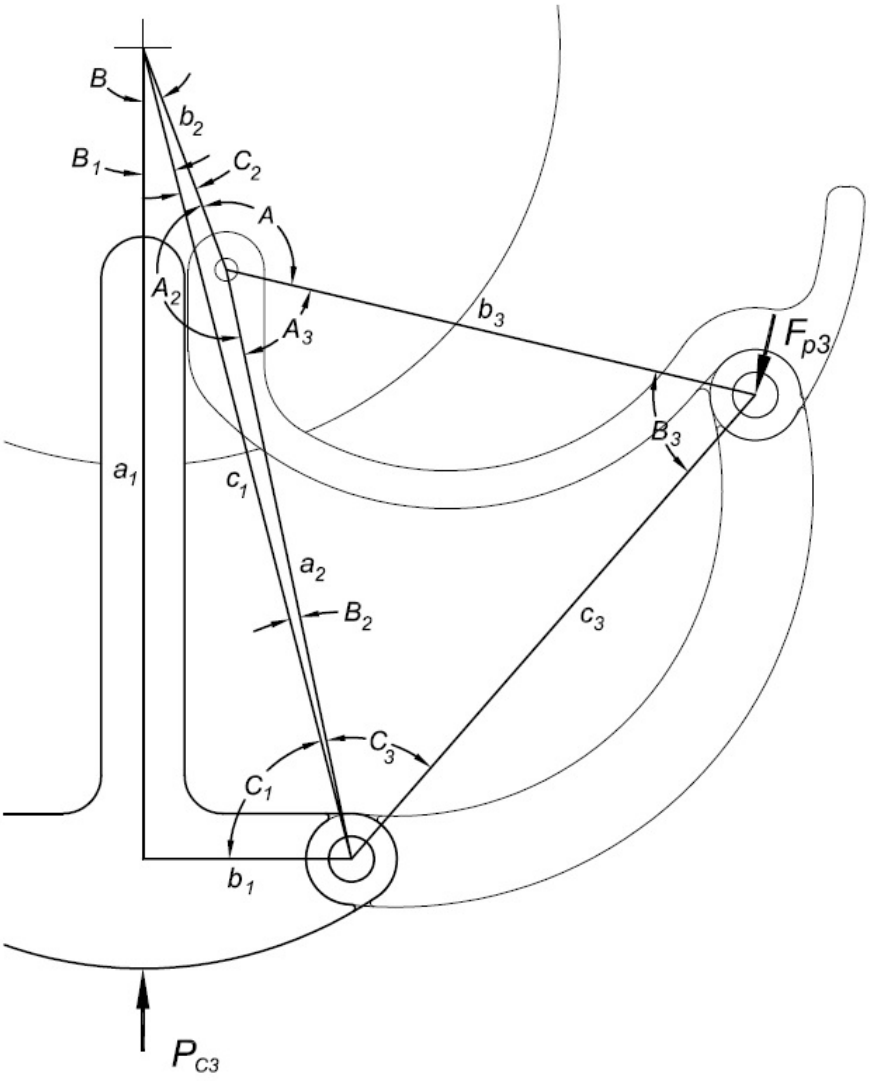


Figure 4.15: Circumferential force acting on the microrobot's centre support P_{c3} results in a perpendicular component force (P_{p3}) and a reaction force F_{p3} acting on the microrobot's leg. The centre support links the two tie bars

Figure 4.15 shows the reaction force F_{p3} acting on the microrobot's leg, as a result of the circumferential peristaltic force acting on the centre support P_{c3}, and can be estimated using the following formula:

$$F_{p3} = \left[\frac{P_{c3}/2}{\sin(180 - (C_3 + B_2 + C_1))}\right] \sin\left[\tan^{-1}\left(\frac{a_2 \sin A_3}{b_3 - (b_2 \cos A_3)}\right)\right] \tag{4.14}$$

Using formula (4.14) the maximum load acting on the centre support equates to 70.47 mN and also occurs at full extension. This can be seen in a plot of a full zero to 90 degrees opening cycle of the microrobot's centre support in Figure 4.16.

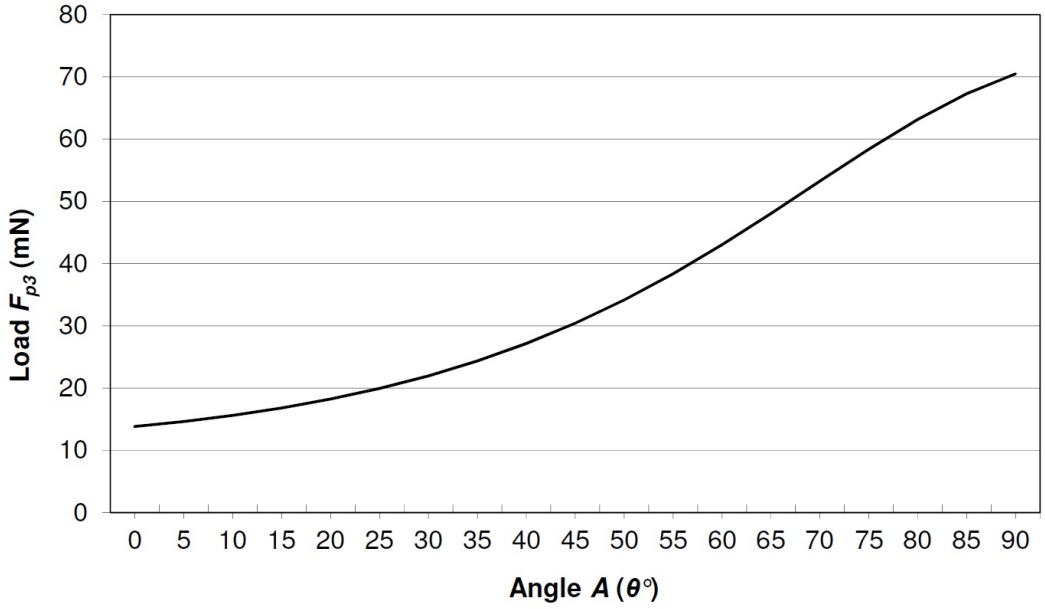


Figure 4.16: Graph plotting the reaction force F_{p3} of a full zero to 90 degrees opening cycle of the microrobot's centre support

4.4.1.2 Summation of Reaction Forces

The reaction forces F_{pn} must be equal to or greater than the sum of the perpendicular component forces P_{pn} acting on the microrobot's leg to ensure a successful holding mechanism deployment. As the micromotor's deliverable torque is known it can be compared to the sum of the reaction forces to determine if it is capable of delivering an equivalent force to the legs to maintain a state of equilibrium. The summation of the reaction forces F_p can be determined by the following formula:

$$F_p = \sum_{n=1}^{6} F_{pn} \tag{4.15}$$

The estimated reaction forces F_{p1}, F_{p2} and F_{p3}, as outlined in the analysis, can be com-

bined with F_{p4} the reaction force for the second tie bar, F_{p5} the reaction force acting on the second leg and F_{p6} the second reaction force acting on the centre support to find the maximum load which will be required to overcome the circumferential peristaltic contractions through a full zero to 90 degree leg movement. Figure 4.17 shows a plot of the combined reaction force F_p for a full leg operating cycle.

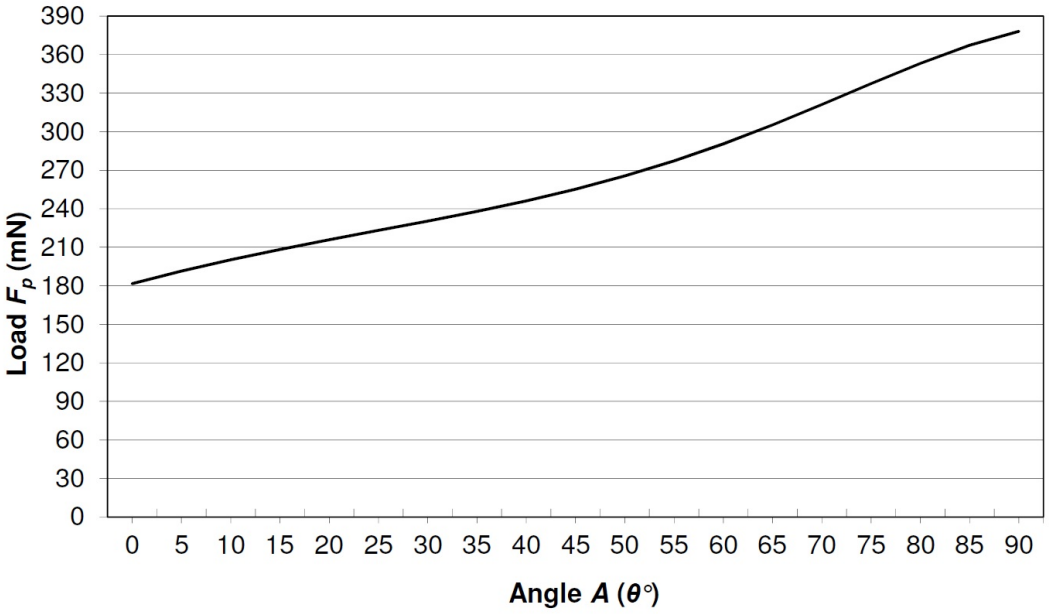


Figure 4.17: Graph plotting the combined individual estimated reaction forces F_{p1}, F_{p2}, F_{p3}, F_{p4}, F_{p5} and F_{p6} for a full zero to 90 degree leg operating cycle

The result of the combined reaction force plot (Figure 4.17) shows a load of 181.7 mN at the start of the opening cycle, rising to a maximum load of 378.15 mN at the end of the cycle. The maximum load occurs when the holding mechanism is fully expanded to 90 degrees, this results in a torque of 2.78 mNm acting on the final gear in the gear train. However the result of equation (4.3) shows an output torque (T_{out}) for the gear train to be 16.2 mNm, this gives a high margin of safety before the micromotor stalls. Further, the circumferential peristaltic force analysis represents a worst case scenario as the microrobot would be orientated at various angles when passing through the GI tract, this would reduce the applied loads on the legs and hence reduce the torque requirement of the micromotor.

4.4.1.3 Leg Member Stress Analysis

The radial peristaltic force (P_c) acting on the six external points of the holding mechanism will develop stress in the leg members as a result of the perpendicular component force (P_p) acting on them. As the available space for the holding mechanism is limited the legs have been optimised for size and shape therefore an evaluation of the stress induced in the leg members has been performed to determine if the legs yield under this load, Figure 4.18.

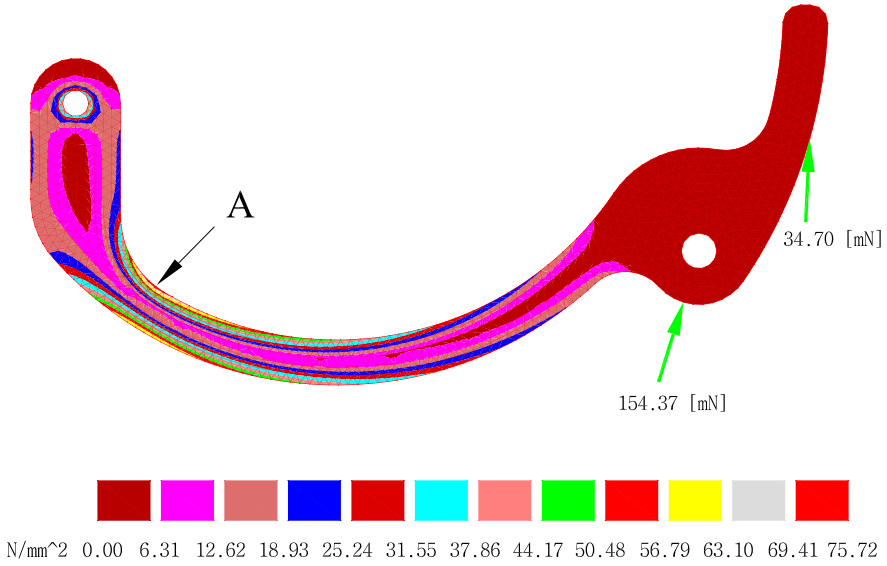


Figure 4.18: Von Mises FEA 2D isoareas analysis of the holding mechanism's leg modelled in stainless steel 304 with the maximum perpendicular component force (P_p) applied

The previous section showed that at the full extension of 90 degrees the maximum load will be distributed through the holding mechanism therefore an evaluation of the stress induced in the legs has been performed at this position. The Von Mises FEA analysis of the stainless steel 304 leg shows that the maximum stress induced in the leg is $75.72\,\mathrm{Nmm}^{-2}$ and that it acts at the surface at point A, Figure 4.18. At these levels of stress a polymer, such as PEEK, is an option for the leg material as its yield point is higher at $97.0\,\mathrm{Nmm}^{-2}$ however a mechanism manufactured from metal would offer greater strength and stability and also limit any deflection from other external forces such as the longitudinal peristaltic force.

4.4.2 Longitudinal Peristaltic Force Analysis

Although the longitudinal peristaltic force does not contribute to the holding function it may have a direct influence on the operating performance of the holding mechanism. The longitudinal force acting on the legs could potentially bend them out of position and prevent them from being retracted back into the microrobot's body and hence become a permanent obstruction. Figure 4.19 shows the longitudinal forces acting on the legs of the microrobot.

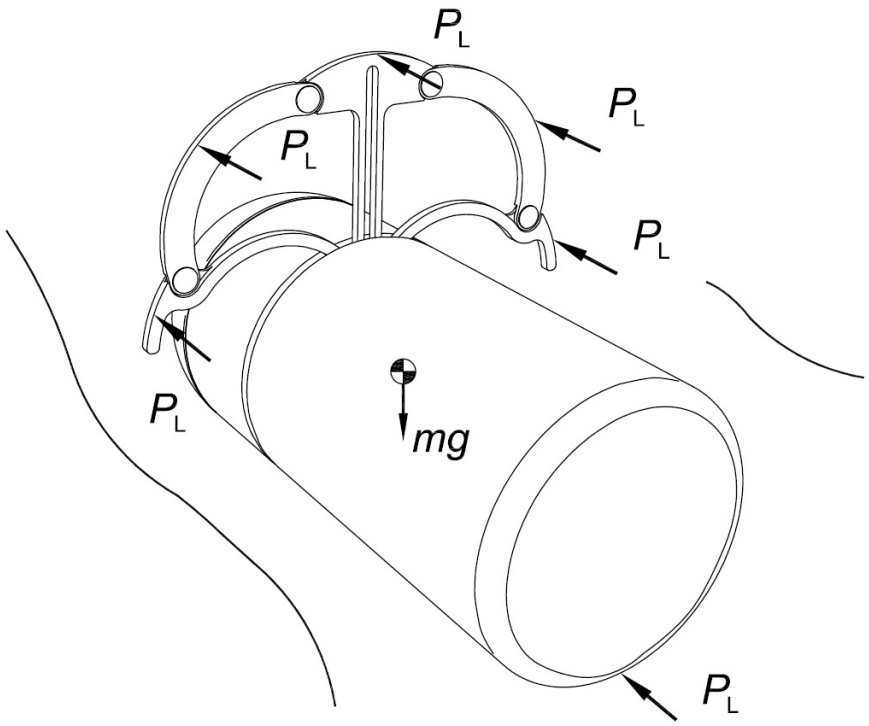


Figure 4.19: External longitudinal peristaltic force P_L acting on the microrobot at six positions

For the purpose of the force analysis the longitudinal peristaltic force contact area has been divided into six contact points positioned linearly with the microrobot's boy, Figure 4.19.

Using the figures determined by Miftahof (2005) [5] the maximum longitudinal amplitude of muscle contraction is 17.2 g/cm. Based on a body length of 32.0 mm long this results in an estimated load of 539.94 mN for the total linear contact area of the microrobot's body.

To determine if the longitudinal peristaltic force P_L will influence the deflection of the legs at full extension we must first calculate the force acting at each point of contact. This can be calculated by the following formula:

$$P_L = \frac{F_L + mg}{6} \tag{4.16}$$

Where F_L is the longitudinal peristaltic force from the GI tract wall, m is the mass of the microrobot and is estimated to be 3.45 g and g is gravity.

Using formula (4.16) the load (P_L) acting at each point equates to 95.63 mN. This load will work towards deflecting the legs however the five points will be focused onto the four main leg supports A, B, C and D, Figure 4.20.

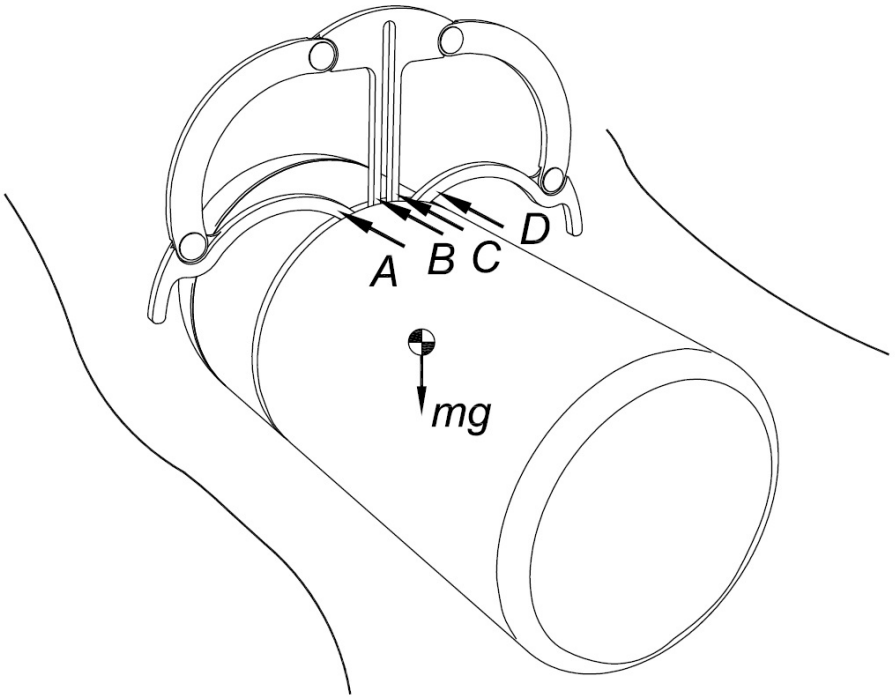


Figure 4.20: Four main leg supports A, B, C and D which will be subjected to the combined longitudinal peristaltic force acting on the holding mechanism

The holding mechanism's leg supports will be subjected to a total force of 478.16 mN. For the purpose of simplifying the bending analysis we will investigate the deflection of

leg support B as this has the smallest cross sectional area (Figure 4.20). It will have a proportional longitudinal load of 119.54 mN applied to it.

Using the principle of a cantilevered beam the load (P) at the free end can be used to determine the displacement (δ) of the beam by rearranging the following formula [6]:

$$P = \frac{3EI_x\delta}{L^3} \tag{4.17}$$

Where L is the length of the leg and E is the material's Young's modulus. I_x represents the moment of inertia through section $x - x$ for a solid rectangular beam and is given by:

$$I_x = \frac{bh^3}{12} \tag{4.18}$$

Where b is the width and h is the height of the beam's cross section.

Using formula (4.17) the calculated maximum deflection of leg support B at full extension equates to 37.10 μm. This is based on the leg being manufactured from stainless steel 304. A plot of the bending profile for a full deployment of leg support B can be seen in Figure 4.21.

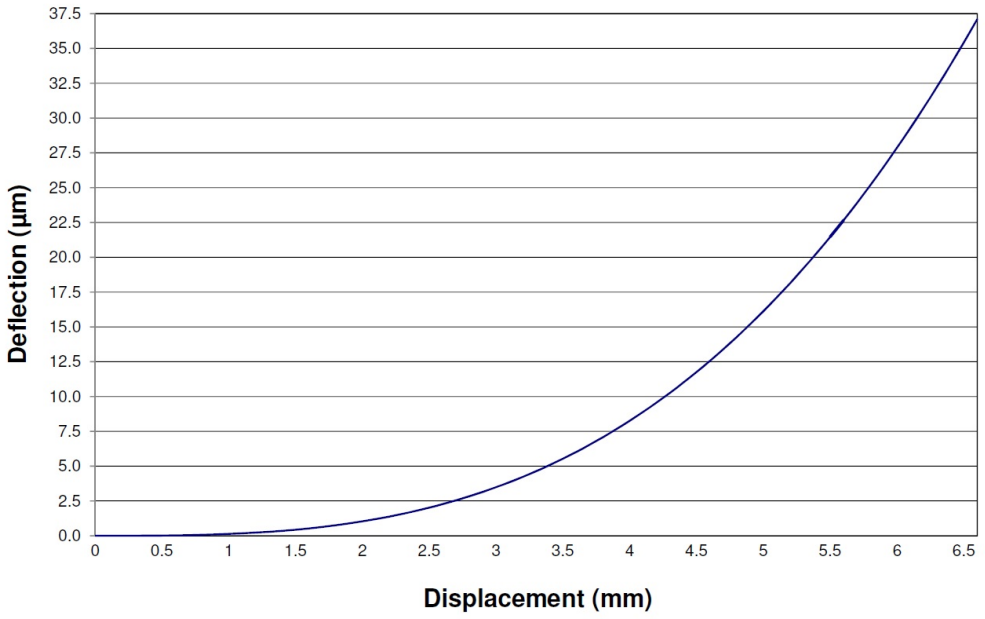


Figure 4.21: Plot of the holding mechanism bending profile for the longitudinal peristaltic force acting on leg support B modelled in stainless steel 304

The effect of the longitudinal peristaltic force acting on the holding mechanism appears to be limited as at maximum extension (6.6 mm) the deflection is only 37.10 μm. However due to the limited space the supports have very small cross sectional areas hence the deflection represents 9.27% of the leg's thickness therefore the deflection may result in potentially high induced stress in the leg.

Using beam bending theory the maximum bending stress induced in the leg can be calculated by the *flexure formula* [6]:

$$\sigma_{max} = \frac{Mc}{I_x} \tag{4.19}$$

Where σ_{max} is the maximum normal stress in the beam and will occur at a point furthest away from the neutral axis, M is the maximum bending moment (comprising of the length L of the beam multiplied by the load P), c is the perpendicular distance from the neutral axis to a point farthest away from the neutral axis and I_x is the moment of inertia of the cross-sectional area through section $x - x$.

At a maximum deflection of 37.10 μm the longitudinal peristaltic force (P_L) will induce a stress of 98.62 Nmm^{-2} in leg support B. At these levels of stress it would be inadvisable to use a polymer for the leg material as there would be insufficient capacity to accommodate unforeseen external forces. However manufacturing the leg support from stainless steel 304, which has a yield point of 290 Nmm^{-2}, would offer a safety factor of approximately three times therefore the structural integrity of the holding mechanism can be assured.

The deflection analysis represents a worst case scenario as the design of the housing for the legs attempts to reduce the impact of bending by supporting the legs between the gearbox housing and a retaining plate. A further degree of support will be gained from the connection between the gears and the legs as the drive shaft connecting the gears to the legs passes through the gearbox housing, the leg and into the retaining plate. This method of assembly will give support to both sides of the drive shaft and hence help to limit the deflection of the legs.

4.5 Prototype Manufacture

The following section presents a discussion of the prototyping methods selected to produce the component parts of the holding mechanism. The advantages and limitations of the cho-

sen manufacturing processes are evaluated and the resulting component parts are presented. The section focuses on the legs, tie bars and gear train components however the gearbox and retaining plate have been manufactured using similar methods.

4.5.1 Gear Train Prototyping

There are a number of process routes which can be used to produce the holding mechanism's gear train, for example hobbing, rapid prototyping or wire EDM are all methods which could be employed to produce the spur gear set which drives the legs in and out. However results from a preliminary trial modeling 1:1 scale model parts using an SLA process yielded component parts which could not perform to the required level, therefore a more conventional manufacturing process was chosen. The need for accurate feature geometry and the restrictions in material choice combined with the costs associated with manufacturing microscale parts resulted in the selection of a CNC milling process to produce the 5:1 scale model prototypes. Figure 4.22 shows a 5:1 scale model of the complete gear train assembled in the gearbox housing.

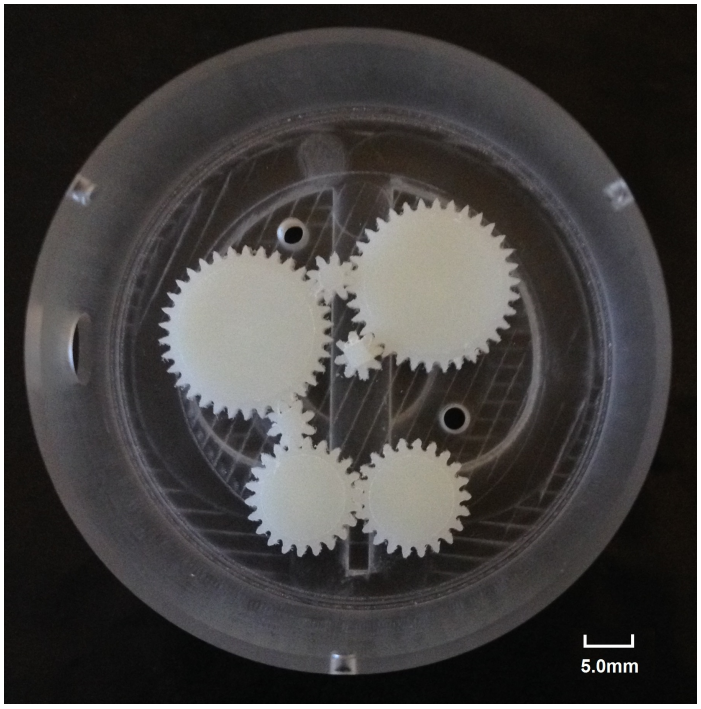


Figure 4.22: 5:1 scale prototype of the holding mechanism's gear train manufactured from Nylon 6 and gearbox modelled in PMMA

Figure 4.22 shows a prototype of the gear train using all the gears specified in the concept design (Figure 4.3 and Table 4.1). However the gears have been orientated in a chain rather than the 8 toothed gears being stacked on top of the 34 toothed gears. The purpose of the simplified prototype was to manually test the functionality of the bevel gear set and the holding mechanism's legs as the simpler design requires only 2.6 turns to fully operate the mechanism whereas the compound gearbox would require 46 turns to fully operate the legs.

Prototyping the gears using a CNC milling machine allowed the use of small diameter end mills (Ø0.5 mm) to generate the tooth profiles and to achieve the tight root radii of the teeth. However the use of Nylon 6, which was selected for its mechanical properties from a limited list of materials, resulted in the gears having significant burrs owing to the manufacturing process, Figure 4.23.

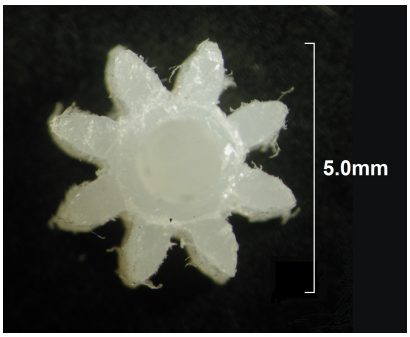


Figure 4.23: CNC milled 8 tooth spur gear manufactured from Nylon 6. The profile of the teeth are obscured by significant burring

There are a number of manufacturing issues which can leave the gears with excessive burrs, for example the end mill feed rate may be too fast or the wrong style of cutter may be selected. Cutter selection is very important as different materials have different requirements. Cutting plastic requires a sharp edged tool therefore a hollow ground edged tool is preferable over a radially ground tool as it will be sharper and result in a cleaner edge.

4.5.1.1 Gear Measurements

Under a microscope at 30X magnification the burrs from the 8 tooth spur gears were removed with a very sharp blade to allow inspection of the gears in order to confirm dimensional accuracy. Inspection was performed on a profile projector type PJ-300 manufactured by Mitutoyo at 10X magnification and a Mitutoyo 0-25 mm digital micrometer. The measured

results have been collated in Table 4.3.

Table 4.3: Statistical measured data for the 0.5 module, 8 tooth spur gears

	Value (mm)	**Average (mm)**	**Min. (mm)**	**Max. (mm)**	**Standard deviation**
Outside diameter (OD)	5.0	5.032	5.02	5.04	0.008
Face width (b_t)	2.25	2.291	2.28	2.30	0.009
Tooth thickness (t)	0.785	0.798	0.79	0.81	0.006
Tooth depth (h_t)	1.2	1.16	1.14	1.18	0.011

Comparing the measured dimensions with the design values shows that the average gear tooth thickness is greater than the nominal value and that the average tooth depth is shallower than nominal. The measured dimensions are well within the expected manufacturing tolerance limit for the given part however the tendency for the teeth to be slightly bigger than required may pose problems with the gears meshing and running smoothly in the assembly.

4.5.1.2 Gear Train Performance

As can be seen from Figure 4.23 there are significant burrs on the top and bottom of the teeth profiles, these burrs are also evident on the larger gears in the train although not to such an extent. The burrs can influence the performance of the gear train in a number of ways, they can directly change the gear profile by being trapped between the rotating teeth and, in addition, the excess material will reduce the clearance between the gears, these two faults may result in a greater bending load being imposed on the tooth. The reduced clearance will also increase the friction within the system which places a greater load on the micromotor driving the train.

The average thickness of the teeth (0.798 mm) suggests that the gear train would not run smoothly due to the reduced clearance however on the larger gears the average thickness of the teeth was undersized (0.71 mm). This compensated for the thicker teeth and resulted in a smooth running gear train, once the burrs had been removed. The slightly larger sized teeth on the smaller gears are an advantage in this instance as they can withstand a greater bending stress during operation.

4.5.1.3 Bevel Gear Set

The bevel gear set allows rotation from the micromotor to be translated through 90 degrees. To allow efficient translation the bevel gear adopts an involute gear profile however the section profile reduces in scale from the larger outside edge to the smaller inner edge. The diminishing form terminates at the pitch apex which is the point where the centre of the two gears meet. The complexity of the gear profile would require a generating type of bevel gear cutting machine [7]. However as the gear tooth loading analysis in Section 4.3.3 reported, the bevel gear will be subjected to limited stress during an operation therefore an SLA manufacturing process was selected. This method of manufacture offered approximately 80% cost reduction compared to CNC milling. Figure 4.24 shows the prototype bevel gears and bevel gear cover designed using AutoCAD Inventor 2014 and modelled in Accura 60.

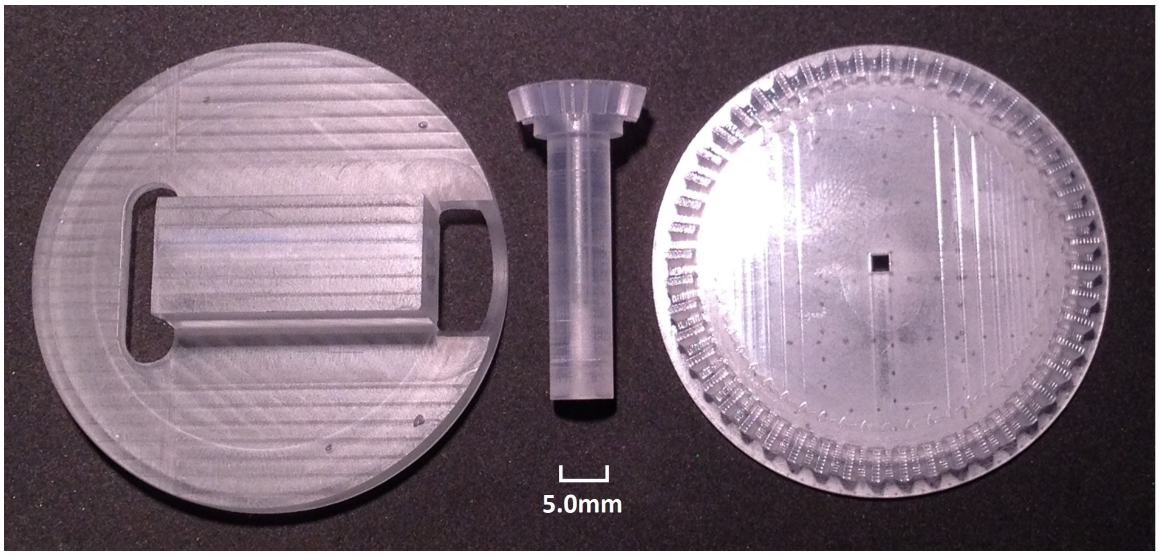


Figure 4.24: Bevel gear set manufactured by SLA in Accura 60 and bevel gear cover manufactured by CNC milling from PMMA

Modelling the gears using the SLA process offered further advantages, for example it was possible to produce a square hole in the centre of the 48 toothed bevel gear for the purpose of mating with and driving the 8 toothed spur gear. Also the dimensional accuracy of the SLA parts, when produced using the high resolution mode, resulted in a tolerance band of ± 0.008 mm for the teeth. The mounting distance, which is the distance from the back of the 48 toothed gear to the centre of the 13 toothed gear, was increased by 0.35 mm from the nominal design specification to allow for running clearance between the gears and

to accommodate for any tolerance stack-up between the parts. A disadvantage of the SLA process is that the surface finish of the component is influenced by the layering technique and can result in a stepped surface. However the orientation in which the gears were made resulted in smooth surfaces at the sides of the teeth and a more pronounced stepped surface at the top of the tooth. This resulted in the gear set running smoothly with very little back lash (0.12 mm).

4.5.2 Holding Mechanism Prototyping

The holding mechanism has been designed to unfold from inside the protective case in a similar way to the unfolding wings of a ladybird. The mechanism is protected on either side by the gearbox housing and a retaining plate. The holding mechanism comprises a micromotor, gearbox, retaining plate, two M3 screws, two legs, a centre support, two tie bars and four pins. Figure 4.25 shows the individual prototyped parts of the holding mechanism.

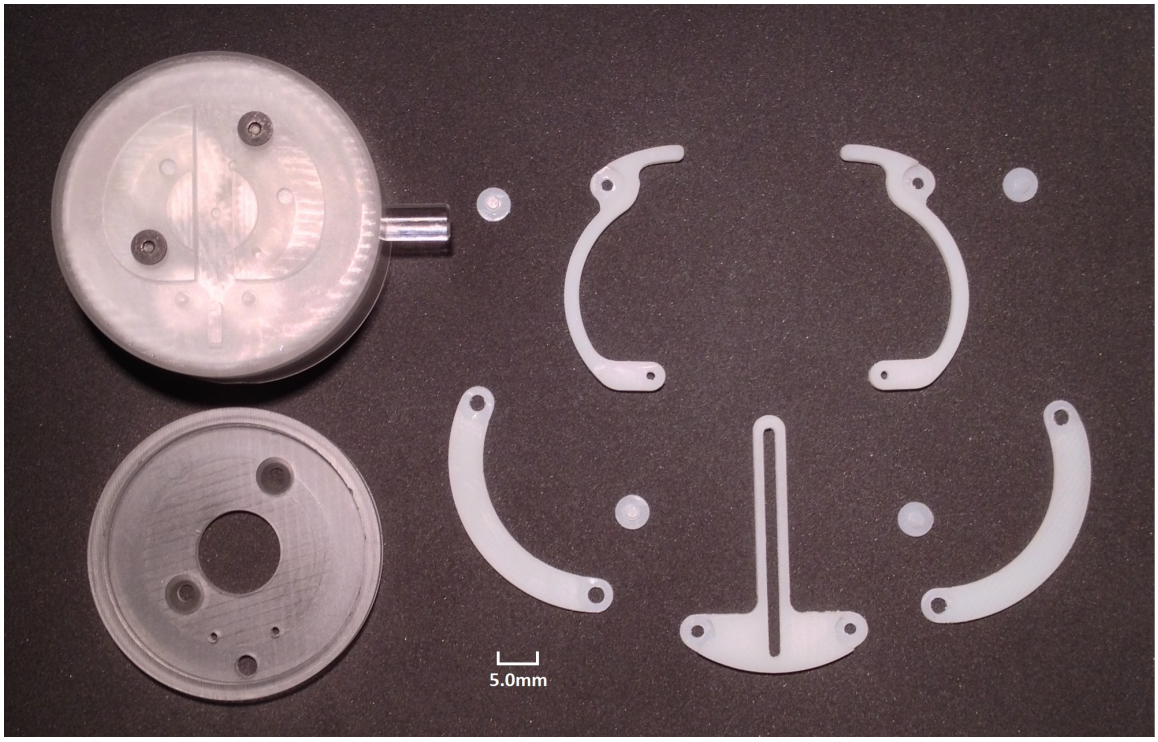


Figure 4.25: Individual parts of the holding mechanism: assembled gearbox, retaining plate, M3 screws, legs, centre support, tie bars and pins

The final two gears in the gear train are the 22 toothed gears, these gears are the means of driving the holding mechanism. A driveshaft protruding from the gear passes through the gearbox, with sufficient clearance to allow the gear to rotate freely, and is press fitted into a corresponding hole at the proximal end of the leg. The driveshaft extends into the retaining plate giving support to both sides of the leg this will help to minimise deflection of the leg when it is at full extension. The gearbox has a centrally positioned boss shaped such that it offers support to the legs when they are in the stored position and prevents them from collapsing inwards. The boss prevents the legs from opening and closing unevenly as it guides the centre support via a channel which prevents the support from twisting, Figure 4.26. The centre support has an integral slot which accommodates a peg mounted on the gearbox. The purpose of the peg is to prevent the mechanism from over running and falling out of the body, Figure 4.27. A greater stroke length could be achieved from the holding mechanism by increasing the length of the slot in the centre support as this would give a greater circumferential reach to the holding mechanism. However the shape of the distal end of the legs has been designed to accommodate cables which must pass through the gearbox to provide power to the micromotor, camera and processor (Figure 4.26).

The Nylon 6 pins are press fitted into the legs and centre support, they facilitate the free movement of the tie bars and centre support however the thickness of the tie bars does not allow for sufficient support from the shank of the pins. Insufficient support may allow the bars to buckle and hence they will not be retracted back into the microrobot's body. To overcome this issue the pins have large diameter heads which act not only to retain the tie bars but also to prevent them from twisting and buckling. Press fitting the pins as opposed to using nuts and bolts for a secure pivoting method significantly reduces the space requirement.

The retaining plate serves two purposes. Firstly it keeps the legs and tie bars from running out of position and secondly it connects the holding mechanism to the main body of the microrobot and allows the holding mechanism to rotate about the body. A second boss is used to align the retaining plate with the gearbox. The benefit of this method of assembly is that it does not add any length to the body yet provides stability and a quick method of alignment. The fixings used to hold the retaining plate in position are M3 countersunk head screws with hexagon sockets manually modified to the correct length. The locations of the screws have been chosen such that their heads miss the legs and the threads miss the gears in the gearbox. Using countersunk head screws takes advantage of their heads' slim profile to minimise the impact on the overall length of the microrobot.

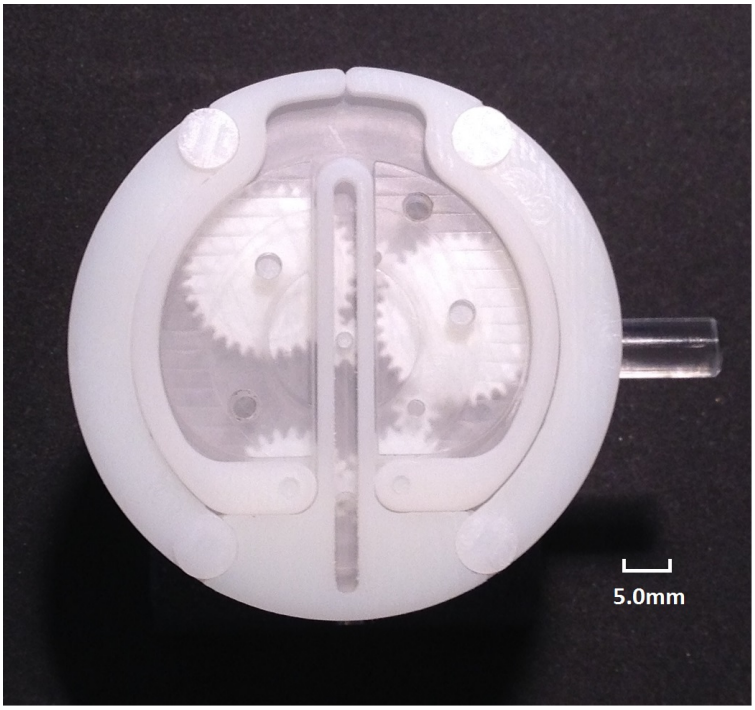


Figure 4.26: Holding mechanism fully collapsed. The shape of the distal end of the legs has been designed to accommodate cables. Retaining plate has been removed for clarity

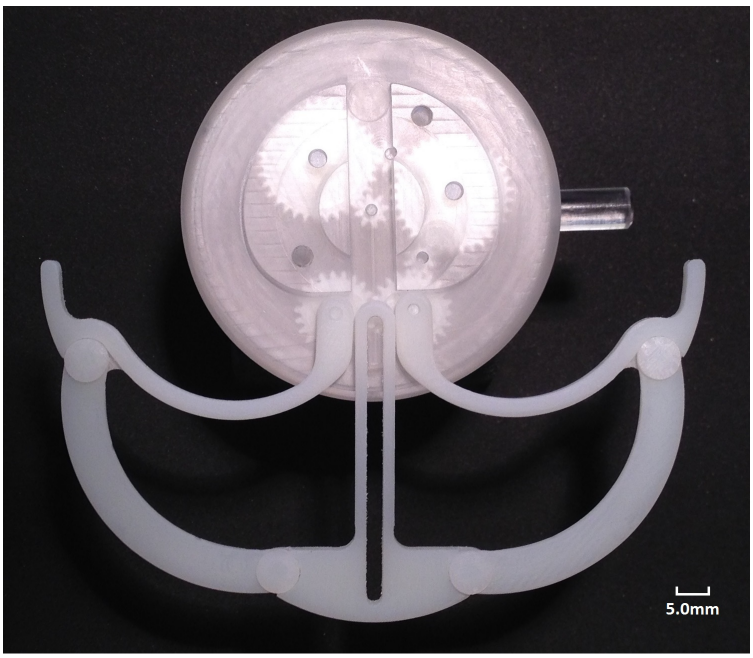


Figure 4.27: Holding mechanism fully expanded. The peg in the centre support slot prevents over expansion of the mechanism. Retaining plate has been removed for clarity

4.5.2.1 Holding Mechanism Performance

The holding mechanism has been designed for ease of manufacture and also for ease of assembly. However there were a number of issues with individual component parts and with the assembly of the parts which required addressing before a working prototype could be realised. Figure 4.28 shows the fully assembled holding mechanism with the retaining plate secured in position with two M3 countersunk head screws and titanium pins fitted to secure the tie bars.



Figure 4.28: Holding mechanism fully extended with retaining plate secured in position and titanium pins fitted to secure the tie bars

Manually operating the gearbox, through a driveshaft mounted onto the 13 toothed bevel gear and protruding through the side of the gearbox (Figure 4.26), resulted in three and a half turns being required to fully expand the holding mechanism and three and a half turns to collapse it. However the calculated number of turns required to operate the mechanism was 2.6 turns. The difference in these two figures can be attributed to the backlash in the gear train which predominantly comprises of the clearance between the gears, required for free running, and also the clearance between the gears' driveshaft

and the housing. A press fit was designed for the gears' driveshaft with the leg however manufacturing methods resulted in an oversized hole in the leg preventing the driveshaft from being securely retained. The issue of slipping was overcome by the application of an adhesive to the driveshaft however a more secure solution for the future would be to integrate the final gear in the train with the leg.

The simple means of connecting the tie bars to the centre support and legs was via a press fitted pin however the manufacturing accuracy of the Nylon 6 pins and the holes in the legs and centre support resulted in an inadequate connection. A further contributing factor was due to the thin section the pins would be mating with as the lack of material offered insufficient support to the press fit and hence it could not retain the pin. To overcome this issue new pins manufactured from titanium were made to suit the holes however if the pins, legs and centre support were manufactured in stainless steel the joint would be secure.

4.6 Measurement and Characterisation of the Holding Mechanism

This section presents a series of experiments designed to validate the holding mechanism. The experiments have been designed to characterise the holding mechanism through quantitative assessment of a 5:1 scale model prototype test rig manufactured using conventional manufacturing processes from Nylon 6 (PA6) and aluminium alloy (7075-T651). The bevel gear set was manufactured using an SLA process in Accura 60. The mechanical properties of the 5:1 scale prototype are related to the materials' Young's modulus and the geometry of the component parts therefore the performance of the 5:1 scale prototype suggests that future prototypes at 1:1 scale will perform as designed.

4.6.1 Motor Torque Protocol

The holding mechanism operates through a micromotor driving a gear train which opens and closes two legs. To determine the overall efficiency of the holding mechanism system the input must first be characterised. The 5:1 scale of the prototype test jig limits the allowable torque which can be transmitted through the gear train; the deliverable torque is further limited by the available manufacturing processes and available materials. Therefore a specifically configured motor will be used which offers the correct input characteristics suitable to operate the 5:1 scale test jig safely.

A 9 V DC motor and 16:1 gearbox have been specifically wound to deliver a speed of 275 RPM and a torque of 5 mNm at 52 mA. The motor's performance at the selected current should deliver the required torque however inaccuracies, such as the variations in resistivity of the coils and also variations in the magnetic flux density of the magnets and how well they are aligned, can cause the torque constant to vary by ±7%. Further manufacturing inaccuracies will also be present in the two stage 16:1 gearbox which is rated at 80% efficiency. To overcome the limitations of manufacturing and establish an accurate output from the motor assembly the actual output torque from the motor will be measured. A motor controller will be used to set the motor's parameters and control the input current. A 20 mm long arm fixed to the motor will be used to measure the torque delivered at the set current.

4.6.1.1 Motor Torque Procedure

The test set-up used to determine the load generated by operating the 9 V DC motor and gearbox is presented in Figure 4.29.

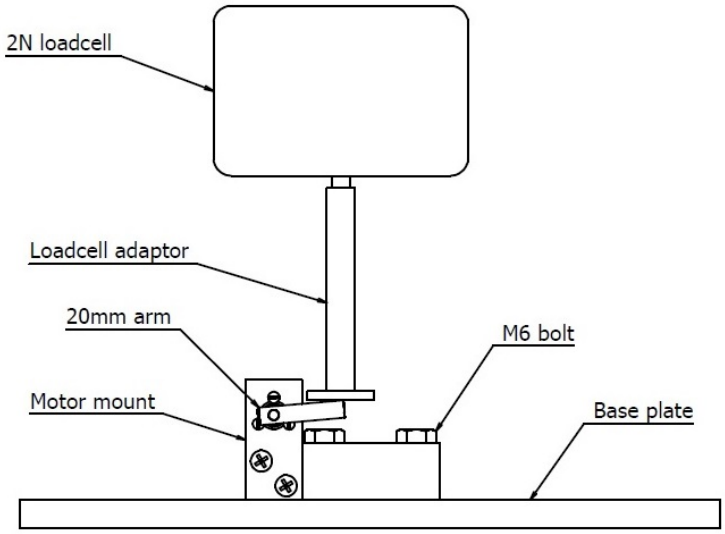


Figure 4.29: Layout of the test fixture to determine the output torque of the 9 V DC motor and 16:1 gearbox at 52m A

To determine the deliverable torque of the 9 V DC motor and gearbox (DCX12S EB KL 9 V DC motor and GPX12 AA 16:1 planetary gearhead, Maxon Motor UK Ltd.) an arm

with a known length is rotated using an input which is set via a motor controller (ESCON 36/2 driver (403112)). The motor controller is programmed to supply a current of 52 mA. The controller is configured via a USB interface and graphical user interface (ESCON studio 2.2). The motor is driven counter-clockwise rotating a 20 mm long arm into a 2 N loadcell (Intelligent loadcell ILC 879-009, ±0.1% of full scale) which is mounted on a MultiTest 2.5-*i* (805-102) test system manufactured by Mecmesin. The stall torque will be measured and recorded for a duration of 10 s on a computer running Emperor^{TM} (force) software (V 1.18-408 (5/10/13)) and connected to the MultiTest system. The test will be performed 10 times and the average force used to calculate the motor's deliverable torque at 52 mA.

4.6.1.2 Results and Discussion

The deliverable motor torque test set-up can be seen in Figure 4.30.

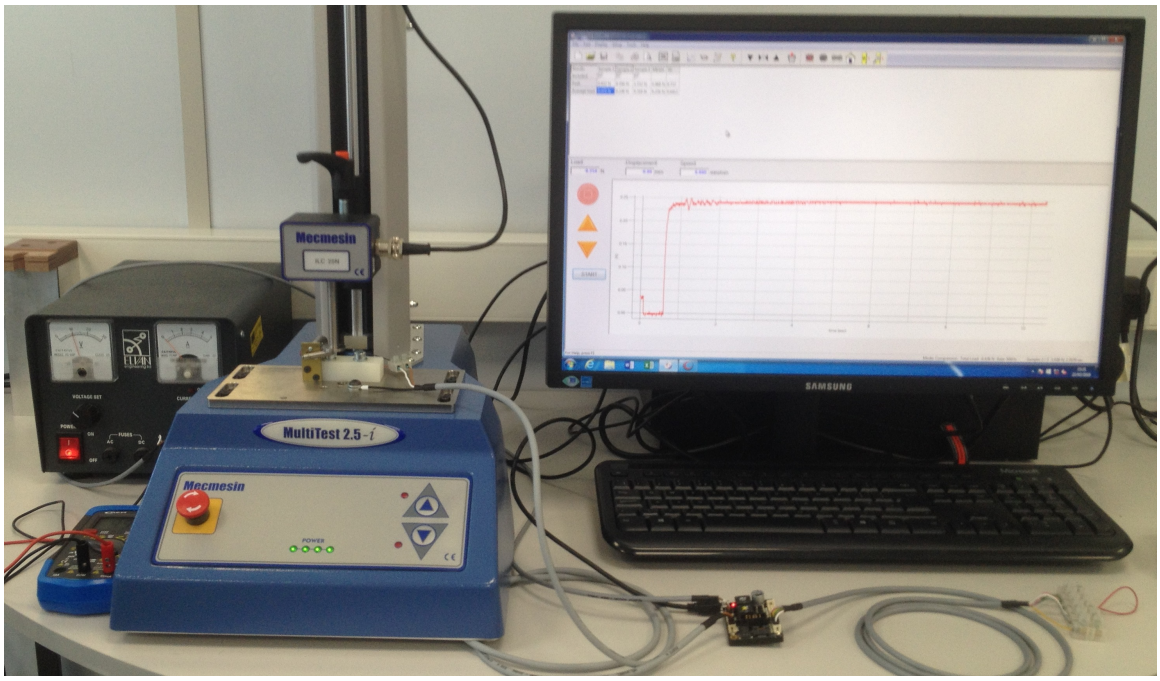


Figure 4.30: Deliverable motor torque test set-up comprising: a motor controller driving a 9 V DC motor and 16:1 planetary gearhead attached to a 20 mm long arm. The arm contacts a MultiTest 2.5-*i* test system fitted with a 2 N loadcell and connected to a computer running Emperor^{TM} (force) software

The average measured load generated by the 20 mm long arm at 52 mA was 248 mN. The measured load equates to a torque of 4.96 mNm which is 99.2% of the required 5 mNm.

The motor and gearbox have been characterised in terms of the input current and output torque. These input parameters can now be used to calculate the efficiency of the gearbox.

4.6.2 Gearbox Torque Protocol

A requirement of the gearbox is to transmit power from the 9 V DC motor to the final gear in the gear train, which has the function of driving the legs of the holding mechanism in and out. To guarantee a successful procedure the final gear in the gear train must supply sufficient torque to drive the legs therefore the efficiency of the gearbox must be validated. Using the established motor input parameters this experiment sets out to establish what torque is being generated at the final gear in the gear train and what the efficiency of the gearbox is.

4.6.2.1 Gearbox Torque Procedure

The test set-up used to determine the efficiency of the 5:1 scale prototype gearbox can be seen in Figure 4.31.

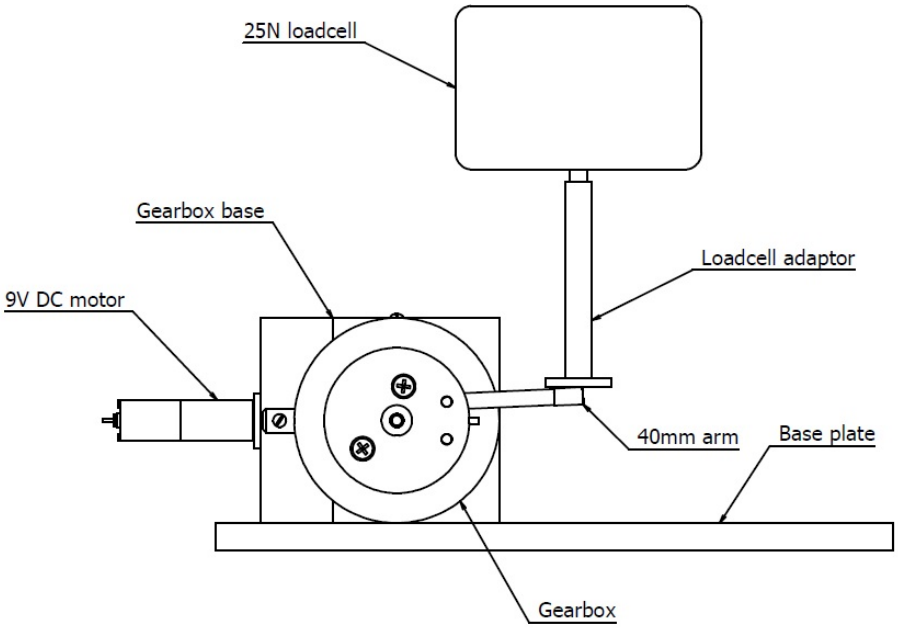


Figure 4.31: Layout of the test fixture to determine the efficiency of the 5:1 scale prototype gearbox with an input motor torque of 4.96 mNm

A 5:1 scale prototype gearbox manufactured from Nylon 6 (PA6) and aluminium alloy (7075-T651) will be tested using a 40 mm long arm attached to the output driveshaft of the final gear in the gear train using a similar test method to the motor torque test protocol. A torque of 4.96 mNm will be applied to the motor driving the gearbox which has a gear ratio of 183:1. The operation of the gearbox will be controlled via a rocker switch connected to a motor controller (ESCON 36/2 driver (403112)). The load developed by the arm will be measured by a 25 N loadcell (Intelligent loadcell ILC 879-002, ±0.1% of full scale) which is mounted on a MultiTest 2.5-*i* (805-102) test system manufactured by Mecmesin. The load profile of the 40 mm long arm will be measured and recorded for a duration of 10 s on a computer running Emperor^{TM} (force) software (V 1.18-408 (5/10/13)) and connected to the MultiTest system. The test will be performed 10 times and the average peak force used to calculate the gearbox's deliverable torque and efficiency.

4.6.2.2 Results and Discussion

The test set-up used to measure the efficiency of the gearbox can be seen in Figure 4.32.

Initial tests showed that the gearbox test fixture (Figure 4.31) was unstable during testing. Therefore to ensure the 40 mm long arm transferred the maximum force available from the gear train into the 25 N loadcell the gearbox test fixture was held securely in a toolmaker's vice which was secured to the base of the test machine via a clamp (Figure 4.32).

A typical load profile of the load developed at the end of the 40 mm long arm with a motor input torque of 4.96 mNm is presented in Figure 4.33.

Figure 4.33 shows a peak load of 5.47 N acting at 2.55 s however it required 2.13 s to achieve this maximum load. The long period of time can be attributed to the backlash in the gear train which allowed the gear train to slowly bind under the input torque. The graph shows that once the peak load had been achieved the load slowly dropped off over a period of 4.5 s until the motor was switched off. This reduction in deliverable force was a result of creep. The Nylon 6 material the gears were manufactured from allowed the teeth to deflect under load and also allowed excessive torsion of the gear's driveshaft.

Using the measured motor input torque of 4.96 mNm the theoretical output torque for the gearbox at 59% efficiency (equation 4.3) would be 537 mNm. However the average peak load for 10 operations was measured at 5.36 N this equates to a deliverable torque of 214 mNm. The measured results equate to a gearbox efficiency of 23.6% which rep-

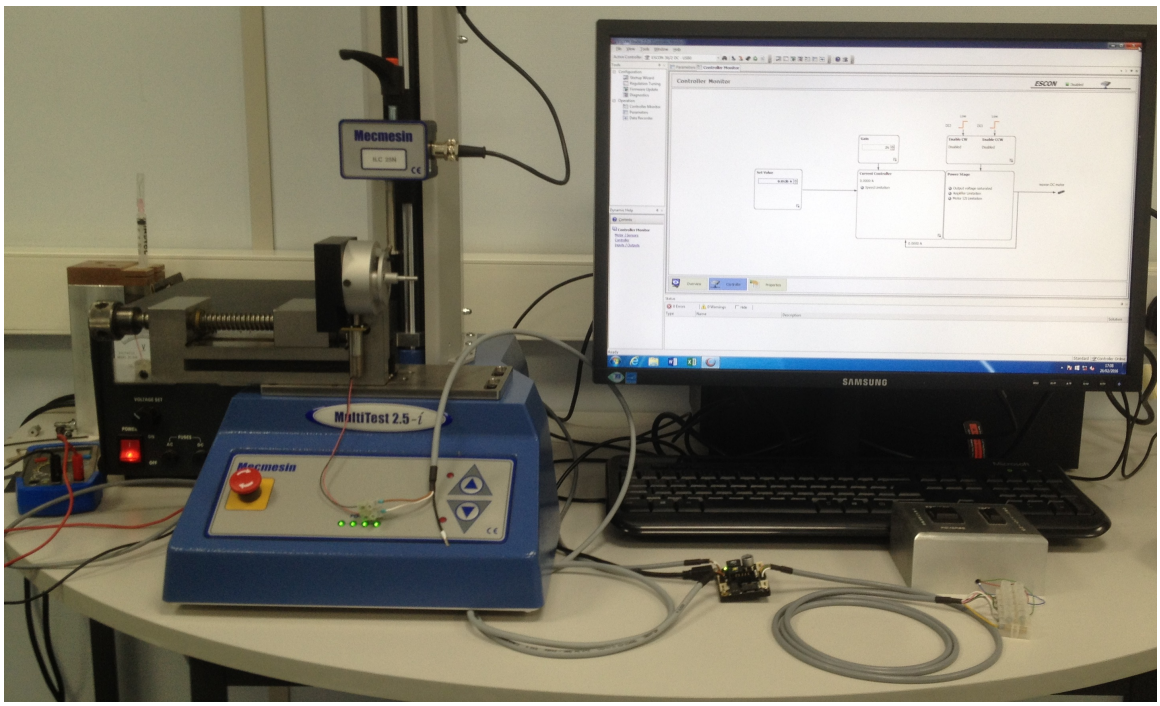


Figure 4.32: Gearbox efficiency test set-up comprising: a rocker switch connected to a motor controller which is controlling the gearbox input motor. A 40 mm long arm connected to the final gear in the gear train contacts a MultiTest 2.5-i test system fitted with a 25 N loadcell and connected to a computer running Emperor^{TM} (force) software

resents a loss of approximately 25% efficiency at each of the five gear stages. The gearbox is designed to deliver 183.4 times the input torque however the actual requirement to guarantee a successful operation is a minimum of 18.5 times the motor's input torque (2.78 mNm/0.15 mNm). Multiplying the input torque (4.96 mNm) by 18.5 results in a minimum torque requirement of 91.9 mNm. Comparing the minimum torque requirement to the measured result (214 mNm) shows that the 5:1 scale prototype would deliver sufficient torque to drive the legs.

Improvements in the efficiency of the 5:1 scale gearbox can be achieved through a number of changes. For example, reducing the backlash and changing the material the gears are manufactured from to a stainless steel would stop the teeth from deflecting and significantly reduce the driveshaft's ability to twist. However the greatest improvement would result from reducing the friction which is generated by the gear train. The 13 toothed bevel gear was mounted in the gearbox base to allow easy alignment and support of the gear however the 29.0 mm length of the gear's driveshaft rubbed on the gearbox housing which then required

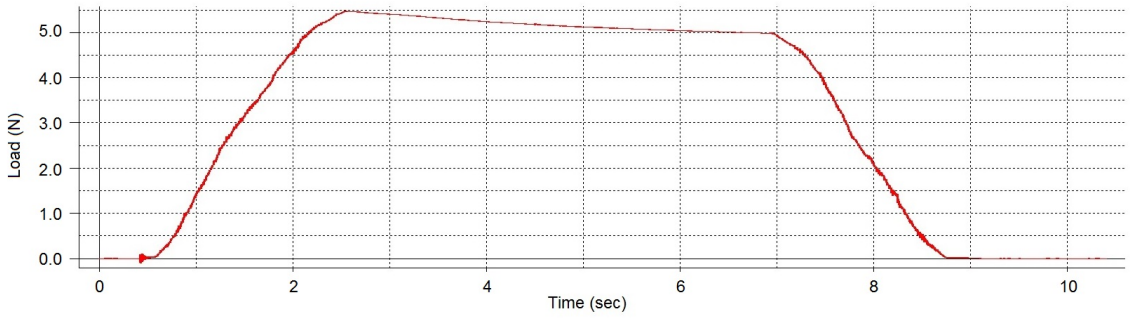


Figure 4.33: Load profile of a typical 40 mm long arm deflection with a motor input torque of 4.96 mNm

a greater degree of torque to overcome the increase in friction. This gear configuration would not be present in the 1:1 scale microrobot.

4.6.3 Holding Mechanism Protocol

The holding mechanism will be required to overcome the external circumferential peristaltic forces imposed on it by the GI tract wall in order for the microrobot to achieve a state of static equilibrium (Figure 4.6). This experiment sets out to measure the load being delivered to the ends of the legs, tie bars and centre support by the motor and gearbox. The measured results will be compared with the individual estimated torques which have been calculated in the circumferential peristaltic force analysis (Section 4.4.1).

4.6.3.1 Holding Mechanism Procedure

An M4 threaded boss mounted in the centre of the 5:1 scale gearbox assembly will be used to hold a series of cylindrical dynamometers to measure the load being delivered to the expanding holding mechanism's legs, tie bars and centre support. The test set-up used to measure the loads can be seen in Figure 4.34.

The holding mechanism comprises the legs, tie bars and centre support which are manufactured from aluminium alloy (7075-T651). The joints of the mechanism are secured together using M2 stainless steel slot pan head machine screws to guarantee the parts cannot separate during an operating cycle. The legs are secured to the final two gears in the gear train via M2 screws which clamp against the gear's driveshaft to ensure there is no slip-

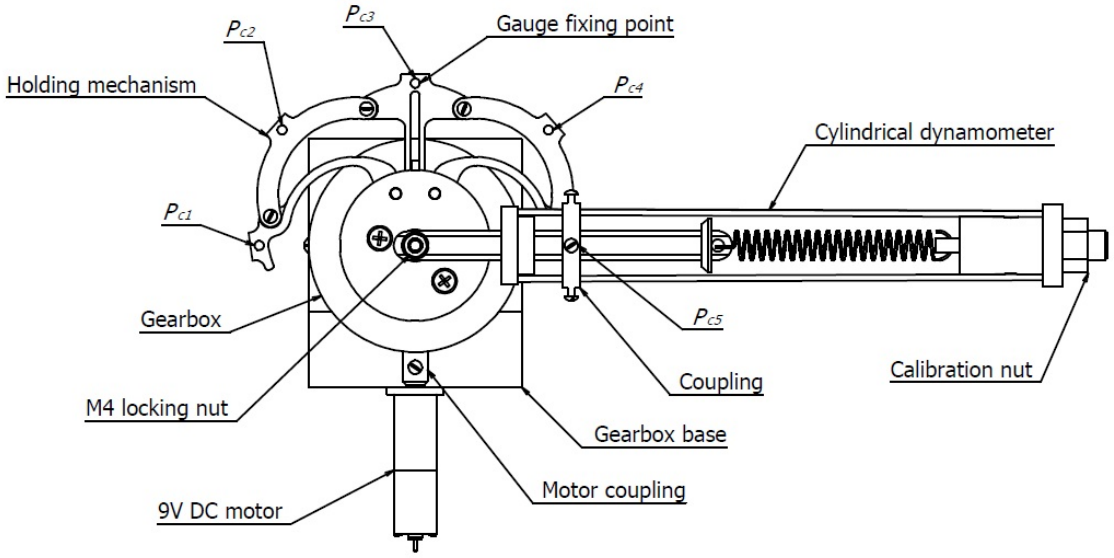


Figure 4.34: Test set-up used to measure the load being delivered to the holding mechanism's legs, tie bars and centre support

ping at the connection. Using a motor controller (ESCON 36/2 driver (403112)) connected to a rocker switch the input torque (4.96 mNm) of the gearbox motor will be controlled. A series of cylindrical dynamometers (manufactured by RVFM) starting at 2.5 N and ranging up to 20 N will be positioned at each of the five circumferential peristaltic positions (P_c) to measure the force being generated by the holding mechanism at that point. The central bar of the dynamometer will be fixed via an M4 locking nut to the central boss of the gearbox assembly, while the body of the dynamometer will be fixed via a specially designed coupling to one of the five gauge fixing points (Figure 4.34). The centre of each fixing point has been designed to correspond with the circumferential peristaltic contact points. The gauge will be set to read zero by adjusting the calibration nut at the end of the dynamometer.

The holding mechanism will be operated five times and the dynamometer's maximum load recorded. If the holding mechanism reaches full expansion without stalling the motor then a higher gauge dynamometer will be fitted and the experiment repeated until the input motor stalls. The average maximum load will be used to calculate the force which can be delivered to the legs, tie bars and centre support by the motor and gearbox.

4.6.3.2 Results and Discussion

The experimental set-up used to measure the force being delivered to the leg tip (P_{c1}) can be seen in Figure 4.35. The set-up shows the holding mechanism performing an opening cycle and reaching full extension with a 2.5 N cylindrical dynamometer interfaced with the leg tip and the central boss.

Each circumferential peristaltic position (P_c) has been tested to its maximum deliverable capacity and the results recorded. Table 4.4 shows the average measured force from the cylindrical dynamometers for each position.

Table 4.4: Measured force from each of the circumferential peristaltic positions (P_c) and calculated perpendicular component forces which have been further evaluated to derive the deliverable torque acting at each position on the final gears in the gear train. A comparison of the derived torque can be made with the minimum torque requirement

Circumferential peristaltic position	**Measured force (N)**	**Perpendicular component force (N)**	**Derived torque (mNm)**	**Minimum torque requirement (mNm)**
P_{c1}	2.8	0.80	33.22	9.43
P_{c2}	2.2	1.53	55.08	19.89
P_{c3}	2.4	6.05	216.92	33.41
P_{c4}	2.8	1.95	70.10	19.89
P_{c5}	3.6	1.04	42.71	9.43

The individual measured forces have been used to calculate the perpendicular component forces acting on the drive gears. Using these figures the deliverable torque acting at each position on the final gears in the gear train has been derived. To make a comparison between the derived torque and the minimum required torque a multiplication factor of 33 has been applied to the minimum torque requirement, this is to compensate for the ratio between the two input motors (4.96 mNm/0.15 mNm). Comparing the minimum torque requirement for each of the circumferential peristaltic positions to the measured results shows that the 5:1 scale prototype would deliver sufficient torque to expand the holding mechanism and achieve a state of equilibrium.

The measured results (Table 4.4) confirm the approximate reduction of 25% in efficiency at each gear stage of the gearbox as P_{c1} is 22.2% lower than P_{c5} and P_{c2} is 21.4% lower than P_{c4}. A further point to note is the deliverable torque of the centre support (P_{c3}) which is higher than that achieved by the other positions. This can be attributed to the 22 teeth

drive gears providing a torque to both legs at the same time which will provide a more balanced and efficient system. Although the gearbox is inefficient the high ratio (183:1) offers an advantage of preventing the holding mechanism from collapsing easily when an external load is applied, furthermore once the mechanism has opened it no longer requires power to maintain its position under load.

4.7 Summary

In this chapter the author has presented a novel holding mechanism concept for the purpose of resisting natural peristalsis in the GI tract. The mechanism has been based on the biologically-inspired concept of a pair of ladybird wings being folded into a protective case. A holding mechanism integrated into a WCE would increase the functionality allowing more active treatment of pathologies of the GI tract to be performed such as the treatment of Crohn's disease.

Through analysis, fabrication and evaluation of a 5:1 scale prototype it has been shown that the 183:1 gearbox, driven by a micromotor with a deliverable torque of 4.96 mNm, can produce sufficient torque to extend the holding mechanism. The results show that in future prototypes a 1:1 scale version with a micromotor delivering a torque of 0.15 mNm would be sufficient to overcome natural peristalsis, however *in-vivo* tests would need to be performed to validate the actual figures. A further advantage of the holding system is the ability to deploy the legs in stages. A staged deployment would act as an anchor and hence offer the ability to slow the transit of the microrobot. This additional feature would enable the microrobot to overcome the issue of differences in transit time in different regions of the GI tract. For example the transit time is more progressive in the proximal section of the small bowel compared to the lower segment [8].

The method in which the holding mechanism unfolds, coupled with the means of positioning the mechanism, ensures that the GI tract has been stretched around the body of the microrobot and is orientated to the site of interest. This novel feature is very important as it guarantees the microrobot is in contact with the GI tract wall which is required for therapeutic treatment to be performed.

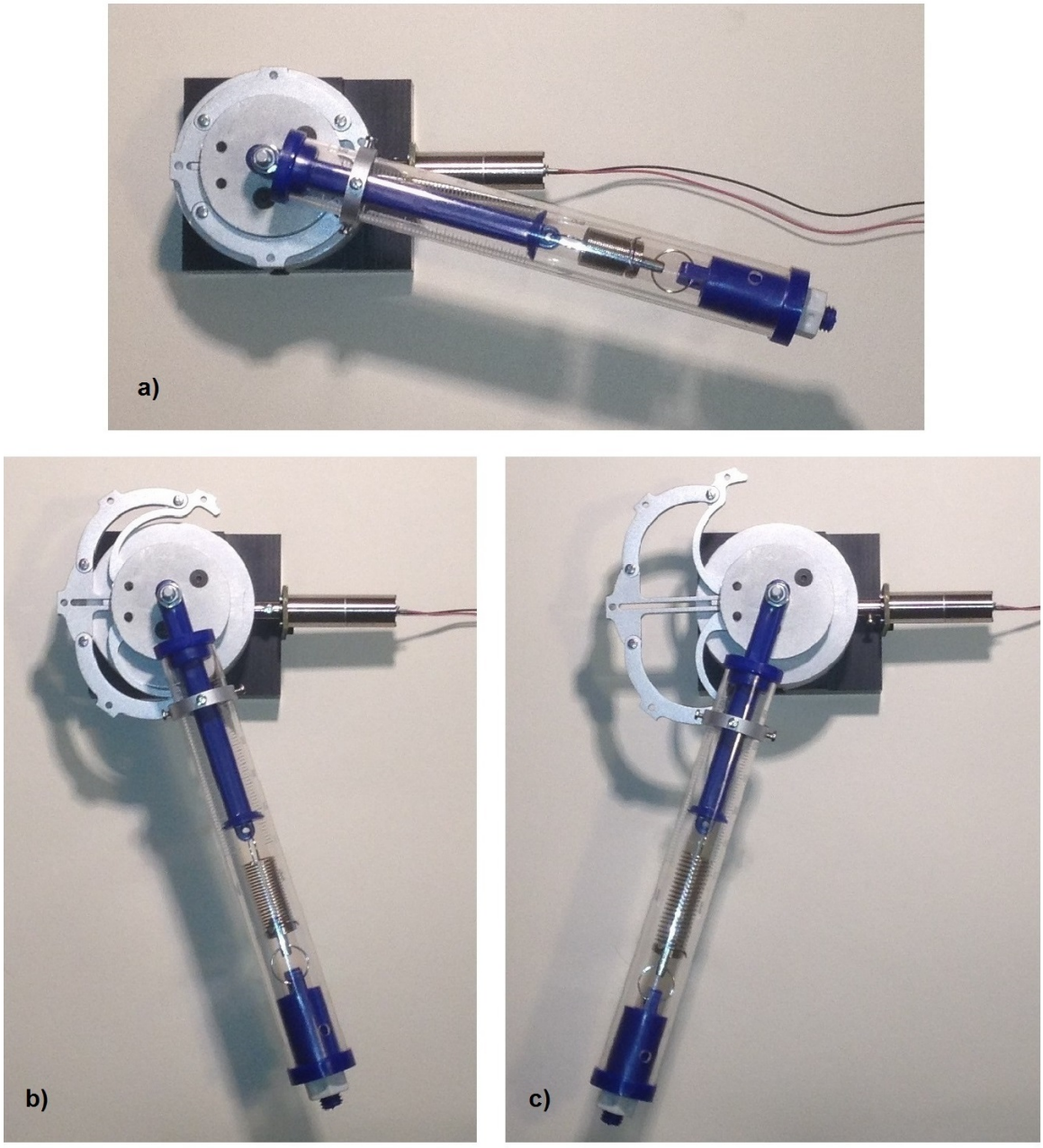


Figure 4.35: Experimental set-up of the holding mechanism's opening cycle with a 2.5 N cylindrical dynamometer interfaced with the leg tip (P_{c1}) and the central boss of the gearbox assembly. Start position with the gauge calibrated to read zero load a), halfway through the opening cycle with a reading of 0.45 N on the gauge b) and the holding mechanism at full extension with a reading of 0.9 N on the gauge c)

References

[1] J. P. Guilford, "The structure of intellect," *Psychological Bulletin*, vol. 53, pp. 267–293, 1956.

[2] Q. Clinical, "Innovations in early development," 2003.

[3] BS ISO 6336-1:2006, "Calculation of load capacity of spur and helical gears - Part 1: Basic principles, introduction and general influence factors."

[4] A. Moulton, J. Grosjean, and G. W. Owen, *The Moulton Formulae and Methods: Directly Useable for Calculations in Mechanical Engineering.* London UK: Professional Engineering Publications, 2005.

[5] R. Miftahof, "The wave phenomena in smooth muscle syncytia," *Silico Biology*, vol. 5, pp. 479–498, 2005.

[6] R. C. Hibbeler, *Mechanics of materials.* Prentice Hall, 8th ed., 2011.

[7] E. Oberg, F. D. Jones, H. L. Horton, and H. H. Ryffel, *Machinerys hand book.* New York: Industrial Press Inc., 23rd ed., 1990, pp. 2201-2203.

[8] A. Koulaouzidis, E. Rondonotti, and A. Karargyris, "Small-bowel capsule endoscopy: A ten-point contemporary review," *World Journal of Gastroenterol*, vol. 19, pp. 3726–3746, 2013.

Chapter 5

Targeted Drug Delivery: Design, Analysis and Evaluation

5.1 Introduction

Chapter 4 presented a holding mechanism for the purpose of resisting natural peristalsis in the GI tract. This chapter builds on the holding mechanism to further increase the functionality of WCE by incorporating a novel targeting mechanism with the aim of delivering a metered dose of medication to a targeted site of interest in the GI tract. Following the medical motivation given in Chapter 1 and the design specification presented in Chapter 3 this chapter will focus on finding a solution to the problem of positioning a needle in the GI tract, operating the needle and safely retracting the needle. A fully functioning prototype targeting mechanism is presented which is capable of positioning a needle within a 360 degree envelope. A discussion of the prototyping methods selected to produce 5:1 scale component parts of the mechanism is discussed and through a series of experiments the novel targeting mechanism is validated.

5.2 Overview

The clinical need to target a specific location or feature within the GI tract for medication delivery can be achieved using a microrobot consisting of an onboard image sensor, a means of resisting natural peristalsis and a drug targeting system. Figure 5.1 shows a concept design of a microrobot with an integrated targeting system.

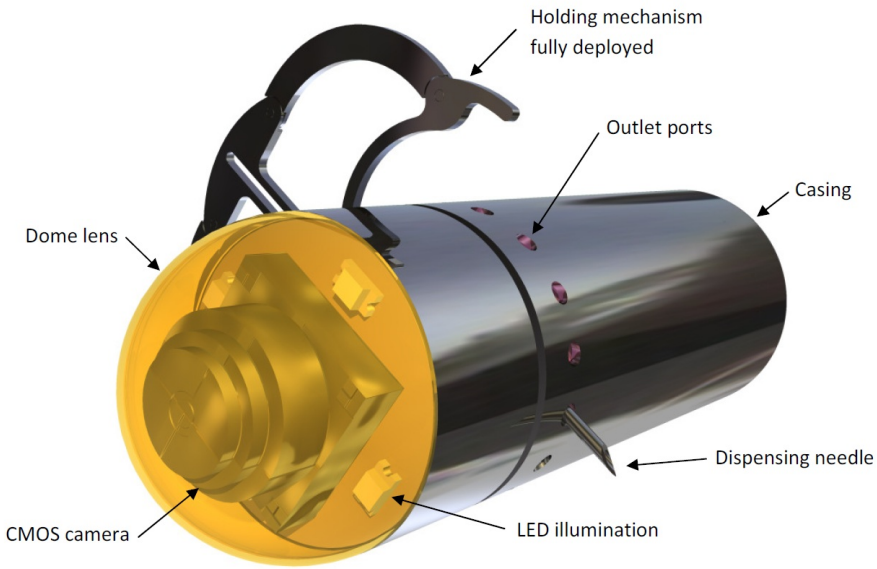


Figure 5.1: Microrobot concept design capable of delivering 1 ml of targeted medication. Needle shown fully extended

There are a number of methods which have been explored that can deliver medication to a SOI in the GI tract such as utilising a micro pump to propel medication to the site or letting the medication naturally release through a side port on the microrobot's body. However these methods do not target a specific location therefore alternative designs have been explored which more specifically address the requirement of targeted delivery. For example a method of using a micromotor to drive a needle in and out was explored, however this method was limited to only targeting one potential location. Alternatively, a combination of two micromotors was explored which orientated the needle radially then extended and retracted the needle, however due to issues of supplying power to the micromotors and the limited available space a single motor drive was selected. Appendix B presents a detailed review of the alternative needle positioning mechanisms which were explored.

The proposed system uses a needle to deliver 1 ml of medication to a target site rather than releasing its payload as a bolus form. This method offers the advantage of being more effective than current systems due to the shorter discharge time and the more accurate delivery position. The shorter discharge time will allow for the correct dosage to be delivered to the required location without it being diluted over the delivery time from the natural passing of the GI tract or from being dispersed by the constant movement from peristalsis.

A significant feature of the targeting mechanism is its ability to penetrate the GI tract wall which guarantees medication has been delivered to the SOI. The needle positioning mechanism (Figure 5.1) utilises a single micromotor to position and operate the dispensing needle. However the same micromotor radially positions the holding mechanism due to a mechanical coupling between the two mechanisms. The dispensing needle is positioned diametrically opposite the holding mechanism therefore when the holding mechanism is fully expanded the GI tract wall will be stretched over the position where the needle will be deployed which guarantees penetration of the GI tract wall.

5.3 Targeted drug delivery

The design of the needle positioning mechanism consists of a 1.5 mm diameter $\times$ 10.5 mm long micromotor manufactured by Namiki, two opposing ratchets, a needle funnel, a needle cam and a movable needle. Also features integral to the microrobot's body are required. The first operation is the angular control of the position of the needle and the second is the extension and retraction of the needle. The 1 ml of medication will be stored in a compartment of the body and be delivered through the needle by means of pressure generated by a piston. The piston will be activated by a spring allowing for a rapid delivery of the medication. The method of deploying the medication will be discussed further in Chapter 6.

It is a requirement that the needle can be positioned at selected points within a 360 degree envelope. For the purpose of prototyping, 16 equally-spaced fixed positions have been chosen. The angular positioning of the needle is achieved by the anticlockwise rotation of the micromotor while the advancement and retraction of the needle is achieved by the clockwise rotation of the micromotor.

5.3.1 Needle Positioning

Manoeuvring the needle to a selected position is achieved by applying a negative voltage to the micromotor. The negative voltage will cause the micromotor to rotate in an anti-clockwise direction. The needle funnel (Figure 5.2, a) rotates anticlockwise by virtue of a ratchet which is mounted on the micromotor's drive shaft. The ratchet engages with a set of sprung legs which are integral to the needle funnel (Figure 5.2, b). The needle is engaged with the needle funnel and will be carried round with it.

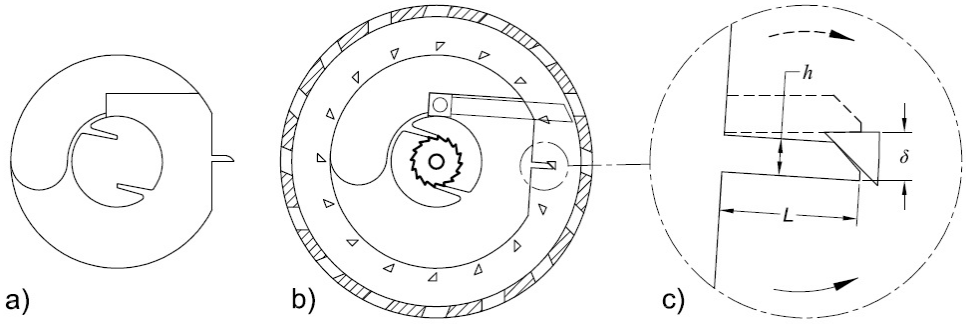


Figure 5.2: Needle positioning mechanism: needle funnel a), ratchet driving the needle funnel and needle b), and enlarged view of the protrusions c)

When the needle funnel is rotating anticlockwise an arm which protrudes from the side of the needle funnel rides over the top of a plurality of protrusions (Figure 5.2, b) on the inside face of the body. The function of these protrusions is to prevent the needle funnel from rotating clockwise when the motor is reversed. It achieves this by engaging the end of the arm with a parallel surface of the protrusion (Figure 5.2, c) preventing any further movement clockwise and aligning the needle with one of the 16 fixed ports on the microrobot's body.

While the needle funnel is rotating anticlockwise it is also carrying with it the needle and the needle cam (Figure 5.4, a). This is achieved through the sprung legs on the needle cam disengaging with the ratchet which would be used to drive it and flexing out of position.

A further improvement to the original concept employs two sprung arms rather than one, Figure 5.3. The orientation of the arms has been modified so that they are now in compression when the needle is being operated rather than bending, this results in a stronger mechanism as the arms will be able to withstand higher compressive forces than bending forces.

Employing two arms will maintain a balanced system giving a smooth action to the mechanism and distributing loads more evenly. The longer arms will facilitate a greater cantilever action reducing the load applied to the beam. In addition the protrusions have been refined and repositioned to impose a smaller deflection to the arms and they have also decreased in contact angle to make a smoother transition over the flexing period.

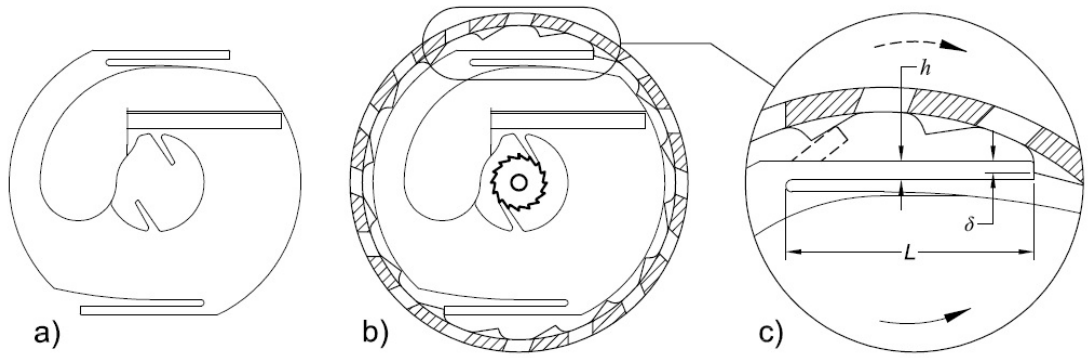


Figure 5.3: Needle positioning mechanism extended cantilever: needle funnel with two arms a), two arms engaged with the protrusions b), and enlarged view of the protrusions c)

5.3.2 Needle Deployment

Applying a positive voltage to the micromotor reverses its direction, this disengages the needle funnel ratchet from its sprung legs and engages the needle cam ratchet with a set of sprung legs that are integral to the needle cam (Figure 5.4, a).

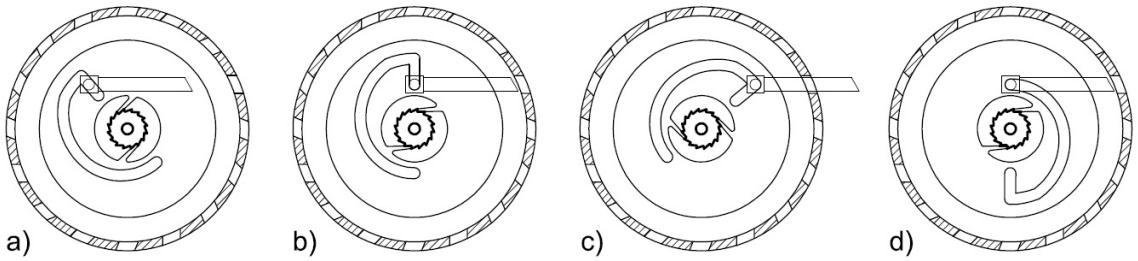


Figure 5.4: Needle cam operating cycle: stored position a), needle ready to exit b), full stroke c), and retracted position d)

When engaged the needle cam ratchet drives the needle cam in a clockwise direction while at the same time the needle funnel legs ride over the ratchet used to drive them. The needle is engaged with a track in the needle cam by means of a driving peg mounted on the side of the needle. The track is shaped to convert the rotational motion of the cam into a variable linear motion. This linear motion allows the advancement and retraction of the needle. The linear displacement of the needle with respect to the rotation angle can be seen in Figure 5.5.

The needle cam displacement profile Figure 5.5 shows the needle advancing forwards to its maximum stroke length of 4.2 mm in the first 90 degrees. This is followed by a delay

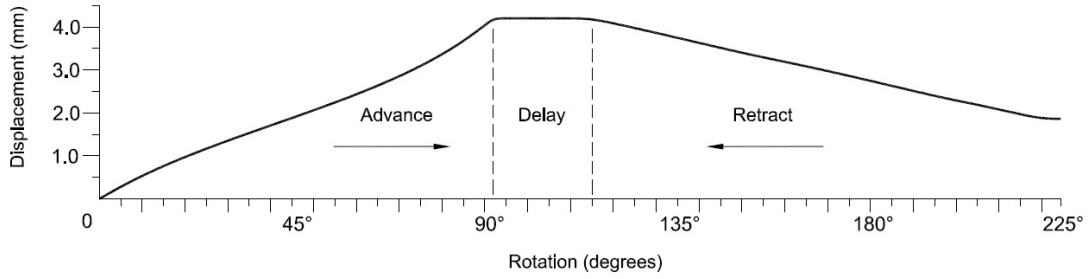


Figure 5.5: Needle cam linear displacement profile

period which is designed to allow the medication to be delivered. The remaining 110 degrees retracts the needle back 2.45 mm to the stored position (Figure 5.4, d). It can clearly be seen from the plotted profile that the needle does not return to its original starting position, this prevents any further operation of the needle.

An improvement to the original design (Figure 5.4) allows the needle to be positioned and repositioned as many times as is required before the medication is released, Figure 5.6. This feature gives an added degree of flexibility to the procedure. The cam has a significantly shorter stroke length (2.0 mm) than the previous design however it has the advantage of allowing the needle to be repositioned even if the needle has been deployed to deliver the medication. This is a safer mechanism than previously envisioned as it gives the operator greater flexibility rather than limiting them to a one shot approach.

Figure 5.6 shows the sequence of operation for the extension and retraction of the needle. Figure 5.6, a) shows the needle in the stored position, this is the position the needle will be in when the microrobot is swallowed and travels through the GI tract to the target site. Figure 5.6, b) shows the needle at full extension giving a reach of approximately 6.92 mm radius and a stroke length of 2.0 mm. The design of the cam utilises a direct linear movement so that a positive force can be delivered to the needle which will be required to penetrate the wall of the GI tract. Figure 5.6, c) shows the needle retracting backwards by virtue of the track slowly spiralling inwards. Figure 5.6, d) shows the needle returning to the stored position once the medication has been delivered.

The 360 degree needle cam linear displacement profile Figure 5.7 shows the needle reaching its maximum stroke length of 2.0 mm in 60 degrees. The proceeding delay period, required for medication delivery, has increased in duration from 23 degrees to 75 degrees. The increase in delay allows for a greater margin of error for the timing of the medication

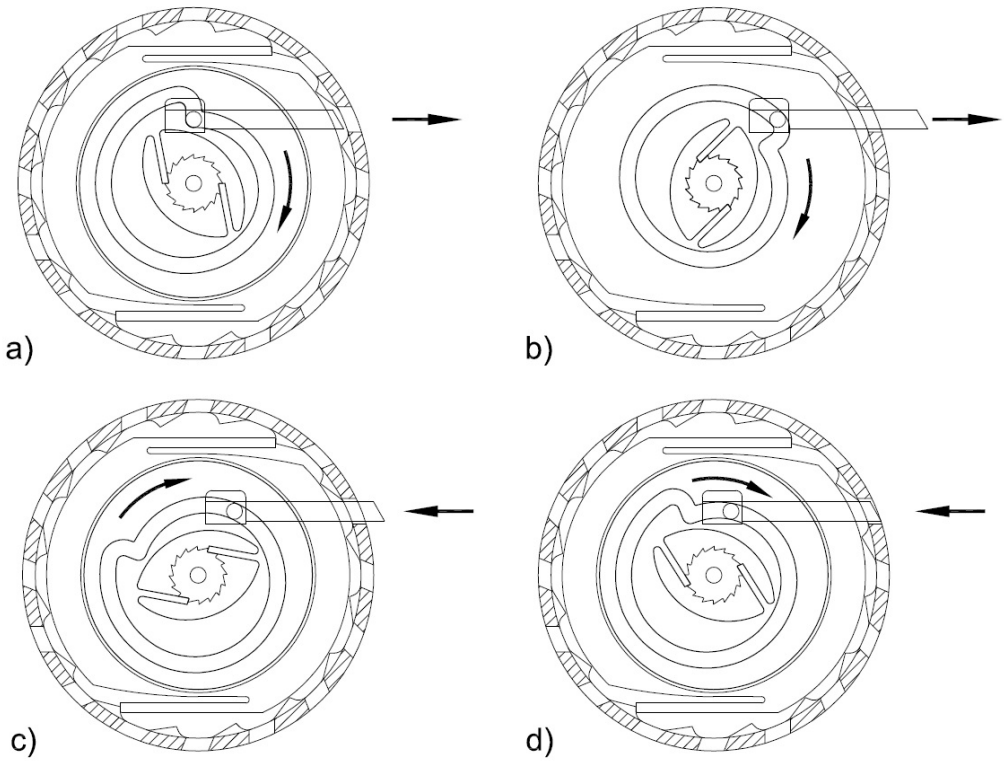


Figure 5.6: 360 degree needle cam operating cycle: stored position a), full stroke b), needle returning to the stored position c), and retracted position d)

release. The remaining 225 degrees gradually retracts the needle back to the starting position, from where the needle can be further deployed. To ensure the needle performs as expected, a spring is required to guarantee the driving peg, mounted on the side of the needle, engages with the cam track throughout the operating cycle.

5.3.3 Needle Cam Spring Design Analysis

A compression spring is required to overcome the possibility of the needle cam moving out of position radially and becoming jammed when the needle positioning mechanism rotates anticlockwise to position the needle. The spring is mounted on the needle and constantly opposes the forward force from the needle cam. The constant force ensures that the needle is always pressed against the needle cam track wall and therefore it will follow the profile of the track. Figure 5.8 shows the position of the spring in the stored position and at full extension.

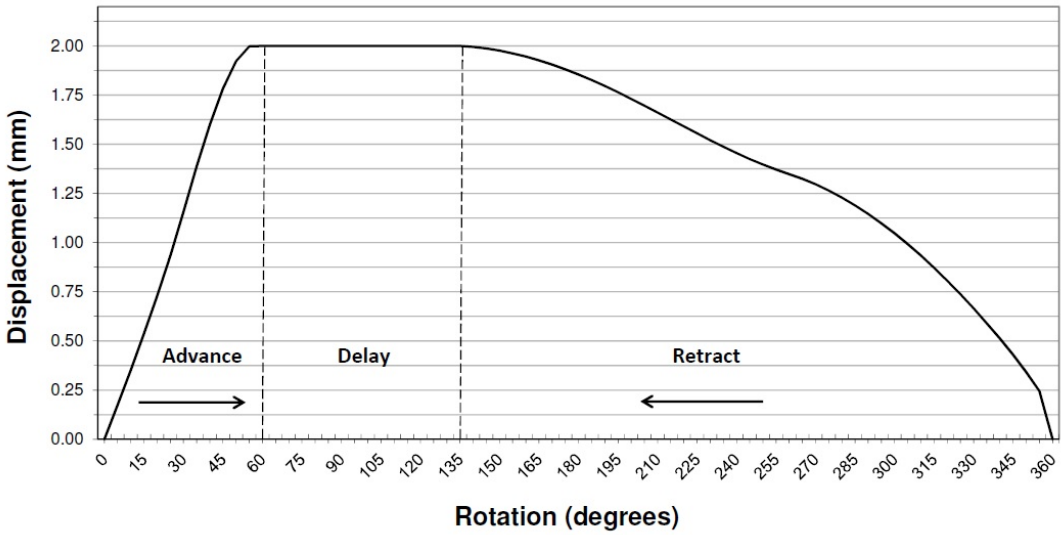


Figure 5.7: 360 degree needle cam linear displacement profile

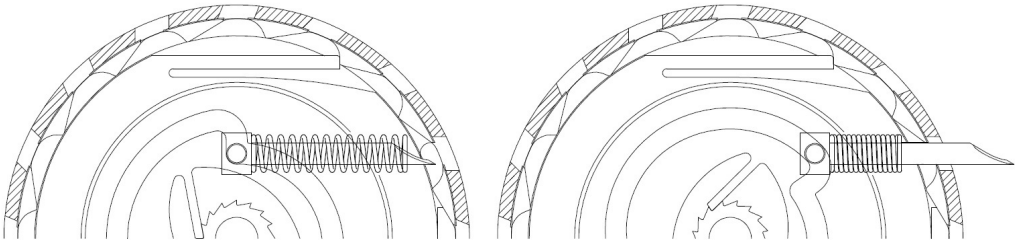


Figure 5.8: Needle cam spring in the stored position and at full extension

The 360 degree needle cam design (Figure 5.6) has a stroke length of 2.0 mm and allows the needle to extend 1.5 mm from the body of the microrobot. This geometry is based on the current literature which suggests that the average wall thickness for the length of the GI tract is between 2.0 mm and 3.0 mm thick [1]. Therefore 1.5 mm will be sufficient to prevent the needle from puncturing the wall of the GI tract when deployed. However the load generated by the compressed spring directly acts against the micromotor driving the mechanism therefore an analysis of the forces involved is required to determine if the micromotor can deliver sufficient force.

The load generated by a deflected compression spring can be calculated from the spring's spring rate and the distance the spring has been compressed using the formula:

$$F = L_t \times S \tag{5.1}$$

Where L_t is the distance the spring has traveled and S is the spring constant of the spring and can be calculated by:

$$S = \frac{Gd^4}{8nD^3} \tag{5.2}$$

Where G is the module of rigidity, d is the wire diameter, n is the number of active coils and D is the mean coil diameter.

Analysing the chosen spring parameters shows that a free length of 4.597 mm long x 0.101 mm diameter stainless steel wire spring with a module of rigidity value of 69.0 GNm^{-2} [2], 12.5 active coils and an outside diameter of 0.889 mm can generate a load of 381 mN at the full 2.0 mm deflection. The selected micromotor can deliver a torque of 1.6 mNm therefore at full extension it will have a potential deliverable force of 800 mN which will be sufficient to compress the spring. The spring's operating sequence can be seen in Figure 5.9.

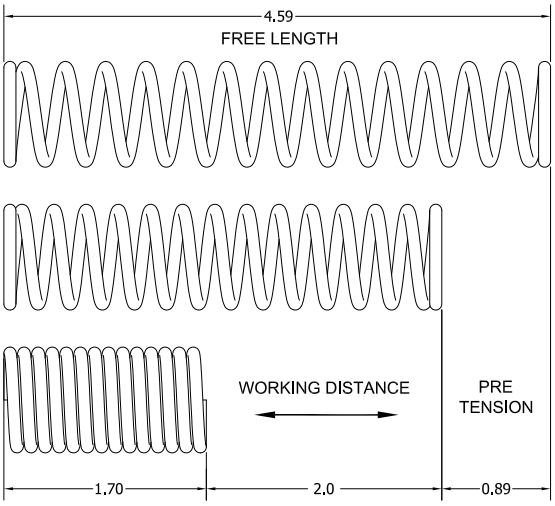


Figure 5.9: Needle cam spring stages of operation

As the operational requirement of the spring is less than 10,000 cycles the spring is categorised as working statically therefore fatigue will not affect its performance. However compressing the spring by 2.0 mm would be operating outside the recommended safe working

limits for minimum working length and therefore an analysis of the stress induced in the spring has been undertaken.

The stress acting on the spring is an important design factor as the spring would be a critical component in the delivery of the medication and failure to perform would result in failure to deliver the medication. For this reason the maximum allowable stresses would be determined as a percentage (59%) of the materials ultimate tensile strength (UTS) [3].

Using the dimensions of the spring, the stress (τ) in the spring can be calculated using:

$$\tau = \frac{8PDK_c}{\pi d^3} \tag{5.3}$$

Where P is the load, D is the mean coil diameter, K_c is a curvature correction factor and d is the wire diameter. The curvature correction factor is used to correct for the uneven stress distribution across the section of the wire as a result of the curvature of the wire and can be calculated using the Sopwith formula [3]:

$$K_c = \frac{D/d + 0.2}{D/d - 1} \tag{5.4}$$

The stress induced in the compressed spring calculated from equation (6.3) equates to $872.7\,\mathrm{MNm}^{-2}$. This can be compared to the calculated maximum allowable stress which is $1{,}298\,\mathrm{MNm}^{-2}$ (59% of UTS $2{,}200\,\mathrm{MNm}^{-2}$). As can be seen the stress in the spring is 67.2% of the allowable stress therefore as the spring will not be cyclically loaded it will be an acceptable design solution in this situation.

5.3.4 Requirements for Needle Penetration

The chosen method for administering medication is through the use of a needle injected into the target location on the GI tract wall. It is therefore essential that the needle can penetrate the GI tract wall sufficiently to allow the medication to be dispersed throughout the tissue.

The force required for the needle to penetrate the GI tract wall can be determined from the following equation [4]:

$$F_{pen} = P_{pen} A \tag{5.5}$$

Where F_{pen} is the penetration force, P_{pen} is the penetration pressure and A is the cross sectional area of the needle.

The penetration pressure (P_{pen}) has been empirically determined by Byun et al. (2005) [5] to be 8.9 MPa from experiments carried out using chicken breast flesh as an equivalent material to the GI tract wall. The dimensions of the needle tip are 0.45 mm in diameter with a wall thickness of 35 μm and a 30 degree bevel 1.25 mm long. Using these figures a penetration force (F_{pen}) of 405.9 mN would be required to successfully penetrate the GI tract wall with the needle.

Combining the calculated penetration force (405.9 mN) with the force required to operate the needle cam spring (381 mN) results in a total force of 786.9 mN required to penetrate the GI tract wall. Comparing the total calculated penetration force to the micromotor's deliverable force of 800 mN (ignoring any losses due to friction) shows that the needle tip design will penetrate the wall successfully.

5.4 Analysis of Needle Positioning Mechanism

The chosen concept for positioning the needle (Figure 5.3) relies on the smooth operation of the flexing arms and rotating ratchets. To ensure that the needle positioning mechanism performs mechanically requires further analysis of the geometry and of the potential materials the needle funnel could be manufactured from.

5.4.1 Anticlockwise Motion: Needle Positioning

The process of positioning the needle requires the needle positioning mechanism to be rotated anticlockwise. This anticlockwise motion will cause the needle funnel arms to be flexed out of position by the protrusions on the inside face of the body (Figure 5.3, c). Once the arm has passed the protrusion it will return to its original configuration. At the same time the legs on the needle cam will ride over the ratchet which is used to drive it.

5.4.1.1 Needle Funnel Arm: Bending Stress Analysis

Flexing the arm out of position will result in a stress induced in the arm. The amount of stress in the arm will be a result of the material's geometry, the Young's modulus for the material and the amount of movement the arm will make. Various materials can be evaluated for their ability to withstand this stress and maintain design integrity. To determine the most suitable for this application Table 5.1 shows a selection of materials and their properties which can be compared for the purpose of evaluating the needle positioning arm. The table data has been sourced from various published results [6, 7, 8].

Table 5.1: Material selection matrix

Material	**Density** $\mathbf{gcm^{-3}}$	**Yield point** $\mathbf{Nmm^{-2}}$	**Shear modulus** $\mathbf{kNmm^{-2}}$	**Young's modulus** $\mathbf{kNmm^{-2}}$	**Poisson's ratio**	**Cost GBP/kg**
Stainless Steel 304	8.08	290	72.4	193	0.3	6.0
Ti Alloy 6AL 4V	4.43	880	42.7	114	0.3	40.0
Nylon 6	1.14	82	1.24	3.3	0.4	2.12
PVC	1.44	58	1.13	3.0	0.4	0.84
Acetal Copolymer	1.41	60	1.01	2.7	0.4	2.80
PEEK 450G	1.32	97	1.31	3.5	0.4	71.2

The material selections have been chosen for their ability to perform in the harsh environment of the GI tract and their biocompatibility with the human body. An examination of the data in Table 5.1 shows that stainless steel 304 will be seven times heavier than an equivalent part made in Nylon 6 and three times more expensive, however its yield point is three and a half times higher than Nylon 6 making it more resistant to induced stress.

To evaluate the resulting stress and strain involved in flexing the needle funnel arm, certain assumptions will be made. Firstly the needle funnel arm will act like a cantilevered beam and secondly the system will be in a state of static equilibrium at the point of maximum deflection. Only the state of maximum deflection will be considered as this is the position which will induce the maximum stress and strain in the beam. Also it is assumed that the beam will be longer than its width or depth, the deformations are smaller than its length, the normal remains normal, straight and un-stretched and the material is both homogenous and isotropic and behaves in a linear-elastic manner when a load is applied.

Using the principle of a cantilevered beam the displacement (δ) of the beam can be calculated by using [9]:

$$\delta = \frac{PL^3}{3EI_x} \tag{5.6}$$

Where P is the load, L is the length of the arm and E is the material's Young's modulus. I_x represents the moment of inertia through section $x - x$ for a solid rectangular beam and is given by:

$$I_x = \frac{bh^3}{12} \tag{5.7}$$

Where b is the width and h is the height of the beam's cross section.

As the geometry of the protrusions are known, the distance the arm will be flexed through can be calculated ($\delta = 0.17\,\text{mm}$), therefore the cantilevered beam equation can be rearranged to find the load (P) that would be required to make the arm deflect by the calculated amount.

Applying the same geometry but varying the material's properties the force (P) required to make the maximum deflection (δ) can be calculated for each material. The results of this comparison are tabulated in Table 5.2. A height (h) of 0.3 mm and a width (b) of 0.2 mm have been used for the purpose of the calculations.

Table 5.2: Resulting load (P) for the selected material properties

Variables	**Units**	**Stainless Steel 304**	**Ti Alloy 6AL 4V**	**Nylon 6**	**PVC**	**Acetal Copolymer**	**PEEK 450G**
δ	mm	0.17	0.17	0.17	0.17	0.17	0.17
L	mm	4.0	4.0	4.0	4.0	4.0	4.0
I_x	mm^4	0.00045	0.00045	0.00045	0.00045	0.00045	0.00045
E	Nmm^{-2}	1.93E+5	1.10E+5	3.30E+3	3.00E+3	2.70E+3	3.50E+3
P	mN	692.0	394.0	11.8	10.8	9.7	12.55

As can be seen from Table 5.2 the material with the greatest generated load is stainless steel 304 with 692.0 mN. This can be compared to the Acetal copolymer which has the

lowest generated load of 9.7 mN. The lower generated loads for the plastic materials can be attributed to their lower Young's modulus values.

Using beam bending theory the maximum bending stress induced in the arm can be calculated by the *flexure formula* [9] and the loads calculated in Table 5.2:

$$\sigma_{max} = \frac{Mc}{I_x} \tag{5.8}$$

Where σ_{max} is the maximum normal stress in the beam and will occur at a point furthest away from the neutral axis, M is the maximum bending moment (comprising of the length L of the beam multiplied by the load P), c is the perpendicular distance from the neutral axis to a point farthest away from the neutral axis and I_x is the moment of inertia of the cross-sectional area through section $x - x$.

To determine the stability and durability of the arm under the calculated loading, the stress and deformation in the components can be calculated using equation (5.8). However as the materials selected for the beam are non-brittle and the beam will not be fatigue loaded the stress concentration due to the change in section at the beam support will be neglected [9]. Table 5.3 shows the maximum calculated stress for all the given materials.

Table 5.3: Induced stress (σ_{max}) in the needle positioning arm

Variables	**Units**	**Stainless Steel 304**	**Ti Alloy 6AL 4V**	**Nylon 6**	**PVC**	**Acetal Copolymer**	**PEEK 450G**
I_x	mm^4	0.00045	0.00045	0.00045	0.00045	0.00045	0.00045
L	mm	4.0	4.0	4.0	4.0	4.0	4.0
P	mN	692.0	394.0	11.8	10.8	9.7	12.55
c	mm	0.15	0.15	0.15	0.15	0.15	0.15
M	Nmm	2.768	1.578	0.047	0.043	0.039	0.050
σ_{max}	Nmm^{-2}	922.78	525.94	15.78	14.34	12.91	16.73

For a structure to be considered stable in operation the maximum stress induced in the structure must be below the limiting property factor of strength for the material, this limit is known as the yield point of the material and it is the point where permanent deformation of the material occurs. The results of the stress analysis for the needle positioning arm can be seen in Table 5.3 and show that only stainless steel 304 exceeds the material's

yield point (which are presented in Table 5.1). Although acetal copolymer has the lowest generated stress levels of the selected materials it represents 23.5% of its yield point however PEEK represents only 17.3% of its yield point making it potentially more suitable to this application.

5.4.1.2 Needle Funnel Arm: FEA Analysis

Selecting PEEK as the preferred material for the needle positioning arm a finite element analysis (FEA) has been performed using AutoCAD Mechanical 2011 software. The FEA program calculates the deformation and stress conditions of the part and presents the results as contours of predicted stress magnitude. Figure 5.10 is a 2D static analysis using the Von Mises stress to display the results.

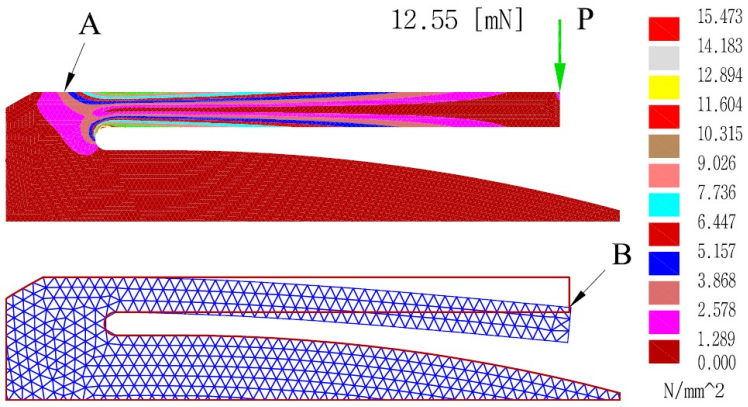


Figure 5.10: Von Mises FEA 2D isoareas and displacement analysis of a PEEK needle funnel arm with a point load of 12.55 mN

The FEA analysis (Figure 5.10) models the needle funnel arm as a cantilever beam with a fixed support running through the centre of the needle funnel, parallel to the arm. The results show the maximum Von Mises stress to be 15.47 Nmm^{-2} from an applied load of 12.55 mN at the end of the arm. The small variation between the FEA figure and the calculated figure (Table 5.3) is due to the size of the mesh used on the FEA simulation and the more accurate modelling of the arm geometry. A stress of 3.86 Nmm^{-2} can also be seen running through the beam as a contour of light brown indicated by arrow (A). The analysis shows that the maximum predicted stress is 6.25 times lower than the 97 Nmm^{-2} yield point of PEEK, this gives an acceptable margin for safety to accommodate for any variations in material and geometry. The displacement analysis, arrow (B), shows the 0.17 mm movement

of the arm. The resulting stress in the arm is of a magnitude which would allow the arm to recover back to its original starting position when the applied load is removed. This will allow the needle funnel to lock into position when it is rotated clockwise. Appendix E presents a bending trial of a PEEK test piece.

5.4.1.3 Needle Funnel Arm: Shear Stress Analysis

It has been determined that the strength of the PEEK arm is adequate to withstand the internal bending stress therefore a further analysis can be completed to determine if the PEEK arm can withstand the shear stress generated from the applied load of 12.55 mN.

To determine if the allowable shear stress for the PEEK material is exceeded the *shear formula* [9] can be used:

$$\tau = \frac{VQ}{I_x t_w} \tag{5.9}$$

Where V is the internal resultant shear force, Q equals $\bar{y}^{'} A^{'}$, where $A^{'}$ is the area of the top portion of the member's cross-sectional area, above the section plane where t_w is measured and $\bar{y}^{'}$ is the distance from the neutral axis to the centroid of $A^{'}$. I_x is the moment of inertia for the cross-sectional area calculated through section $x - x$ and t_w is the width of the member's cross-sectional area measured at the point where τ is to be determined.

The results of the shear stress analysis show that a shear stress of 313.7 $\mathrm{mNmm^{-2}}$ is developed across the beam. Comparing this result with the material's allowable shear modulus, 1.31 $\mathrm{kNmm^{-2}}$ confirms it would be an acceptable material choice for the needle positioning arm.

5.4.1.4 Actuator Stall Torque Analysis

The needle positioning mechanism comprises of a stainless steel needle, a needle funnel, a needle cam, two ratchets and a micromotor with a four stage gearbox. The micromotor will be required to rotate these parts from a stationary position up to the maximum RPM of the micromotor. However the chosen micromotor manufactured by Namiki has a limited deliverable torque of 1.6 mNm available. It is therefore necessary to determine if the micromotor is capable of operating the system.

To determine the torque required to operate the needle funnel system an analysis of the two separate stages of the system is required.

The first stage of the system is to calculate the torque (T) required to accelerate the mass of the needle funnel from rest to its maximum angular velocity. This can be calculated using the following formula for torque:

$$T = I_o \alpha \tag{5.10}$$

Where I_o is the moment of inertia and α is the angular acceleration. The needle positioning mechanism can be modelled as a uniform disc and the moment of inertia for a uniform disc can be calculated as follows:

$$I_o = \frac{mr^2}{2} \tag{5.11}$$

Where m is the total mass of the body and r is the radius of the disc. The mass can be calculated from the volume of the parts and the specific density of the material they are to be manufactured from.

The acceleration can be calculated from:

$$\alpha = \frac{\omega_2 - \omega_1}{t_r} \tag{5.12}$$

Where ω_1 is zero and it is the initial angular velocity at the start, ω_2 is the maximum angular velocity and can be calculated from the motor's RPM ($N = 76$) as follows:

$$\omega_2 = \frac{2\pi N}{60} \tag{5.13}$$

t_r is 30 ms and it is the rise time. The rise time is the time required to achieve the micromotor's maximum RPM [10].

Using equation (5.10) the torque required to rotate the needle funnel mechanism from zero to the maximum angular acceleration of 265.3 rad/s^2 is 0.4 μNm. However this figure does not take into consideration the braking action of the needle funnel arms and the needle cam legs. Therefore the second stage is to calculate the couple required to maintain

a constant velocity when the needle funnel arms and needle cam legs come into contact with the protrusions and ratchet teeth and act like brakes.

The needle funnel arms will be analysed as a static system which is in equilibrium. The arms will be statically determinate as the unknown couple (M) can be determined from the static equilibrium equation [11].

The unknown couple can be calculated by generating a free-body diagram of the needle funnel to obtain a relation between M and the reaction exerted on the needle funnel by the arms for a state of equilibrium.

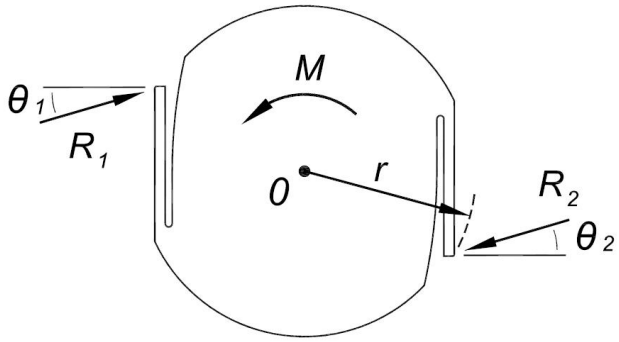


Figure 5.11: Free-body diagram of the extended cantilever needle funnel design

Figure 5.11 is a free-body diagram of the needle funnel with the forces exerted by the arms being represented by the forces R_1 and R_2. The forces R_1 and R_2 oppose the counter clockwise rotation of the needle funnel and the angles θ_1 and θ_2 are the maximum angle of deflection of the arms due to the protrusions on the inside face of the body and they have been calculated at 16.36°.

Summing moments about point 0 we obtain:

$$\sum M_0 = M - (R_1 \sin\theta_1)r - (R_2 \sin\theta_2)r = 0 \tag{5.14}$$

Resolving for the couple M:

$$M = (R_1 \sin\theta_1)r + (R_2 \sin\theta_2)r \tag{5.15}$$

The moment (M) required to maintain a state of equilibrium equates to 33.8 μNm. This is derived from the 12.55 mN force generated by a PEEK arm (Table 5.2) and a maximum

deflection angle of 16.36 degrees. This process of analysis has also been completed for the needle cam legs with a result of 33.4 μNm required to maintain a state of equilibrium.

The total torque required to operate the needle positioning mechanism would be the sum of the initial torque required for acceleration and the torques required to overcome the braking action of the needle funnel arms and needle cam legs, as a worst case scenario could position the arms and legs at their maximum deflection at the start-up of an operation. However the combined figures equate to a torque of 67.68 μNm which is 23.6 times smaller than the 1.6 mNm stall torque of the Namiki micromotor, therefore the chosen micromotor will operate the needle positioning mechanism.

5.4.2 Clockwise Motion: Needle Deployment

Once the desired position of the needle has been established through the anticlockwise rotation of the needle funnel it is then ready for deployment. Reversing the voltage on the micromotor reverses the direction of the needle funnel arms, this clockwise rotation will cause the ends of the needle funnel arms to engage with the protrusions on the inside face of the microrobot's body (Figure 5.3, c). This interaction with the arm tips and the microrobot's body will prevent any further rotation of the needle funnel and align the needle with the desired port ready for deployment.

5.4.2.1 Needle Funnel Arm: Buckling Analysis

The micromotor will be applying a constant clockwise torque to the needle funnel to enable it to maintain its position and deploy the needle, however due to the rotation being prevented a compressive force will be applied to the ends of the arms. Therefore it is important that the integrity of the needle funnel arms are maintained under this constant compressive loading and that they do not fail due to buckling. The compressive load acting on the end of the arms as a result of the moment generated by the micromotor can be calculated from the equilibrium equation determined from the static state of the system.

Figure 5.12 is a free-body diagram of a needle funnel arm under a constant load from the micromotor. It shows the reactions at the end of the arm for a state of equilibrium.

The reaction force A_x opposes the force delivered by the needle funnel arm (F). The force generated by the arm is 164.98 mN, this has been calculated from the 0.8 mNm deliverable

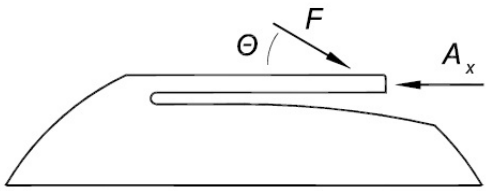


Figure 5.12: Free-body diagram of the forces acting on the needle funnel arm end

torque at the arm radius of 4.85 mm. The angle Θ is a result of the geometry of the protrusion on the inside face of the body and has been calculated at 30.19°. The compression force acting on the arm can be calculated as follows:

Summing forces about the x coordinate we obtain:

$$\sum F_x = (F \cos \Theta) - A_x = 0 \tag{5.16}$$

Resolving for the force A_x:

$$A_x = F \cos \Theta \tag{5.17}$$

Using the derived formula, equation (5.17) the compressive force acting on each arm equates to 142.6 mN. This axial compressive force will deflect the arm laterally or sideways. If the extent of this lateral movement is excessive then buckling will occur resulting in misalignment of the needle with the port in the body or total failure of the mechanism. Therefore it is essential that the arms can safely support the 142.6 mN compressive force without buckling.

Assuming the arms behave in a linear-elastic manner when the compressive force is applied and there is no side load, the calculated compressive force can be checked to determine the stability of the arm by using Euler's buckling equation [9]:

$$P_{cr} = \frac{\pi^2 E I_y}{(K_e L_e)^2} \tag{5.18}$$

Where P_{cr} is the critical load the column can carry, E is the material's Young's modulus, L_e is the *effective length* of the beam and K_e is the *effective-length factor* which represents the unsupported distance between the points of zero moment. As one end of the arm is

fixed and the other end is restrained as a result of the body's geometry the *effective-length factor* becomes $K_e = 0.7$. I_y is the moment of inertia for a solid rectangular beam and is given by:

$$I_y = \frac{hb^3}{12} \tag{5.19}$$

Where h is the height and b is the width of the beam's cross section.

The critical load required to buckle the needle funnel arm equates to 881 mN using Euler's buckling equation (5.18). This can be compared to the calculated compressive force in the arm of 142.6 mN. As can be seen, the load required to buckle the arm is far in excess of the load which can be delivered by the micromotor.

5.5 Prototype Manufacture

The following section presents a discussion of the prototyping methods selected to produce the component parts of the targeting mechanism. One-to-one scale component parts prototyped through an SLA manufacturing process are presented and also 5:1 scale component parts manufactured through conventional CNC milling are presented. The finished components are evaluated for their dimensional accuracy and for their functionality.

5.5.1 SLA Alpha Prototyping

One-to-one scale parts of the body, needle funnel, needle cam, ratchets, retaining plate and needle have been produced through an SLA manufacturing process, Figure 5.13 and Figure 5.14. SLA prototyping was selected as it was a very quick and cost effective method of realising parts. The purpose of the 1:1 scale prototypes was to test the functionality of the mechanism and also to determine how easily the parts could be assembled together as the physical size of the components could make handling potentially very difficult.

Figure 5.13 shows the component parts of the needle positioning mechanism manufactured from Accura 60 which is a resin with similar mechanical properties to polycarbonate (tensile strength of 58 - 68 Nmm^{-2} and an elongation at break of 5 - 13%). The spring was manufactured from stainless steel. The 1:1 scaled parts have been produced on a Viper si2 SLA system at high resolution with a laser beam diameter of 0.075±0.015 mm and a layer

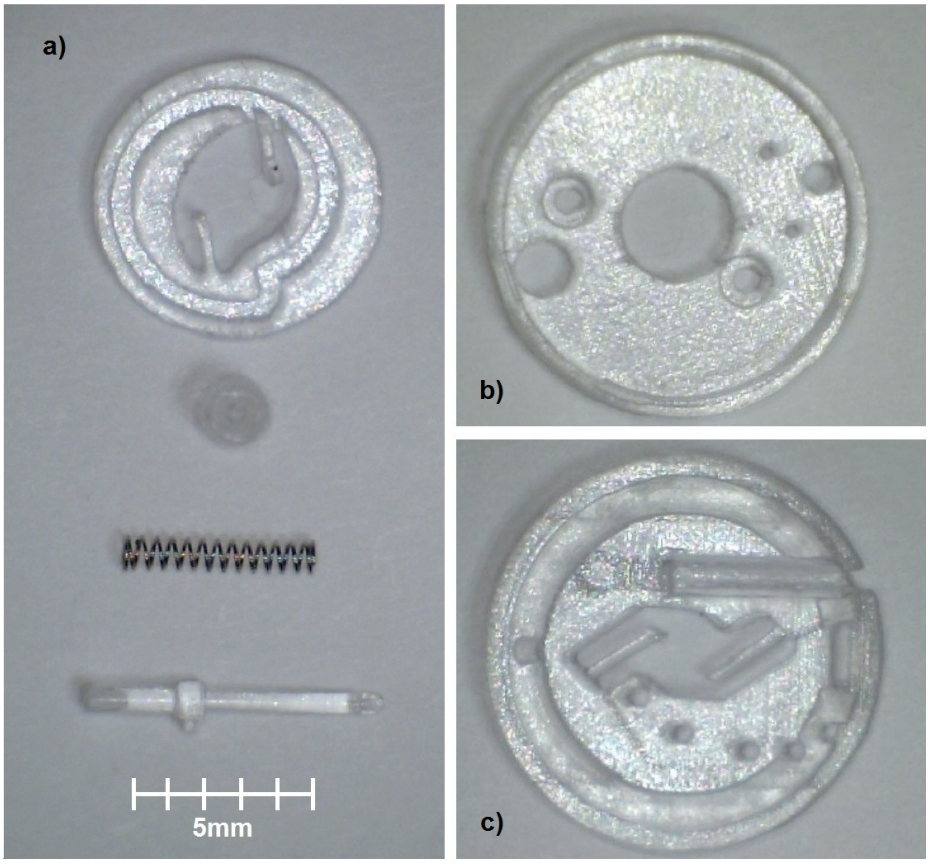


Figure 5.13: 1:1 scale SLA prototypes. a) shows the needle cam, ratchet, spring and needle combined with the driving peg b) shows the retaining plate and c) is the needle funnel

thickness of 0.05 mm. The SLA process offers the advantage of producing complex shapes without the need to invest in expensive tooling, this can clearly be seen with the needle funnel, Figure 5.13, c). The complex shape of the needle funnel combined with the cross holes and undercuts would have required complex tooling with movable cores to produce it through an injection moulding process.

The assembled needle positioning components can be seen in Figure 5.14. Figure 5.14, a) shows the needle funnel fitted with the needle and spring. Figure 5.14, b) shows the needle cam mounted in the needle funnel and engaged with the needle's drive peg. Figure 5.14, c) shows the needle funnel ratchet and the needle cam ratchet mounted on a drive spindle and the cavity in the case which will house the targeting mechanism. Figure 5.14, d) shows the case fitted with the mechanism and the drive spindle at the rear.

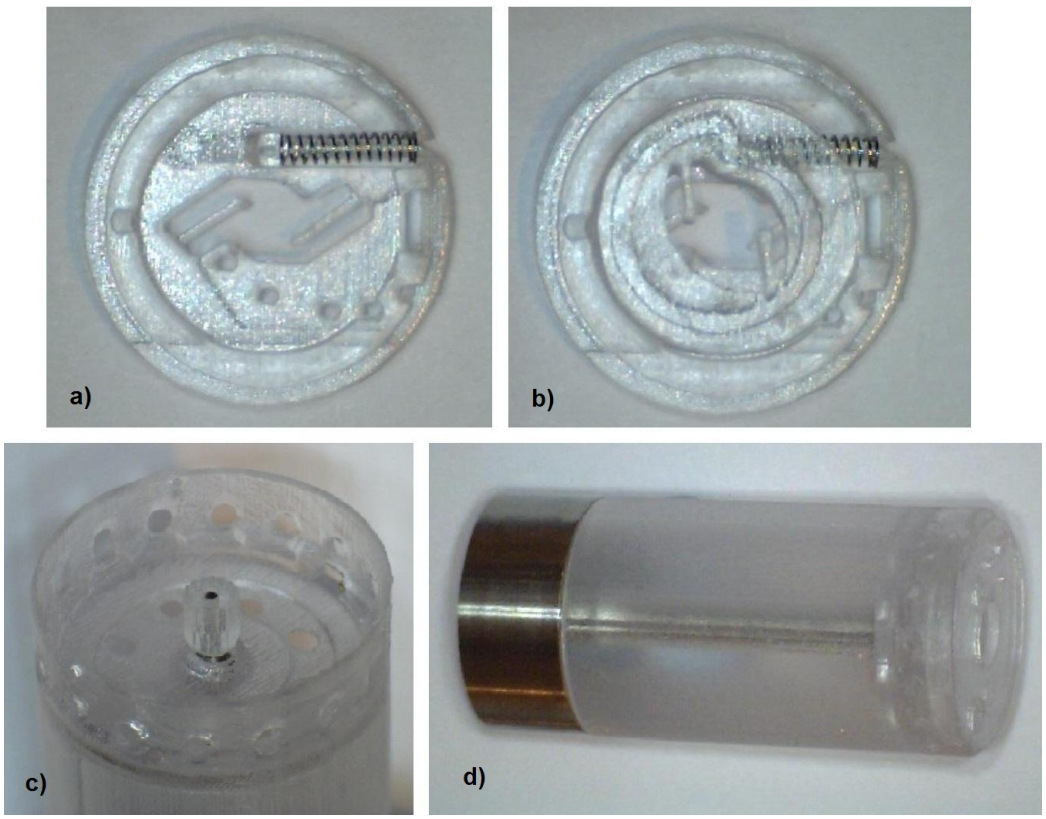


Figure 5.14: Assembled needle positioning mechanism. a) shows the needle funnel, spring and needle assembled b) shows the needle cam in position c) shows the ratchets and case cavity and d) shows the case fitted with the mechanism and coupled to a drive spindle

The proof of concept prototypes performed within the allowable design limits for the material with the arms and legs flexing and returning to their original positions. The spring allowed the needle to advance 2.0 mm and then return back to rest. However the performance of the mechanism was severely hindered due to features which were not fully formed. To drive the mechanism round requires the sharp edges of the ratchet to engage with the ends of the arms mounted on the needle cam (Figure 5.13, a)). However the arm tips were not fully formed and the radius of the laser beam resulted in rounded edges on the ratchet, these combined issues produced an intermittent engagement of the needle cam arms with the ratchet and therefore resulted in an intermittent operation.

5.5.2 Needle Positioning Mechanism Prototyping

To validate the efficacy of the needle positioning mechanism a 5:1 scale prototype was produced using conventional CNC milling techniques. The body and retaining plate were manufactured in PMMA to allow visualisation of internal component parts. Also a rigid material was required for the plurality of protrusions in the body which deflect the needle funnel arms. The needle cam, needle funnel and needle were manufactured from Nylon 6, which was chosen for its mechanical properties. The material for the spring was stainless steel. The mechanical properties of the 5:1 scale prototype are related to the materials' Young's modulus and the geometry of the component parts therefore the performance of the 5:1 scale prototype suggests that future prototypes at 1:1 scale will perform as designed. Figure 5.15 shows the component parts of the needle positioning mechanism.

The stainless steel spring is mounted onto the front section of the needle and butts up against the drive peg boss. Both the spring and the needle are fed into a captivating recess in the needle funnel (Figure 5.15). The needle can move linearly in the recess and is independent of the needle funnel however it will be under constant pressure from the spring as the end of the spring is retained by the end of the recess. The drive peg on the side of the needle protrudes outwards from the recess allowing it to engage with the needle cam.

The needle cam sits inside a counter bore in the front of the needle funnel. The counter bore captivates the needle cam and only allows the cam to rotate. The needle cam sits with the cam groove engaged with the drive peg on the needle. To prevent the needle cam from falling out during an operation the retaining plate is placed over the front of the needle funnel. A boss located towards the outside edge of the needle funnel engages with a corresponding hole in the retaining plate. The reason for this arrangement is to provide rotational drive to the holding mechanism for the purpose of positioning the holding mechanism diametrically opposite the needle.

The assembled needle funnel is loaded into the front of the body where the corresponding legs engage with the needle funnel ratchet, the needle cam ratchet and the arms engage with the protrusions. Three equally spaced pins are used to prevent the assembly from separating from the body when it is being operated. The pins are stepped which allows a press fit with the body and for them to pass through the body and into a groove which runs around the outside edge of the retaining plate. To prevent the pins from engaging with the bottom of the groove and to facilitate easy assembly and removal a larger diameter shoulder has been incorporated at the end of the pin. The retaining plate would be connected to the holding

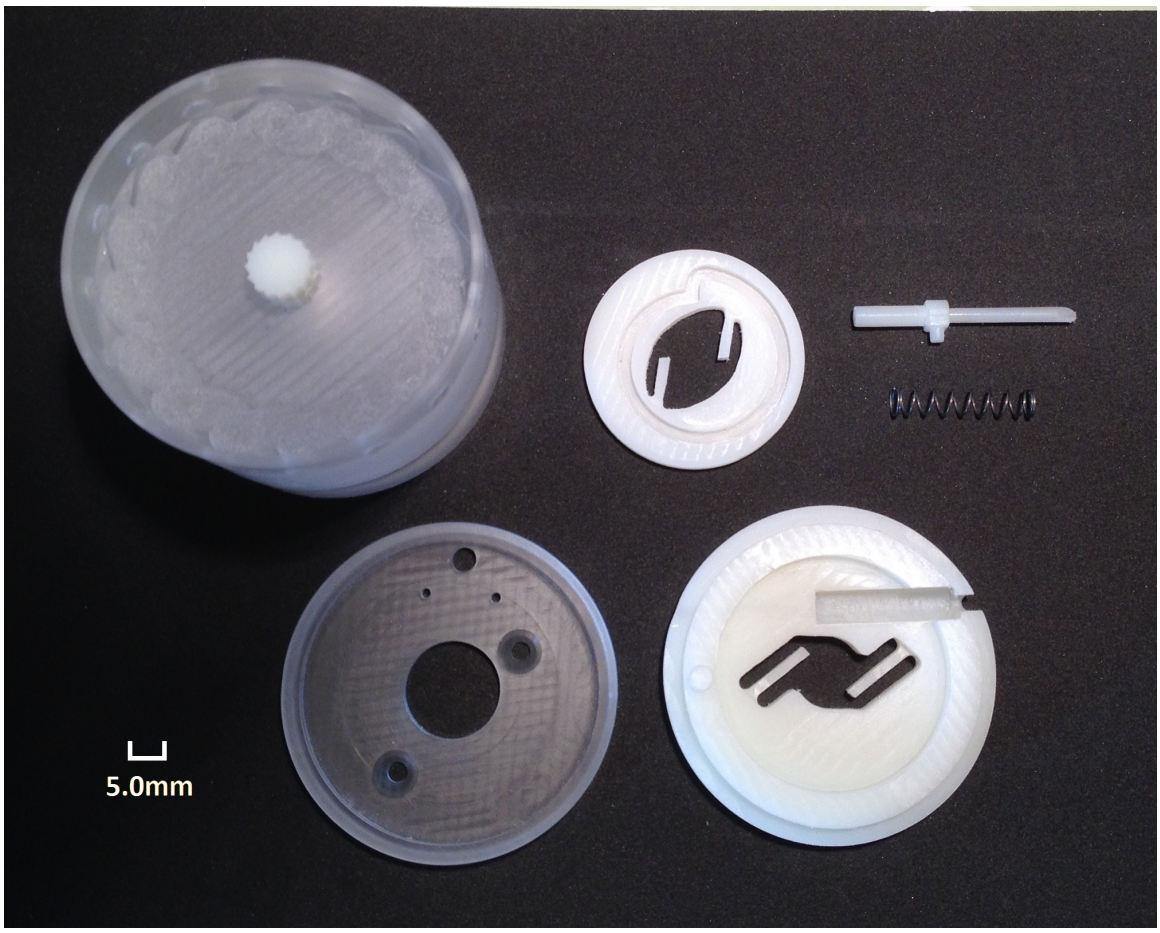


Figure 5.15: 5:1 scale prototypes of the body and ratchets, needle cam, needle and spring, retaining plate and needle funnel

mechanism via two M3 countersunk head screws which can be clearly seen in Chapter 4, Figure 4.28.

5.5.3 Needle Deployment

To simplify the operation of the mechanism the needle cam ratchet and the needle funnel ratchet were joined together to make a drive shaft which was extended such that it could pass through the body. The end of the drive shaft was threaded allowing a locking nut arrangement to be secured to it which would prevent the ratchet drive shaft from becoming unfastened when manually operated. The assembled needle positioning mechanism can be seen in Figure 5.16 and the mechanism at full extension can be seen in Figure 5.17.

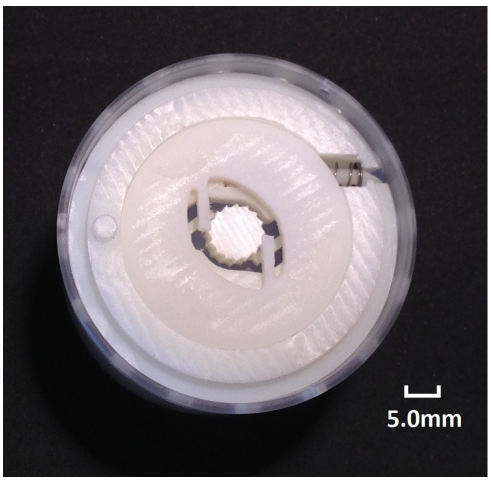


Figure 5.16: Assembled needle positioning components. Retaining plate has been removed for clarity

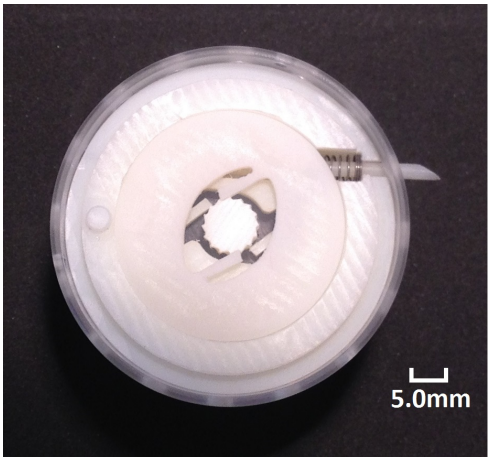


Figure 5.17: Needle positioning mechanism at maximum extension. Retaining plate has been removed for clarity

5.5.4 Needle Positioning Mechanism Performance

The needle positioning mechanism performs well under manual operation however modifications to the geometry of key parts were required to allow smooth operation. The dimensional accuracy of the manufactured parts was the largest problem in the assembly of the needle positioning mechanism prototype. For example, the needle funnel was designed with radial clearance between it and the inside bore of the body to allow it to freely rotate when

positioning the needle and driving the holding mechanism. However the outside diameter of the needle funnel and the overall thickness had been manufactured outside the expected tolerance of the part (± 0.1 mm). Also, even though a degree of working clearance was designed into the axial alignment of the parts the over-sized geometry caused the mechanism to lock up. Due to the complex shape of the needle funnel it was a difficult task to manually remove the excess material however this issue can be overcome in the future by attributing specific tolerances to the geometric features.

A significant issue contributing to the performance of the mechanism was the straightness of the ratchet drive shaft. As already discussed, the ratchets were joined together to simplify the operation of the mechanism. However on inspection of the drive shaft it was clear that the part was outside the limits for straightness. The bent shafts resulted in a concentricity error with the manual driving nut causing the mechanism to tighten up intermittently. Also significant radii were left in the base of the ratchets teeth this prevented the needle funnel arms from engaging correctly and driving the mechanism round. The problems with the drive shaft can be attributed directly to the manufacturing method selected by the company who produced them. They chose to mill the diameters rather than turn them and also to mill the ratchet teeth using a bull nose cutter. These manufacturing choices resulted in the shaft being out of straightness and out of concentricity.

It became evident through manual operation that the needle cam ratchet used to deploy and retract the needle was potentially redundant in normal use as the drive shaft could be linked directly to the needle cam. A scenario which utilises the needle cam ratchet would be if the needle is in the fully forward position and the micromotor was inadvertently driven anticlockwise the cam ratchet would act as a safety device and allow the micromotor to slip without causing damage. However it is unlikely this scenario would take place therefore it would be recommended that the ratchet be removed as this would simplify the design and ultimately reduce the cost.

5.6 Measurement and Characterisation of the Needle Positioning Mechanism

This section presents a series of experiments designed to validate the needle positioning mechanism. The experiments focus on the performance of the needle funnel through quantitative assessment of two 5:1 scale model prototypes manufactured from Nylon 6. The

mechanical properties of the 5:1 scale prototype are related to the materials' Young's modulus and the geometry of the component parts therefore the performance of the 5:1 scale prototype suggests that future prototypes at 1:1 scale will perform as designed.

5.6.1 Needle Funnel Arm Deflection Protocol

To determine whether the performance of the needle funnel arms correlates with the calculated load at maximum deflection an independent examination of the needle funnel arm has been performed.

As the calculated forces developed by the needle funnel arms are very low (<2 N) it is important that the test set-up be stable with limited external influences. Therefore purpose-built fixtures will be used to perform the protocol on as they offer a stable base and a means of securely holding the test piece during testing, Figure 5.18.

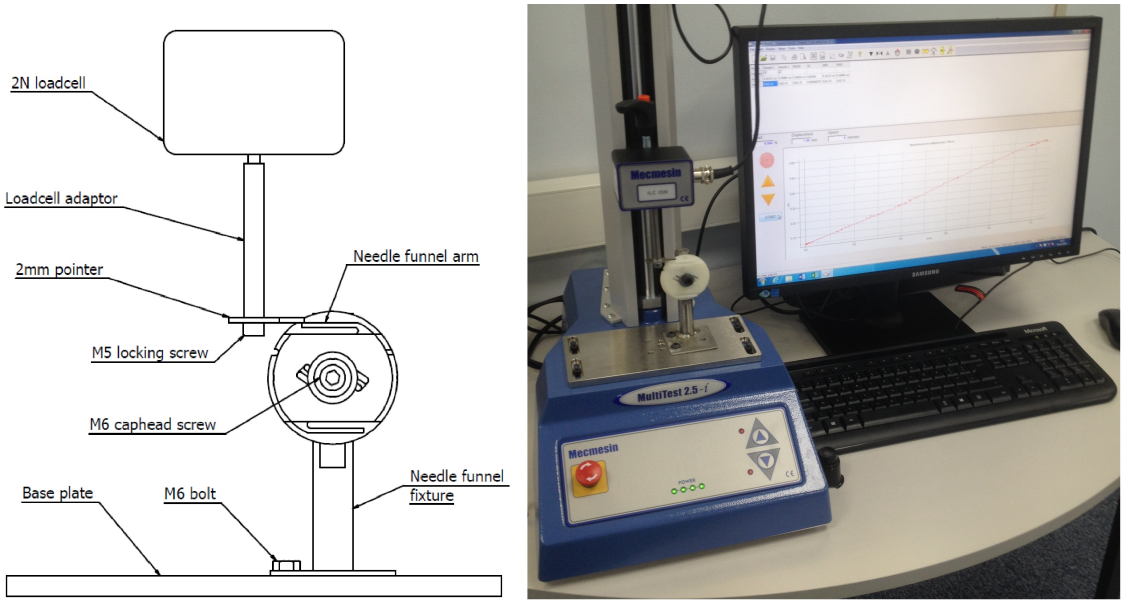


Figure 5.18: Left: Layout of needle funnel arm deflection fixture; Right: Experimental set-up comprising: a needle funnel mounted on the test bed of a MultiTest 2.5-i test system which is fitted with a 2 N loadcell and connected to a computer running Emperor^{TM} (force) software

5.6.1.1 Needle Funnel Arm Deflection Procedure

Figure 5.18 shows the test set-up used to determine the load generated by deflecting one of the needle funnel arms. The needle funnel is securely mounted to a fixture using an M6 caphead screw. The needle funnel arm is positioned such that it is aligned horizontally with the test bed and the tip of the needle funnel arm aligns with the tip of the 2 mm pointer.

During an operation the needle funnel arm will deflect 0.17 mm this equates to a deflection of 0.85 mm for the 5:1 scale prototype. A MultiTest 2.5-i (805-102) test system manufactured by Mecmesin is fitted with a 2 N loadcell (Intelligent loadcell ILC 879-009, $\pm 0.1\%$ of full scale) to measure the load generated by the deflection of the arm from its static state through a given distance. A computer running Emperor^{TM} (force) software (v. 1.18-408 (5/10/13)) is connected to the MultiTest system and used to record the deflection data. The deflection program will be run five times and the data for each run recorded. The results of the peak deflection load will be combined and the average of these runs will be used for the comparison with the calculated figure.

5.6.1.2 Results and Discussion

A profile of the load recorded for a needle funnel arm deflection of 0.85 mm is presented in Figure 5.19. It can be seen in Figure 5.19 that a displacement of 0.85 mm has been reached and a maximum peak load of 509.9 mN has been recorded at the end of the deflection.

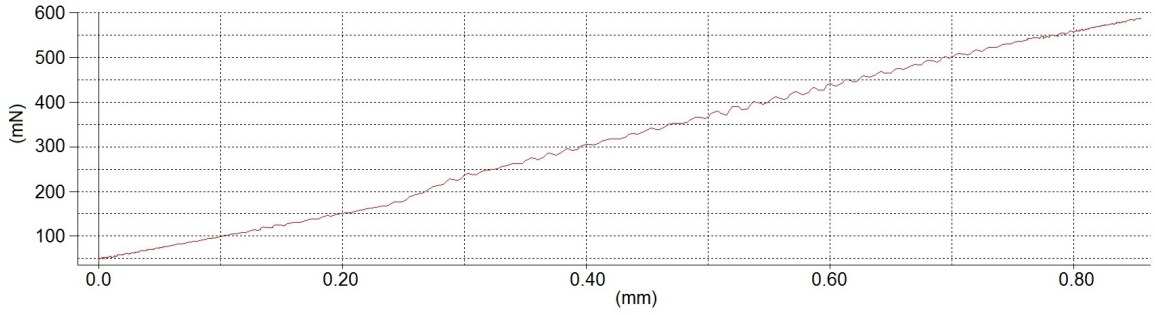


Figure 5.19: Needle funnel arm load deflection profile of a 0.85 mm deflection

Table 5.4 shows the average measured results for a series of deflection experiments on two prototype needle funnels. To minimise any inaccuracies with the experimental set-up and with the test procedure a series of results have been recorded from a deflection range

of 0.75 mm up to 1.05 mm for each of the needle funnel arms, as recording the deflection data for multiple values will highlight any inconsistencies with the measured results.

Table 5.4: Average recorded loads developed through a deflection range of 0.75 mm to 1.05 mm for each of the needle funnel arms

Deflection value (mm)	**Prototype No. 1 (mN)**	**Prototype No. 2 (mN)**	**Average force (mN)**
0.75	474.8	511.25	493.03
0.85	532.8	571.75	552.28
0.95	588.4	631.9	610.15
1.05	634.8	688.4	661.60

As can be seen from Table 5.4 the average load developed by deflecting the needle funnel arms at the optimum design value of 0.85 mm is 552.28 mN. This figure is approximately 48% lower than the calculated figure and is consistent with the measured figures across the range of deflections.

The geometry of the arm will influence its performance. The measured figures for the cross-sectional area of the arms showed that they were marginally undersize and that the lengths of the arms were an average of 0.1 mm longer than the designed value (with the material being removed from the back of the slots). These small variations in geometry are due to inaccuracies in the manufacturing process and will result in a reduced load being generated by the deflecting arm. The change in geometry only accounts for approximately 3% reduction in performance. However close dimensional inspection of the arms showed that, in all cases, the arms exhibited a degree of deflection already set into the arm at rest. The position of the arm tips varied from the designed nominal value by -0.2 mm up to -0.37 mm.

The movement of the arms can be attributed to stress relieving of the material due to the chosen manufacturing method and the selected material. The sequence of machining operations, the speed and cutter selected can all influence the stress developed in the component material. The net result of the arms positional movement reduces the effective spring pressure the arms can deliver and therefore could account for the 48% reduction in the measured results. Changing the material to an engineering material such as PEEK or annealing the material before machining would reduce the effects of the material's internal stress resulting in more dimensionally stable needle funnel arms.

5.6.2 Durability and Performance of Needle Funnel Arms

The objective of the experiment is to determine the stability of the needle funnel arms when subjected to multiple operations. During an operation the arms engage with protrusions on the inside edge of the body causing them to deflect inwards when rotating anticlockwise and to compress when rotated clockwise (Figure 5.3). Therefore the experiment will manually simulate a number of operations by subjecting the needle funnel arms to multiple deflections.

5.6.2.1 Needle Funnel Arm Performance Protocol

To determine the stability of the needle funnel arms the 5:1 scale prototype needle funnel, CNC machined from Nylon 6, is coupled to the retaining plate and mounted inside the PMMA body. The assembly is subjected to multiple operating cycles with each cycle combining a 360 degree anticlockwise rotation with a 22.5 degree clockwise rotation. The needle funnel and assembly can be seen in the top and bottom left of Figure 5.20.



Figure 5.20: Top left: Needle funnel arms, measurements are taken between the arrows; Bottom left: Needle funnel assembly; Right: TESA Vision 200 measuring system

A measurement is taken across the protrusions on the inside of the body to confirm they are within specification (Ø47.75 mm±0.05 mm). The needle funnel arms are measured from the outside edges of the tips (top left, Figure 5.20). Inspection of the dimension across the arms and protrusions will be carried out on a digital vision measuring system (TESA Vision 200, TESA Technology UK Ltd.) at 42.4X magnification (right, Figure 5.20). The assembly is mounted back into the body and manually operated for 10 cycles. On completion of the 10 cycles a further measurement across the needle funnel arms tips is taken. This process is repeated 10 further times giving a total number of operations of 100 cycles.

5.6.2.2 Results and Discussion

The performance protocol was carried out on two needle funnel assemblies. The results of the measured dimensions across the tips, series 1 and series 2, can be seen in Figure 5.21.

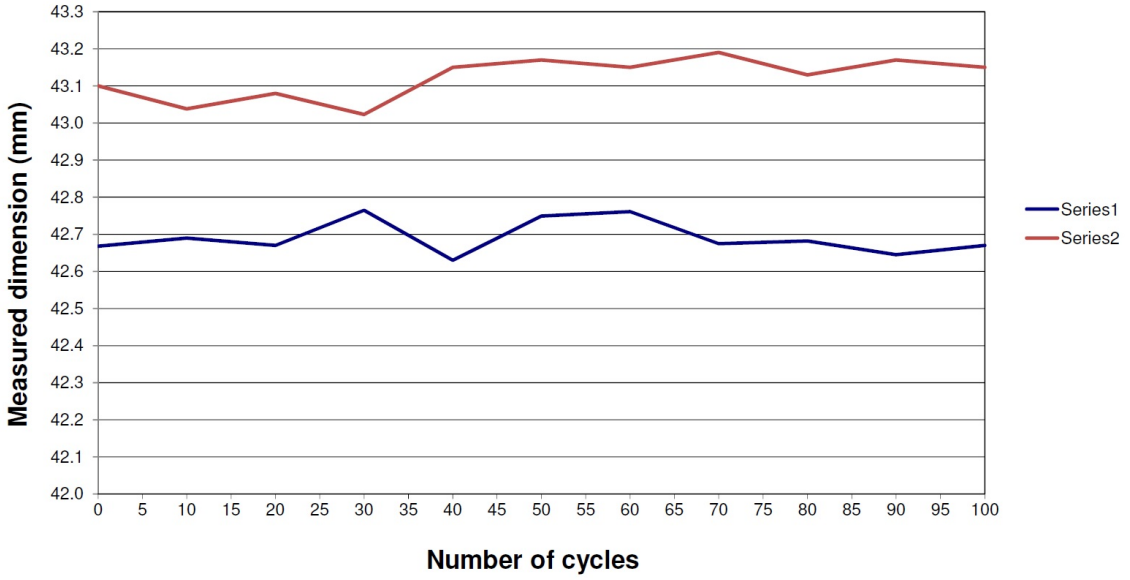


Figure 5.21: Plot of the measured arm dimension across the tips of two prototype needle funnels during repeated manual cycling

The results of the performance protocol show both needle funnel arms varying in dimension across the tips. The maximum standard deviation was 0.05 mm. The variations on the measured dimensions can partly be attributed to the inaccuracy of the test method as the needle funnels were manually aligned on the vision system before measurements were

taken. Further inaccuracies in measurement can be attributed to the material's colour as it proved very difficult to define the edges of the white feature when set against a white background.

The needle funnel assemblies performed within expected limits, the arms engaged and disengaged with the protrusions as expected. Series 1 (Figure 5.21) shows an initial starting dimension across the arm tips of 42.67 mm which is 0.16 mm shorter per side than the nominal design value of 43 mm. However the design of the mechanism would provide 0.73 mm of engagement with the protrusions. The results show that the needle funnels can maintain their performance through repeated operations.

5.6.3 Needle Funnel Ratchet Arm Deflection Protocol

For the needle positioning mechanism to function, the needle funnel arms must perform as designed however the needle funnel ratchet arms, which drive the needle funnel anticlockwise, must also perform. The needle funnel ratchet arms can be seen in Figure 5.22.

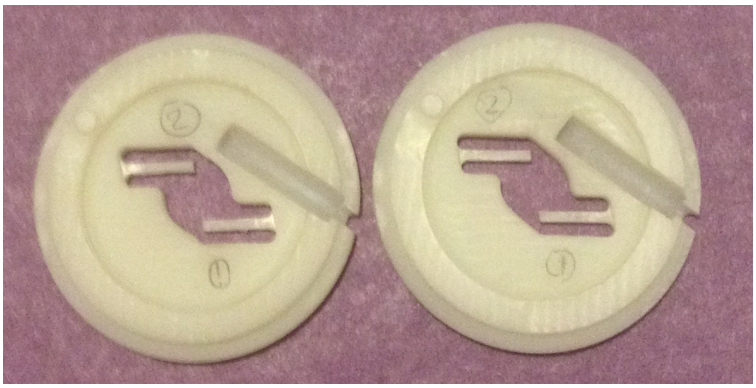


Figure 5.22: Prototype needle funnels CNC machined from Nylon 6. The ratchet arms can be seen in the centre of the parts

5.6.3.1 Needle Funnel Ratchet Arm Deflection Procedure

The set-up employed to test the deflection load generated by the needle funnel ratchet arms is in principle similar to the method used to test the needle funnel arms. However a different method of fixing the needle funnel ratchet to the needle funnel fixture is required. The test set-up can be seen in Figure 5.23.

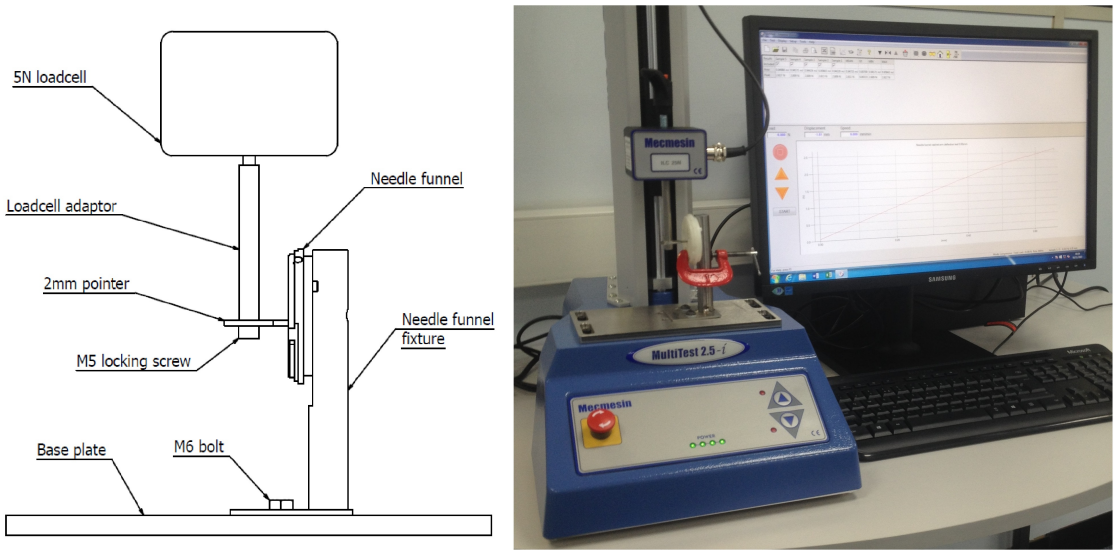


Figure 5.23: Left: Layout of needle funnel ratchet arm deflection fixture; Right: Experimental set-up comprising: a needle funnel mounted on the test bed of a MultiTest 2.5-i test system which is fitted with a 5 N loadcell and connected to a computer running Emperor^{TM} (force) software

The needle funnel is secured to the needle funnel fixture via a 1" G-clamp, making sure that the G-clamp does not interfere with the load cell adaptor and pointer when it performs a deflection procedure. The needle funnel ratchet arm is positioned such that it is aligned horizontally with the test bed and perpendicular to the 2 mm pointer. The side edge of the 2 mm pointer is positioned such that it just touches the tip of the needle ratchet arm.

A MultiTest 2.5-i (805-102) test system manufactured by Mecmesin is fitted with a 5 N loadcell (Intelligent loadcell ILC 879-010, $\pm 0.1\%$ of full scale) to measure the load generated by the deflection of the ratchet arm from its static state through a given distance. The deflection data is captured through a computer running Emperor^{TM} (force) software (V 1.18-408 (5/10/13)) and connected to the MultiTest system. The deflection program will be run five times and the data for each run recorded. The results of the peak deflection load will be combined and the average of these runs will be used for the comparison with the calculated figure.

5.6.3.2 Results and Discussion

The average measured results for a series of deflection experiments on each ratchet arm on two needle funnels are presented in Table 5.5. To limit any inconsistencies with the test procedure a series of results have been recorded from a deflection range of 0.55 mm up to 0.75 mm for each of the needle funnel ratchet arms.

Table 5.5: Average measured loads developed through a deflection range of 0.55 mm to 0.75 mm for each of the needle funnel ratchet arms

Deflection value (mm)	**Prototype No. 1 (N)**	**Prototype No. 2 (N)**	**Average force (N)**
0.55	2.04	1.92	1.98
0.65	2.37	2.25	2.31
0.75	2.70	2.55	2.63

Table 5.5 shows the average load developed by deflecting the needle funnel ratchet arms at the optimum design value of 0.65 mm to be 2.31 N. This figure is approximately 33.6% lower than the calculated figure.

Although the average deflection force is lower than the calculated force the individual loads for each arm presents a different result as arm number one on prototype number one performed within an average of 25.3% of the expected load at deflection, therefore the lower results recorded for the remaining three arms significantly influenced the overall average deflection force.

Inspection of the arms under 42.4X magnification showed that the arms were not of uniform thickness across their length as they ranged from 1.48 mm at the base of the arm to 1.65 mm at the tip. The manufacturing process has resulted in push-off when machining the arms, this is evident in the larger thickness at the tips of the arms. However the arms also exhibited a degree of deflection of an average of 0.295 mm already set into the arm at rest. These inconsistencies in geometry due to the manufacturing process could account for the reduction in the spring pressure the arms can deliver.

5.6.4 Durability and Performance of Needle Funnel Ratchet Arms

The durability of the needle funnel arms has been established, however to complete the operation of positioning the dispensing needle the needle funnel must engage with the ratchet, Figure 5.24. The ratchet engages with the tips of the needle funnel ratchet arms and drives the needle funnel anticlockwise to position the dispensing needle. Reversing the micromotor's direction results in the ratchet arms disengaging with the ratchet and riding over the ratchet teeth, this results in repeated flexing of the arms. Therefore the durability and stability of the needle funnel ratchet arms must be established through multiple cycling.



Figure 5.24: Needle funnel ratchet arms engaged with the ratchet

5.6.4.1 Needle Funnel Ratchet Arm Performance Protocol

The stability of the needle funnel ratchet arms can be determined through repeated manual cycling of the needle funnel. The needle funnel is mounted inside the PMMA body and engages with the ratchet, which is manufactured from Nylon 6. The assembly is subjected to multiple manual operating cycles with each cycle combining a 720 degree anticlockwise rotation followed by a 720 degree clockwise rotation. Two rotations clockwise and anti-clockwise have been selected for the protocol to simulate the possibility that the operator

may require a number of rotations before selecting the optimum position for delivery.

A measurement is taken across the peaks of the ratchet protrusions on the inside of the body to confirm they are within specification (Ø9.0 mm±0.05 mm). The needle funnel ratchet arms are measured from the inside edges of the tips. Inspection of the dimension between the arm tips will be carried out on a digital vision measuring system (TESA Vision 200, TESA Technology UK Ltd.) at 42.4X magnification. The needle funnel is mounted back into the body and manually operated for 10 cycles. On completion of the 10 cycles a further measurement between the needle funnel arm tips is taken. This process is repeated 10 further times giving a total number of operations of 100 cycles.

5.6.4.2 Results and Discussion

After the completion of each 10 cycles the measurements between the needle funnel ratchet arms was taken and recorded. The results for two sets of prototype needle funnel ratchets can be seen in Figure 5.25.

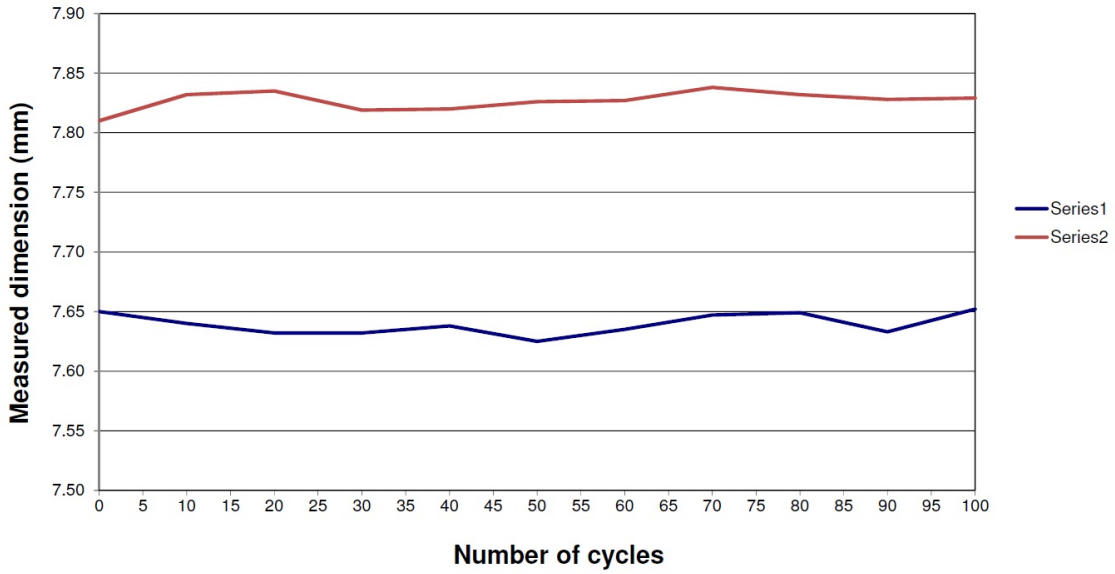


Figure 5.25: Plot of the measured arm dimension between the tips of two prototype needle funnels during repeated manual cycling

Measurement of the ratchet geometry showed that it was at the bottom of the tolerance limit (Ø9.0 mm±0.05 mm). However the tips of the arms engaged with the ratchet teeth

and drove the ratchet anticlockwise successfully. The edges of the ratchet teeth retained a sharp edge from the manufacturing process, this resulted in a positive transition of the arm tips when riding over the ratchet teeth. However it is recommended for a 1:1 scale prototype ratchet that it be made from a metal to prevent the edges from being damaged and to guarantee a positive engagement with the arm tips.

Figure 5.25 series 1 shows that the initial measurement between the arm tips was 7.81 mm which is 0.06 mm greater than the nominal design value of 7.75 mm. The increase in value will have the effect of reducing the amount of engagement the arm tip will have with the ratchet tooth. However the 5:1 scale prototype offers 0.65 mm of engagement therefore the small reduction will have a negligible effect on its performance. Series 2 shows that the initial measurement between the arm tips was 7.65 mm which is 0.1 mm smaller than the nominal design value. The reduction in value will have the effect of closing the arms on the ratchet and therefore it would offer a benefit to its performance.

The dimensional stability of the arms was very good as the greatest standard deviation was found to be 0.008 mm for series 1. The results show that the needle funnel ratchet arms can maintain their performance through repeated operations. The outcome of the needle funnel ratchet arm performance protocol confirms the durability and performance of the needle positioning mechanism.

5.7 Summary

In this chapter a novel concept targeting mechanism has been presented for the purpose of delivering a targeted dose of medication to a specific site of interest in the small intestinal tract. It has been shown through analysis, prototyping and testing of a 5:1 scale prototype that the targeting mechanism is durable and capable of being positioned within a 360 degree envelope to target a specific location.

The mechanical properties of the 5:1 scale prototype are related to the materials' Young's modulus and the geometry of the component parts, therefore the performance of the 5:1 scale prototype suggests that a scaled down version would perform equally as well. However *in-vivo* tests would need to be performed to validate the actual figures.

References

[1] L. Phee, D. Accoto, A. Menciassi, C. Stefanini, M. Chiara, Carrozza, and P. Dario, "Analysis and development of locomotion devices for the gastrointestinal tract," *IEEE Transactions on Biomedical Engineering*, vol. 49, pp. 613–616, 2002.

[2] T. Kunimine, S. Yoshioka, and K. Matsue, "The relations between modulus of rigidity and young's modulus for various kinds of wire," *IEIC Technical Report (Institute of Electronics, Information and Communication Engineers)*, vol. 98, pp. 33–36, 1998.

[3] D. Matthew, *Springs & Pressings: A Designers' Guide*. Hampshire: Southern Springs & Pressings Limited, 1st ed., 2001.

[4] R. Sharaf, P. Aggarwal, K. Kaler, and W. Badawy, "On the design of an electronic mosquito: design and analysis of the micro-needle," in *MEMS, NANO and Smart Systems, 2003. Proceedings. International Conference on*, pp. 32–35, 2003.

[5] S. Byun, J. Lim, S. Paik, A. Lee, K. Koo, S. Park, J. Park, B. Choi, J. Seo, K. Kim, H. Chung, S. Song, D. Jeon, and D. Cho, "Barbed micro-spikes for micro-scale biopsy," *Journal of Micromechanics and Microengineering*, vol. 15, pp. 1279–1284, 2005.

[6] "CES selector 4.1: Various technical data sheets," Granta Design Ltd, 2006.

[7] "Materials property guide: A comprehensive review of the materials properties of VICTREX PEEK high performance polymer," Victrex plc, 2007.

[8] "Polypenco materials: Physical properties," Nippon Polypenco Ltd, 2008.

[9] R. C. Hibbeler, *Mechanics of materials*. Prentice Hall, 8th ed., 2011.

[10] T. Aoyagi, "Namiki SBL015PG1609 rise time measurement," Namiki Precision of Europe SA, 2011.

[11] A. Bedford and W. Fowler, *Engineering Mechanics: Statics.* Addison Wesley, 1995.

Chapter 6

Drug Delivery System: Design, Analysis and Evaluation

6.1 Introduction

Targeting pathologies of the GI tract such as small intestinal Crohn's disease or ulcerative colitis requires the application of medication direct to the specific site [1]. The increased functionality presented in Chapter 4 and Chapter 5 allows a microrobot to resist peristalsis and to target a pathology of the GI tract. However the challenge of releasing medication from the microrobot still remains. This chapter presents the drug delivery system, the mechanism responsible for the delivery of an onboard supply of medication. This medication can be in the form of either a suspension or a concentrated volume, however it must be a liquid. A 1 ml volume of medication has been selected as the optimum dose as it is representative of the dose published in the prior art [2] and also the quantity being used in current trials stated in the literature [3]. This chapter focuses on the design and analysis of solutions to administer a metered dose of medication and the validation of the system through experimentation.

6.2 Overview

The clinical need to treat pathologies of the GI tract has been discussed in previous chapters. Chapter 4 and Chapter 5 address the issues of resisting natural peristalsis and targeting a specific location in the small intestinal tract, however the curative treatment of administer-

ing a metered dose of medication is required for a successful procedure. Figure 6.1 shows a concept design of a microrobot with an integrated drug delivery system.

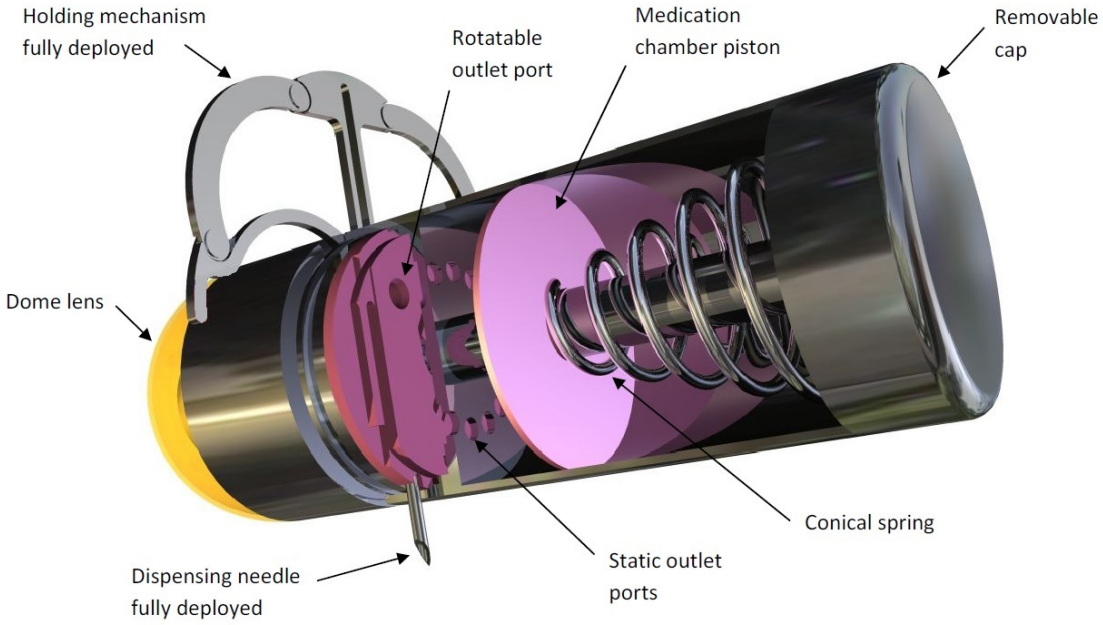


Figure 6.1: Microrobot concept design capable of delivering 1 ml of targeted medication. Needle shown fully extended and the medication partially deployed

Delivering an onboard supply of medication can be achieved through various means. For example a number of ideas were explored which utilised a micromotor to drive a leadscrew which in turn pushed a piston that forced medication out through a port. Another idea was to utilise a balloon which could be filled with liquid medication. A number of designs which employed a compression spring were also explored, however all these potential solutions posed a number of issues such as the requirement for a method to release the spring or balloon, space constraints or the practicality of swallowing such large devices. Therefore a solution which utilised a conical spring was chosen as this method offered reduced space requirement yet retained the potential for high energy release. A selection of delivery concepts which were explored are presented in Appendix C.

The chosen drug delivery system has the capacity to store a 1 ml volume of medication onboard the microrobot. The force generated by a compressed conical spring is proposed to expel the medication. The conical spring engages with a piston and when activated it will force the medication out of one of sixteen preset holes at the base of the medication chamber.

The holes have a thin membrane across them to protect the integrity of the medication and to prevent the medication from leaking into the needle positioning mechanism. Rotating the needle positioning mechanism will align a port on the back of the needle funnel with one of the sixteen holes, the remaining holes would automatically be blanked off and therefore prevent any ingress of the medication. The novel configuration of the conical spring provides a compact design however a triggering mechanism will also be required to automatically release the spring.

The following sections discuss the design and analysis of the drug delivery system, the trigger mechanism and the issue of power distribution through the microrobot. A series of experiments are presented which validate the drug delivery system.

6.3 Drug Delivery System

Using a compressed spring to drive the delivery of the medication would require allocating a volume of space within the microrobot for the spring's solid state volume and for the spring's actuation mechanism. A novel way of minimising the spring's volume is to use a conical compression spring, Figure 6.2.

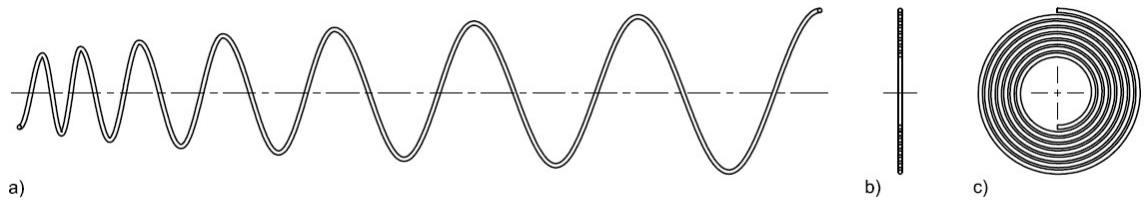


Figure 6.2: Conical compression spring configurations, 7.5 coils fully expanded with a variable pitch a) collapsed section view b) and fully coiled position c)

Figure 6.2 shows a variable pitch conical compression spring in its free state a) in the primed position b) and a plan view in the fully coiled position c). Winding the coils such as they lie inside each other (Figure 6.2, c) enables the same number of coils to be used as in a conventional compression spring to generate a force, however it significantly reduces the space required to hold the spring. For example, a conical compression spring with six Ø0.5 mm coils would occupy a solid state volume of 40.1 mm^3 this can be compared to a volume of 55.0 mm^3 for a conventional compression spring with the same geometry.

Providing clearance between the coils enables them to be spiralled inside each other. A variable pitch is required between each coil to allow the spring to collapse at the same rate, this is due to the larger coils collapsing faster than the tighter coils. This configuration allows the active coils to bottom simultaneously resulting in a straight line force versus deflection curve similar to the output of a conventional compression spring. To release the spring from the compressed position a trigger mechanism will be required. Appendix D compares the volume of the alternative designs which have been explored.

The conical compression spring will require analysing to determine the optimum medication delivery force. This will involve analysing a number of spring variables such as the number of coils, the diameter of the wire and the force required to operate the system. All these factors will influence each other's performance and a balance will need to be determined which will minimise the space required to house the system.

6.3.1 Drug Delivery

To deliver a 1 ml volume of medication to a target site requires the onboard supply of medication to be pushed through a series of holes allowing it to be expelled through the needle tip. To achieve this task an evaluation of the force required to expel the medication must be performed.

The bore of the needle is the most restrictive section of the delivery system for the flow of medication. The needle has an internal diameter of 0.38 mm and a length of 6.7 mm. As the needle has a consistent diameter and length Poiseuille's equation can be used to model the flow of medication through the needle. The assumptions which will be made with Poiseuille's equation are that the medication is incompressible and Newtonian, the flow is laminar and friction will be ignored [4].

The flow rate of a needle Q_f can be calculated as follows:

$$Q_f = \frac{\pi r^4 (P_2 - P_1)}{8 \eta_v l} \tag{6.1}$$

Where r is the radius of the needle's bore, η_v is the viscosity of the medication and l is the length of the needle. P_1 is the pressure at the end of the needle and P_2 is the pressure required to expel the medication. For the purpose of analysis the viscosity of the medication will be based on water at 36^oC ($0.705 \,\mathrm{x}\, 10^{-3}$ Pa s). P_1 is the pressure resistance of

the medication being introduced into the GI tract wall. The interstitial hydrostatic pressure in subcutaneous tissue can range from -8 mmHg to +6 mmHg for normal tissue however for tissue with a tumour the pressure can be much greater. Therefore P_1 will be taken as the subcutaneous pressure in a tumour which is approximately +20 mmHg (2.6 kPa) [5].

As the medication must be absorbed by the subcutaneous tissue a delivery time has been set at 3.5 s (Table 3.1). The flow rate (Q_f) can be calculated by dividing the 1 ml volume of medication stored onboard the microrobot by the target delivery time (3.5 s).

Rearranging equation (6.1) allows the pressure difference ΔP to be calculated (2.63 kPa). As the pressure difference $\Delta P = P_2$ - P_1 the pressure required to deliver the medication in 3.5 s (P_2) can be determined, 5.23 kPa. The delivery pressure (P_2) multiplied by the area of the medication chamber's plunger gives the delivery force required to expel the medication. The force applied to the medication chamber's plunger equates to 0.43 N.

The flow of the medication through the needle was assumed to be laminar however to confirm this the Reynolds number can be used to determine how the medication flow is acting:

$$R_e = \frac{\rho d v}{\eta_v} \tag{6.2}$$

Where ρ is the density of the medication, d is the diameter of the needle, v is the velocity of the medication and η_v is the viscosity of the medication.

The Reynolds number for the system equates to approximately 1.9. For $R_e < 2100$ the flow is laminar and for $R_e > 4000$ the flow is turbulent. A Reynolds number between these two limits results in transition flows which can either be laminar or turbulent. The low Reynolds number confirms the flow will be laminar and therefore no compensation for changes in pressure will be required.

There are a number of variables which can affect the delivery time, for example if the viscosity of the medication were to decrease it would speed up the delivery time while a decrease in temperature would slow down the delivery time.

6.3.2 Spring Design Analysis

The geometry of the microrobot places limits on the allowable design parameters which can be used in the design of a conical spring. However the spring must be designed to fit within a volume of 40.0 mm^3 and deliver a force of 0.43 N over a stroke of 12.05 mm. As the spring's deliverable force is known the spring's deflection f can be calculated by the following formula for conical compression springs [6]:

$$f = \frac{16n(r_1 + r_0)(r_1^2 + r_0^2)F_d}{d^4 G} \tag{6.3}$$

Where n is the number of active coils, r_0 is the mean coil radius of the first coil and r_1 is the mean coil radius of the last coil, F_d is the force, d is the wire diameter and G is the module of rigidity. A stainless steel wire spring with a module of rigidity value of 69.0 GNm^{-2} [7] will be used for the spring analysis.

Using an input force of 0.43 N and a combination of 0.254 mm diameter wire, 7.5 active coils, a mean coil radius of 2.1 mm for the first coil and a mean coil radius of 5.0 mm for the final coil results in a spring with a free length deflection of 49.73 mm and which only occupies a volume of 17.89 mm^3. However equation (6.3) calculates the deflection (f) based on a solid length of n x d whereas the compact design of the conical spring requires the spring wires to be coiled inside each other, this will result in a greater deflection length and therefore an increase in the initial starting load. As the deflection is known the new starting load F_c can be calculated as follows:

$$F_c = \frac{F_d}{f}((nd) - d + f) \tag{6.4}$$

The increased spring deflection results in a new starting force (F_c) of 0.59 N however at the end of the 12.05 mm stroke length the conical spring will be delivering 0.43 N. The deflection force can be used to determine the stress (τ) in the spring and can be calculated by rearranging the following formula:

$$F_c = \frac{\pi d^3}{16 r_1}\tau \tag{6.5}$$

The 0.59 N force which is generated by the spring at the start of the stroke results in 915.16 MNm^{-2} of stress induced in the compressed spring. The requirement for the spring

is for a single operation therefore the maximum allowable static stresses would be limited to 59% of the material's ultimate tensile strength (2,200 MNm^{-2}) [8]. The resulting stress in the spring represents 41.6% of the allowable static stress therefore the variable pitch conical compression spring design will be acceptable for the application.

6.3.3 Trigger Mechanism

To deliver the 1 ml volume of medication a trigger mechanism is required to release the compressed conical spring. Releasing the spring remotely at the required moment in time is a challenging requirement. The system chosen to release the spring is a thermo mechanical method. This method of triggering the spring relies on the Joule's effect to heat an igniter which in turn ignites a pyrogen that melts a Nylon wire. The Nylon wire is employed to retain the compressed coiled spring. Figure 6.3 shows a layout of the proposed system.

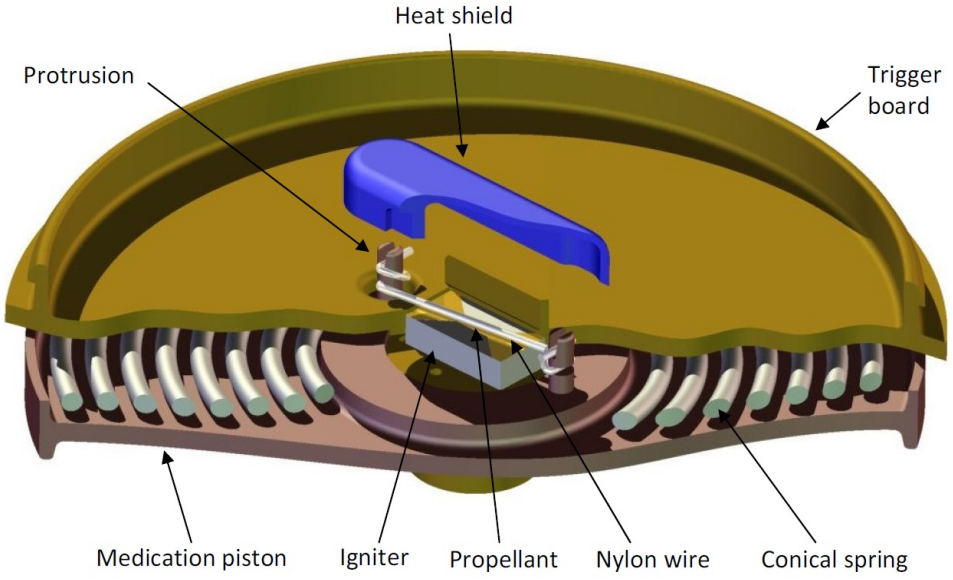


Figure 6.3: Cut-through view of the thermo mechanical trigger mechanism. Heat shield shown suspended above the igniter and Nylon wire

Figure 6.3 shows a section view through the thermo mechanical trigger mechanism. The trigger mechanism utilises a Nylon wire to retain the medication chamber piston (Figure 6.1) which in turn traps the conical spring, preventing it from expanding. The medication chamber piston has two protrusions which pass through the trigger board. The trigger board

connects the power supply section to the main body of the microrobot. The protrusions have been designed with two perpendicular tapered slots. The tapers in the slots retain the Nylon wire when it is manually wrapped around the protrusions. The Nylon wire passes over the igniter and propellant. A heat shield is placed over the top of the Nylon wire and it also encompasses the protrusions. The heat shield is retained by two vertical arms mounted on the trigger board to prevent it from separating at the point of ignition. Once the thermo mechanical mechanism has been fired the medication piston will be propelled towards the front of the microrobot, this action will simultaneously suck the exhaust fumes and heat from the propellant into the medication chamber, therefore dissipating any heat generated and preventing heat radiating into the power supply area.

The compressed conical spring will be delivering a load of 0.59 N at maximum compression therefore the Nylon wire must be capable of holding this force without breaking prematurely or elongating under the strain and partially delivering the medication. A Nylon monofilament wire has been selected which melts at 220 °C, has a Young's modulus of 3,300 $\mathrm{MNm^{-2}}$ and a diameter of 0.10 mm. The technology chosen to ignite the propellant, which in turn will melt the Nylon wire, is an electro-pyrotechnic initiator thin film chip (EPIC) (Vishay Intertechnology, Inc.). The microjoule energy device is a surface mount device (SMD) (size 0603) comprising a ceramic (alumina) based substrate with a tantalum nitrogen (Ta_2N) deposit as the activating resistor. A deposit of boron potassium nitrate ($BKNO_3$) (25% boron/75% potassium) propellant is applied to the EPIC igniter. Boron potassium nitrate ignites at 730 K (456.85 °C) [9] and reaches a flame temperature of 3,000 °C [10] therefore it will be capable of melting the Nylon wire.

The resistance (R_{tn}) of the tantalum nitrogen heating element is dependent on the resistivity of the material and the geometry of the element. It can be calculated as follows:

$$R_{tn} = \frac{r_{tn} l}{wt} \tag{6.6}$$

Where r_{tn} is the resistivity of the tantalum nitrogen material (400 $\mu\Omega$ x cm), l is the length of the heating element, w is the width and t is the material's thickness.

Using the geometry of 75 μm for the length (l), 50 μm for the width (w) and 2 μm for the thickness (t) results in a heating element resistance (R_{tn}) of 3.0 Ω.

The electrical energy (E_i) required to ignite the propellant and melt the Nylon wire can be calculated by the following formula:

$$E_i = lwt\rho C_p \Delta T \tag{6.7}$$

Where l is the length of the heating element, w is the width, t is the material's thickness, ρ is the density of tantalum nitrogen ($11.5\,\mathrm{gcm}^3$), C_p is the specific heat of the material ($0.14\,\mathrm{J\ g^{-1}\ °C^{-1}}$) and ΔT is the adiabatic temperature required at the heating element.

Using equation (6.7) with the heating element geometry already specified and an ignition temperature (ΔT) of 456.85 °C results in an electrical energy of 5.5 μJ required to ignite the propellant. However a safety factor is required to ensure that the electrical pulse delivered to the EPIC device is sufficient to ignite the propellant therefore a safety factor of 10 will be applied. Incorporating the safety factor into equation (6.7) results in 55 μJ of electrical energy required to ignite the boron potassium nitrate propellant.

The firing time (F_t) required to ignite the propellant can be calculated using the following formula:

$$F_t = \frac{E_i}{R_{tn} I^2} \tag{6.8}$$

Where E_i is the electrical energy required to ignite the propellant, R_{tn} is the resistance of the heating element and I^2 is the supply current.

Using equation (6.8) with a supply current of 0.5 A results in a firing time of 74 μs. Increasing or decreasing the current will affect the firing time. However the combination of the heating element geometry and the supply current must be chosen to guarantee the device does not fire through external influences, such as electro-magnetic interference from the environment, and can only be fired by the activation energy pulse.

6.4 Measurement and Characterisation of the Drug Delivery System

This section presents a series of experiments designed to validate the drug delivery system. The experiments focus on determining the parameters required for the delivery of the medication and on the performance of the conical spring through quantitative assessment of a 1:1 scale model prototype manufactured from stainless steel (BS 2056 Austenitic 302).

6.4.1 Drug Delivery Performance Protocol

The purpose of the drug delivery experiment is to determine if the chosen delivery speed of 3.5 s is a suitable delivery speed to expel the 1 ml of onboard medication. The analysis performed in Section 6.3.1 (equation 6.1) was based on water at body temperature (36^oC) however ex vivo experiments will be performed at room temperature therefore the viscosity of the water will increase to 1×10^{-3} Pa s to compensate. The implications of this change will be a reduction in delivery speed to 5 s to maintain the calculated delivery force.

The test set-up used to measure the delivery force required to expel the 1 ml of medication is presented in Figure 6.4, a). A specially designed plunger has been produced which can be used with a conventional syringe body. The plunger is independent of the loadcell adaptor and any sideways movement between the plunger and body has been minimised for the purpose of reducing friction within the system. The reduction in friction will result in a consistent force being generated by the plunger assembly.

The mathematical model (equation 6.1) presented for calculating the force required to deliver the medication assumed a straight through needle orientation and presented no difference between a vertical and horizontal configuration due to the Reynolds number being very low, however comparing the flow of a liquid in the vertical configuration (Figure 6.4, b) with the flow of liquid in the horizontal configuration (Figure 6.4, c) will prove the validity of this hypothesis.

6.4.1.1 Drug Delivery Procedure

Figure 6.4 shows the test set-up used to determine the force required to deliver a 1 ml volume of water. The body of a 2.5 ml capacity syringe (300185, BD Plastipak) is securely held in a fixture. The bore of the syringe (Ø8.60 mm) is used to calculate the linear movement of the plunger (17.20 mm) required to deliver 1 ml volume of liquid. A MultiTest 2.5-*i* (805-102) test system manufactured by Mecmesin is fitted with a 5 N loadcell (Intelligent loadcell ILC 879-010, ±0.1% of full scale) to measure the load required for a delivery. The loadcell has been programmed to travel at the required delivery speed of 207 mm/min for a distance of 17.20 mm from the tared zero position. A computer running Emperor^{TM} (force) software (v. 1.18-408 (5/10/13)) is connected to the MultiTest system and used to record the delivery data.

The delivery program will be run multiple times with no liquid being delivered and the

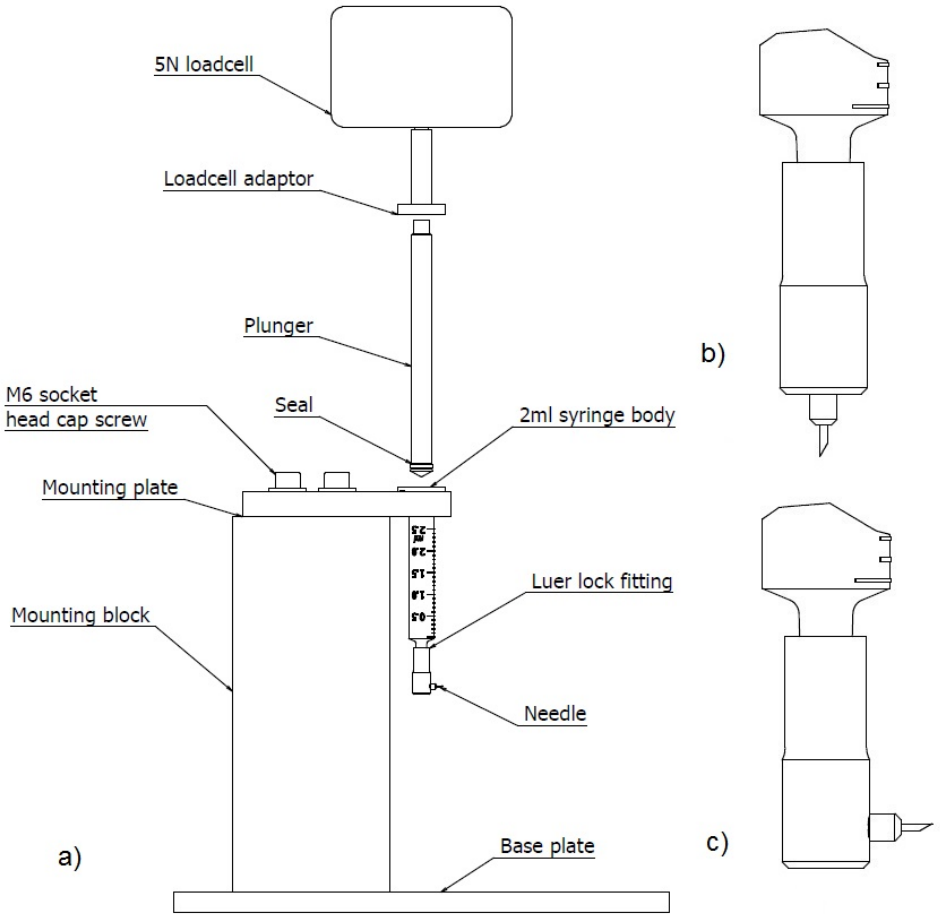


Figure 6.4: Layout of the medication performance delivery test fixture a), vertical needle configuration b) and horizontal needle configuration c)

data for each run recorded. The results of the average delivery force will be combined and the average of these runs will be used to calculate the friction in the system due to the seal on the plunger. The syringe will be filled with water and a piece of chicken breast flesh positioned such as the needle tip is embedded into the chicken by approximately 1.5 mm. Chicken breast flesh has been chosen as it has significant similarities to the tissue of the GI tract wall [11]. The delivery program will be run multiple times with the data for each run recorded. The results of the average delivery force will be combined and the average of these runs will be used to calculate the delivery force required to deliver the 1 ml volume of water.

6.4.1.2 Results and Discussion

Measurement of the force required to operate the plunger assembly with the luer lock and needle fitted were first taken to establish a baseline friction force for the plunger assembly. Due to the sensitivity of the measuring system and the variability of the results a large number of deliveries were performed. Over a set of 30 runs the average delivery force for a dry delivery was 2.32 N.

A series of deliveries were performed which expelled a 1 ml volume of water with the needle orientated in the vertical configuration and also with the needle orientated in the horizontal configuration, as this would more closely match the needle orientation in the microrobot. The needle configurations can be seen in Figure 6.5.

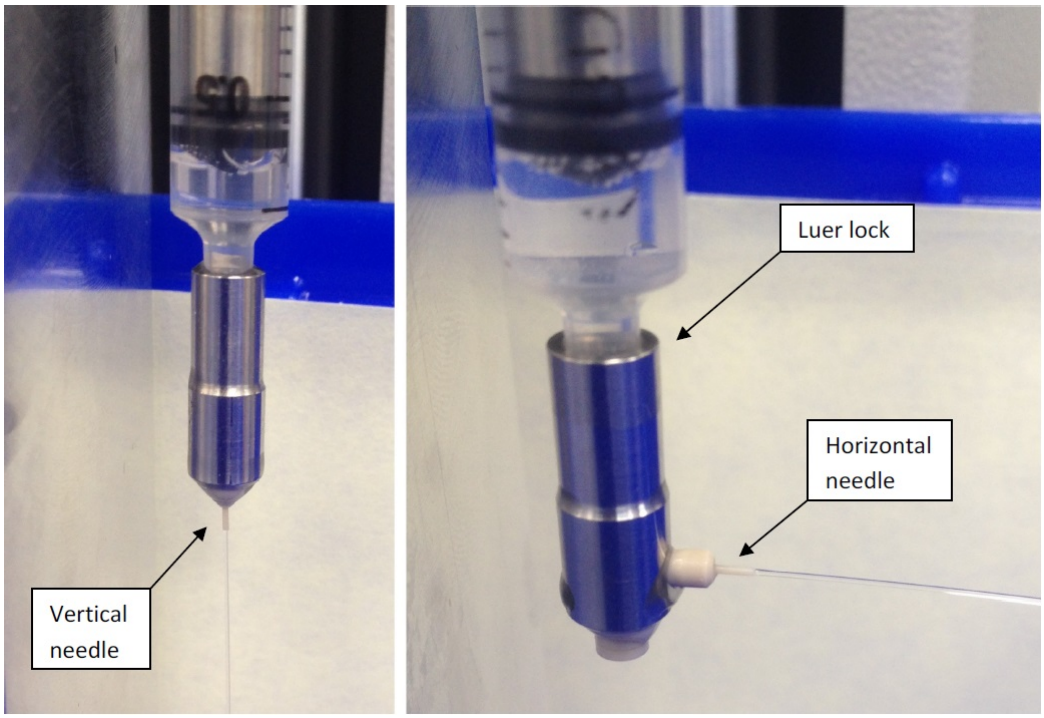


Figure 6.5: Left: Vertical needle configuration; Right: Horizontal needle configuration

The average delivery force for a 1 ml volume of water over 10 runs for the vertical configuration was 2.755 N, this can be compared to the average delivery force for the same volume of water over 10 runs for the horizontal configuration which was 2.738 N. The results show that the average horizontal delivery force is lower than the vertical delivery force. The small difference in delivery force (17 mN) can be attributed to the sensitivity of the test

method. However the results confirm that there is very little turbulence in the system and hence confirms the low Reynolds number and that the flow will be laminar.

A series of deliveries were performed which expelled a 1 ml volume of water into chicken breast flesh to simulate the intestinal pressure at the end of the needle tip. The needle was orientated in the vertical configuration as it guaranteed needle penetration and prevented the chicken breast flesh from being pushed away from the needle due to the pressure of the delivery force. The set-up used to measure the delivery force can be seen in Figure 6.6.

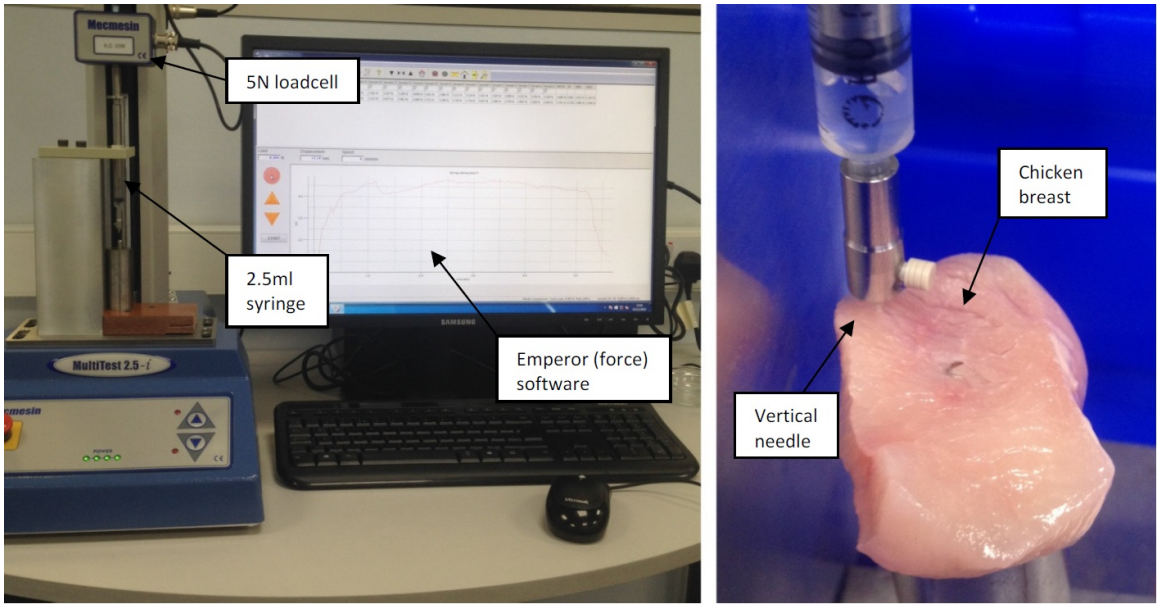


Figure 6.6: Left: Medication delivery force experimental set-up comprising: a 2.5 ml syringe body mounted on a block, the Ø0.38 mm bore needle fitted to the syringe and a MultiTest 2.5-i test system fitted with a 5 N loadcell and connected to a computer running Emperor^{TM} (force) software; Right: Needle delivering liquid into a chicken breast test piece

An overlay of the measured load profiles for three deliveries of a 1 ml volume of water into chicken breast flesh can be seen in Figure 6.7. The average delivery force required to expel the volume of water was 2.95 N with a standard deviation from the mean of 40 mN. However subtracting the baseline friction force for a dry delivery of 2.32 N from the delivery force results in a delivery force of 0.63 N. This figure is very close to the spring's calculated start force of 0.59 N (equation 6.4).

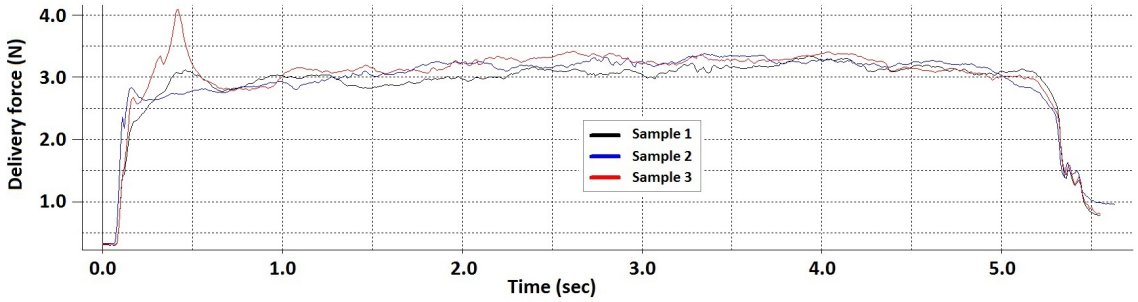


Figure 6.7: Overlay of three plots of the measured delivery force required to deliver a 1 ml volume of water into chicken breast flesh

The test result plots highlight the behaviour of the delivery method, for example a spike of 4.08 N can be seen in sample 3 at the beginning of the delivery (Figure 6.7). The spike can be attributed to the build-up of liquid due to the chicken breast flesh not absorbing the water quickly enough and hence causing a back pressure. The measured data suggests that the delivery speed of 5 s should be increased to allow the medication to penetrate and be absorbed by the tissue however this is based on the behaviour of chicken breast flesh at room temperature and *in-vivo* tests would need to be performed to validate the actual figures.

6.4.2 Spring Deflection Protocol

To deliver the medication in 5 s the variable pitch conical compression spring must be capable of delivering the calculated force of 0.59 N at the start of the delivery. Therefore the design of the spring must be validated to ensure its suitability to perform the task. There are no British Standards or industry standards for the design of conical compression springs however the Institute of Spring Technology (IST) provides a software package which is based on theoretical mathematical models and empirical data to aid in the design and analysis of conical compression springs and also to determine their suitability for manufacture. The IST software will be used to verify the calculations derived in Section 6.3.2.

The space available onboard the microrobot to house the spring has changed due to the requirements imposed by the trigger mechanism therefore the spring parameters will be modified from those used on the theoretical mathematical model (equation 6.4) to accommodate the available space. Using the IST spring calculator professional software (v1.0.18) a prototype 1:1 scale variable pitch conical compression spring will be designed and eval-

uated for its suitability to deliver the required starting load and also to perform within acceptable stress levels (59% of UTS).

A stainless steel wire spring (BS 2056 Austenitic 302S26 G2) with a module of rigidity value of 70.3 GNm^{-2} has been selected for the prototype spring. The 0.25 mm diameter wire has 7.5 active coils, 2 dead coils for the purpose of stabilising the spring during testing, a mean coil radius of 2.6 mm for the first coil and a mean coil radius of 5.12 mm for the final coil and a free length of 48.84 mm. The modified spring parameters result in a linear spring rate of 10.9 mN/mm which equates to a theoretical solid state load of 0.53 N however the software predicts a solid state load of 0.79 N and a solid state stress of 991 Nmm^{-2} (45% of UTS). The discrepancy in load can be attributed to one of the coils prematurely touching at the final stage of compression, this will result in the coil collapsing which in turn will increase the spring rate. However it is anticipated that manual modification of the spring end will eliminate this issue and result in the calculated load (0.53 N).

6.4.2.1 Spring Deflection Procedure

The stainless steel variable pitch conical compression spring will be mounted on a mandrel and held between two supports which have been designed to hold the end coils in position while the spring collapses. The test set-up used to measure the force delivered by the compression of the conical spring is presented in Figure 6.8.

The spring will be tested on a MultiTest 2.5-i manufactured by Mecmesin. A 2 N loadcell (Intelligent loadcell ILC 879-009, $\pm$0.1% of full scale) will measure the load generated by the compression of the spring from its free state to its solid state. The test will be run at a velocity of 145.0 mm/min which matches the calculated delivery speed. The compression program will be run multiple times with the data for each run recorded. The results of the average peak force at solid state will be combined and the average of these runs will be used to calculate the delivery force. A further measurement at 12.05 mm deflection will be recorded and the average force from the deliveries will be used to determine the spring's force at the end of its stroke.

6.4.2.2 Results and Discussion

A total of 10 springs were dimensionally inspected on a digital vision measuring system (TESA Vision 200, TESA Technology UK Ltd.) with the results showing that the 2.6 mm

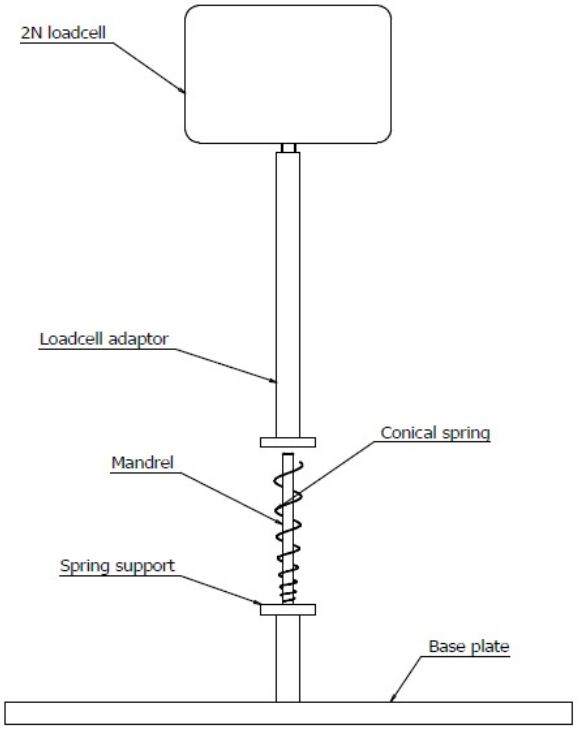


Figure 6.8: Variable pitch conical compression spring deflection load test fixture

mean coil radius for the first coil was outside of the design specification at 2.76 mm and the springs' free length was 47.7 mm compared to the design value of 48.84 mm. The reduced clearance between the coils due to the larger radius of the first coil resulted in the coils touching during the final stages of compression. The coils could not be manually modified to reinstate the clearance as initially anticipated therefore the springs were tested through a stroke length of 46.65 mm to minimise the impact of the coils colliding. Figure 6.9 shows the conical compression spring in its free state.

The test jig was configured such that the mandrel could pass freely in and out of the load-cell adaptor without generating a false reading on the loadcell due to friction. A 0.50 mm by 10.30 mm diameter counter bore was positioned in the loadcell adaptor support to accommodate the large coil and to prevent it from moving during compression. The 0.50 mm depth of the bore allowed clearance for the coils at the end of the stroke. Figure 6.10 shows the test set-up used to hold the spring vertically between two supports and via a central mandrel. The spring is also shown in the fully compressed configuration.

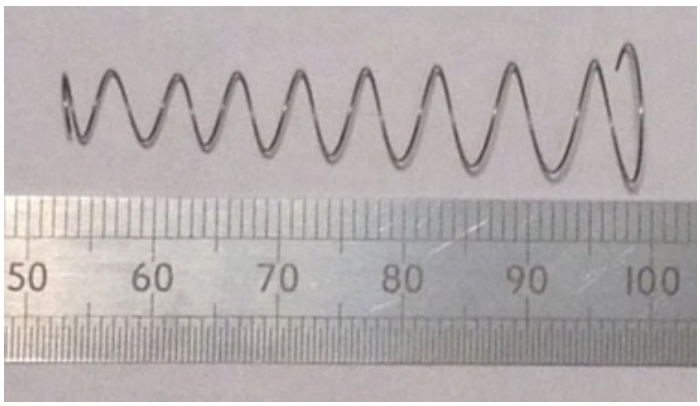


Figure 6.9: 1:1 scale prototype stainless steel variable pitch conical compression spring

A total of 10 springs were compressed 10 times each from a preloaded compression of 0.20 mm through a stroke length of 46.45 mm to give a total working compression of 46.65 mm. The stroke length allowed 1.05 mm of clearance at the end of the stroke for the solid state of the spring. The springs were preloaded to stabilise the coils during the compression sequence and to accommodate slight variations in the overall length of the spring. A typical load profile of a spring compression can be seen in Figure 6.11.

Figure 6.11 shows a peak load of 0.94 N at the end of the stroke. As the coils could not be modified manually to eliminate touching during the compression the measured result can be compared to the calculated figure of 0.79 N. The higher result can be directly attributed to the coils contacting each other and increasing the spring rate. Figure 6.11 highlights the change in spring rate through the compression sequence. Between zero and 30.0 mm the spring rate is 10.93 mN/mm resulting in a peak load of 0.32 N and between 30.0 mm and 46.45 mm the spring rate significantly increases to 37.6 mN/mm, resulting in the peak load of 0.94 N. The results for the series of tests show that the springs are consistent with an average spring rate of 10.97 mN/mm for compression up to 30.0 mm and 32.8 mN/mm up to 46.45 mm. The abrupt changes in load which are evident at 41.85 mm and 46.1 mm are due to the coils slipping over each other.

It is a requirement that the spring can deliver a force of 0.43 N at the end of its 12.05 mm stroke to guarantee delivery of the medication in 5 s. It can be seen in Figure 6.11 that a load of 0.42 N is developed at 35.65 mm compression which represents the end position of the piston (12.05 mm). The results of the protocol show that the conical compression spring will deliver sufficient force to expel the medication in 5 s and that the stress in the

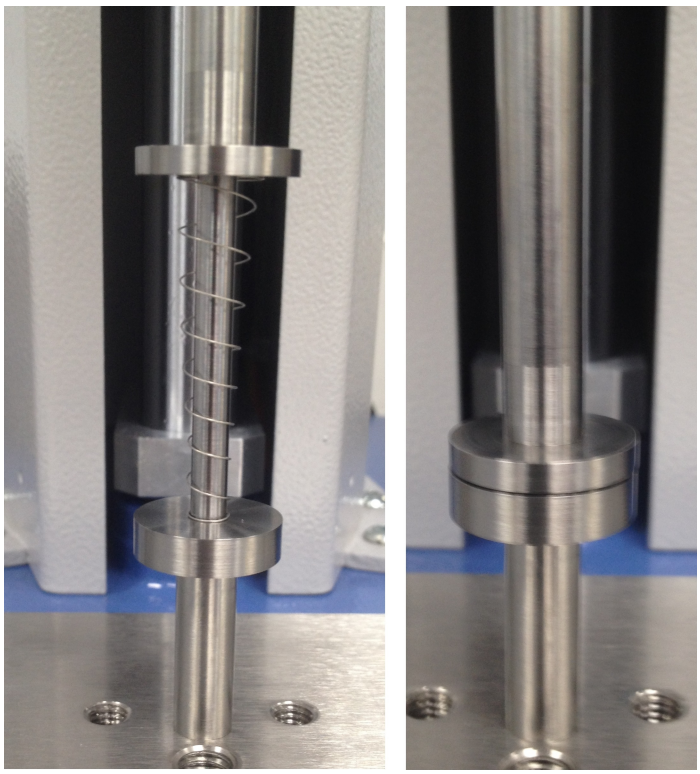


Figure 6.10: Left: Conical spring held vertically between two supports and further supported via a mandrel; Right: Spring in the fully compressed configuration

spring will be at a safe level as the overall length of the springs remained the same after repeated operations. The performance of the spring could benefit from some improvements. For example, generally increasing the clearance between the coils, reducing the number of coils and increasing the wire diameter would result in a more stable spring which would deliver a consistent load and have lower levels of stress. However the deliverable force at the end of the 12.05 mm stroke would drop off slightly resulting in a longer delivery time.

6.5 Summary

This chapter has presented a novel method for the deployment of a metered dose of medication which can be stored onboard a WCE. The delivery solution allows manual loading of medication at the point just prior to administration. This feature gives flexibility in the choice of medication which can be prescribed to the patient therefore broadening the scope of its use. The medication will pass through a needle which penetrates the tissue of the GI

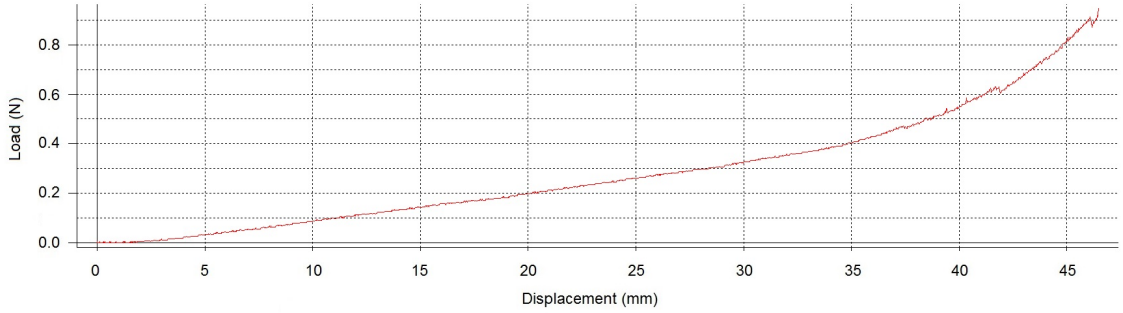


Figure 6.11: Load profile of a typical spring compression

tract wall. During the delivery of the medication any air which is trapped in the needle will quickly disperse into the subcutaneous tissue causing no adverse effects.

The medication delivery analysis and the delivery force analysis (presented in Section 6.3.1 and Section 6.3.2) have been discussed and validated through experimentation using 1:1 scale prototype parts. It has been shown that a stainless steel variable pitch conical spring can be wound such that it has a solid state thickness of the wire diameter and that it can deliver sufficient force to expel 1 ml of medication in approximately 5 s. The parameters chosen to achieve the delivery speed of the medication can be tailored to suit the specific viscosity of the medication formula by modifying the spring. However examination of Poiseuille's equation (6.1) shows that greater control of the medication flow can be gained by increasing or decreasing the bore of the needle, this would overcome the limitations imposed on the design of the conical spring due to the limited available space.

To fully validate the medication delivery mechanism a number of design challenges will be required to be overcome. For example the trigger mechanism will need to be prototyped and tested at 1:1 scale and *in-vivo* experiments will be required to validate the release mechanism and delivery times. The issue of sealing the medication into the chamber and preventing the medication from leaking through the front ports requires further work. Also the impact of the additional friction due to the sealing will need to be taken into consideration when designing and validating the spring.

References

[1] N. I. Goldfarb, L. T. Pizzi, J. P. Fuhr, C. Salvador, V. Sikirica, A. Kornbluth, and B. Lewis, "Diagnosing crohn's disease: An economic analysis comparing wireless capsule endoscopy with traditional diagnostic procedures," *Disease Management*, vol. 7, pp. 292–304, 2004.

[2] A. Lambert, F. Vaxman, F. Crenner, T. Wittmann, and J. F. Grenier, "Autonomous telemetric capsule to explore the small bowel," *Medical and Biological Engineering and Computing*, vol. 29, pp. 191–196, 1991.

[3] A. Parr, E. Sandefer, P. Wissel, M. McCartney, C. McClain, U. Y. Ryo, and G. Digenis, "Evaluation of the feasibility and use of a prototype remote drug delivery capsule (RDDC) for non-invasive regional drug absorption in the GI tract of man and beagle dog," *Pharmaceutical Research*, vol. 16, pp. 266–271, 1999.

[4] C. G. Caro, T. J. Pedley, R. C. Schroter, and W. A. Seed, *The Mechanics of the Circulation*. Cambridge University Press, second ed., 2011.

[5] S. Kurbel and J. Flam, "Interstitial hydrostatic pressure: a manual for students," *Advances in Physiology Education*, vol. 31, no. 1, pp. 116–117, 2007.

[6] A. van Beek and T. U. Delft, *Advanced Engineering Design: Lifetime Performance and Reliability*. TU Delft, 2006.

[7] T. Kunimine, S. Yoshioka, and K. Matsue, "The relations between modulus of rigidity and young's modulus for various kinds of wire," *IEIC Technical Report (Institute of Electronics, Information and Communication Engineers)*, vol. 98, pp. 33–36, 1998.

[8] D. Matthew, *Springs & Pressings: A Designers' Guide*. Hampshire: Southern Springs & Pressings Limited, 1st ed., 2001.

[9] K. R. Krishnan, R. A. Ammal, B. Hariharanath, A. Rajendran, and C. Kartha, "Addition of RDX/HMX on the ignition behaviour of boron-potassium nitrate pyrotechnic charge," *Defence Science Journal*, vol. 56, no. 3, pp. 329–338, 2006.

[10] J. A. Conkling and C. Mocella, *Chemistry of pyrotechnics: basic principles and theory*. CRC press, 2010.

[11] S. Byun, J. Lim, S. Paik, A. Lee, K. Koo, S. Park, J. Park, B. Choi, J. Seo, K. Kim, H. Chung, S. Song, D. Jeon, and D. Cho, "Barbed micro-spikes for micro-scale biopsy," *Journal of Micromechanics and Microengineering*, vol. 15, pp. 1279–1284, 2005.

Chapter 7

Conclusion

This thesis has presented a novel microrobotic platform concept for targeted drug delivery in the GI tract, Figure 7.1. To facilitate this aim, three novel micromechanical mechanisms have been investigated: the first mechanism allowed the microrobot to expand sufficiently to overcome natural peristalsis; the second mechanism achieved the positional control of a dispensing needle to allow for targeted drug delivery in the small intestinal tract and the third mechanism achieved delivery of the onboard medication. The additional functionality represents the state-of-the-art in mechanism design for WCE. It is hoped that the mechanisms will act as a platform for further research into methods of delivering targeted therapy. Detailed engineering drawings of the mechanisms can be found in Appendix F.

7.1 Contributions

Chapter 2 reviewed the state-of-the-art in WCE through the evaluation of current and past literature. A review of the limitations of current practises in colonoscopy was presented and a review of the clinical benefits of performing endoluminal capsule monitoring was discussed. An evaluation of the background relating to the main themes of methods for resisting peristalsis, drug targeting systems and drug delivery systems was presented. A review of actuators was presented, in the context of WCE, with a view to evaluating their suitability for adding functionality to current WCEs. The specific problems of available space when it comes to achieving functionality of actuators was highlighted. Fabrication methods for manufacturing low-volume high-precision component parts were compared and their process parameters presented. A discussion of current WCE systems highlighted the

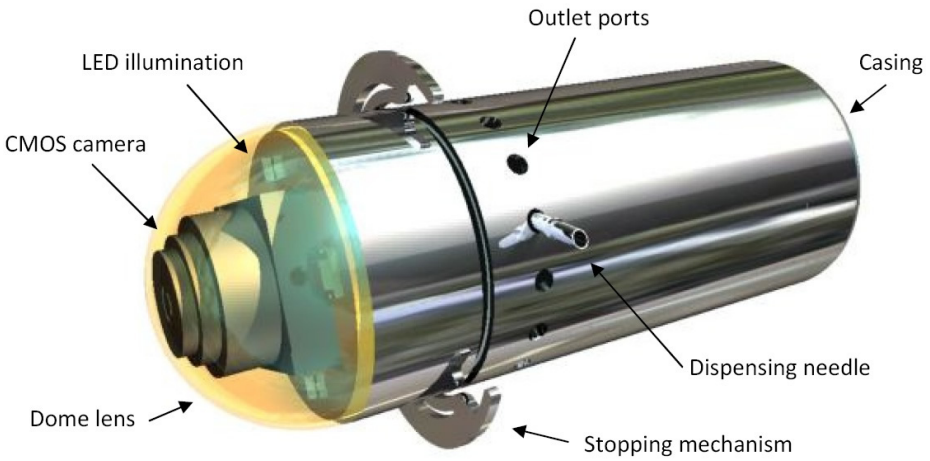


Figure 7.1: Microrobot concept design capable of resisting peristaltic pressure through an integrated holding mechanism and delivering 1 ml targeted medication. Holding mechanism shown partially open and the needle fully extended to give 1.5 mm of needle penetration

relevance of the development status of capsule research as the type of category a capsule is in highlights the capsule's technology status.

Chapter 3 set out the aims and objectives for this research project. A methodology was presented which evaluated three research questions which were chosen for their impact on the design of the microrobot at the early design concept stage. The questions looked at the optimal physical geometry of the microrobot, which actuator technology was best suited for the application and what method of resisting peristaltic contractions could be incorporated into a WCE. Solutions to the complex issue of delivering power through the microrobot were presented and methods of controlling the orientation of the needle positioning mechanism were discussed. A comprehensive technical specification of the microrobotic platform was presented.

Chapter 4 presented a novel biologically-inspired holding mechanism which could be incorporated into the next generation of WCE for the purpose of resisting natural peristalsis in the GI tract. The expanding holding mechanism was the first reported circumferential holding mechanism driven by a single micromotor. The presented mechanism utilises a novel configuration of gearing to allow the compact design to drive the holding mechanism. The detailed analysis of the gear train and the loading on the gears were presented with the results confirming the materials the gears are to be manufactured from. An analysis of the two components of peristaltic force were presented and the circumferential and longitu-

dinal peristaltic contractions were evaluated for their effect on the micromotor's ability to deliver torque. Through analysis it was shown that the proposed mechanism was capable of withstanding the forces generated by the GI environment. A fully functioning 5:1 scale prototype of the holding mechanism was evaluated and validated through trials.

Chapter 5 presented a novel targeting mechanism capable of delivering a 1 ml dose of medication to a target site of interest in the GI tract. The targeting mechanism overcame the problems of positioning a needle in the GI tract, operating the needle and safely retracting the needle. The operation of the mechanism has been analytically evaluated which resulted in the selection of the optimum geometry for the features of the mechanism and also which materials the mechanism should be manufactured from. The evaluation of a 5:1 scale prototype of the mechanism was presented and through experimentation the function and operation of the system was validated.

Chapter 6 presented a novel drug delivery system. The system utilised a stainless steel variable pitch conical compression spring to expel a 1 ml dose of onboard medication through a retractable needle which has an internal diameter of 0.38 mm and a length of 6.7 mm. A thermo mechanical trigger mechanism concept was presented which could potentially release the compressed conical spring. Through experimentation using 1:1 scale prototype springs and a specially designed plunger combined with a conventional syringe the method for delivering the onboard supply of medication was validated.

7.2 Recommendations for Future Work

The microrobot concept mechanisms presented in this thesis have been designed to be manufactured using conventional machining techniques. For example the holding mechanism could be manufactured using a 9 axis sliding head machining centre (Star SV-20) and the needle positioning mechanism could be manufactured using injection moulding techniques. A 1:1 scale prototype is a feasible next step however limited resources prevented a scale prototype from being manufactured at this stage. It is an important requirement that the component parts can be manufactured using conventional manufacturing techniques as the ultimate goal of this research is to produce a low cost microrobot which is disposable.

There are a number of elements of the proposed microrobotic system which were not analysed and validated as part of this investigation such as the complex electronics required for the control of the microrobot. However to realise a fully functioning prototype capable

of delivering targeted therapy these elements will need to be addressed. For example the method for power distribution described in Chapter 3 requires prototyping and validating at 1:1 scale, also the concept rotary encoder and the modular power supply unit will also require prototyping and validating.

A number of experiments designed to validate each of the mechanisms have been performed however further work is required on the mechanisms to allow them to be integrated into a 1:1 scale WCE and then to validate its ability to perform *in-vivo* targeted drug delivery. Specifically the holding mechanism requires testing at 1:1 scale to confirm the efficiency of the gear train and the successful operation of the holding mechanism in the GI environment. The micromotor chosen to operate the drug targeting mechanism requires testing at 1:1 scale to confirm it is capable of repeatedly positioning and deploying the needle, also the needle requires prototyping and testing to confirm it is capable of penetrating the tissue of the GI tract wall. The drug delivery mechanism has been tested at 1:1 scale however further work is required on the method of sealing the medication chamber and preventing premature leaking of the medication through the ports. Also further research is required in the area of localisation as tracking the progress of the microrobot through the GI tract is an important requirement.

The proposed mechanisms could be adapted to perform a number of different procedures. For example, reversing the direction of the drug delivery system would allow the retrieval of a tissue sample from the intestinal tract rather than the delivery of medication. The following medical procedures may benefit from future developments in the swallowable microrobotic platform proposed in this thesis:

7.2.1 Gastrointestinal Biopsy

Examination of histological changes in the GI tract is the gold standard in diagnosing celiac disease [1]. This method of examination can only be performed through the application of a biopsy procedure. However the small intestines is a very difficult environment to gain access to with repeated attempts causing increasing discomfort for the patient. Future research could focus on modifying the positioning mechanism and adapting it to take a biopsy sample. The basic principle of reversing the system would enable a sample to be stored safely onboard.

7.2.2 Pancreas

There has been much research into methods for replacing the pancreas with a device capable of releasing the required levels of insulin into the body [2]. A limitation with implantable devices is that they require the insulin supply to be replaced on a regular basis. The microrobot would provide a simple system which could be adapted to perform this function.

7.2.3 Electrosurgery

Limitations of conventional endoscopes restrict the treatment of diseases such as angiodysplasia as the area of interest can only be treated by bipolar electrocoagulation techniques if it is within the reach of the endoscope [3]. Adapting the microrobot so that it could perform electrocoagulation would overcome this issue. Future research could look at adapting the needle positioning mechanism to carry bipolar probes which would administer an electric current that would result in localised heat. However a further challenge would be in the development of batteries which would be required to hold sufficient charge to carry out the operation and still fit within the package size.

7.2.4 Surgical Tools

The ability to surgically remove pathologies of the GI tract such as polyps would bring great benefits to patients. This function may be realised by research into a chip-scale particle accelerator [4]. This new technology may be integrated into a WCE through the modification of the targeting mechanism. The system could then be utilised to manoeuvre the laser such that it ablates the target site.

References

[1] W. El-Matary, "Wireless capsule endoscopy: indications, limitations, and future challenges," *Journal of pediatric gastroenterology and nutrition*, vol. 46, pp. 4–12, 2008.

[2] M. Ho, P. Georgiou, S. Singhal, N. Oliver, and C. Toumazou, "A bio-inspired closed-loop insulin delivery based on the silicon pancreatic beta-cell," in *Circuits and Systems, 2008. ISCAS 2008. IEEE International Symposium on*, pp. 1052–1055, IEEE, 2008.

[3] A. C. Steger and J. Spencer, "Obscure gastrointestinal bleeding," *British Medical Journal*, vol. 296, p. 3, 1988.

[4] Y. Shi and A. Lal, "Integrated all-electric high energy ion beam guidance on chip: Towards miniature particle accelerator," in *Micro Electro Mechanical Systems (MEMS), 2011 IEEE 24th International Conference on*, pp. 137–140, 2011.

Appendix A

Holding Mechanism Concept Designs

A.1 Holding Mechanism Concepts

The microrobot is required to be sufficiently small to pass through the small intestines without becoming an obstruction, however it is also required to expand in some way to prevent it from moving when a section of the intestinal wall is being examined or when medication is being administered. This section presents a selection of concept designs potentially capable of stopping the microrobot.

Concept design 1 attempts to stop the microrobot by utilising a centrally aligned micromotor and leadscrew to operate two axially aligned legs, Figure A.1.

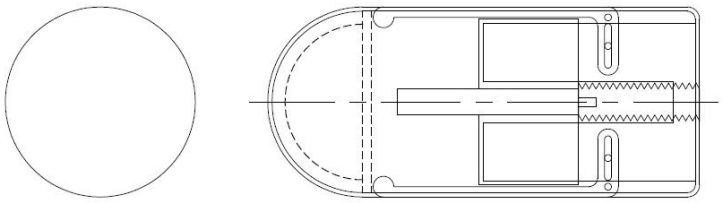


Figure A.1: Design concept 1 - two axially aligned legs operated by a centrally aligned leadscrew and micromotor

A single micromotor is employed to perform multiple operations. Concept design 1 uses the action of the leadscrew delivering the medication to operate two legs. As the leadscrew rotates it drives a piston forwards pushing the medication out. Attached to the piston are pins located in slots at the ends of the legs, hence as the piston moves forwards it pulls the pins in the slot causing the legs to be deployed.

There are numerous disadvantages with this system. For example, the lever ratio pushing the legs out is too high and therefore the micromotor cannot generate the required torque to allow the legs to distend the GI tract wall. In addition, the legs cannot be deployed before the medication is released and the speed of the micromotor is too high causing the legs to deploy too quickly.

Concept design 2 (Figure A.2) overcomes the problems of delivering torque, controlling the operation of the legs and the speed of deployment by aligning the legs circumferentially.

The two-legged design utilises a micromotor which is orientated in a vertical position. The micromotor is engaged with an annular ring through a small gear which drives the ring. The annular ring is connected to a gear train which drives the legs in and out. This

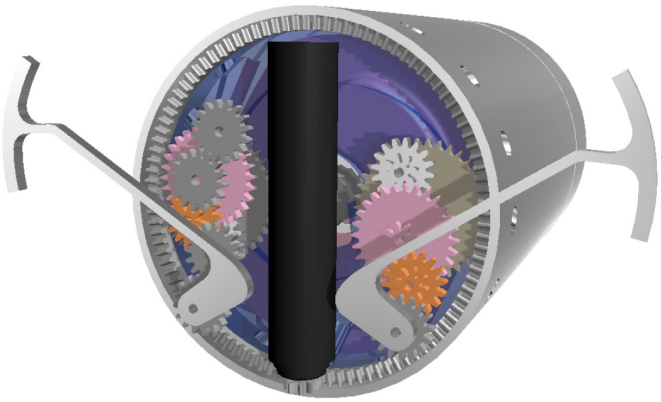


Figure A.2: Design concept 2 - two-legged mechanism

novel configuration reduces the micromotor's RPM. The reduction in RPM will result in a multiplication of the micromotor's torque which will give the legs the strength required to distend the GI tract wall and hold the microrobot in place.

The advantage of the vertical configuration of the micromotor is that it makes for a very compact design, resulting in efficient use of space. The two legs, along with the microrobot itself, will give four points of contact against the GI tract wall. This will distribute the load from the wall evenly about the microrobot. The rate at which the legs are deployed can be controlled by the ratio of the gears.

The disadvantage with this configuration is that it can only expand the lumen to a diameter of 15.14 mm which may not be sufficient to hold the microrobot in position for the majority of patients.

To try and overcome the limitations of expanding the lumen a third leg has been introduced, Figure A.3.

Design concept 3 uses the same gearing mechanism and micromotor configuration as design concept 2 however it utilises a third leg to distend the lumen further. The third leg would simply be driven from the existing gearing (through the addition of a gear) which would allow the leg to be deployed at the same time as the horizontal legs, Figure A.4.

Figure A.4 shows the basic configuration of the proposed design. The gears driving the legs are positioned inside the annular ring to reduce the volume of the mechanism however this configuration has potential problems as the gears will be required to sit one on top of another making fixation in the centre of the gears difficult. This may be overcome by

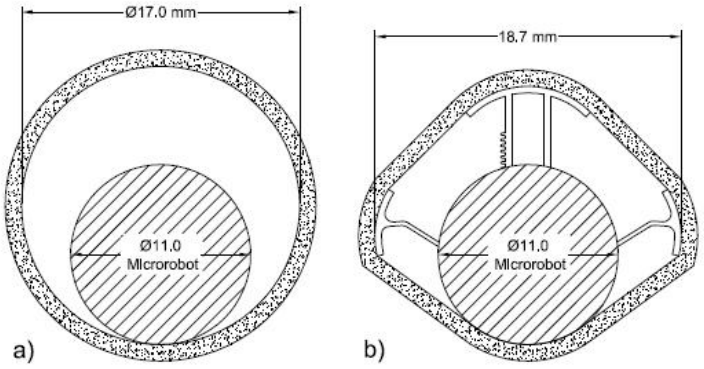


Figure A.3: Design concept 3 - section view through the small intestines (a) three-legged mechanism (b)

supporting the outside diameter of the gears.

The addition of the third leg results in a circumferential length equivalent to a diameter of 16.56 mm. The 1.42 mm increase in diameter is still below the >53.0 mm target circumference.

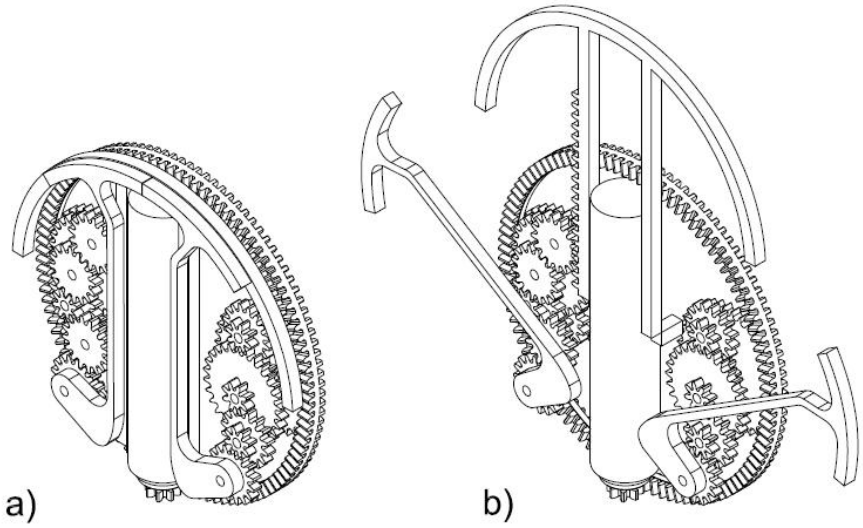


Figure A.4: Three-legged design - legs in the stored position (a) legs in the fully extended position (b)

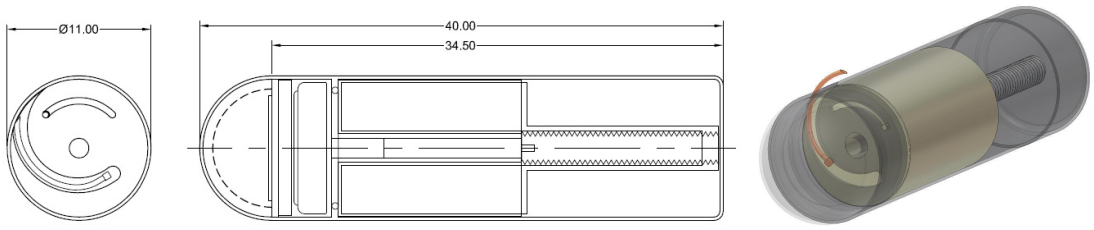
Appendix B

Targeting Mechanism Concept Designs

B.1 Targeting Mechanism Concepts

A number of design configurations have been investigated for their potential to achieve the goals of positioning a needle in the GI tract, operating the needle and delivering medication from within the confines of geometry based on the Enterion capsule. Each new design concept is intended to overcome the limitations of the previous versions.

An early concept design which showed potential utilised a micromotor mounted along the central axis of the microrobot to rotate a needle which would deliver medication to a specific location within the GI tract, Figure B.1.



(a) CAD layout drawing (b) 3D view

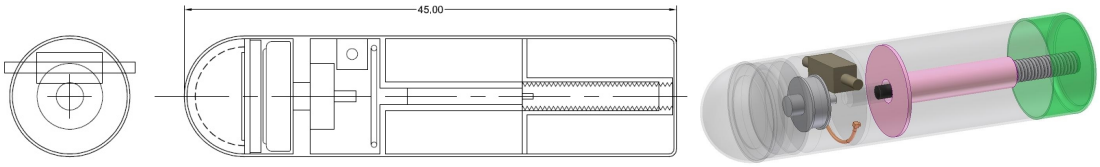
Figure B.1: Design concept 4 - a centrally aligned micromotor and leadscrew for the operation of the needle and deployment of medication

The principle behind design concept 4 (Figure B.1) was to utilise a single micromotor to perform the multiple operations required such as deploying the needle, delivering the drug and retracting the needle. The design consisted of a micromotor connected to a leadscrew. The leadscrew rotated a cover which was attached to the medication chamber. The pressure in the medication chamber made it act like a solid mass therefore on initial rotation of the leadscrew the medication chamber would rotate propelling a pivoting needle out of the side of the microrobot. The distance the needle protruded was dependent on a pin reaching the end of a slot in the main body. Once the pin stopped the medication chamber from rotating, pressure in the medication chamber forced the medication out through the needle. When delivery was complete the medication cover would automatically lock in the forward position enabling the reverse action of the micromotor to retract the needle.

After discussion and evaluation of the concept with a medical representative[1] it was agreed that the microrobot should have the ability to position the needle within a 360 degree envelope as this would provide maximum control for the operator to deliver therapy.

[1]N. Oliver, Clinical Research Fellow, Imperial College London, (Personal communication 18 Feb. 2010).

Concept design 5 (Figure B.2) utilises a combination of micromotors from Faulhaber and Maxon Motor, and a Squiggle piezoelectric motor to solve the problem of positioning a needle within the GI tract.

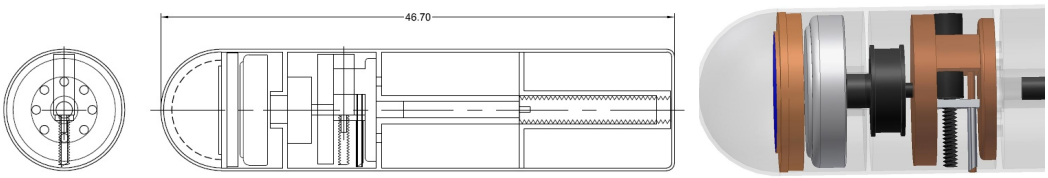


(a) CAD layout drawing (b) 3D view

Figure B.2: Design concept 5 - micromotor combination for needle advancement and retraction

As can be seen from Figure B.2 the Faulhaber motor would be employed to deliver the medication through the operation of a leadscrew, the Maxon motor would be employed to rotate the needle 360 degrees while the Squiggle motor would be utilised for the advancement and retraction of the needle. The linear movement of the Squiggle motor makes it an ideal choice to operate the needle however attempting to mount the motor inside the dimensions of a capsule proves difficult as the geometry of the Squiggle motor prevents it from being mounted perpendicular to the central axis of the capsule.

A further design concept, concept 6 (Figure B.3), overcomes the dimensional constraints of the Squiggle motor by replacing it with a Ø1.9 mm x 5.5 mm long micromotor mounted on a platform. The platform can be rotated by the Maxon motor and has access to medication through ports in the medication chamber wall.



(a) CAD layout drawing (b) 3D view

Figure B.3: Design concept 6 - rotating medication platform driven independently from the needle operating micromotor

It is clear that using these motors in this type of configuration not only presents technical challenges, such as supplying power to the motor which would be used to drive the needle in and out, but also that the overall length of the resulting microrobot (>45 mm) would be prohibitive due to the constraints imposed by swallowing.

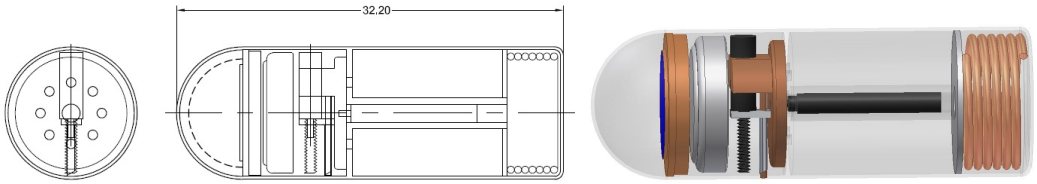
Appendix C

Medication Delivery Concept Designs

C.1 Medication Delivery Concepts

Once the target location has been reached and the needle deployed, the final stage of the procedure is to deliver the medication. This section presents a selection of concept designs potentially capable of administering medication.

Using a leadscrew as a delivery method substantially increases the length of the microrobot. Design concept 7 (Figure C.1) maximises the use of space by employing a spring to activate the medication delivery mechanism. The spring would be employed to push a disc which in turn would force the medication out through small apertures in the capsule body. The apertures are inline with a medication delivery mechanism. The medication delivery mechanism is shaped such that it funnels the medication out through a needle. The needle is mounted on the medication delivery mechanism and can be driven in and out by a second micromotor which is also mounted on the medication delivery mechanism.



(a) CAD layout drawing (b) 3D view

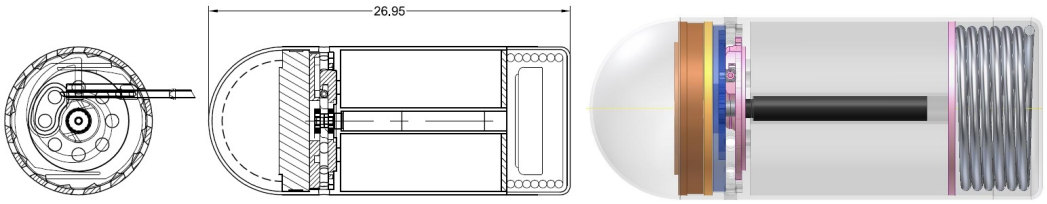
Figure C.1: Design concept 7 - spring activated medication delivery mechanism and autonomous needle operation

Using the spring as the medication delivery method releases the micromotor in the centre of the capsule. The micromotor can now be re-orientated so that it can be employed to rotate the medication delivery mechanism. This configuration drastically reduces the volume of the microrobot.

Design concept 8 (Figure C.2) overcomes the requirement for a second motor to drive the needle in and out by employing a novel mechanism to position and operate the needle.

The design of the needle positioning mechanism consists of a Ø1.5 mm x 10.5 mm long geared micromotor manufactured by Namiki, two opposing ratchets, a needle funnel, a needle cam and a movable needle. In addition, features integral to the microrobot's body are required.

The novel aspect to this mechanism is that it uses a micromotor to perform two separate



(a) CAD layout drawing (b) 3D view

Figure C.2: Design concept 8 - novel single micromotor configuration performing two separate operations

operations. The first operation is the angular control of the position of the needle and the second is the advancement and retraction of the needle. The medication will be stored in a compartment of the body and delivered through the needle by means of pressure generated by a piston. The piston action will be similar to the operation of a syringe and will be activated by a spring.

It is a requirement that the needle can be positioned at selected points within a 360 degree envelope. For the purpose of prototyping, 16 equally-spaced fixed positions have been chosen. The angular positioning of the needle is achieved by the anticlockwise rotation of the micromotor while the advancement and retraction of the needle is achieved by the clockwise rotation of the micromotor.

An overall reduction in length for the microrobot can be achieved by reconfiguring the component parts. By placing the power supply inside the area of the compressed spring (Figure C.2, a) the length of the microrobot reduces from 32.2 mm to 26.95 mm, it also has the added advantage of allowing easy connection to the micromotor's terminals.

Appendix D

Volume Comparison of the Proposed Concepts

D.1 Volume Comparison

The continued improvements from the design iterations presented in Appendix B and Appendix C can be seen through an analysis of the total volume of the concept designs compared to the target volume of the Enterion capsule (Table D.1). The higher the resulting merit index the more easily the design can be swallowed.

Table D.1: Concept design volume merit index

	Enterion	**Design 4**	**Design 5**	**Design 6**	**Design 7**	**Design 8**
Design volume cm^3	2.86	3.62	4.10	4.26	2.88	2.38
Enterion volume cm^3	2.86	2.86	2.86	2.86	2.86	2.86
Merit Index	1	0.79	0.70	0.67	0.99	1.2

Concept designs 1, 2 and 3 have been omitted as they are only partial designs

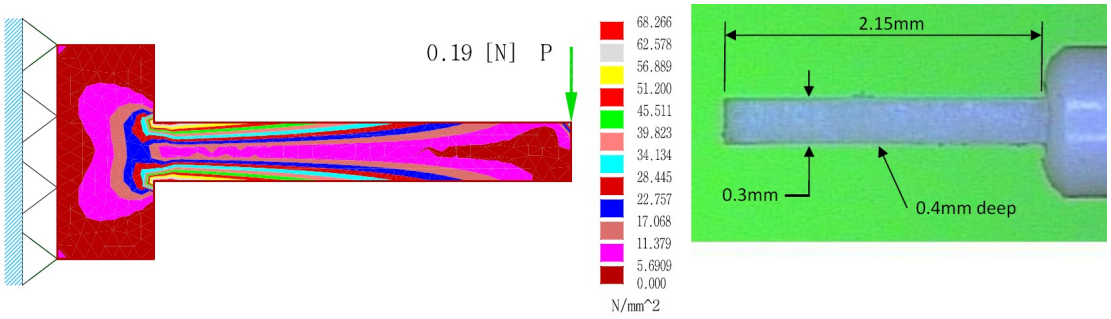
As can be seen from Table D.1, the results from the volume merit index show that design concept 7 closely matches the target volume of the Enterion capsule. However design concept 8 has a volume merit index of 1.2 which is a 16.8% reduction in volume compared to the target Enterion capsule. This highlights the improvement which has been gained by employing the novel needle positioning system and power configuration.

Appendix E

Bending Trials

E.1 PEEK Beam Bending Trial

Before prototyping a scaled model of the needle funnel (Chapter 5, Figure 5.3, a)) it was necessary to gain an idea of how the chosen PEEK material would perform in reality rather than relying on simulated results. For this purpose a PEEK test piece was devised and subjected to a range of bending loads, Figure E.1, b).



(a) Von Mises FEA analysis (b) PEEK test piece

Figure E.1: Von Mises FEA 2D isoareas analysis (a) and plan view of PEEK test piece at 42.4X magnification (b)

Figure E.1 represents a Von Mises FEA analysis (a) and a magnified view of the actual PEEK test piece (b). The dimensions of the arm are 2.15 mm long by 0.3 mm high and 0.4 mm wide. The test piece is shorter than the required 4.0 mm long needle positioning arm as a result of the restrictions imposed by the available manufacturing method. However the results will be valid as a longer lever arm will result in a lower applied load and hence a lower induced stress in the beam.

An FEA analysis has been carried out on the test piece before prototyping the piece to ensure the geometry is within reasonable operating parameters. Using a calculated maximum load of 0.19 N from the predicted deflection of 200 μm it was found that the maximum Von Mises stress of 68.26 Nmm^{-2} was restricted to the surface of the corners of the test piece with only a contour band of dark blue penetrating through the arm between 17.06 Nmm^{-2} and 22.75 Nmm^{-2}. The predicted results show that there would be no areas of the arm which would exceed the 97 Nmm^{-2} yield point of PEEK.

The deflection experiment was performed on a profile projector type PJ-300 manufactured by Mitutoyo at 10X magnification. The edge of the test piece was aligned with the profile projector's cross hairs to ensure the test piece was in a horizontal alignment at the

start. The cross hairs were then advanced 50 μm away from this edge. The arm tip was gently pushed until it reached the cross hairs whereupon it was released allowing the arm to return to its original position. This process was repeated for 100 μm, 150 μm and 200 μm positions with the arm successfully returning to its origin after each new position. This method of testing ensures the accuracy of the deflection measurement.

The successful movement of the arm through to the 200 μm position gives added confidence that the prototype needle positioning arm will perform as required, as the 200 μm distance exceeds the design requirement of 170 μm.

Appendix F

Detailed Engineering Drawings

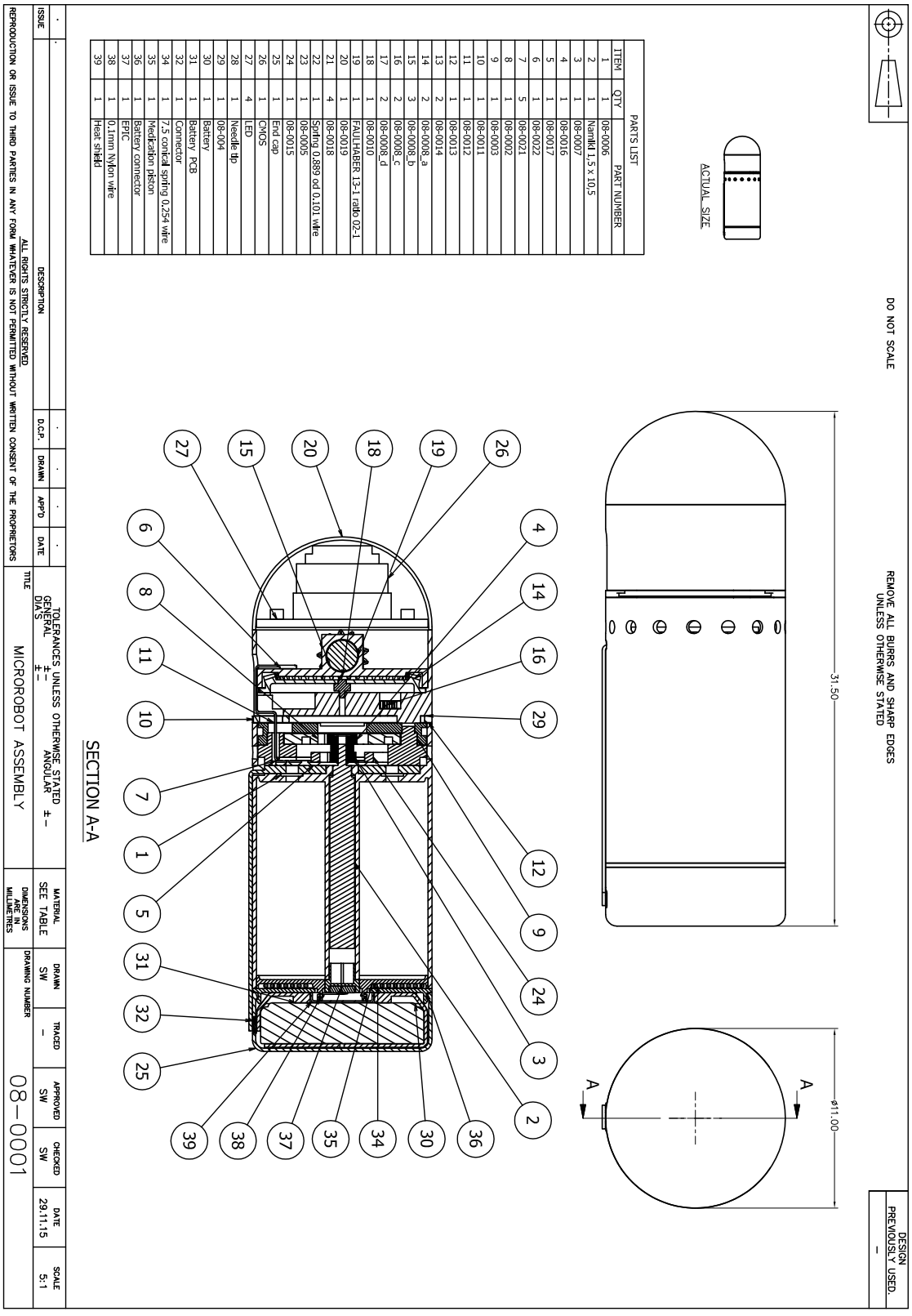


Figure F.1: Final assembly drawing

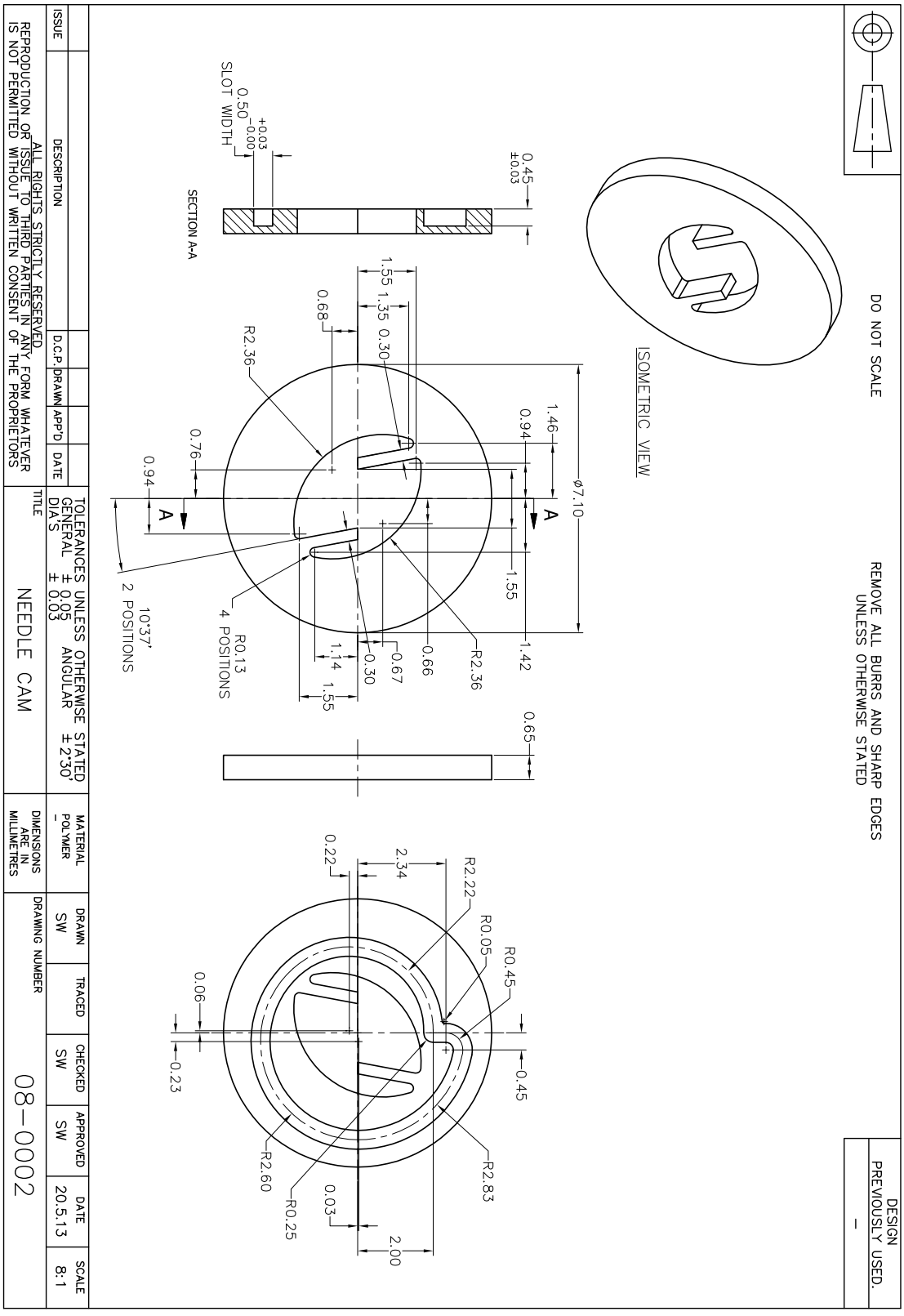


Figure F.2: CAD layout drawing of the needle CAM

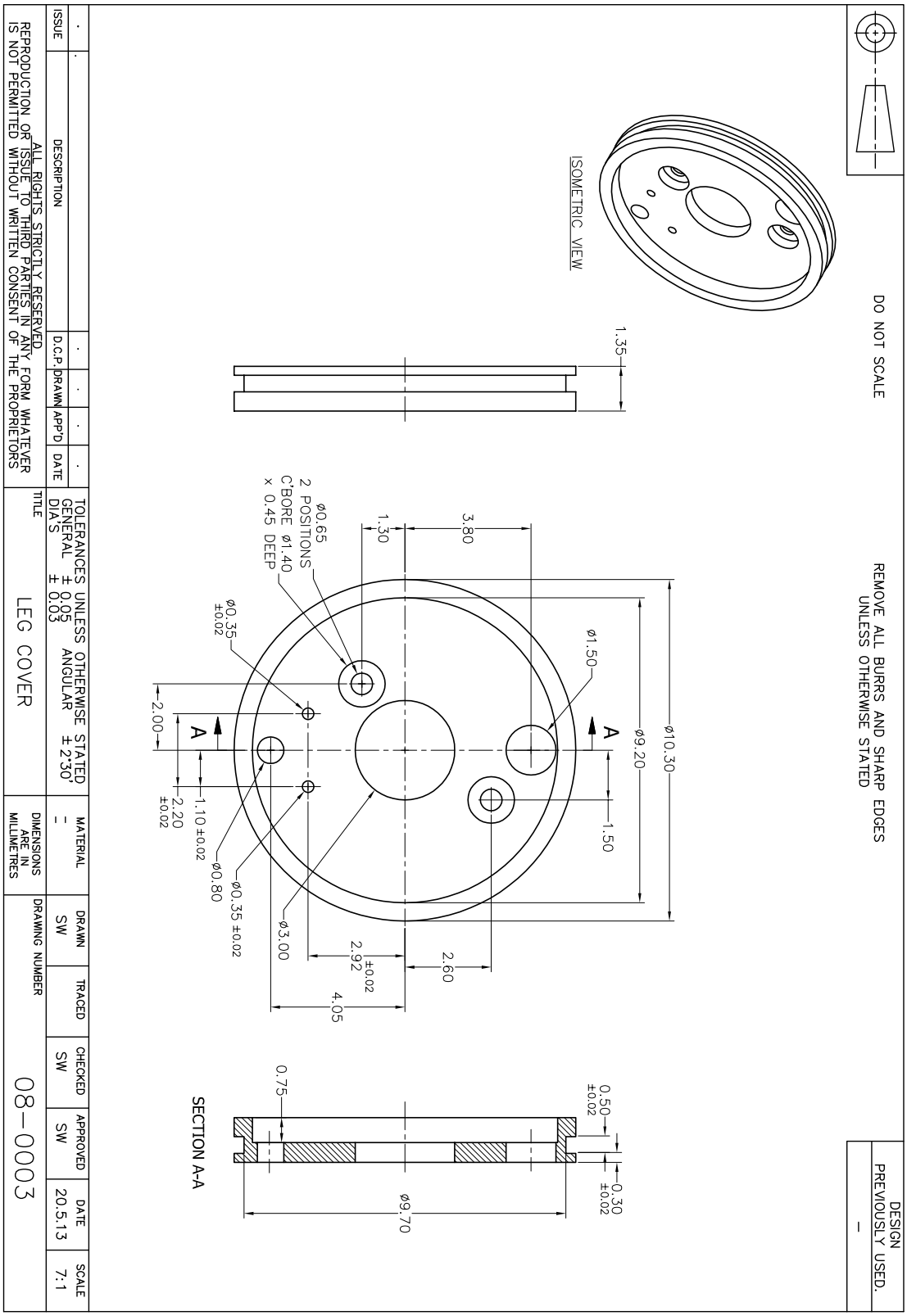


Figure F.3: CAD layout drawing of the leg cover

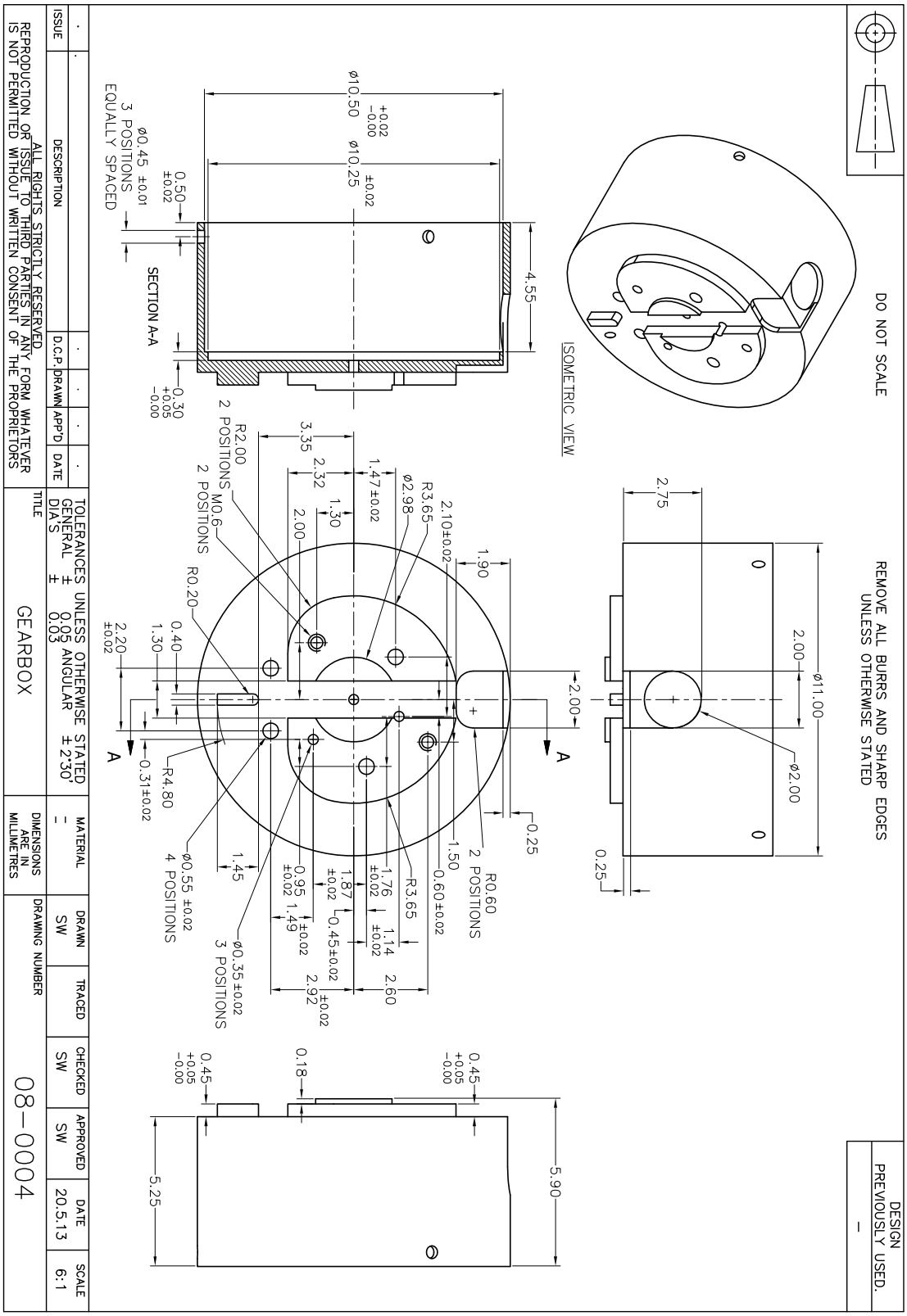


Figure F.4: CAD layout drawing of the gearbox - legs

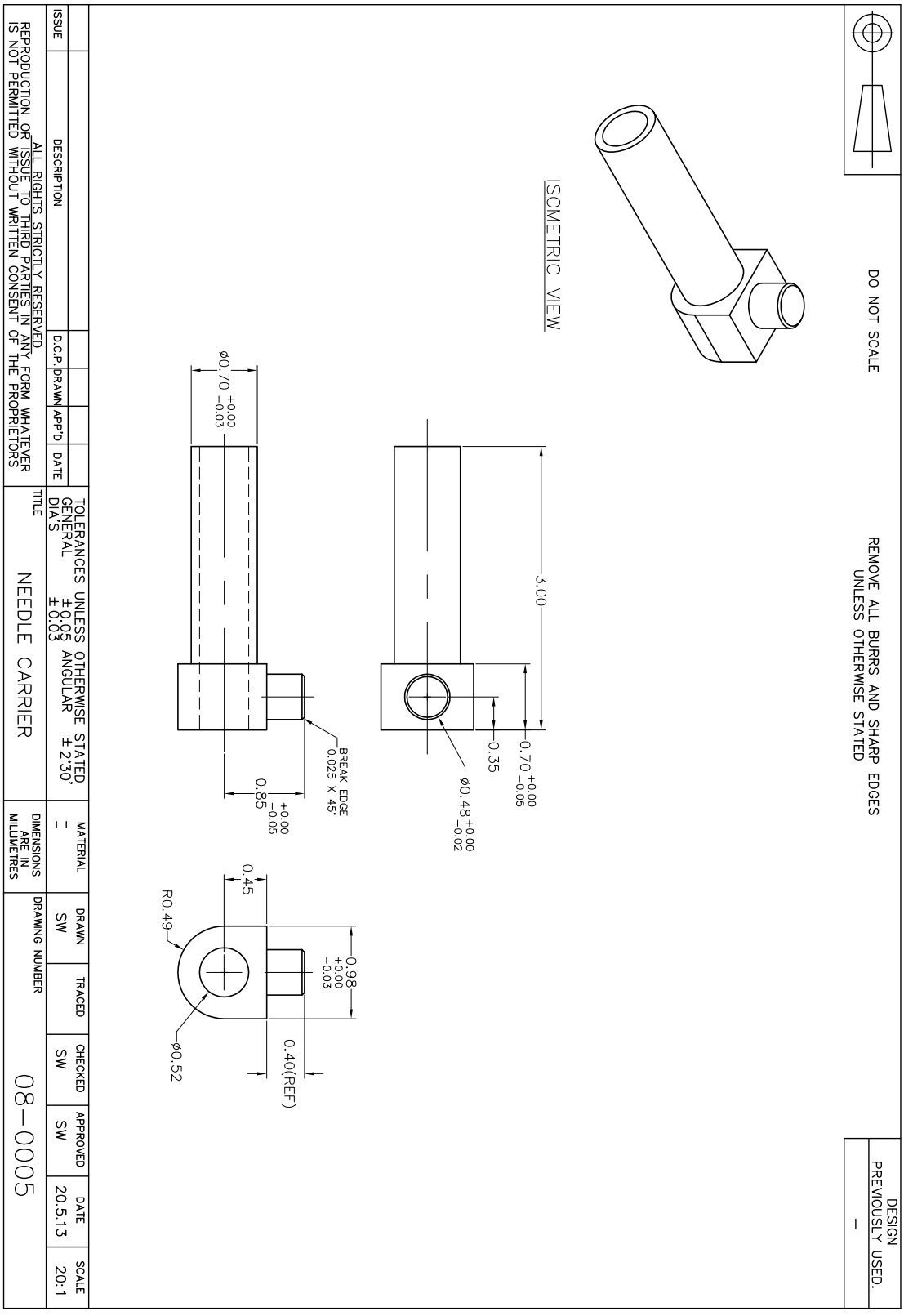


Figure F.5: CAD layout drawing of the needle carrier

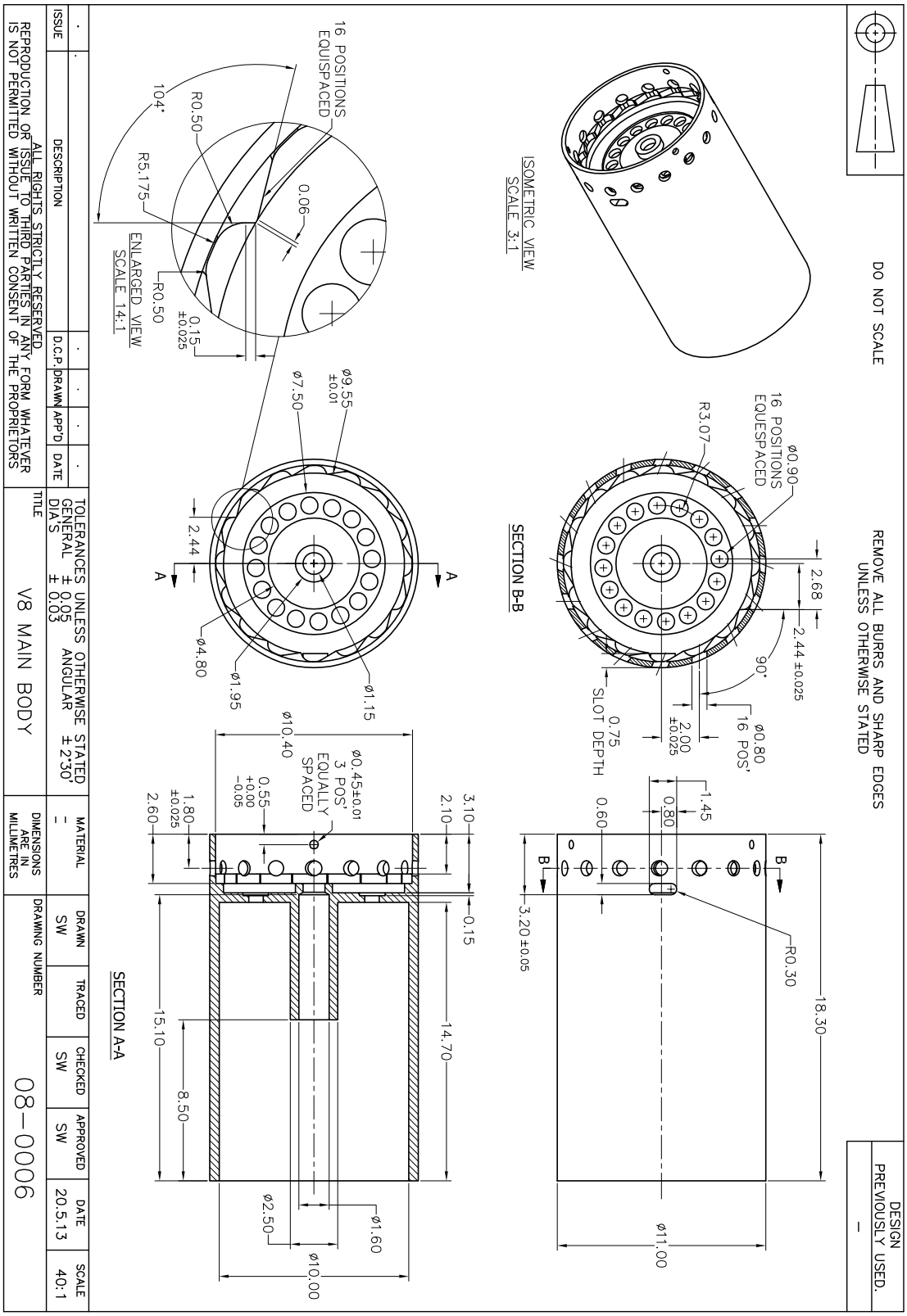


Figure F.6: CAD layout drawing of the main body

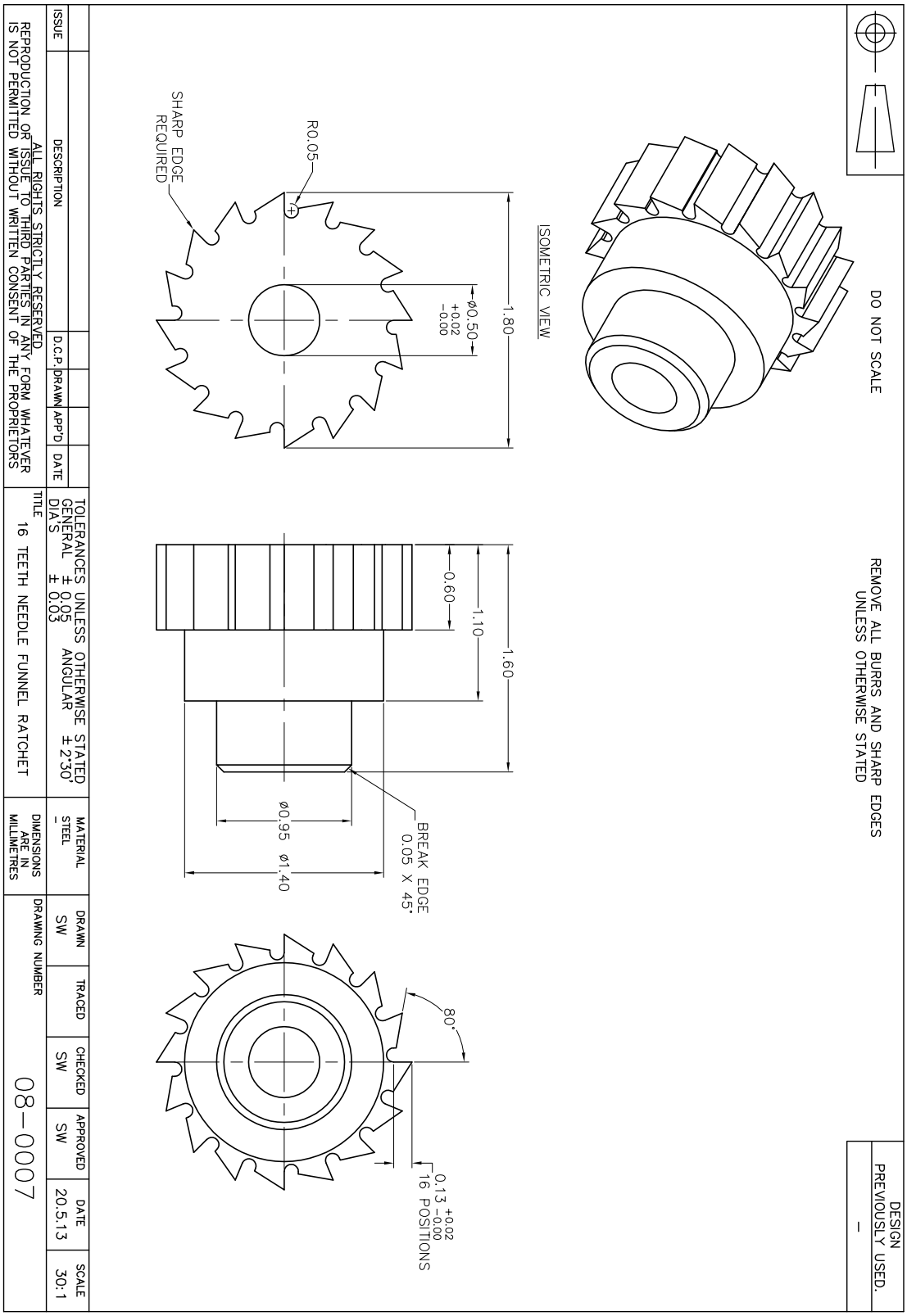


Figure F.7: CAD layout drawing of the 16 teeth needle funnel ratchet

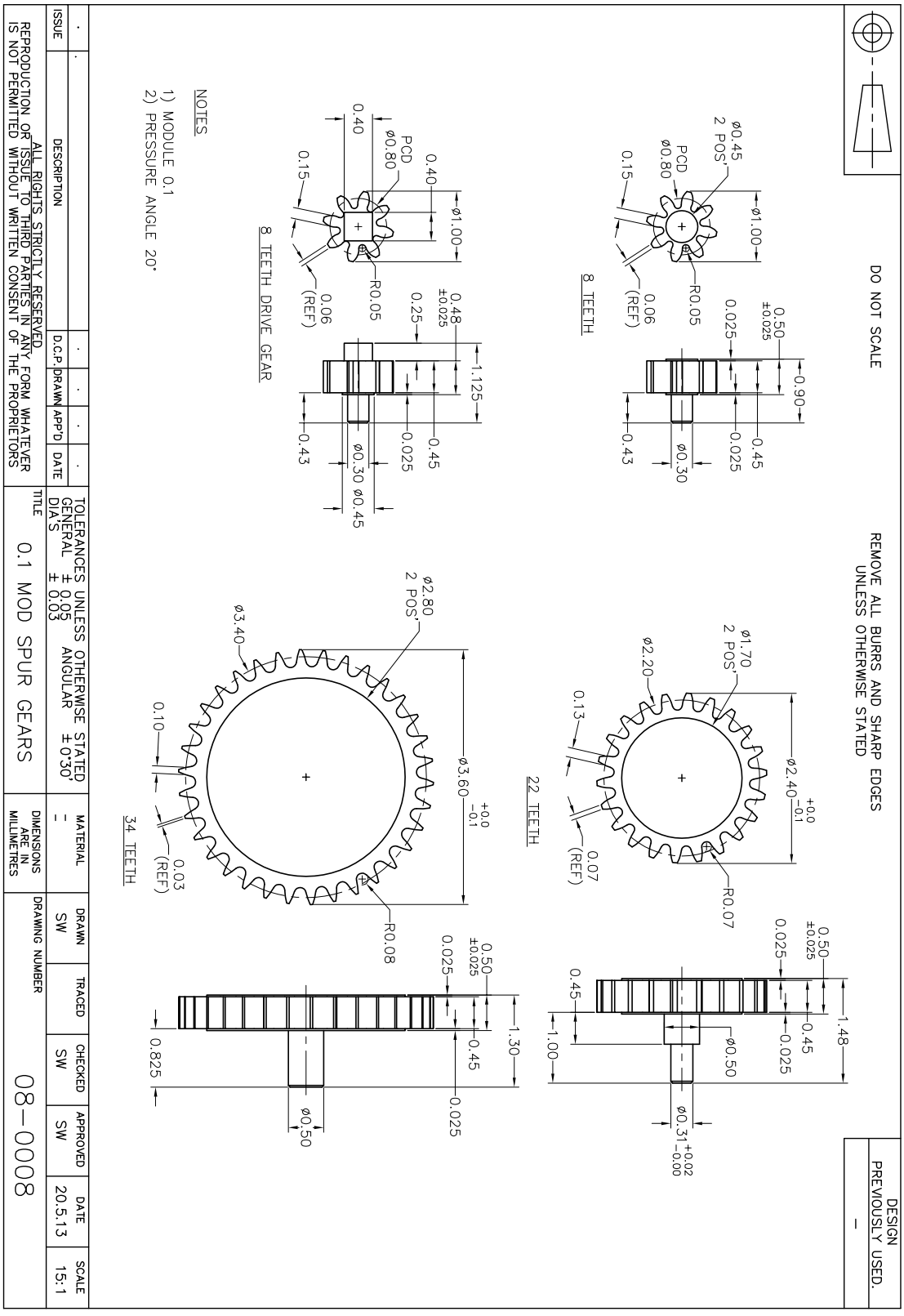


Figure F.8: CAD layout drawing of the 0.1 mod spur gears

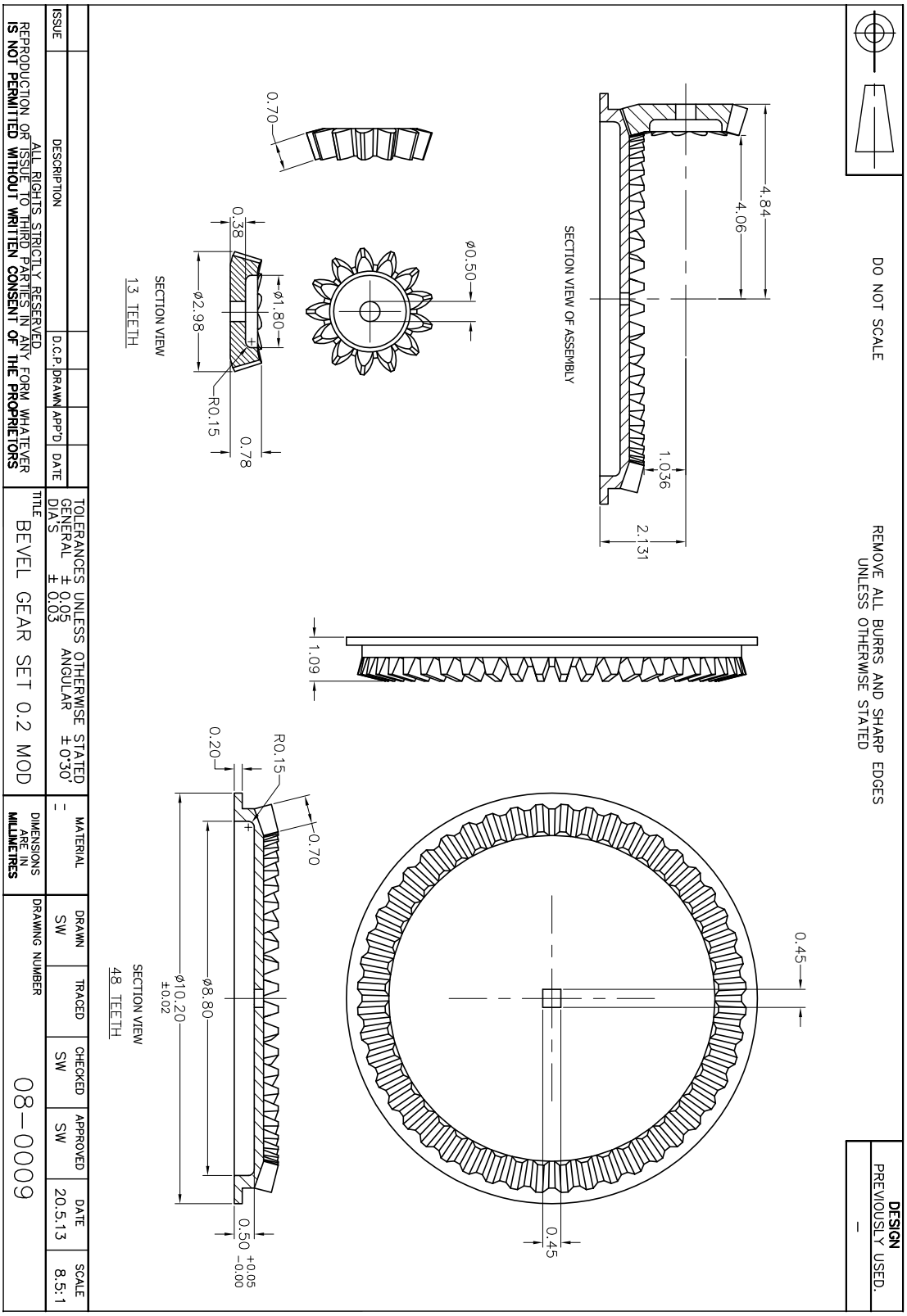


Figure F.9: CAD layout drawing of the 0.2 mod bevel gear set

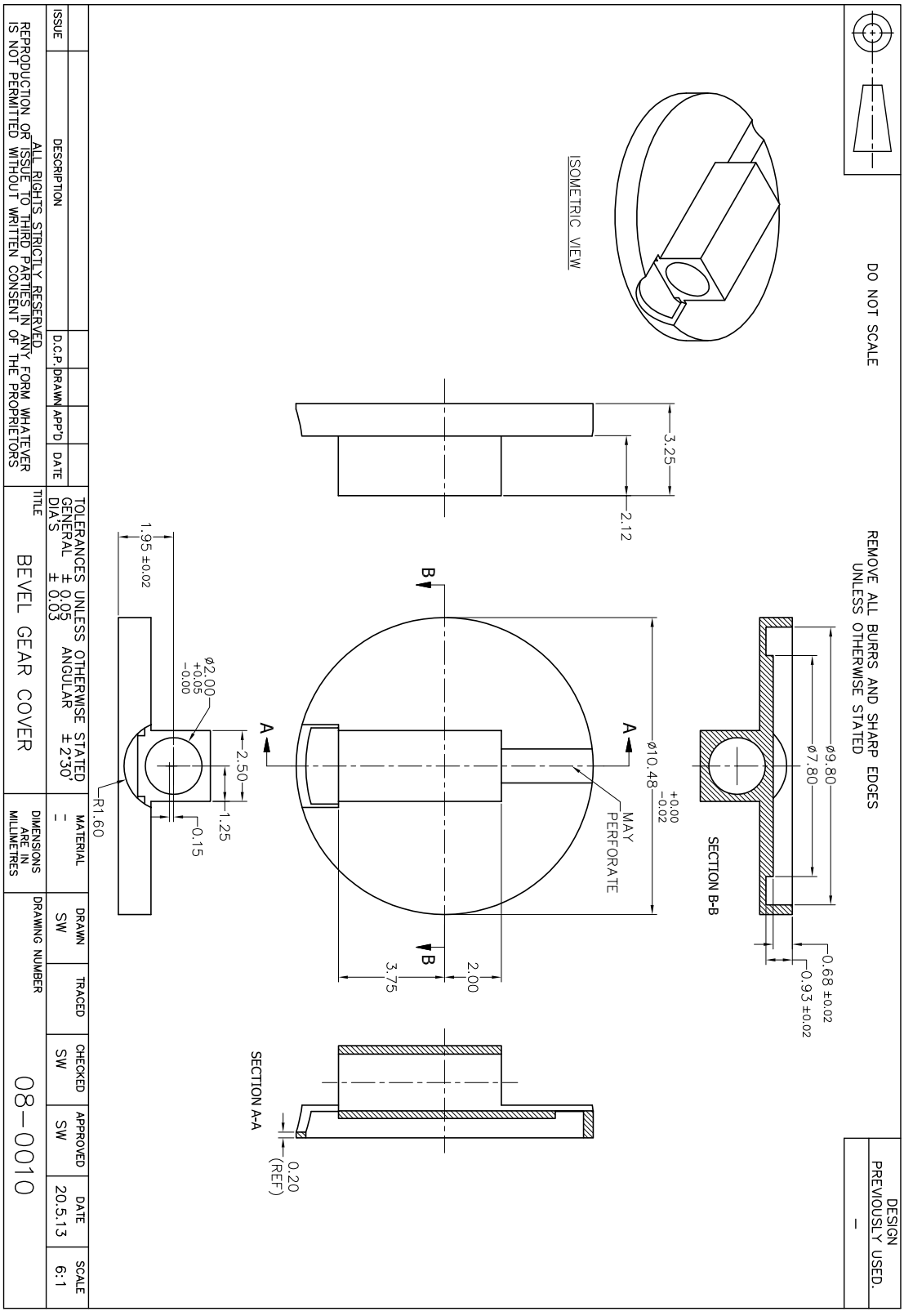


Figure F.10: CAD layout drawing of the bevel gear cover

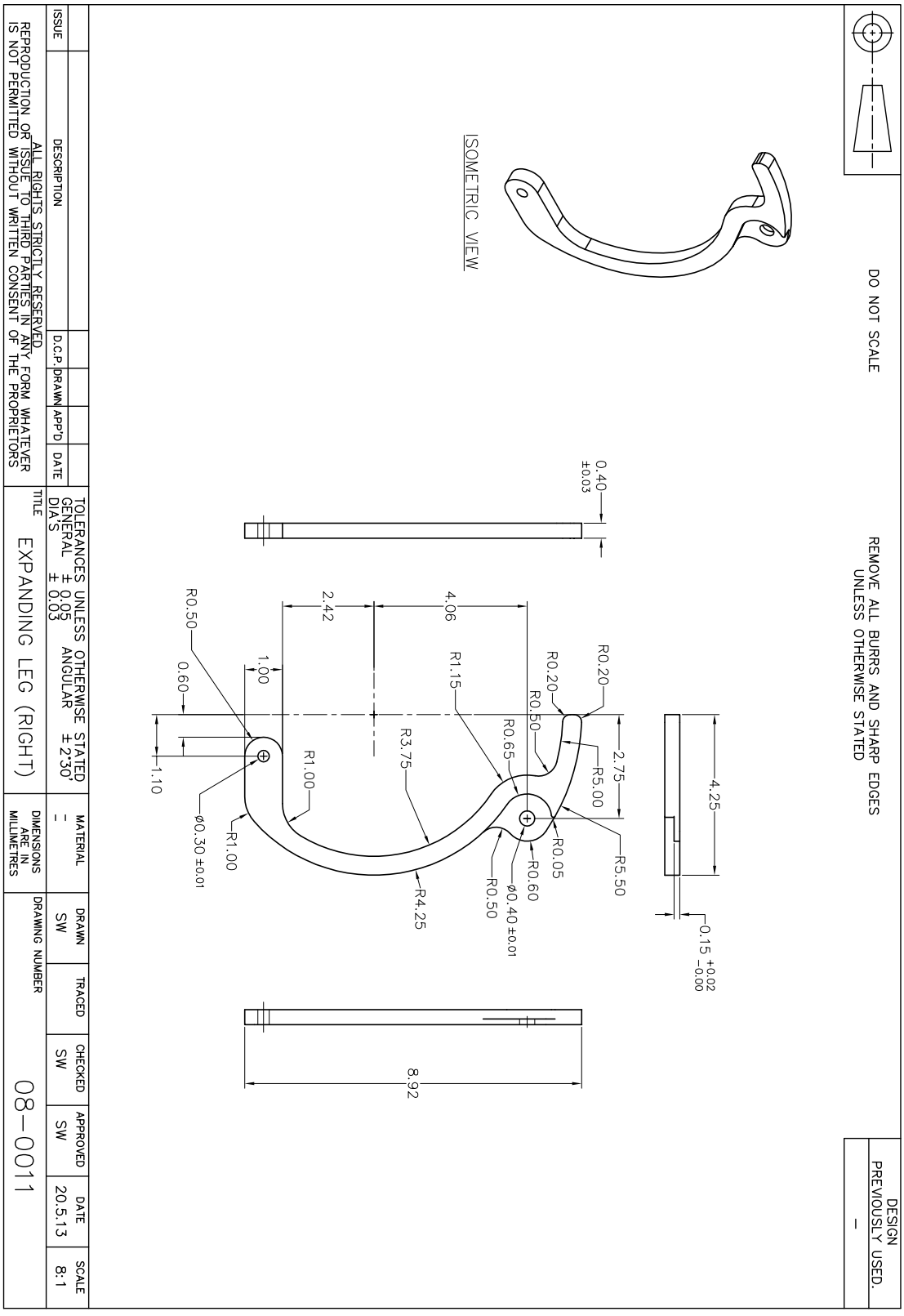


Figure F.11: CAD layout drawing of the expanding leg (right)

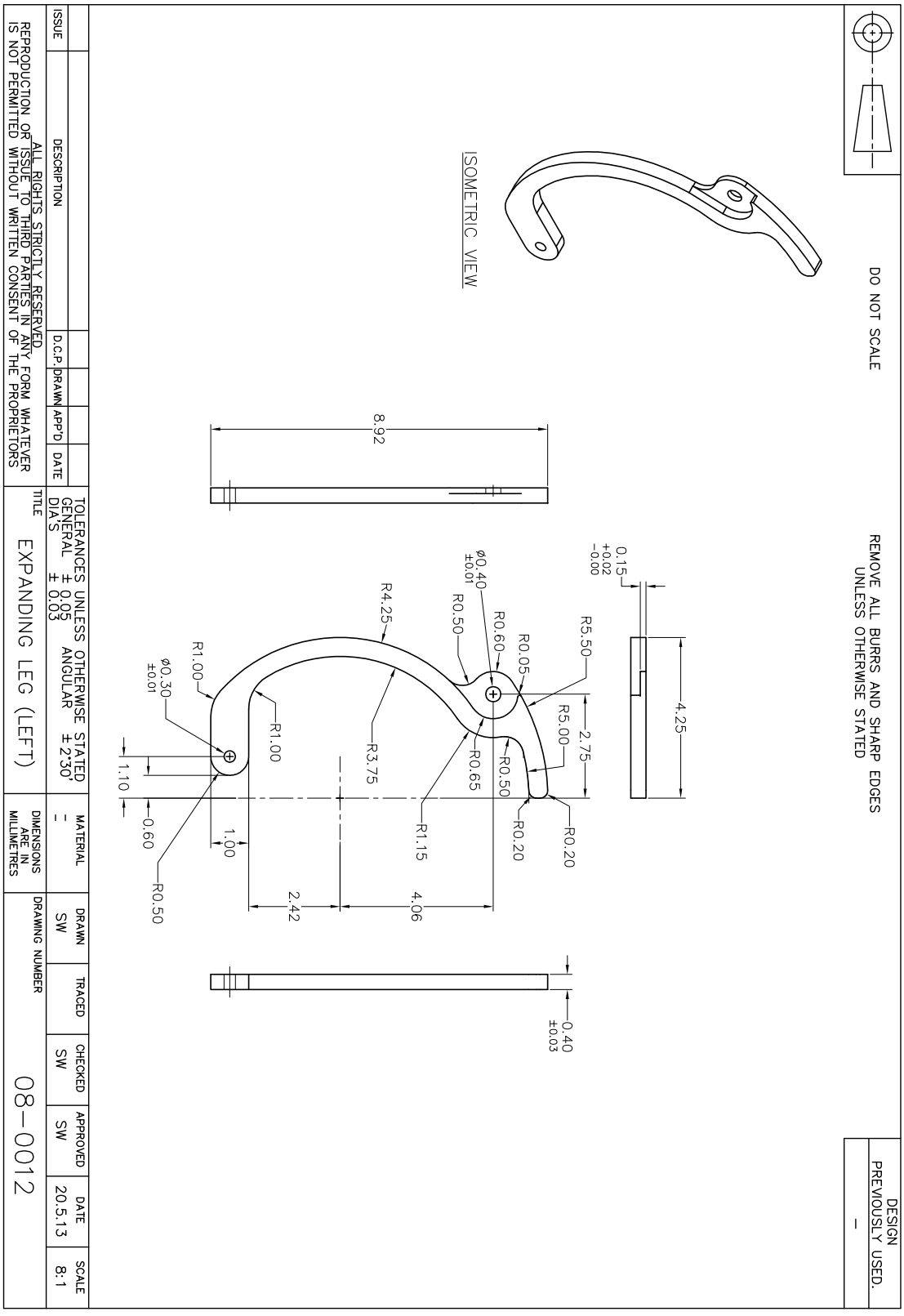


Figure F.12: CAD layout drawing of the expanding leg (left)

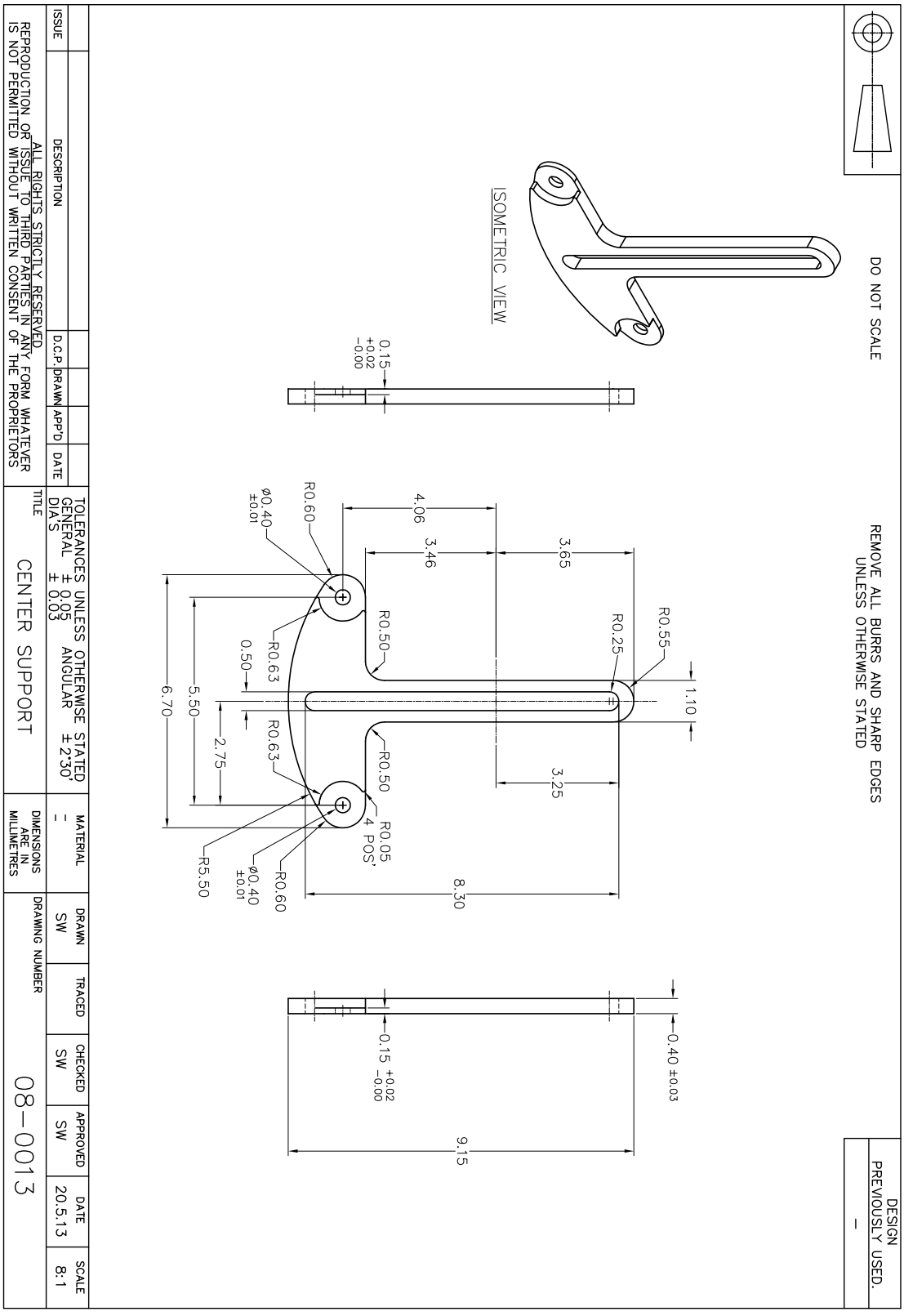


Figure F.13: CAD layout drawing of the centre support

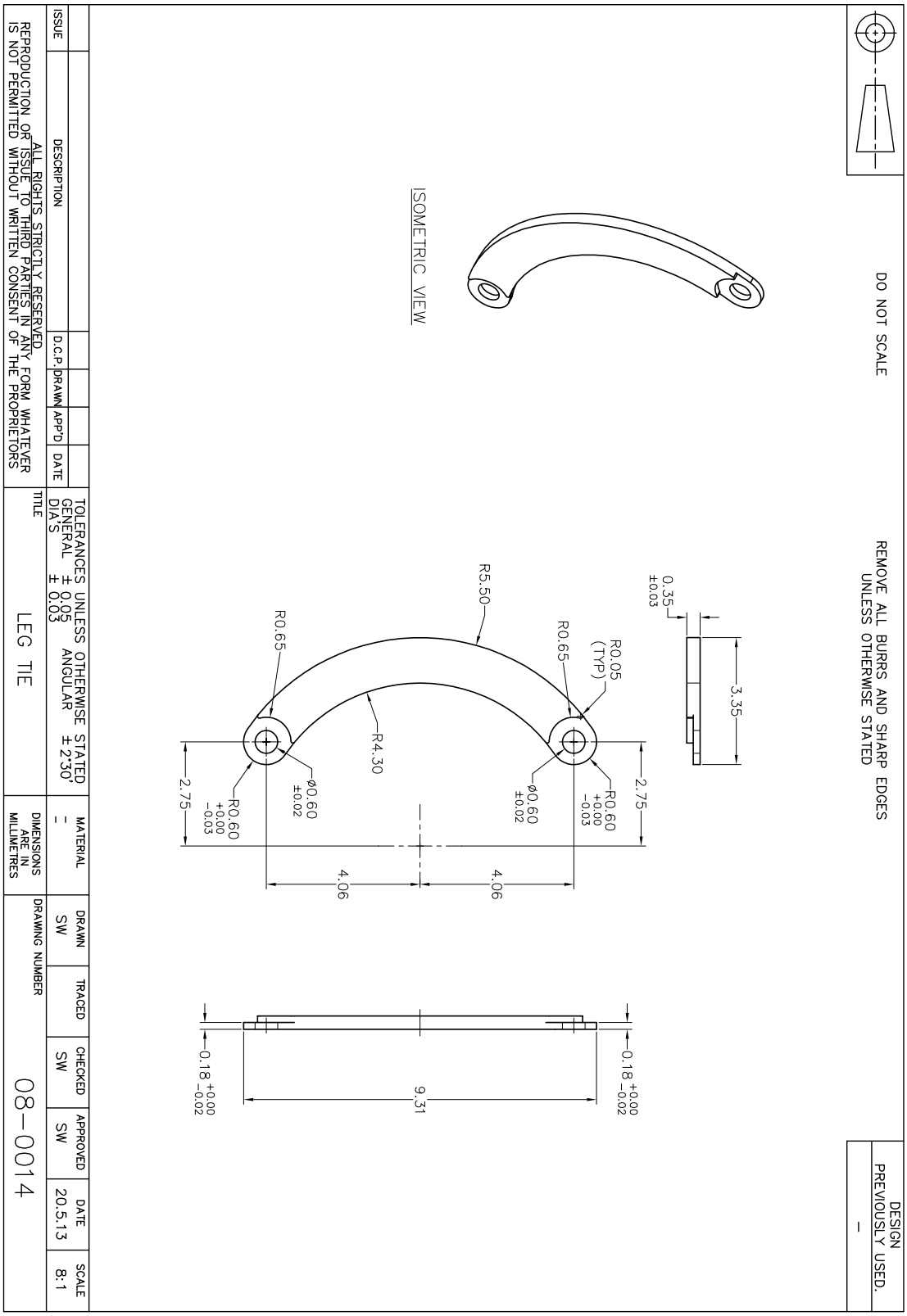


Figure F.14: CAD layout drawing of the leg tie

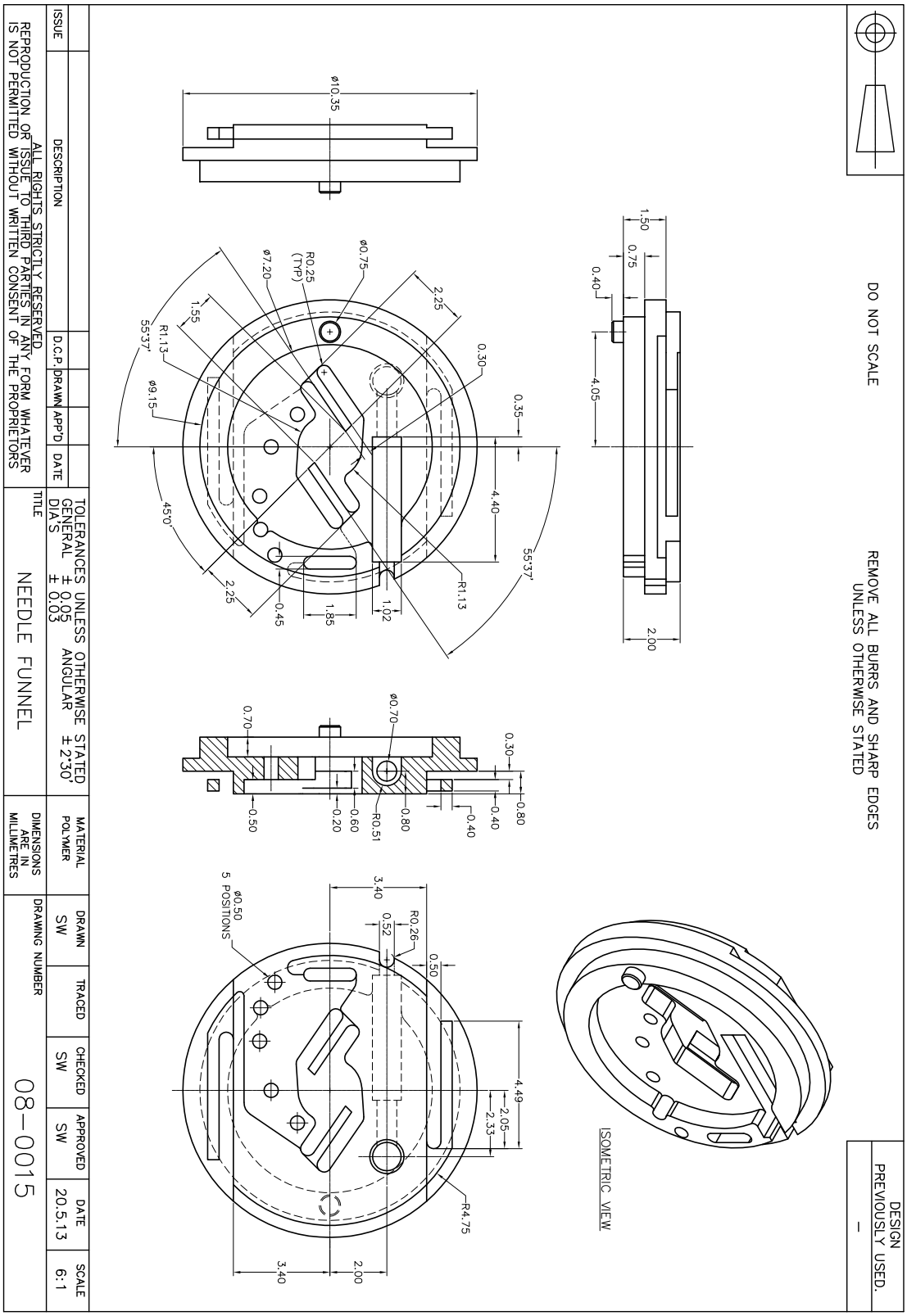


Figure F.15: CAD layout drawing of the needle funnel

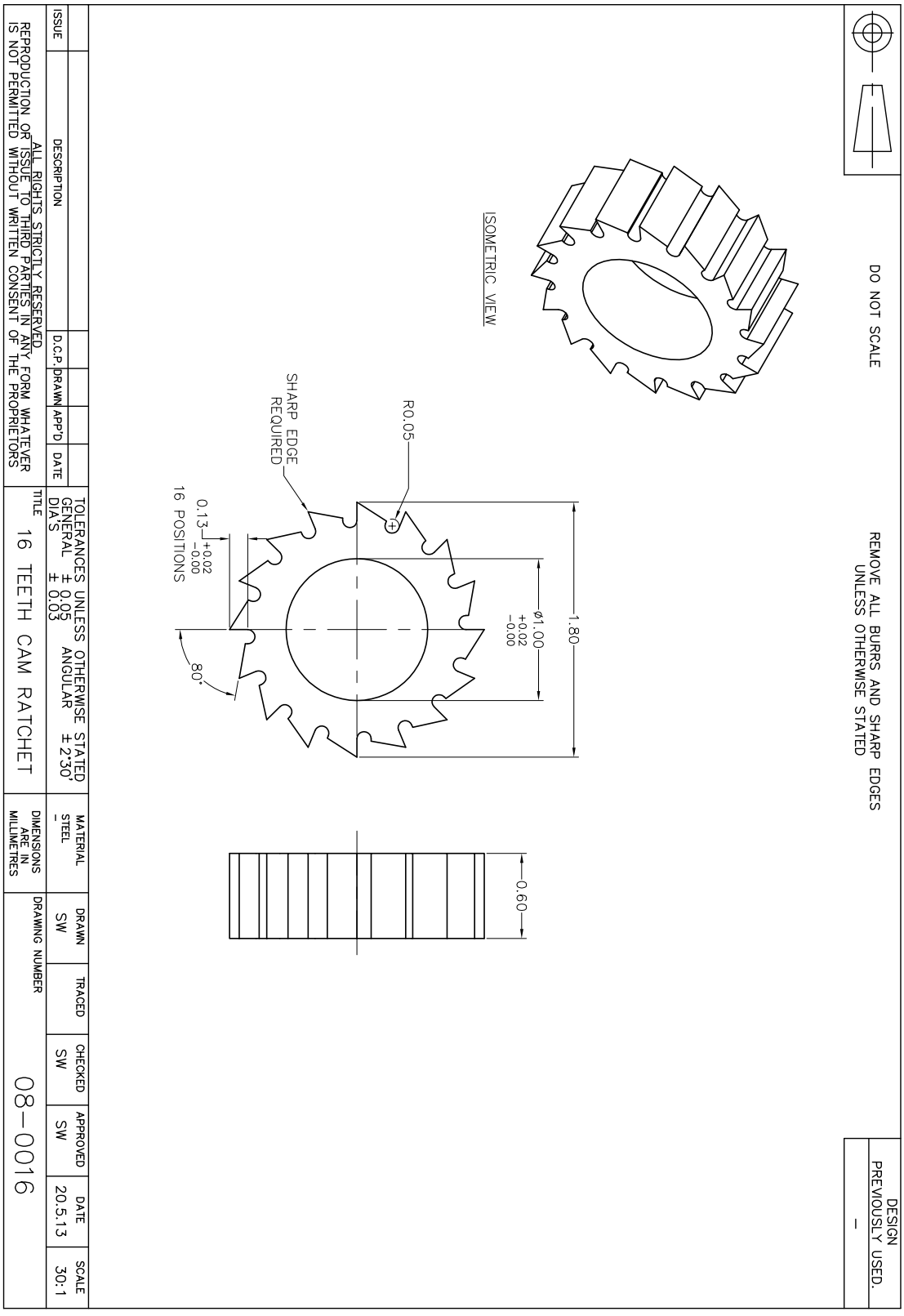


Figure F.16: CAD layout drawing of the 16 teeth cam ratchet

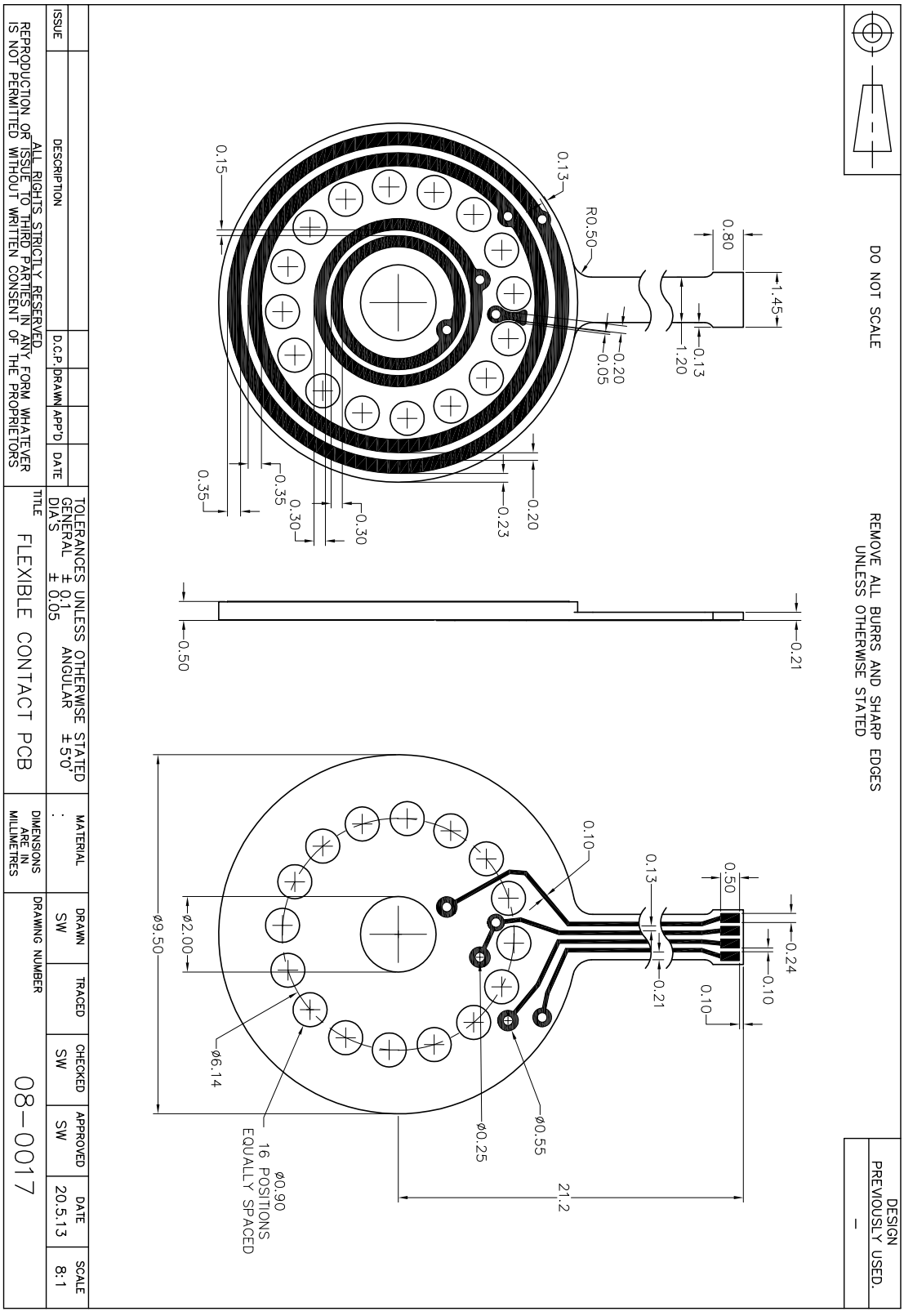


Figure F.17: CAD layout drawing of the flexible contact PCB

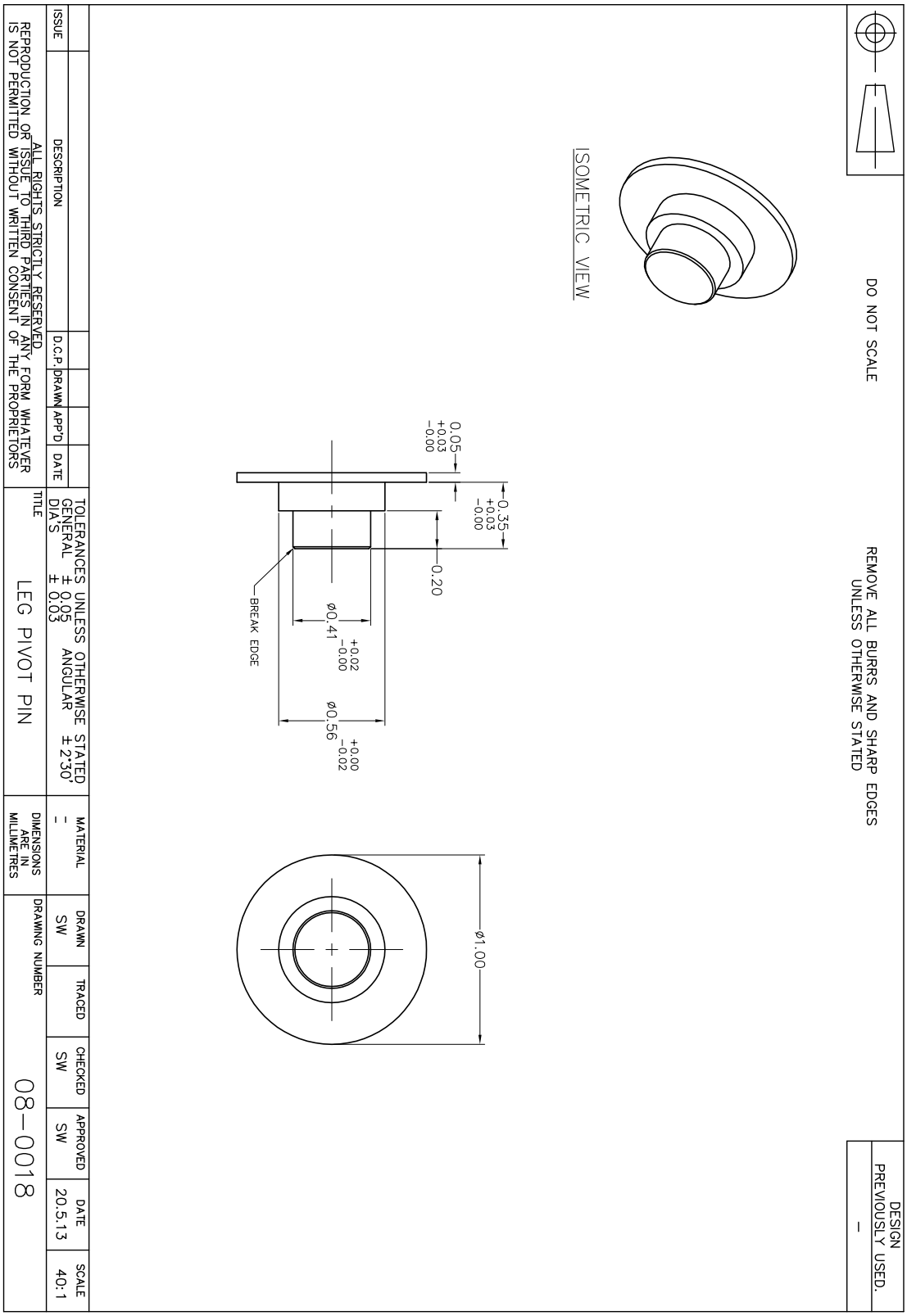


Figure F.18: CAD layout drawing of the leg pivot pin

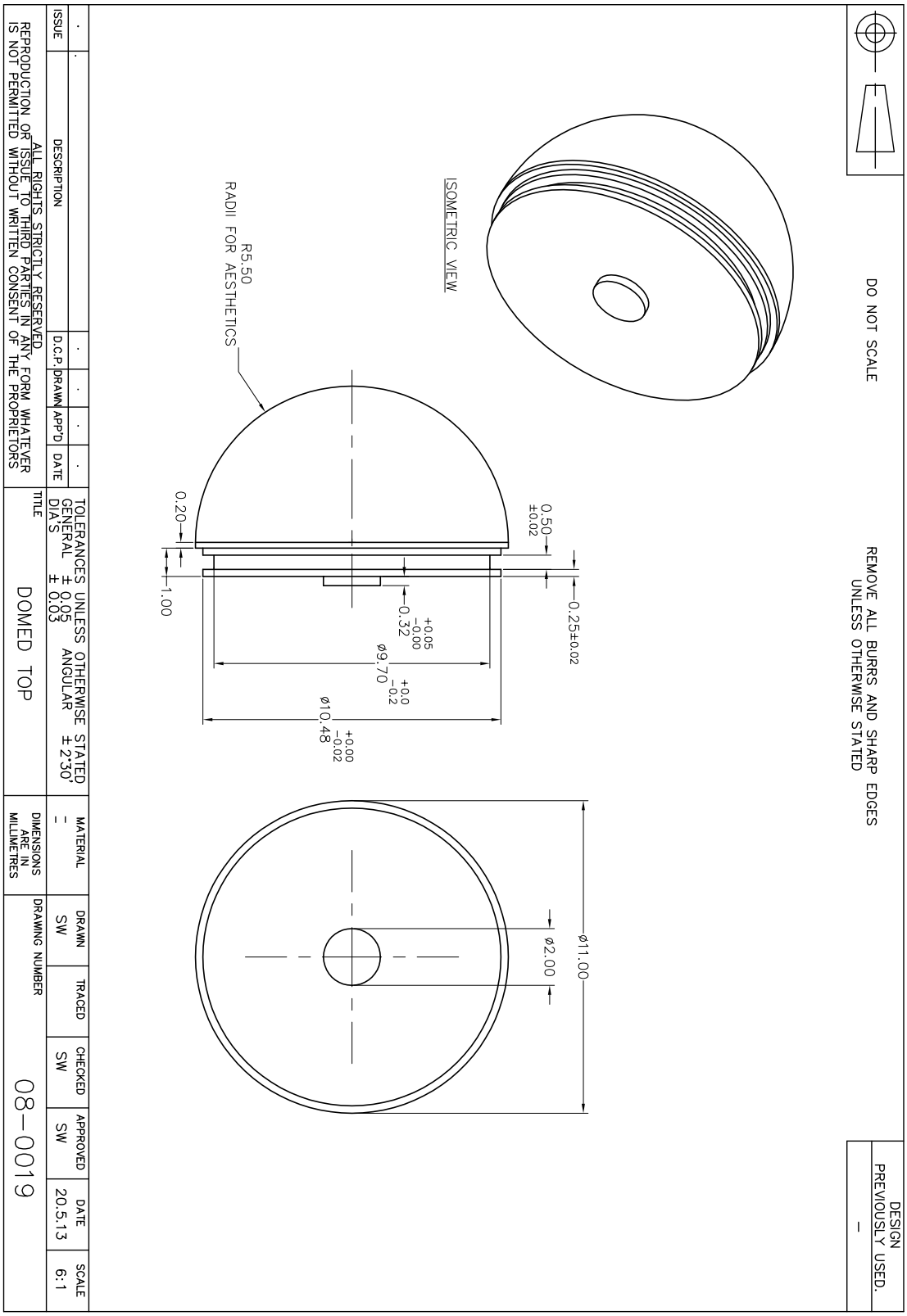


Figure F.19: CAD layout drawing of the domed top

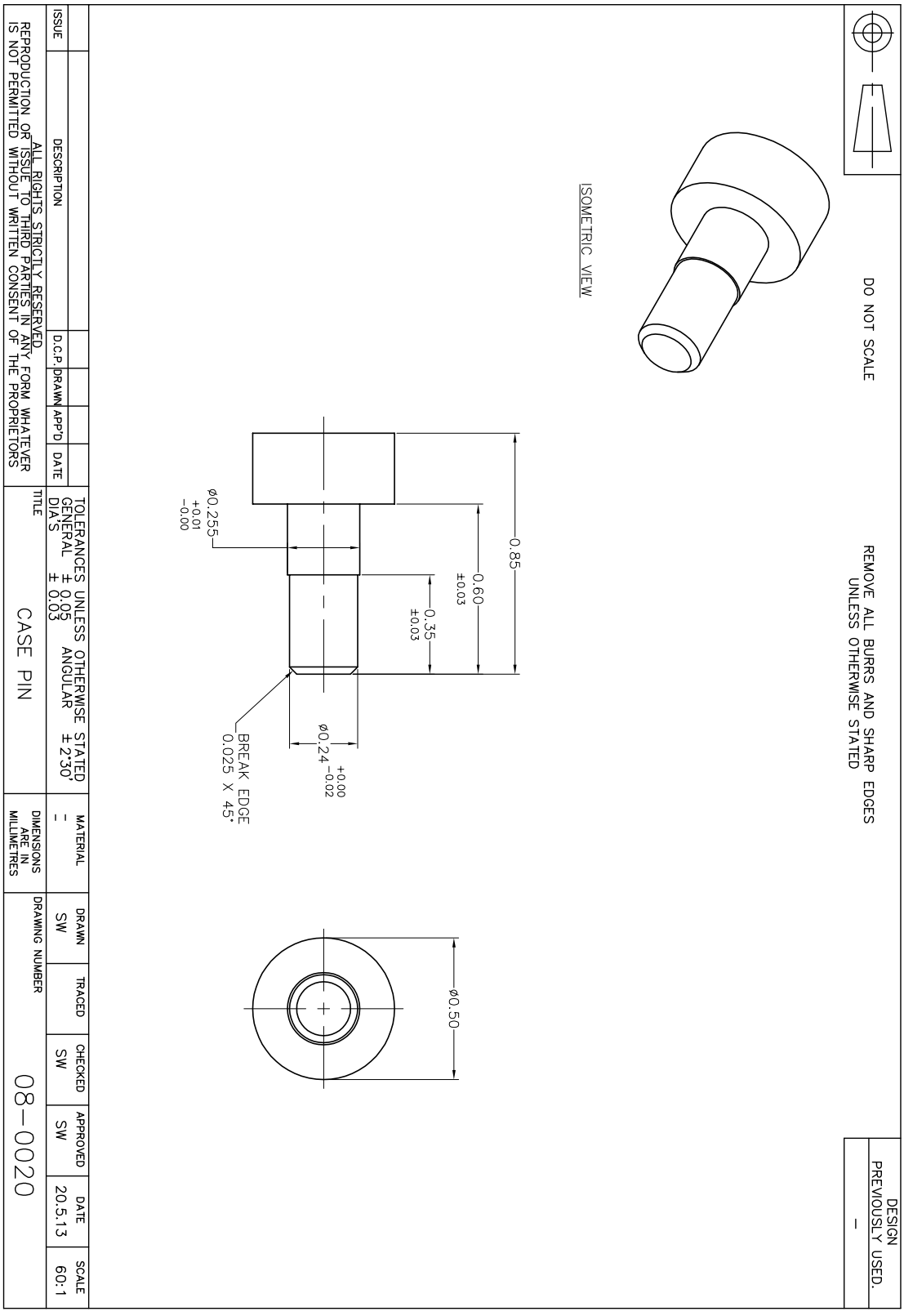


Figure F.20: CAD layout drawing of the case pin

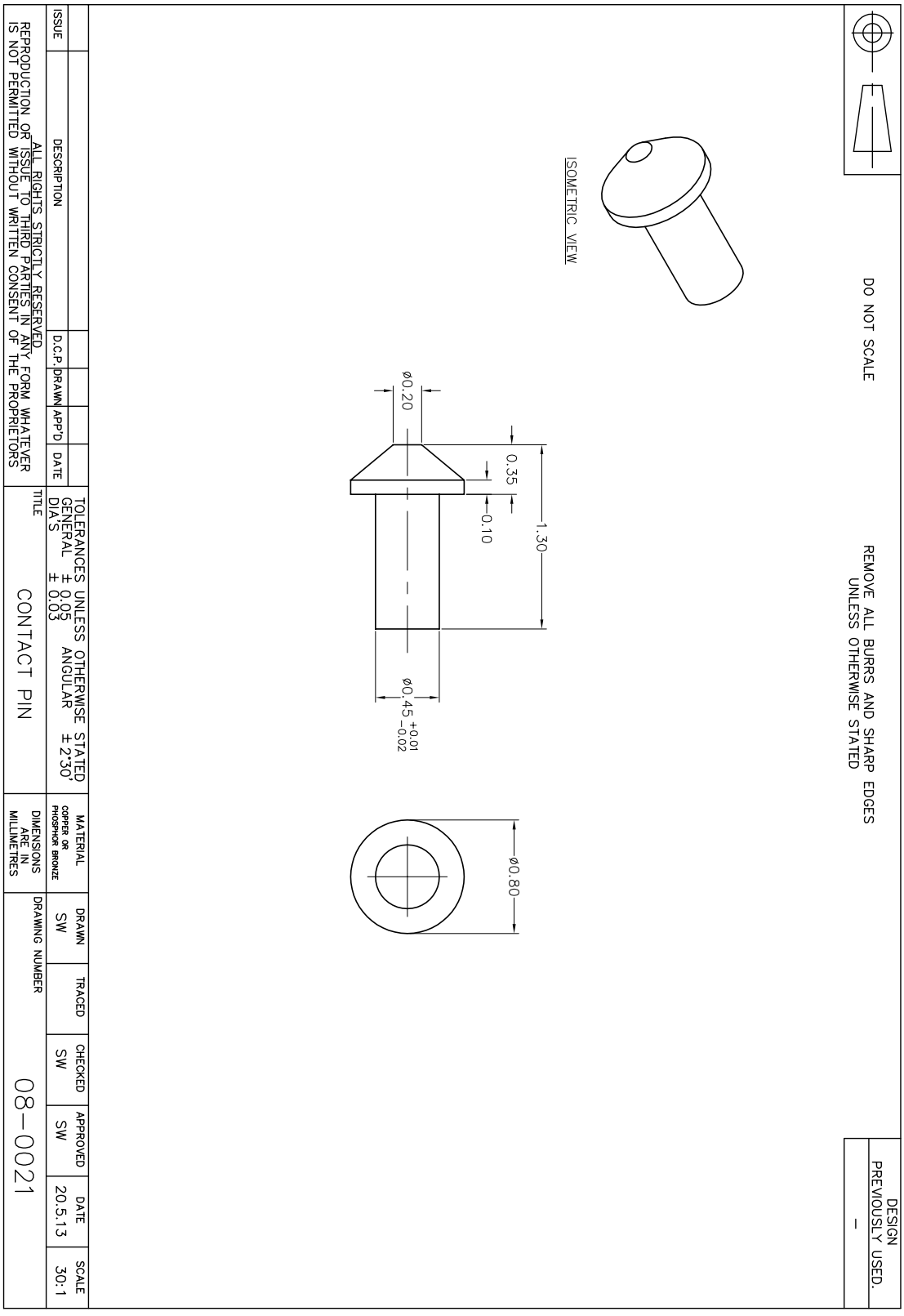


Figure F.21: CAD layout drawing of the contact pin

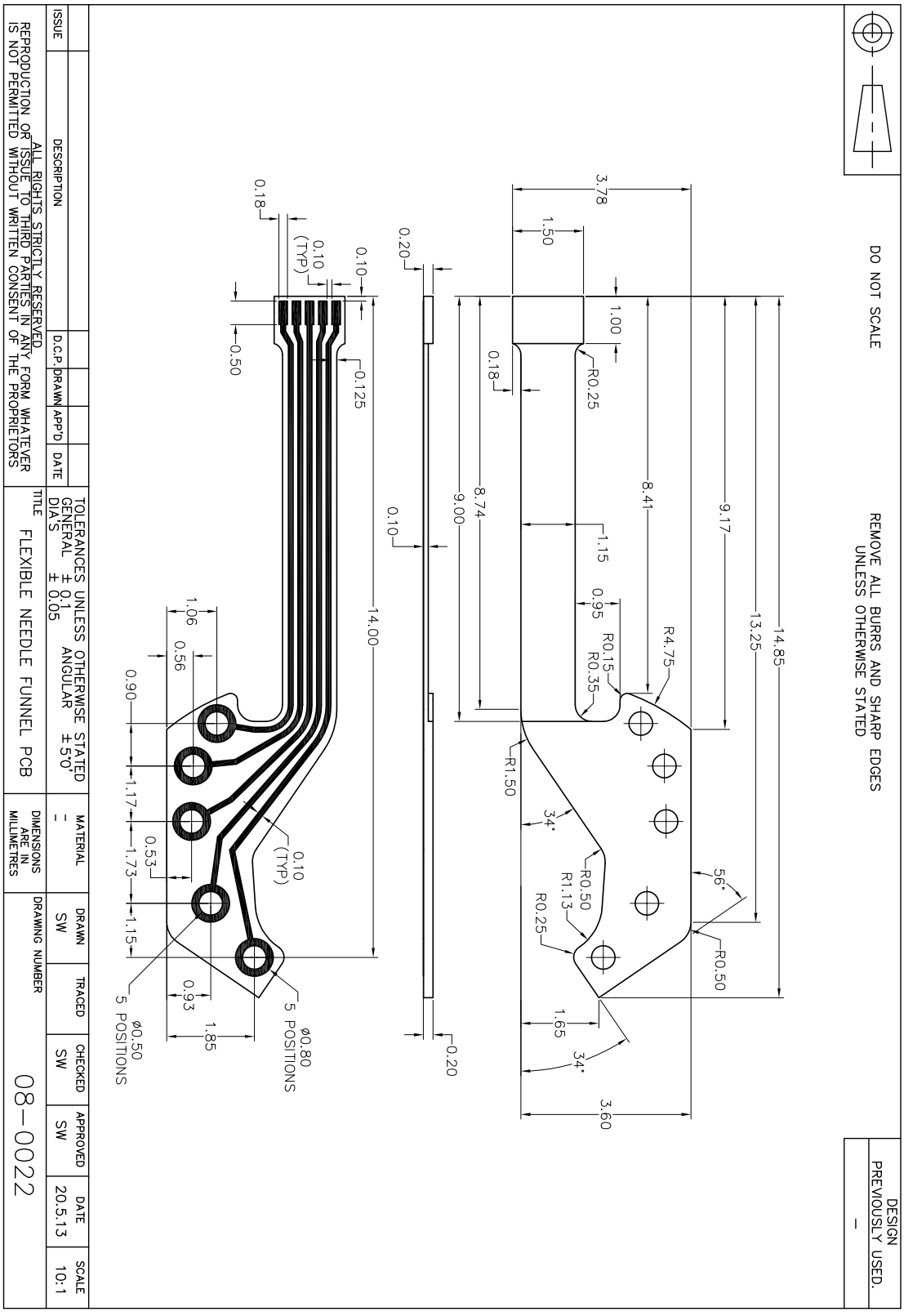


Figure F.22: CAD layout drawing of the flexible needle funnel PCB

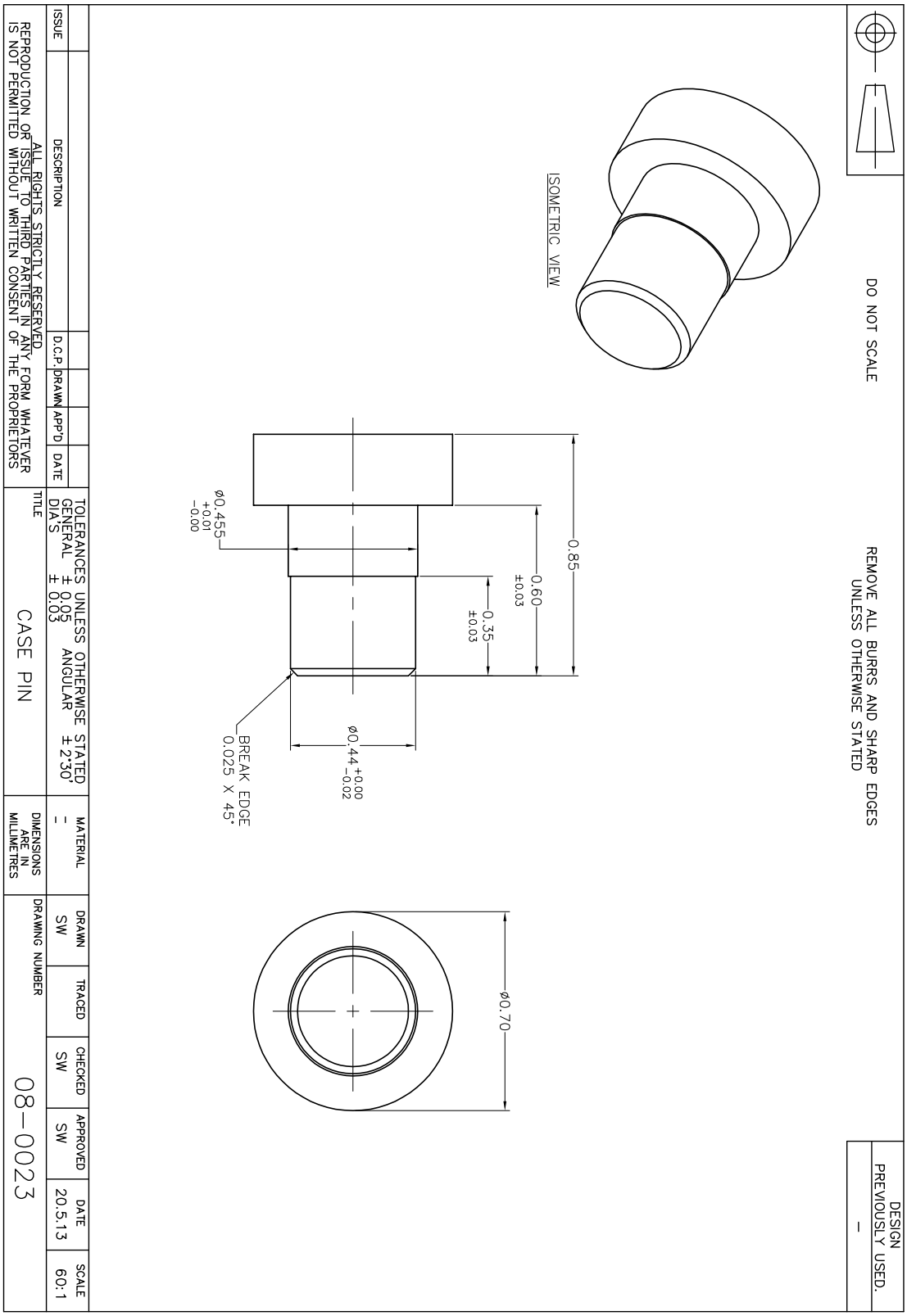


Figure F.23: CAD layout drawing of the case pin (large)

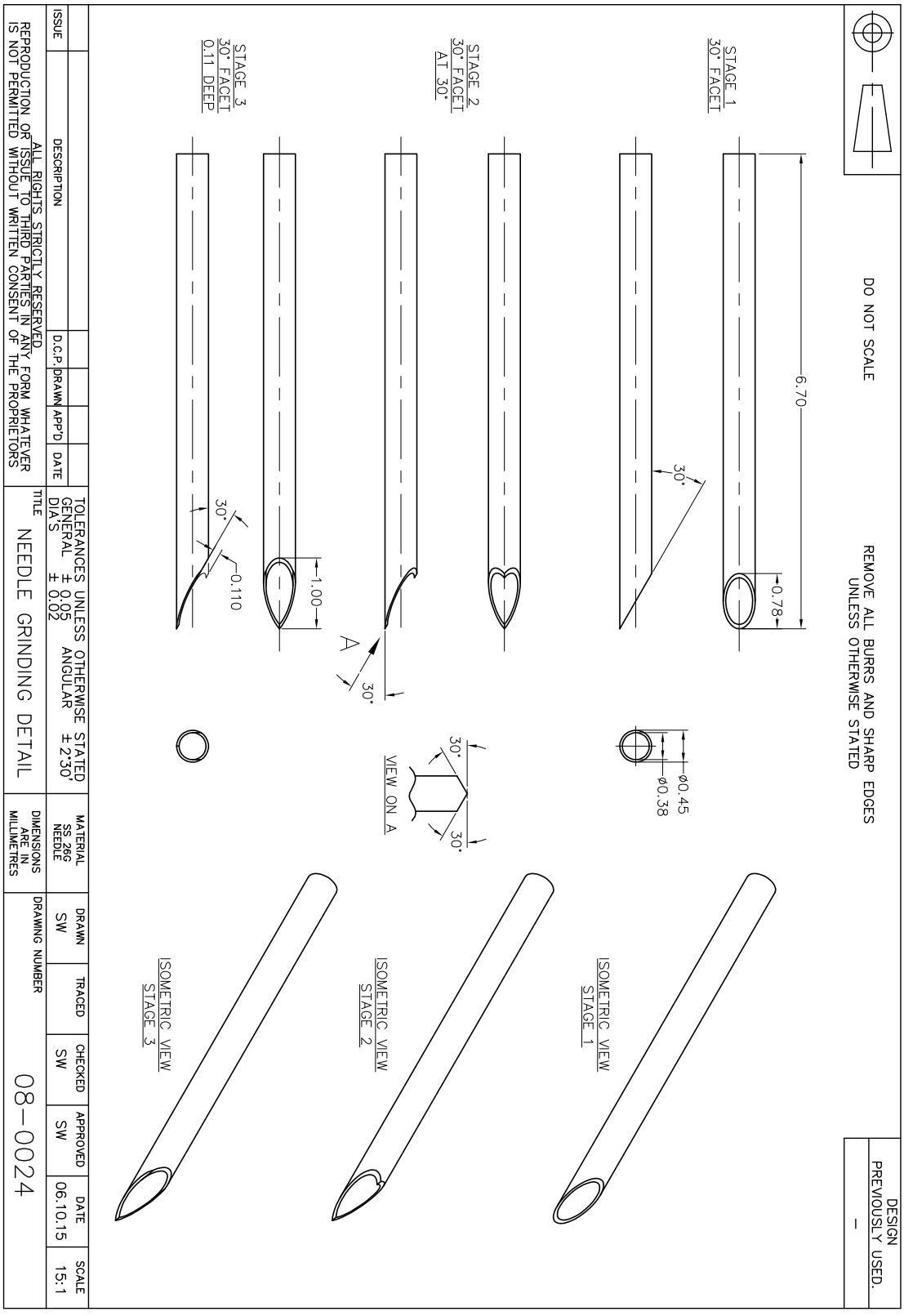


Figure F.24: CAD layout drawing of the needle grinding details

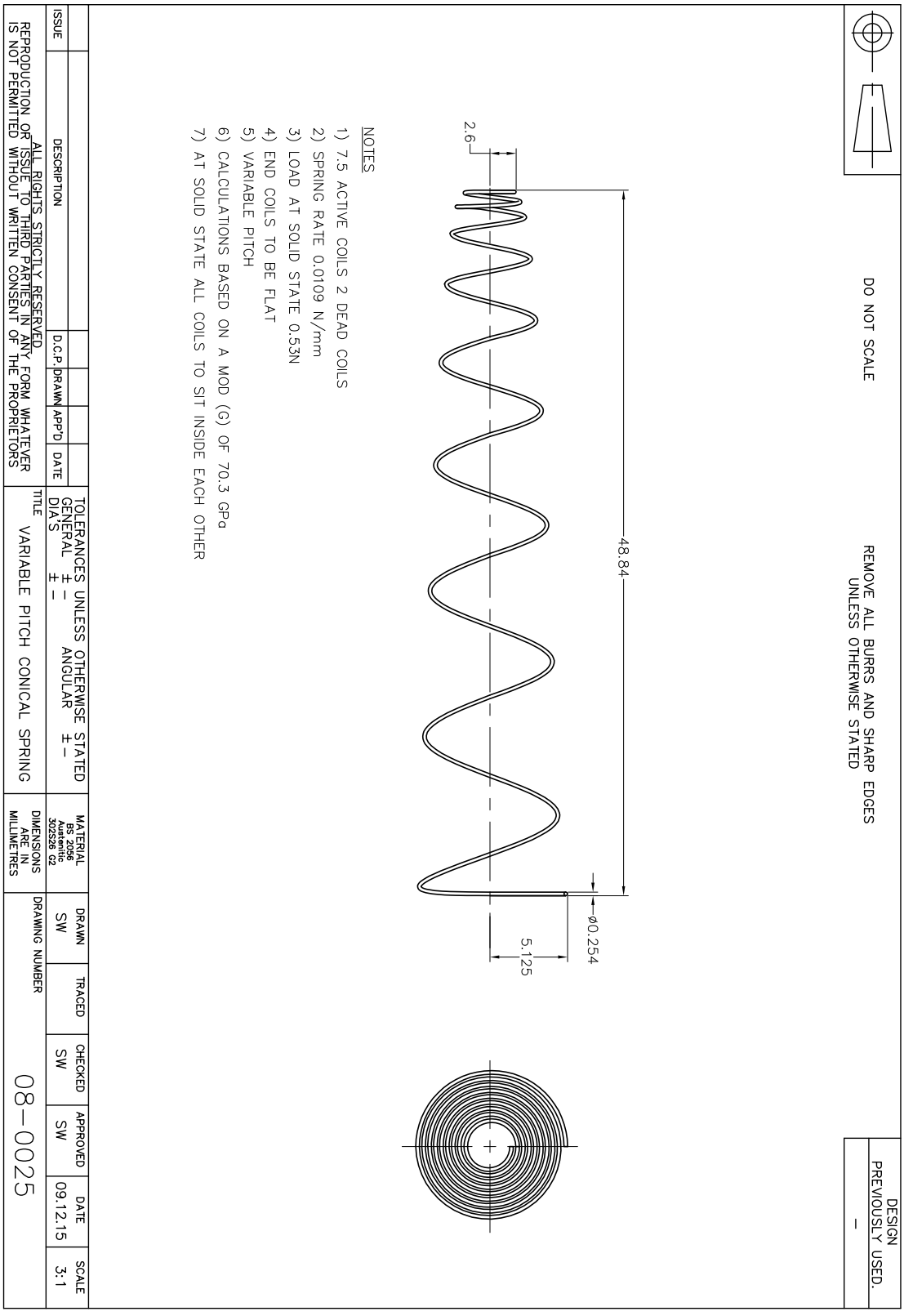


Figure F.25: CAD layout drawing of the variable pitch conical compression spring